TARGETED FLUORESCENT OPTICAL NANOSENSORS FOR IMAGING AND MEASURING FUNCTION IN INTRACELLULAR MICRODOMAINS

Paul Coupland, BSc.

Thesis submitted to the University of Nottingham for the degree of Doctor of Philosophy

June 2008

Abstract

Nanosensors offer the opportunity to measure intracellular domains with minimal chemical or physical perturbation. Typically only 60 nm in diameter and synthesised from polymer matrices they entrap chemical sensing elements and can be surface functionalised allowing for further chemical modification. Upon intracellular localisation the cellular environment can be monitored using conventional techniques such as confocal laser scanning microscopy. Reported here is one use of nanosensors to investigate the mechanisms of intracellular delivery mediated via the cell penetrating peptide, Tat. It is shown that information obtained from the nanosensors reveals that the post-delivery environment is representative of a lysosome in terms of both pH and morphology. The delivery mechanism of Tat, however, is shown to be dependent upon the cargo being delivered, corresponding to the absence or presence of a body of polymer matrix; thus nanosensors have been used to further the understanding of the cell penetrating mechanisms of Tat peptide. Technological aspects of nanosensor development have been investigated including polymer matrix modification and different methods of incorporating fluorophores into the nanosensor body. Addressing nanosensors located in an intracellular domain has historically been achieved with epi-fluorescent and confocal microscopy acquiring data from individual or low numbers of cells only. Reported here is the combination of nanosensors with flow cytometry as a technique for *en masse* investigation into entire cell populations.

Glossary of terms

APS	Ammonium persulfate
ATP	Adenosine triphosphate
cAMP	Cyclic adenosine monophosphate
CD Marker	Cluster of differentiation
CHO-K1	Chinese hamster ovary cells
CLSM	Confocal laser scanning microscopy
CPP	Cell penetrating peptide
DLS	Dynamic light scattering
DMEM PRF	Dulbecco modified Eagle's minimal phenol red free
DMSO	Dimethyl sulfoxide
EDTA	Ethylene diamine tetraacetic acid
FACS	Fluorescent-activated cell sorting
FITC	Fluorescein isothiocyanate
FSC	Forward scatter channel
GFP	Green fluorescent protein
GPCR	G protein-coupled receptor
HEPES	4-(2-hydroxyethyl)-1-piperazineethanesulfonic acid
K_d	Dissociation constant
LC50	Median lethal dose / Lethal Dose, 50%
LD50	Median lethal dose / Lethal Concentration, 50%
LIF	Leukemia inhibitory factor
MSC	Mesenchymal stem cell
NADPH	Nicotinamide adenine dinucleotide phosphate
NLS	Nuclear localisation signal
PBS	Phosphate buffered saline
PEBBLE	Probes entrapped by biologically localised embedding
PEG	Polyethylene glycol
PMT	Photo multiplier tube
poly-R-PTD	Poly arginine protein transduction domain
PTD	Protein transduction domain
ROI	Region of interest

PE	Phycoerythrin
SCC	Side scatter channel
SMBS	Sodium metabisulphite
sulfo-SMCC	Sulfosuccinimidyl 4-N-maleimidomethyl cyclohexane-1-carboxylate
TEMED	N,N,N',N'-Tetramethylethylethylenediamine
TRITC	Tetramethyl Rhodamine Isothiocyanate
UTP	Uridine triphosphate
UV	Ultra violet
VOCs	Volatile organic compounds

Acknowledgements

I would like to thank my supervisors Jonathan Aylott and Steve Briddon for their continued support and patience over these last few years, and many thanks go to John Keyte in the School of Biomedical Sciences, Nottingham, for solid-phase synthesis of the Tat peptides used throughout this study. I would also like to thank my friends from the lab, Andy, Bernie, Helen, Karen, Leo, and Matt, we had some great discussions, and arguments, both in and out of B38, that developed some good, and some not so good, ideas. Finally special thanks go to Dr Rhodri Jones, Department of Immunology, University of Nottingham, Queens Medical Centre, who helped me with the MSC and flow cytometry work, and showed true embodiment of that what my old boss, Prof Steve Haswell once taught me; all the best meetings take place in the pub.

'...when they say theoretically, they mean not really'

1 Table of Contents

Chapter 1 – Introduction: Biomedical sensing and techniques

1.1 Introduction

Cell biology, biochemistry, and biomedical research drives the development of sensors and sensing techniques used for investigation; in effect advancements in all fields of scientific research progress in parallel with advancements of new and emerging investigative tools. As research into a particular field advances and the requirement for detailed analysis increases, the usefulness of the tools and techniques used to attain the present understanding can become exhausted. Consequently the development of novel and innovative technologies, from which the continuance of research is possible, is required. The advent of improved techniques and equipment prevents applied scientific research from faltering when the point is reached at which the current tools provide no more insight. This outlines a model of research progression, efforts flow between the advancement of a scientific understanding followed by the development of improved tools to further that understanding. In practice advancements in both research and the development of the required tools proceed concurrently, and occasionally the simple step of applying an already existing technology to another field may allow for new area to be investigated. The *in situ* spatial and temporal study of the intracellular environment of viable and unperturbed cells is the focus of this study, achieved through the development of a new class of intracellular optical sensors – *Nanosensors*.

A sensor is a type of transducer – a device which converts one type of energy into another. They are used in virtually all facets of modern day life and take on many different forms and function. Some sensors are capable of being read directly (direct-indicating sensors), for example, the fluctuation in temperature can be 'seen' by an individual when using a mercury thermometer. Most sensors however must utilise a display or indicator to translate their message; this generally requires the backing of an electrical system although in scientific research several types exist which can be addressed by eye, when for example, watching a colour change. However for analysis and quantification the modern laboratory tends to record an output signal from the sensor which requires an additional system surrounding the sensing component. A sensor therefore is typically thought of as a device which contacts the environment in question; this device contains a sensing component which converts the presence of a

particular factor into a measurable change or signal. This signal is conveyed through the sensor's display systems into a readable result for the user.

1.1.1 Types of sensor

There are a great number of sensors available which are classified by the type of energy transfer which they detect. The range of sensors available include, among others, thermal sensors (thermometers, thermocouples, calorimeters), electromagnetic sensors (voltmeters, ammeters, a magnetic compass, metal detectors and Radar), mechanical sensors (altimeter, pressure gauges, flow sensors, gas meters), ionising radiation sensors (Geiger counter, particle detector), acoustic sensors (microphones, seismometers, ultrasound, Sonar), chemical sensors (ion-selective electrodes, oxygen sensors, redox electrodes) and optical radiation sensors (Lidar, photocells, photodiodes, CCDs, photo multiplier tubes, fibre optic sensors and fluorochromes). It is these last two types of sensor, chemical and optical sensors, which are of particular importance to the progress of intracellular understanding, and which have been used most exclusively in recent years; in particular fibre-optic based sensors, and free-dye fluorochrome / fluorophore based sensing schemes. It is from these predecessor sensor technologies that nanosensors are being developed to improve on their respective abilities.

1.1.2 Fibre-optic sensors and biosensors

Optical sensors for scientific research have really been developed in the slip stream of the R&D of integrated optical devices for optical telecommunication which has both developed the equipment and processing as well as driving down the costs [1]. Fibre-optic sensors are often classified into two major groups referred to as extrinsic / hybrid fibre-optic sensors or intrinsic / all fibre sensors [2]. Extrinsic fibre-optic sensors consist of optical fibres which lead to and from a housing at which the environmental signal is impressed upon the light beam passing through this housing. The return fibre (which can be the same as the input fibre) carries light with the environmental factor impressed upon it to a detector. The manner in which the light can be 'impressed' may include

differences in intensity, frequency, phase, polarisation, or spectral content; remission measurements (changes in the absorbance of reflected light) and fluorescence effects are the most simple sensing methods [3]. Intrinsic fibre-optic sensors utilise complete optical fibres which are submerged in the environment to be monitored, which impresses its effect upon the light contained within the fibre, e.g. due to light loss through the fibre as a particular factor surrounding the fibre fluctuates. There are many examples of fibre-optic sensors which rely on a multitude of basic concepts allowing for the measurement of practically every environmental factor imaginable. The simplicity with which these devices work is quite astounding when considering the detailed information gathered with such techniques. An early review that gives a comprehensive covering of the different concepts utilised in fibre-optic sensors development is by Udd [2]. Fibre-optic sensors have found wide spread acceptance and use in the biological sciences within the last couple of decades, including optical fibre arrays applied to the understanding of chemical biology [4], for optical imaging using high density cell assay platforms linked to fibres [5], and simple extracellular measurements such as pH [6, 7]. The scope of fibre-optic sensors is considerably enhanced when coupled to a biological sensing component (i.e. biosensor). Several recent reviews highlight the developments seen in the field of optical biosensors in the last decade, driven by the need for simple, rapid, and continuous *in-situ* monitoring in a wide range of scientific disciplines [8-10]. A biosensor contains a biologically derived constituent sensing element integrated into the transducer – detector system. The effect of the environment upon the biological constituent of the sensor is transduced to the detector. Fluorescence is a very common technique employed in fibre-optic biosensors (and fibre-optic sensors in general) – in the last decade reagentless fibre based sensors have been developed capable of detecting changes in cell behaviour, metabolism and cell death when exposed to toxic reagents [8]. Optical biosensors are available for the detection of numerous agents as described by Bosch [8], including urea by urease enzyme-catalysed hydrolysis [11] and food-borne pathogens [12] ongoing development into every aspect of this class of sensor (for example the application of sol-gel technology to optical biosensor development described by Jerónimo [13]) are further improving their scope and applicability; it is said that biosensors in general are improving the quality of life [14].

1.1.3 Free-dye probes, fluorochromes and fluorophores

There are different terminologies for describing fluorescent molecules, dyes and probes. For clarity a free-dye molecule is referred to as a fluorochrome, the same molecule when attached to a protein or dextran, for example, is termed a fluorophore. Further descriptions include fluorescent conjugates, fluorescent constructs or simply by its constituent parts, e.g. CPP-RPE (a cell penetrating peptide attached to R-Phycoerythrin in this example).

Utilising intrinsic fluorescent molecules has had wide application in plant science for ion imaging and morphological information [15] utilising the auto-fluorescent compounds such as NAD(P)H, chlorophylls, phycobiliproteins of cyanobacteria and red algae, flavoproteins, phenolics, and lignins, particularly if UV excitation is available [16]. One of the central questions in cell biology today regards the *in vivo* role of proteins and other key metabolites, and the development of tools to visualise these constituents and events in living cells is an active and interdisciplinary area of research [17]. Recent development of fluorescent probes for cell biology, particularly by Tsien and the exceptional work from his group [18, 19] has allowed for an increase in the scope of fluorescent microscopy techniques being applied to cell biology. These include internal morphological studies, ion flux, small molecule messenger dynamics, enzyme activation and protein-protein interaction studies to name but a few. Immunology is one field which has benefited greatly from the advent of fluorescent applications, the key advantage of fluorescence tools is their inherently greater sensitivity and dynamic range in comparison to other optical techniques. This inherent greater sensitivity over chemiluminescent emission comes from the number of photons emitted per 'event'. Petty [20] points out that only one photon per molecule is emitted during chemiluminescent applications whereas hundreds to thousands of photons can be emitted by one fluorochrome. The available tools such as confocal laser scanning microscopy (CLSM) are driving experimental cell biology, immunology and biochemistry and will continue to do so in the coming years, helping to improve our knowledge of biological mechanisms. Even with the current resolution of conventional and confocal microscopy being limited to approximately 500 – 800 nm, Weiss shows

that single fluorescent molecules can be distinguished if similar molecules are far enough apart [21]. Two recent reviews by Hell [22] and Garini [23] describe the current methods being investigated to increase the resolution limit of microscopy beyond the Rayleigh criteria. The Rayleigh criteria describes the resolution limit of a conventional optical microscope as being limited by the wavelength of light and the numerical aperture (NA) of the objective lens. Near-field optics [24] and Fluorescence nanoscopy [22] are real possibilities which will enhance the utility of fluorescent probes and techniques within the next decade.

1.2 Sensor technology application and miniaturisation

The importance of sensing technologies is very much apparent in areas other than intracellular investigation in single cells. Medical diagnostics and clinical therapeutics are two fields which are investing heavily into sensor technology for a variety of reasons. One particular area is glucose monitoring, Pickup [25] describes an urgent need to develop technology for continuous *in vivo* monitoring in subjects with diabetes mellitus, a view which is echoed many times over accounting for the health ramifications caused by inadequate glycemic control which provides a strong argument for continuous glucose monitoring systems [26, 27]. Modern biomedical sensors have benefited from recent advancement in microelectronics, microfabrication, and inexpensive signal processing paving the way for a vast array of novel biomedical sensors, impacting biology and medicine alike [28]; it is widely accepted that the biomedical sensor field has matured enough to be poised for commercial success [29]. Away from medicine and therapeutics new sensor technologies are providing increased capabilities in many areas such as bioprocessing and biotechnology [30], environmental analysis and monitoring [31], and for electronic nose systems that can detect and analyse volatile organic compounds (VOCs) [32] which are receiving particular interest in these times of bioterrorism, avian flu, and other bio-threats [33].

Coupled with advancements in sensors and sensing technologies the emergence of microfabrication techniques and nanotechnology in general is providing added means for better, smaller scaled sensors. Nanotechnology is expected to by a very disruptive

technology having a significant impact in many industrial sectors and applications, one recent review by Kim highlights the nanotechnology platforms making headway in cancer therapeutics [34] and Levy [35] describes the synthesis of multifunctional nanoclinics for targeted diagnosis and therapeutics which are ~ 50 nm Ø nanoparticles surface functionalised with various moieties for interaction with specific cells or biological sites. Obviously the miniaturisation of sensors has great appliance to biological research, particularly with individual live cell investigation. The effect of the sensors or sensing technique upon viability and metabolism of the cell is paramount as any appreciable damage negates the effort of sensing. There is a very real likelihood of interfering with the normal state of a cell when investigating its function so a degree of effort has been employed in developing techniques which silently observe the intracellular environment – this is where miniaturisation plays a key role. Coupled with non-contact optical observation of cells maintained within a physiological-like environment, such as a humidified compartment on a confocal microscope's stage (held at 37 °C with 5 % CO_2) it would seem reasonable to argue that there would be no physical damage. However in any research requiring investigation into the intracellular environment, by the insertion of a sensing or probing device, the question of perturbation *as a whole* becomes very important; significant because any appreciable damage, either physical *or* chemical, to the cell will evoke an abnormal cellular response. In extreme cases damage to a cell can induce auto-cell lysis or apoptosis. Regardless of the severity of the perturbation any induced cellular damage is greatly detrimental. It is essential to remove cellular stress induced through the sensor, in order to understand the cell in a state representative of normality, induced cellular stress is not characteristic, and therefore the results will be uncharacteristic also.

When culturing cells for investigation environmental conditions are optimised and essential growth media and nutrients are in plentiful supply, providing cells that remain typical of cells as close to *in vivo* as possible. Similarly then, during investigation, cells should remain in this state and not be stressed by the actions of investigation. In short, if it was not for the inherent cytotoxicity of fluorochromes and the problems of intracellular interference from random protein binding the use of free-dyes for intracellular analysis would be a practically perfect technology.

1.2.1 Miniaturisation of optical sensors for intracellular micro domain investigation

The emergence of nanotechnology has broadened the horizon for the development of nanosensors and nanoprobes with sub-micron dimensions suitable for intracellular measurements and many technologies are being developed allowing for insights into metabolite dynamics in real-time at cellular and sub-cellular resolution [36-38]. The application of nanotechnology to the development of other types of nanosensor including electrochemical nanobiosensors [39] has an equally impressive array of advantages. This work focuses on the technologies based on optical methods, as these are the prerequisites to nanosensors described in this research, namely probes entrapped by biologically localised embedding (referred to as PEBBLE nanosensors or merely nanosensors). Single cell biological analysis really drove the importance of miniaturising analytical instrumentation although there is great application to chemical measurements generally and for the micro-environmental analysis in material science, analytical chemistry and environmental monitoring. The main benefits to research fields, away from single cell investigation, are the vast reduction in the necessary sample volume and the increase in signal response. Tan and Kopelman, in 1995, pioneering early sensor miniaturisation state that the thousand-fold miniaturisation of the sensor results in at least a million-fold reduction of the necessary sample volume and millisecond or less response times [40]. Nanosensors are a further development in miniaturisation benefiting from the relative advantages of free-dyes in combination with miniaturised pulled fibre-optic sensors developed by Vo-Dinh [41-44] and Kopelman [40, 45, 46]. The miniaturisation of fibre-optic sensors was based on the reduction in tip size to sub-micron dimensions. This is achievable through the process of laser heated optical fibre pulling which produces a nano-scale tip easily small enough for cellular insertion. As shown in Figure 1 only limited equipment is necessary and the process can be carried out with minimal precaution in the laboratory environment.

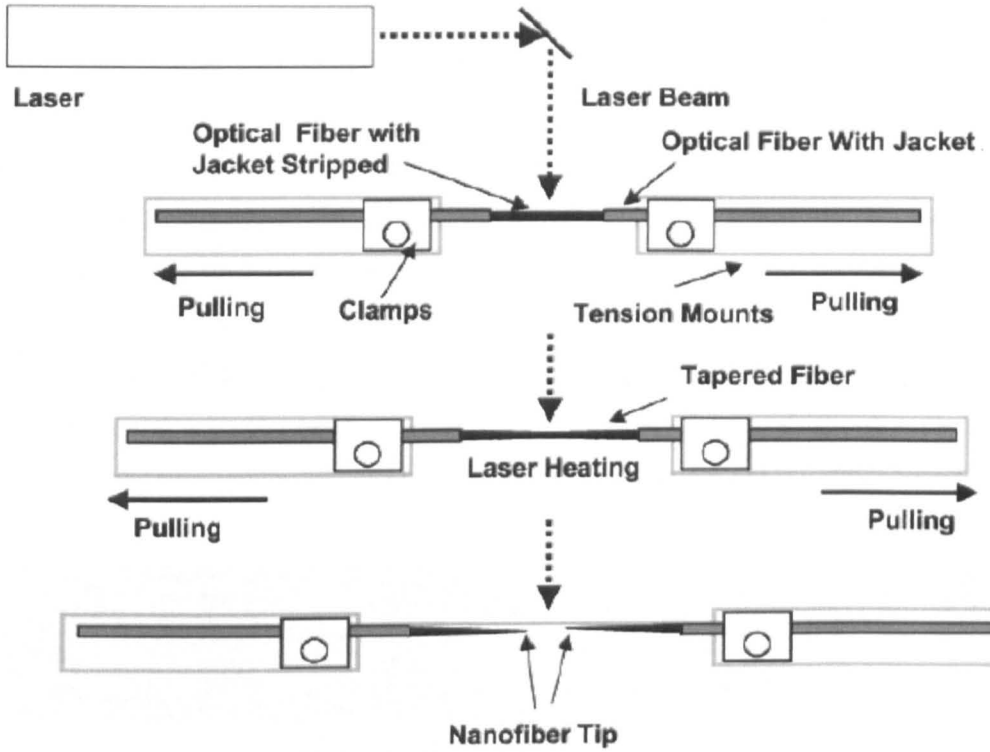

Figure 1 Schematic representation of the process of producing tapered ends of optical fibres down to nanoscale dimensions [41].

Once the tapered fibre is produced the chemical or biological sensing element is attached to the probe's tip via chemical or physical means. In some instances the tip is coated with the sensing element after silanisation of the fibre for the binding of antibodies for example [42, 43]. This approach however leaves the sensing element exposed directly to the intracellular environment when inserted inside a cell (Figure 2) and the associated problems of interference from random protein binding as well as cytotoxic effects of the sensing element upon the cell are present; free-dyes suffer these effects in the same way. Kopelman's key step was to entrap the sensing element within a polymer matrix via a photo-nanofabrication technique [46] producing a similar material as those developed by Wolfbeis [47] where polymer membranes doped with fluorescent dyes sensitive to anions and cations were produced. The photo-nanofabrication Kopelman developed consists of submerging the tapered fibre-optic in a solution of monomer molecules and fluorescent dextran bound dyes and initiating photochemical polymerisation with a light source travelling down the fibre. The profile of the light source is mapped by the photochemical reaction meaning the resulting polymer body

forming on the tip is defined by the light-emitting aperture and only forms in the near-field region where photon numbers are high. The resulting polymeric tip of the fibre-optic probe is thus a nano-sized body with suitable dimensions for intracellular positioning. The probe tip also plays a crucial role in housing the sensing element and preventing interaction of these elements with the intracellular environment. Overcoming the problem of sensing molecules leaking from the polymeric matrices of, for example, ion selective electrodes is reported [48]; this is even more crucial when the matrix is inserted directly into the cell. This is why dextran bound fluorescent dyes play such a crucial role; the large molecular weight allows the physical entrapment of the sensing element - preventing intracellular interference and cytotoxicity.

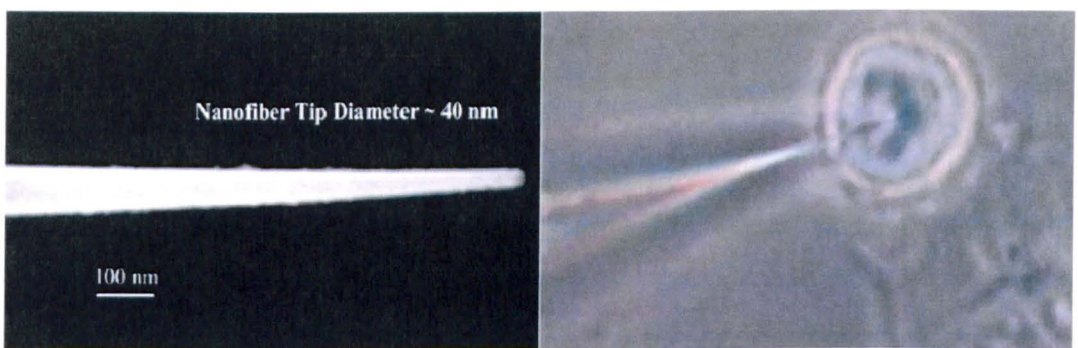

Figure 2 Electron micrograph of a pulled fibre-optic tip with dimensions applicable to intracellular insertion [41] and *in situ* during intracellular measurement [44].

A generalised system for internalisation and intracellular measurement using fibre-optic nanoprobes is shown in Figure 3. Insertion of the probe into a single cell is achieved with micro-manipulators which offer micrometre control over three dimensional positioning of attached glass needles, as used widely in *in vitro* fertilisation and single cell sampling. The nano fibre-optic probe is then attached to a suitable light source (in this example a helium cadmium laser, 442 nm wavelength) and the cells are placed on the confocal microscope stage. Illumination of the sensing element and the effect of the surrounding intracellular environment provide optical data in the form of localised fluctuations in fluorescence which is collected by the detection system of the confocal microscope.

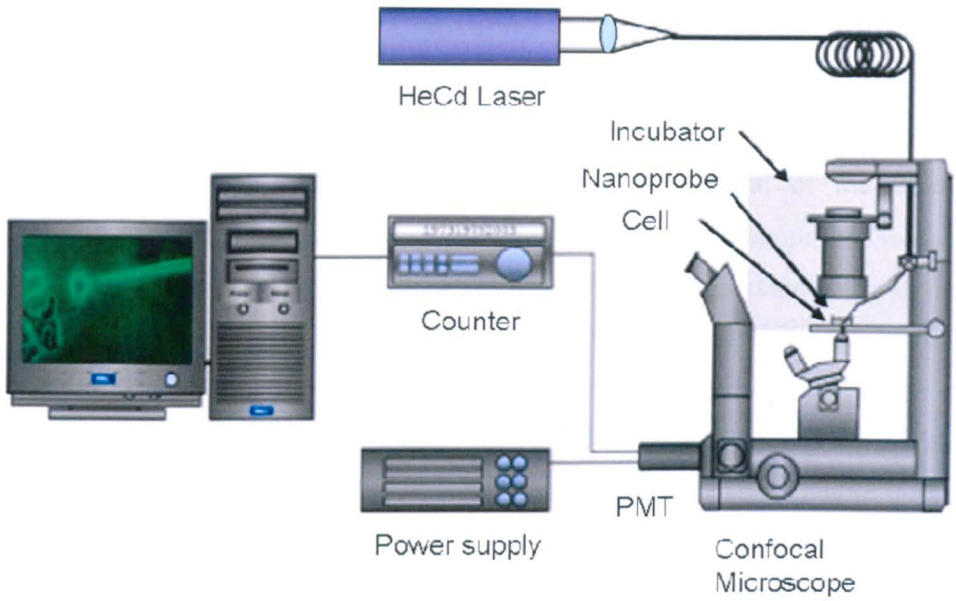

Figure 3 Nano-biosensor schematic representative of the optical measurement system used for making fluorescent measurements within single living cells [44].

Regarding the physical perturbation to the cell, pulled fibre-optic nanoprobes, even with tip sizes down to 20 nm, were presumed to cause a significant degree of mechanical damage. Commonly used as a description of this problem is the relative penetration volume of a fibre-optic nanoprobe when internalised in a 100 μm diameter mouse oocyte. If a nanoprobe is inserted into the cell (puncturing the cell wall) to a penetration depth which is half that of the diameter of the cell - the volume of the inserted apparatus attains nearly 4% of that of the whole cell volume, approximately 20,000 μm^3 and 524,000 μm^3 respectively [49]. This physical size limitation of the fibre-optic nanoprobes is greatly augmented when applied to the research of other mammalian cell lines, typically smaller than that of the large oocyte cell. It is clear to see that the PEBBLE nanosensors had to alleviate the size problem; the very small size of the fibre-optic polymer tip alone, approximating a 50 – 100 nm sphere (admittedly not as small as a single fluorophore) would cause only minimal physical perturbation to the cell compared to the rest of the probe.

1.2.2 The emergence of nanosensors

The development of PEBBLE nanosensors by Kopelman came from the logical next step in miniaturisation which paved the way for the removal of the fibre-optic component entirely. Realising that the very tip of the fibre-optic nanoprobes was all that was needed for sensing, Kopelman endeavoured to fabricate the same polymer tip as a stand alone unit and a means to address these isolated polymer nanosensors without fibre-optics. Addressing the probes was never an additional complication as the use of fluorescence microscopy for intracellular measurements with free-dyes was already commonplace [50, 51], e.g. using green fluorescent protein (GFP) as dynamic cell cycle sensors with automated microscopy [52].

PEBBLE nanosensor technology combines the benefits of both preceding technologies into a new, more robust, sensor capable of more selective measurements. A (PEBBLE) nanosensor is a small (~50 nm Ø) spherical body of inert bio-compatible polymer matrix incorporating a fluorescent based sensing scheme. The nanosensor is capable of surviving within a cell body without signal fluctuation through cellular activity other than that being observed – whilst simultaneously protecting the cell from the toxicity of the sensing constituents. It provides a means by which intracellular activity can be observed without evoking a cellular response, allowing silent observation.

1.2.3 Intracellular delivery

Although the nanosensor provides a platform technology from which we can observe and analyse intracellular domains with minimal cellular perturbation, current methods by which nanosensors are inserted do not yet afford similar low levels of cellular damage.

The main delivery methods used so far include gene gun delivery which was originally developed in biological research for the delivery of DNA into living cells, and was easily adapted for nanosensor delivery [53]. It can be described as a shotgun method where nanosensors are fired into cells. Nanosensors are layered onto a disc, by applying

a thin layer of suspended nanosensors solution and allowing it to dry. In one example of a gene gun, pressurised helium is used to propel the carrier disc a controlled distance before an abrupt stop causing the nanosensors to be thrown into the cell culture. It is reported that by controlling the original concentration of nanosensors in the suspension when layered onto the carrier disc it is possible to deliver single or thousands of sensors into the cell culture sitting a short distance away. It is also argued [53, 54] that certain levels of spatial delivery are possible by altering the helium pressure, distance from carrier disc to cell culture, and the chamber vacuum. As the nanosensors are intrinsically fired in a random pattern this only serves to selectively choose the distance the nanosensors will travel through the cell – with a certain amount of luck this will allow one to deliver sensors to the nucleus or have them remain in the cytosol.

Macrophages automatically take up nanosensors when in the surrounding solution which provides an ideal delivery method for these types of cells [55]. The concentration attained relies on both the original concentration of nanosensors in the solution and the amount of time the macrophages are placed in the solution. As it is a non-mechanical technique of internalisation cell viability is excellent. The disadvantages are that the technique is highly selective for macrophages, the sensors end up in certain cellular regions, and these specialised immune system cells are difficult to culture and maintain. Another delivery method utilises commercially available liposomes to produce nanosensor-liposome complexes which are incubated with cells. The technique exploits the natural fusion of liposomes with some cells due to the similarity of lipid structure of the cell membrane with the liposome micelle. As the nanosensor-liposome complexes fuse with the cell membrane nanosensors internalised or bound to the wall of the liposomes can become internalised within the cell. It is possible to deliver a wide range of concentrations in a similar fashion to the macrophage system but additionally the concentration of loaded liposomes plays a key role in delivering final concentrations [53, 56]. Delivery is really only possible to the cytosol of the cell and delivery requires specific modification of cell / nanosensor / liposome concentration and not all cell lines are applicable to liposomal delivery.

Finally, pico-litre injection is a technique applied to nanosensor internalisation although physical damage and distress to the cell is a problem faced during delivery. Needles are

formed using a standard pipette puller and are used to inject a nanosensor solution directly into the cell. Generally cell viability is good although normal cellular activity is likely affected. The deliverable range of nanosensor concentration is broad as this method dopes the cell with increasing numbers of nanosensor aliquots until the required number is delivered, or the cell becomes physically damaged. This method requires a high level of skill and is a batch technique meaning only one cell at a time can be addressed [56]. These limitations have lead to this technique becoming generally obsolete for the purpose of nanosensor intracellular delivery.

Each delivery method described suffers from a particular disadvantage limiting its applicability. Most notable disadvantages are the distress and physical perturbation to the cell from gene gun and pico-litre injection, and the limited cell types for which macrophage uptake can be utilised. Presently liposomal delivery is a realistic contender as a suitable delivery technique and is under investigation to provide a routinely successful technique. However it remains that tailoring liposomal delivery for each cell line is very time-consuming and applicability to cell types is notably limited. The development of a different method based on the attachment of cell penetrating peptides is investigated here which is hoped to provide a simple and universal technique enabling nanosensor internalisation without disruption to the cell wall or cellular biochemical activity of the cell. This is hoped to complement the silent observing nature of nanosensors.

Delivery of the sensors into the cell is the fundamental part of a model delivery system, once the sensors have crossed the cell wall the question of where the sensor locates needs to be addressed. The ultimate goal is to target nanosensors to a particular location or micro domain within the cell of interest. This concept of targeted delivery of particles to a specific area within a cell is currently an engaging area of drug delivery research; it makes sense therefore that our own investigations into targeted nanosensor delivery initially looked to these drug delivery techniques for insight into the available possibilities.

1.3 Fluorescence

Fluorescence is a process of luminescence which is distinct from incandescence (i.e. emission of light due to high temperatures). Luminescence describes a number of processes by which light (photons) is emitted from certain molecules which have attained excited states. A common result of directing light on a molecule that absorbs rather than transmits is that one or more of the electrons of the molecule are promoted into a higher energy state. The ways in which these higher states are brought about are physical (light absorption) mechanical (friction) or chemical (chemiluminescence). Formally the process of luminescence generation through the absorption of infra red or visible light is known as photoluminescence which is further subcategorised into fluorescence and phosphorescence. In the theoretical model of molecules the electrons occupy distinct orbits and energy levels, although a simple view of molecules, it does serve to outline the general process of fluorescence. The excited electronic states are unstable; sooner or later the electrons forced into these higher energy states lose their excess energy and fall back to lower energy ground states. This excess energy can be dissipated in several ways, the most common being simply to increase atomic vibrations within the molecule. But some molecules are capable of emitting some of the energy as light. This is what we see as fluorescence or phosphorescence. The difference between the two is the electronic configuration of the excited state and the emission pathway. In fluorescence the excited electron is in a singlet state, that is to say it is spin paired (i.e. opposite spin) with the second electron in the ground state orbital. This allows return of the excited electron to occur rapidly, in the order of nanoseconds, with the resulting emission of a photon. In phosphorescence the excited electron is in the triplet state, not spin paired with the ground state electron, meaning that return to the lower energy level is forbidden. This ultimately means return to the ground state takes significantly longer, in the order of $10^3 - 10^0$ s^{-1} (milliseconds to seconds). The timescale between the absorption of one photon and the emission of another is termed the fluorescence lifetime. Depiction of these processes is typically exemplified with one form of a Jablonski diagram (Figure 4). Professor Alexander Jablonski (1898 – 1980) is regarded as the father of fluorescence spectroscopy due to his significant accomplishments in the field, although it was British scientist, Sir George G. Stokes, who first described

fluorescence in 1852 and was responsible for coining the term in honour of the blue-white fluorescent mineral fluorite [57]. An excited electron in a fluorescent molecule (one that fluoresces when illuminated with a particular wavelength (λ) of light) quickly falls to a lower, more stable, energy level – the relaxed electronic singlet state. This occurs as the fluorochrome undergoes some conformational change which allows some of the absorbed energy from the incident photon to be released as heat. However heating is generally detrimental to the process of fluorescence, and most molecules, when fluorescing, produce very little heat. From here the electrons more steadily move back to the original ground state releasing the remaining energy ($E_{emission}$) as fluorescence. Because some energy of the original photon has been lost through heat, $E_{emission}$ has less energy than $E_{excitation}$ and as such is of a longer wavelength i.e. is red shifted with reference to the visible electromagnetic spectrum.

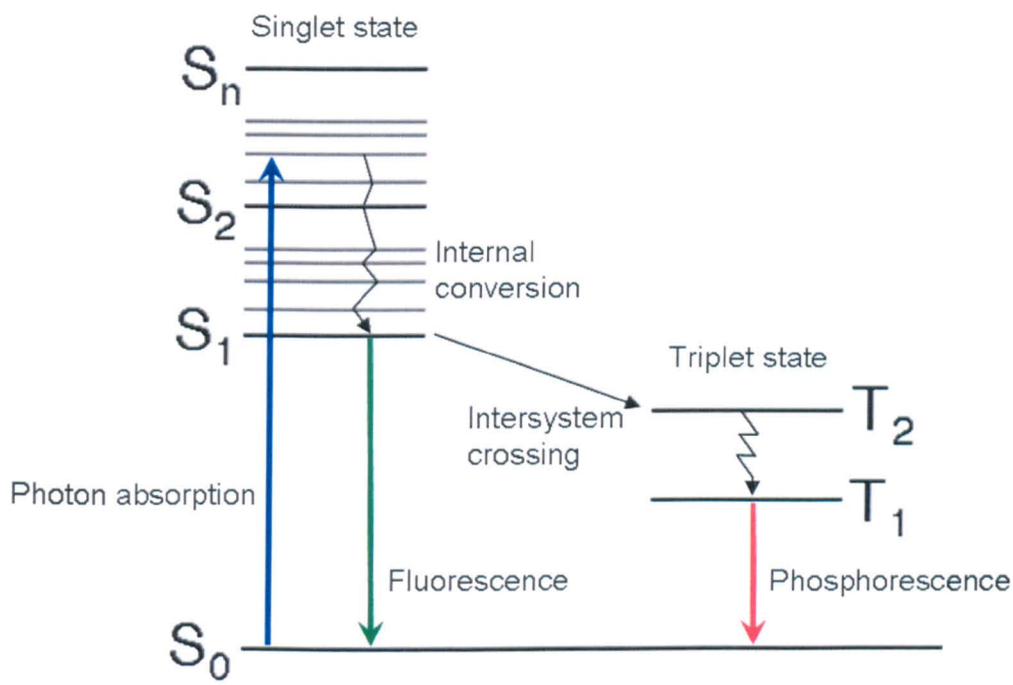

Figure 4 Fundamental Jablonski diagram.

This effect, in practice, means the emission wavelength of a fluorochrome will be longer than the excitation wavelength required to excite the electrons. The difference between the excitation and emission wavelength of a fluorochrome is termed the Stokes shift. A larger Stokes shift often means the fluorochrome is better for fluorescent studies

as the emission can more easily be distinguished from the excitation, it also allows for broader excitation wavelengths to be used.

When the excitation and emission spectra of a fluorochrome are viewed they most often look like a mirror image of one another with regards to wavelength, e.g. FITC in Figure 5. The emission spectra of a fluorochrome almost always stays the same irrespective of the excitation wavelength used [58]. This is due to the fact that excess energy is quickly dissipated with conformational change allowing the excited electron to quickly fall to the lowest excited vibrational state, S_1. This occurs prior to fluorescence so, regardless of how excited the electron became initially (i.e. the energy of the incoming photon) fluorescence emission is generated from the same excited state. Only the intensity of the emission alters depending on the excitation wavelength. Many fluorescent molecules alter their fluorescent intensity when the environment around them changes. This can be due to the association of the fluorescent molecule with a particular analyte or pH change which causes a change in the quantum yield of the fluorochrome. Quantum yield in a radiation-induced process refers to the number of times that a defined event occurs as a photon is absorbed by the system. Therefore, the quantum yield is a measure of the efficiency with which absorbed light produces some effect. In fluorescence, the quantum yield is defined as the ratio of the number of photons emitted to the number of photons absorbed. As you can see an increased quantum yield means that the molecule will fluoresce more strongly, measured by an increase in light. Responding to an environmental factor, which is an inherent feature in many recently developed fluorescent probes, has made fluorescent probes one of the cornerstones of real-time imaging of live cells and a powerful tool for cell biologists [19].

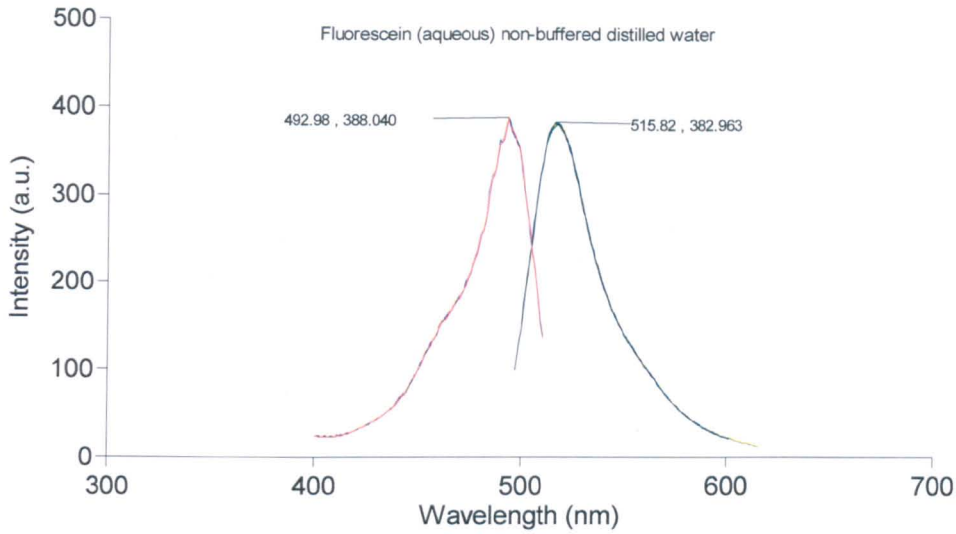

Figure 5 Fluorescence spectra of FITC. Excitation profile monitored at 520 nm (red trace) and emission profile excited at 488 nm.

1.4 Spectrofluorometry

This is a specialised technique dealing with fluorescence, part of a number of techniques termed spectrophotometry that investigate the interaction between light and substance as a function of wavelength, or the type of material under observation. In general the equipment used for this purpose is simple consisting of a light source, a monochromator, sample holder, another monochromator, and a detector. The necessity of a second monochromator is so that the individual wavelengths of emitted light can be observed also. Monochromators are dispersive optics allowing the selection of very narrow bands of wavelength to be chosen from a light source. They can work on optical dispersion, like a prism separates light, or diffraction using what is known as a diffraction grating. These devices have a surface covered with parallel lines with a distance between them similar to the wavelength of light used, these lines serve to diffract the light, the degree of diffraction depends upon the wavelength, consequently spreading out the light into its constituent colours. A common diffraction grating effect can be seen when one holds up a compact disc, the parallel grooves of data act as a diffraction grating. In the Varian, Carey Eclipse, model of spectrophotometer used in

this research the monochromator is of the diffraction grating type, a visual explanation of this can be seen in Figure 6.

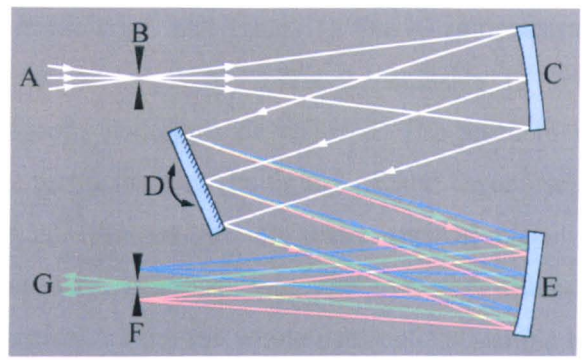

Figure 6 Light (A) is focused onto an entrance slit (B) and is collimated by a curved mirror (C). The collimated beam is diffracted from a movable grating (D) and the dispersed beam re-focused by a second mirror (E) at the exit slit (F). Each wavelength of light is focused to a different position at the slit, and the wavelength which is transmitted through the slit (G) depends on the rotation angle of the grating. These optics have similarities with the pinholes used in a confocal microscope.

The light source is a pulsed xenon arc lamp which is focussed onto the sample holder; the emitted light is collected at a 90 ° angle to the source. A second monochromator receives the light much in the same way as the source monochromator, the difference being that the mechanics of the system allow for the second monochromator to be rotated, separating out and detecting the individual wavelengths present in the emitted light. Similarly, the source monochromator must allow for this when carrying out an excitation profile of a particular fluorochrome. The ease in which a solution can be measured in terms of fluorescence with this technique made it a valuable tool for the assessment of nanosensors and was used throughout to demonstrate the functionality of various nanosensors.

1.5 Confocal microscopy

In the field of microscopy, which has its beginnings as far back as the early 1600's, confocal laser scanning microscopy (CLSM) is a relatively new technique, an invention borne from the necessity and desire to improve image clarification within thick samples. Development of the confocal microscope is credited to Marvin Minsky; he never

published his ideas but filed for a patent of his invention in 1957. This remarkable step in microscopy development was not the focus of Minsky's research at the time, he was pursuing an interest in neuronal morphology and nerve cell mapping, but due to the inability of current microscopy techniques to derive information from within thick samples, such as neuronal tissue, he found it necessary to divert his attention to developing the microscopy technique he required. The problem wasn't being able to stain the cells, but the architecture of the tightly packed tissue itself. With conventional epi-fluorescent full-field illumination the entire vertical plane of the specimen is illuminated simultaneously meaning that the returned fluorescent signal is an amalgamation of information from the whole depth of the sample rather than just at the focal plane; the serious problem was scattering. Most of the light collected by the objective lens comes from above and below the selected focal plane affording out of focus haze to the final image, unless each view could be confined to a thin enough plane, nothing came out but a meaningless blur [59]. In the fascinating memoirs of Minsky detailing this time he describes "solving that problem of scattered light became my conscious obsession" [60]. Minsky realised that an ideal microscope would examine each point of the specimen allowing the user to obtain information about the amount of light scattered or absorbed at that point. If one tries to look at many points at once then each will be clouded by the aberrant rays of light coming from adjacent points. It became apparent that it was necessary to view each point exclusively whilst omitting the out of focus light in the surrounding sample, the idea of a new microscope type was defined and was to be developed. Figure 7 shows that Minsky used a dual microscope set up, one microscope (rather than a condenser lens) was used to image a pinhole aperture in the sample which removed all incident light not initially focussed at the focal point; this also reduced the amount of light in the sample by orders of magnitude without reducing the intensity at the focal point. The image plane, though, still receives scattered light from out of focus parts of the specimen above and below the focal point (as there will be a double cone of illumination above and below the focal point); this too was removed through the use of a second pinhole aperture lying beyond the exit side of the objective lens. Ultimately Minsky developed a symmetrical system with pinholes and objective lenses on either side of the specimen, the first set prevented full-field illumination allowing only the illumination of a single focal point, the other set only allowed image capture of the single point.

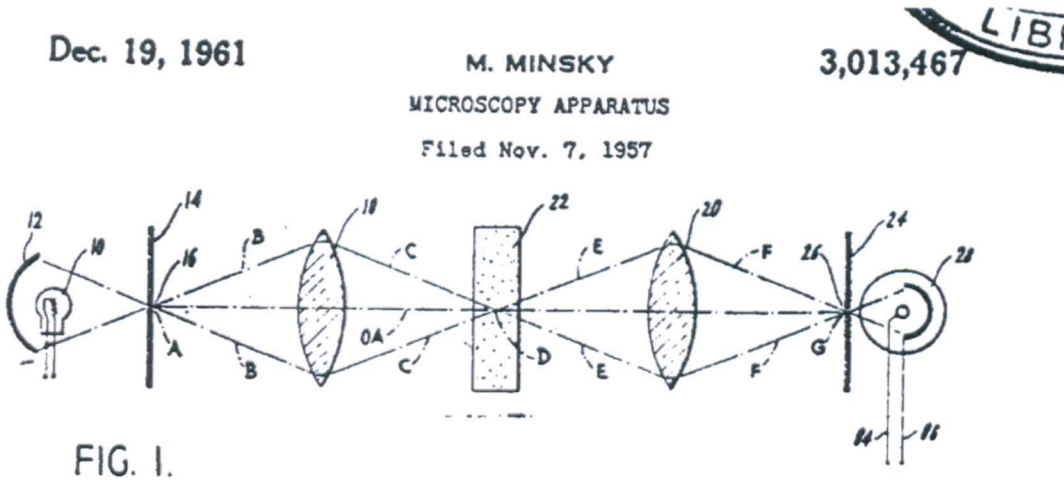

Figure 7 Minsky's dual microscope 'confocal' set up. Taken from the original 1957 patent application [61]. Here a pinhole in front of a zirconium arc source provides a point source of light.

Even though this design was patented in 1957 and Minsky presented the invention to several colleagues and visitors, the advent of the technology never really came about until the 1980's with the development of powerful lasers and the entire opto-electrical system necessary to take advantage of Minsky's confocal apparatus [62, 63]. The theoretical basis of confocal microscopy leads to the associated advantages as evidenced in Figure 8. Almost all out of focus light is removed by the confocal set up giving rise to much clearer images with enhanced contrast.

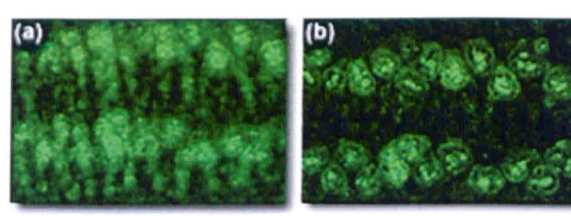

Figure 8 Butterfly wing epithelium. Out of focus fluorescence in (a) seriously impairs the quality of the captured image with conventional epi-fluorescence microscopy. In contrast confocal microscopy removes the glare of out of focus fluorescence creating much clearer images (b) [64].

The manner of illumination in a confocal optical path allows for very discrete illumination of a point in space called the Point Spread Function (PSF). In the sample the light imaged from the point source forms a double cone (as shown in Figure 9) which is most intense at the centre, some 10^5 more intense than the outer areas with a

point source PSF [65]. One way to think of the PSF is in probability; the probability that a photon will reach the centre of the point spread function is 10^5 more likely than another point within the light cone.

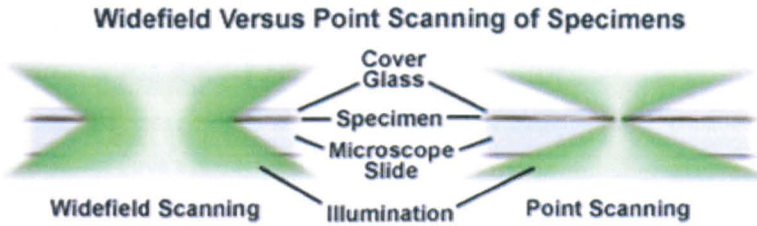

Figure 9 Difference between wide-field and point source illumination [64]. With wide field illumination the resulting image suffers with interference from reflected or emitted light from above and below the optical focal plane as well as scattered light from areas adjacent to the point of interest. In comparison, the very small point of illumination (PSF) created with point scanning increases contrast as adjacent areas are not illuminated in the first instance and remitted light from above or below the focal plane is prevented from reaching the detector by the pinhole located on the exit side of the objective lens.

The pattern in figure 10 shows that there is a highly structured order to the intensity distribution. This is what is specifically meant by the PSF. The reason the PSF has these areas of diminishing high and low bands of intensity is due to the wave nature of light [66].

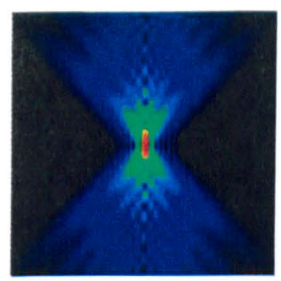

Figure 10 Arbitrary image of a confocal PSF expressed with a logarithmic scale.

Light is diffracted when passing through the objective lens, just as all waves are diffracted as they pass through or around an object, and the resulting constructive and deconstructive interference yields the pattern observed in the PSF. If one were to bisect the PSF perpendicular to the *z*-axis then the resulting pattern (cross section) of the PSF would look similar to that in Figure 11.

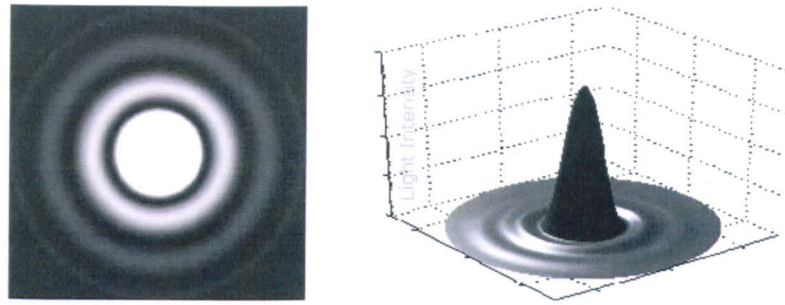

Figure 11 Airy disc: PSF cross section at Z = 0, Logarithmic scale and 3-D visualisation. On a linear scale only the peak would have any intensity [67].

The centre spot of this pattern is known as the airy disc and it can be used to measure the resolving power of the microscope, the term 'diffraction limitation' is referred to when the airy disc is greater in size than the resolution required to distinguish between two smaller objects in close proximity. The diffraction effects seen with confocal microscopes are due to the objective lens, which is why the numerical aperture (NA (a measure of the lens aperture in angle [68])) of the lens has such a profound effect over the resolution of the microscope. A lens with a greater NA has a smaller PSF so provides better resolution, but with greater cost.

A confocal microscope uses a point source of light to image a PSF within the sample; remitted light from this point in turn travels through a pinhole aperture (a second PSF) to the detector. The intensity of the image captured is therefore made up of the mutual intensities from both PSF which means the confocal microscope has an overall PSF, the product of the two.

$$PSF_{CF} = PSF_S \text{ X } PSF_P$$

CF = confocal microscope, S = source, P = pinhole

The PSF_{CF} is a representation of the probability of a photon travelling from the point source (laser) to the correct point viewed in the sample, being remitted in a manner which allows it to then travel through the pinhole and to the detector, being that they are both probabilities the sum of the two creates a much smaller PSF than either the point source PSF or pinhole PSF alone. This reduction factor is why the confocal microscope has such improved contrast and optical sectioning ability.

Being able to create a defined point of illumination in the sample is one half of a confocal microscope, the other is being able to image many individual points across the sample and render these into a coherent image. The manner in which this is achieved is alluded to in the name confocal laser *scanning* microscopy. In most systems today the optical path is adjusted through the use of motorised mirrors which scan the PSF_S across a section of the sample being addressed [62]. The resulting series of intensities are put together by the microscope's computer and software systems providing the user with an *x-y* image of the sectioned sample. Further to this optical sections can be overlaid in series providing three dimensional information of the sample, which is inaccessible with full-field microscopy. Recent advancements in the mechanics and software rendering techniques have turned confocal microscopy into one of the most successful imaging techniques to date and is used heavily in the biological sciences [51, 69-73], has had wide application in morphological studies and ion imaging in plants [15] as well as many other scientific disciplines including polymer science, thin film, and topographical investigations [63, 74]. Figure 12 is a schematic of a Leica Microsystems TCS SP2 confocal microscope similar to the one used throughout this research. The relative simplicity of the mechanics of the confocal microscope are illustrated very clearly in this diagram, in particular the manner in which each photomultiplier tube (PMT, see section 1.6) can be set to detect specific bands of light in order to separate out information from several different fluorophores within the sample. The spectrophotometer prism splits the remitted light into a broad spectrum which can be mechanically filtered by adjusting the gates located prior to the PMT detectors. The viewer can then see the individual channels with the option of overlaying several at once, creating images of specific fluorescence within the sample. For easily accessed information, Olympus, Leica-Microsystems, and Nikon all have very informative websites which describe the theory of confocal microscopy in great detail.

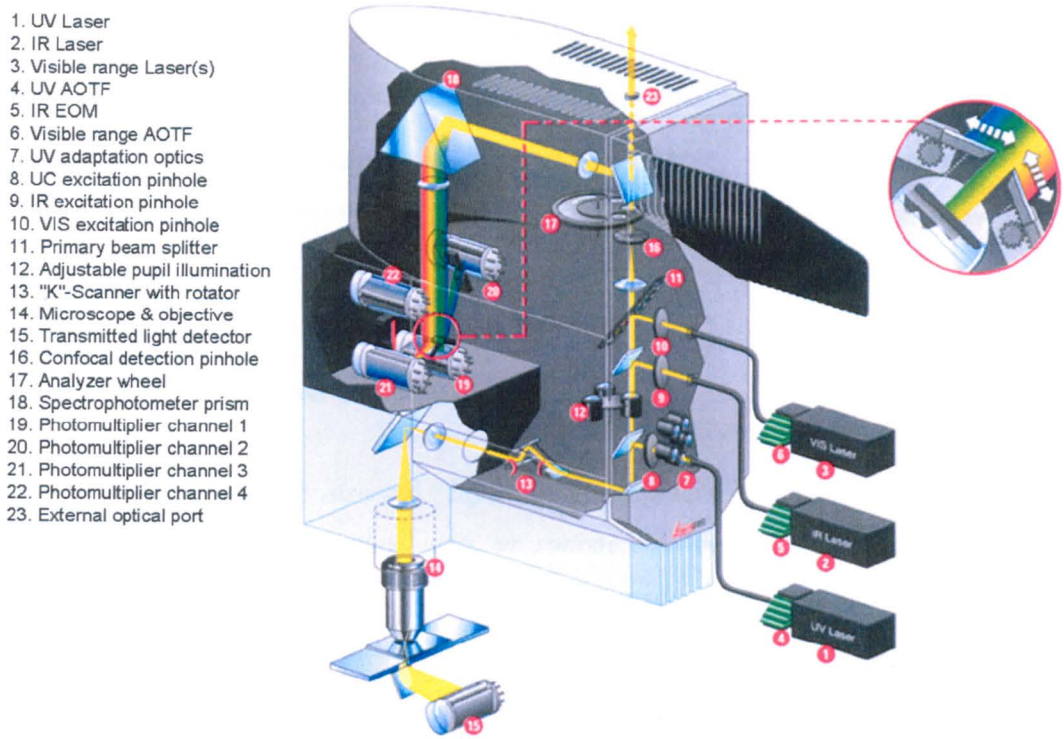

Figure 12 Leica Confocal Microscope with Spectrophotometric Detection: Schematic illustration of the beam path in the Leica TCS SP2. The prism splits the beam into its spectral components. The enlarged detail shows the detector system with the motorized slit plates, which can be opened and closed [75].

1.6 Photo Multiplier Tubes

As these devices feature in all the main techniques used during this research it is worth mentioning them specifically. PMTs amplify the signal produced by incident light by as much as 10^8, allowing single photon events to be resolved. This is essential for low level fluorescence applications such as those within this research.

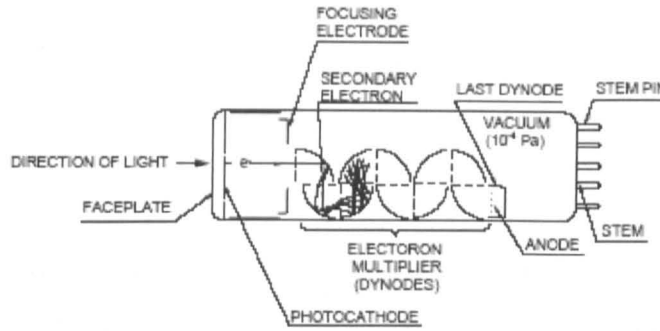

Figure 13 Cross section of Head-On type PMT [76].

Photomultipliers are constructed from a glass vacuum tube which houses a photocathode, several dynodes, and an anode. A typical PMT consists of a photoemissive cathode (photocathode, typically made from multiple alkali metals) followed by focussing electrodes (dynodes) an electron multiplier and an anode. Incident photons strike the photocathode material which is present as a thin deposit on the entry window of the device, with photoelectrons being produced as a consequence of the photoelectric effect (a quantum electronic phenomenon in which electrons are emitted from matter after the absorption of energy from electromagnetic radiation such as x-rays or visible light [77]) and emitted into the vacuum. The electrons leave the photocathode, having the energy of the incoming photon and are directed by the focusing electrode voltages towards an electron multiplier (dynode). As they move towards this first dynode they are accelerated by the electric field and arrive with much greater energy. On striking the dynode, more low energy electrons are emitted by the process of secondary emission (additional electrons, called secondary electrons, are emitted from the surface of a material when an incident particle, in this case an electron, impacts the material with sufficient energy, the yield of secondary electrons depends upon the type of material and energy of the impacting electron). These, in turn, are accelerated toward the second dynode. This process is repeated, as the electron multiplier contains a number of dynodes; secondary electrons strike a subsequent multiplier allowing electron multiplication to proceed up an electron multiplying cascade (each held at a more positive voltage than the previous one). The geometry of the dynode chain is such that a cascade occurs with an ever-increasing number of electrons being produced at each stage. Finally, at the end of the cascade the anode is reached where the accumulation of charge results in a sharp current pulse (an output

signal) indicating the arrival of a photon at the photocathode [76]. They come in various guises, including side-on type geometry where incident light is received though the side of the glass bulb. The number of electron multipliers (dynodes) ranges typically from 8 to 19 and there are also several different classes of dynode in use including the circular cage type generally used in side-on types of PMT, e.g. Leica-Microsystems TSP confocal microscope shown in Figure 12. In general a PMT provides extremely high sensitivity with a fast response time and exceptionally low noise which is why they are used so commonly in light detection systems.

1.6.1 Current amplification (gain)

One of the easiest and quickest ways to increase the signal during fluorescence detection on any apparatus utilising a PMT is to increase the gain. This means that the voltage across the PMT is increased. As mentioned, photoelectrons emitted from a photocathode are accelerated by an electric field so as to strike the first dynode and produce secondary electron emissions. By increasing the voltage across the photocathode / anode the intensity of the electric field is increased. This promotes the acceleration of the photoelectrons giving them more energy when they strike subsequent dynodes – consequently more secondary electrons are emitted. This added acceleration also applies to all secondary emitted electrons meaning the output signal of the PMT is very susceptible to fluctuations in the power supply voltage. This is why the uniformity in the gain of the PMTs between experiments is often stated. The use of increased gain should be approached with caution; the significant differences in apparent fluorescence can be useful when presenting low level fluorescence images but the increased noise more than often clouds the image and loses data. If the only way to produce visually appealing results is through the use of high PMT voltages there is more than likely a more serious factor needing attention within the experimental design.

1.7 Flow cytometry

Flow cytometry or FACS analysis (fluorescence activated cell sorting) is a technique in which entire populations of cells, circa 50,000, can be quickly analysed and sorted on the basis of fluorescence or scatter (the pattern of scattered incident laser light from individual cells) [78-81]. To be specific, cells were not sorted during this study and therefore true FACS analysis was not performed, however sorting would be logical and easy next step to the flow cytometry carried out. FACS could be a very interesting tool in future experiments for the purifying of cells which have specific, or a certain number of nanosensors internalised. The fluorescence measured from the cell usually comes from fluorescently labelled antibodies chosen specifically for surface markers on the cells under examination [82]. Cell surface receptors or surface markers can be used in the diagnosis of several diseases in a process called immunophenotyping. Diseases including Human Auto Immune Deficiency and leukaemia can be diagnosed on the basis of cell-surface markers using FACS [78, 83]. Obviously FACS is an important clinical application, used widely today and is applicable to nearly all biological fluids [84] including bacterial analysis [85]; in the scope of this research the feasibility of flow cytometry was investigated as a technique to monitor different aspects of nanosensor technology.

1.7.1 The flow cytometer

The flow cytometer is made up of three parts, the fluidics system, the optical system, and the electronic detection, sorting, and analysis system. The fluidics system is essential in producing a fluid flow in which a uniform stream of cells is created before they pass through the laser beam. This is achieved by tuning the size of the channels the sample fluid flows through and a process known as hydrodynamic focussing. The suspension of randomly distributed cells is injected into the central part of a microfluidic system consisting of a core channel surrounded by a sheath fluid (or carrier fluid), basically one small tube within another, see Figure 14 for an illustration. The

central core narrows to a point at which the central fluid (containing cells) exits into the surrounding sheath fluid which, importantly, is flowing at a faster rate.

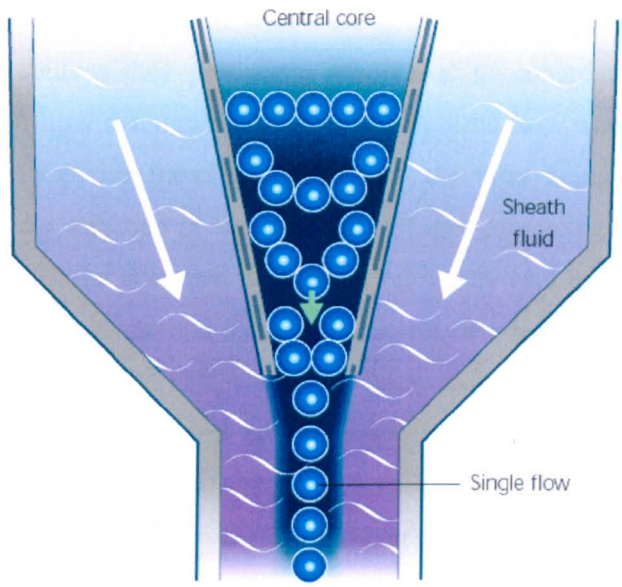

Figure 14 Schematic of single cell stream being produced by hydrodynamic focussing [80].

$$\mathrm{Re} = \frac{pVD}{\mu}$$

Equation 1 Reynolds number, when Re < 2300 flow will be laminar. At Re > 2300 flow will be turbulent between the two streams.

p = fluid density
V = fluid mean velocity
D = tube or channel diameter
μ = fluid viscosity

The faster flowing sheath fluid creates a drag effect on the central core ultimately leading to the formation of a single file of cells. Optimal conditions can be achieved by altering fluid velocity and channel diameters until a laminar flow system is attained, i.e. the two fluid streams do not mix. Laminarity can be achieved with reference to the Reynolds number (a measure of fluid turbulence) of the fluid system, see Equation 1. Hydrodynamic focussing is vital to flow cytometry for allowing single cell analysis and also in preventing the nozzle from getting blocked. Information on the particle is attained through optical illumination, the effects of the particle upon the incident light is representative of its characteristics. The role of the optical system is to provide the light

source and collect scattered or emitted (in the case of fluorescent molecules) light from each particle. Typical light sources are lasers or arc lamps, although lasers provide a better light source (coherent and of a particular wavelength) they are more expensive. Arc lamps use ignited gases within sealed tubes to provide light, although they are cheaper than laser sources they produce a mixture of un-coherent wavelengths. The light used during the flow cytometry investigation reported here was laser originated, λ = 488 nm. As the particles travel out of the nozzle after being hydrodynamically focussed they pass through one or more beams of light producing scattered light and fluorescence emission. The scattered light is picked up by two lenses at two different angles from the scattering event and focussed onto relevant detectors. Forward scatter is picked up at typically 17 – 20 ° offset from the lasers axis and side scatter at 90 °. The channels are known as the Forward scatter channel (FSC) and Side scatter channel (SSC) respectively. Both reveal information about the particle, the FSC provides an estimation of the particle size and is useful in telling cells apart from cellular debris, the SSC informs on the granular content of the particle so can distinguish between live and dead cells. Fluorescence data from each particle can be both qualitative and quantitative and can provide data on both cell-surface residing fluorophores, for example when conjugated to antibodies attached to cell-surface markers, or intracellular fluorophores such as DNA intercalated dyes, or perhaps nanosensors? The number of fluorescence channels available differs between machine depending upon the number of detectors, light sources, and the complexity of the optical filtering system prior to detection. The detectors for the SSC and fluorescence channels are PMTs similar to the detection systems in confocal microscopes however a silicone photodiode is used to collect the stronger signal of the FSC. The similarity in detection systems, as can be expected, between FACS and fluorescence confocal microscopy is very similar consisting of long, short, and band pass filters, dichroic mirrors, and the aforementioned detectors, PMTs and silicone diodes.

Signal processing again is very similar to that for confocal microscopy so need not be discussed here except to clarify some terminology specific to this technique. Each detector provides data which is referred to as a parameter, e.g. forward scatter, side scatter, and fluorescence 1, 2, 3, etc. The individual data acquired in each parameter, i.e.

from each cell displaying a physical or fluorescent feature, are known as the events. A typical set up for the detection system in a flow cytometer is shown in Figure 15.

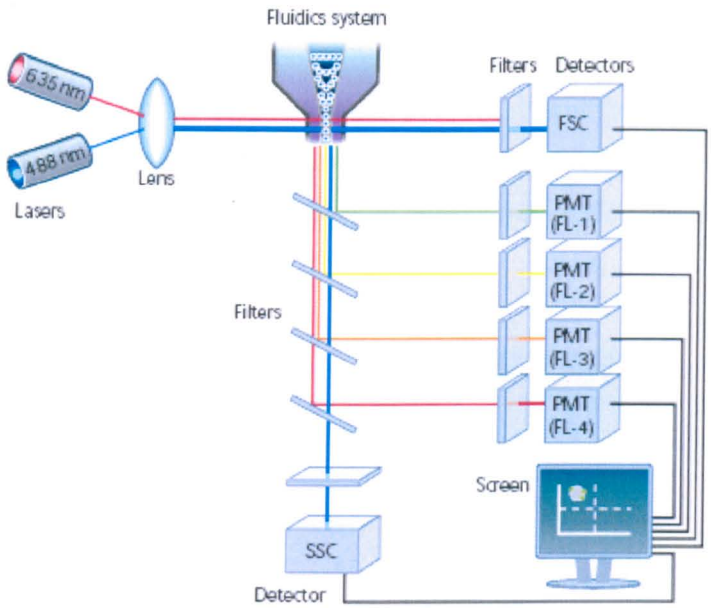

Figure 15 A typical flow cytometer detection system [80].

FACS, as mentioned previously, is a major application of flow cytometry allowing the separation of cells from a heterogeneous sample into pure sets for further biological experimentation. To achieve this data acquired from the optical detection system is processed and the resulting action, based upon the set of pre-loaded criteria, is passed to the electrostatic cell sorter. Historically cell sorters had a mechanical sorting system in which an arm would move a collection vehicle into the fluid stream and remove the desired cell. As one can imagine this action, however technically stream-lined, would take considerably longer than more recently developed electrostatic based systems with no moving parts. The relative numbers of cells that could be sorted were 300 cells s^{-1} mechanically, compared to 100,000 s^{-1} with an electrostatic sorter. The promise of FACS for nanosensor research could be to separate out cell populations providing a sample in which 100 percent of cells contain nanosensors. This would allow subsequent tracking of nanosensors through progeny lineage determining if they can pass through to daughter cells or not.

During cell sorting, if the cell is flagged up as being of a particular type the fluid stream is charged when exiting the nozzle of the microfluidic system. Obviously the cells cannot be removed from the fluid stream without serious disruption which is why the interaction with the fluid occurs at a precise moment called the break-off point. This is the point when and where the fluid stream breaks up into droplets, each containing a single cell if all parameters are optimal, Figure 16. This is achieved by vibrating the nozzle at low amplitude but with a very high frequency. This ensures the break-off point is consistently reproduced and allows the sorting mechanism to charge the correct droplet.

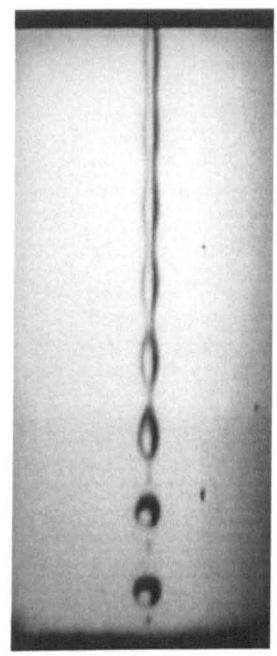

Figure 16 Break off point in FACS flow cytometer [86].

The journey the cell takes during FACS can be summarised thus – after experimental treatment, including labelling with fluorescent antibodies / loading with dyes, the cell starts off at a random position within a cell suspension. This suspension is drawn up into the central channel of the microfluidic system and proceeds through a tapered exit into the sheath fluid flow where it becomes one of many cells exiting in a single file located in the centre lamina of the now combined sample and sheath fluids. As the cell travels downwards with the fluid it passes through one or more laser beams which interrogate the cell on the basis of scatter and fluorescence. This site of interrogation is

sometimes referred to as the flow cell. After passing through the laser beam(s) the fluid stream breaks up in a uniform fashion into discrete droplets, the cell is located within one of these droplets. At this, the break-off point, the droplet is electrostatically charged in response to the data acquired in the laser interrogation and is directed from the main droplet flow when falling between two voltage plates. The cell is then collected in an appropriate vessel, tubes, plates, and eppendorfs can all be used, and the sorting is complete. Figure 17 shows this process schematically.

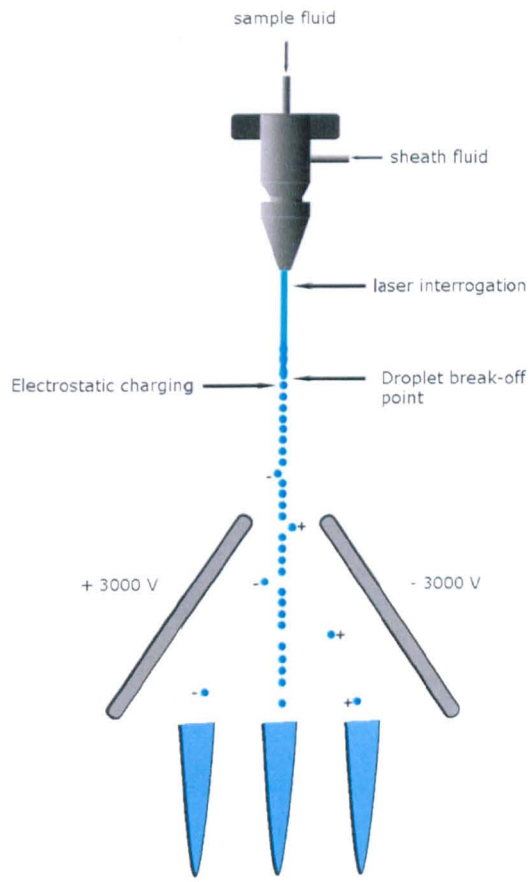

Figure 17 Schematic overview of FACS, adapted from [86].

2 Chapter 2 – Nanosensors: fabrication and tailoring of surface functionality

2.1 Introduction

2.1.1 Nanosensors

Polymeric nanosensors are a relatively new tool for biological research and bring the possibility of being a true 'silent observer' closer than ever before [53, 54, 87-89]. Conventional techniques employed in this vein of intracellular research include the use of fluorescent dyes with confocal microscopy [90], and opto-chemical sensors, generally a pulled optical fibre with a modified tip which is inserted directly into the cell [44, 46]. When using free dye molecules one must acknowledge the problems associated with a naked sensing element in direct contact with the intracellular environment and the possible cytotoxic effects this may have upon the biological system. In addition the effect that the intracellular environment exerts upon the dye can be detrimental to obtaining successful and reliable measurements from within the cell [49, 56]. The small size of the free sensing molecule is a key advantage providing high spatial resolution and allowing information throughout the cell to be collected *en masse*. However random protein binding and intracellular sequestrations are major complications [55] as well as simply retaining the dye within the cell during the life time of an experiment [91]. In contrast, pulled fibre sensors provide a bio-compatible platform which protects both the dye and the cell from one another and negates adverse interaction. The polymer matrix, which entraps the chemical sensing elements, also allows for more complex sensing schemes to be devised due to the close proximity of several elements which can interact complimentarily [42, 92]. This comes at a price, however, as the large size relative to a single cell causes severe physical perturbations to all but the largest cells. The perturbation comes from the need to collect the signal generated at the tip of the sensor when inserted into the cell, requiring a physical pathway to the detector. Additionally, only low spatial resolution is achievable as very few optodes can be successfully inserted into a cell before it is damaged irreversibly [45, 55].

Fibre-optic sensors and fluorochrome / fluorophores both have significant advantages over each other but both also suffer from serious limitations preventing them from being ideally suited to single cell intracellular measurement. Combining key aspects of both

fibre-optic nanoprobes and individual molecular probes (fluorochromes) PEBBLE nanosensors were developed as a response to the problems faced by conventional technologies and designed specifically to exploit the benefits of both the opto-chemical sensors and free dyes whilst excluding the negative. They most resemble the very tip of an optode in form, as they are essentially a polymer matrix body entrapping chemical sensing elements, such as fluorophores. All components necessary for carrying the signal out of the cell have been removed - thus being more akin to free dyes - but the protective capacity of a bio-compatible polymer matrix is retained. Typically only 50 nm in diameter these sensors take up approximately 1 ppb of a typical mammalian cell and cause negligible physical perturbation [88]. Chemical perturbation to the cell caused from free dyes is negated as is the effect of the intracellular environment upon the efficiency of the reporter molecule; in essence the polymer matrix protects the cell from the dye and the dye from the cell [93]. Reports show that fluorophores which are adversely affected through random protein binding respond characteristically when entrapped within the polymer matrix of a nanosensor [94, 95]. In brief, a nanosensor is a polymeric sphere of nanometer size in which chemical sensing elements (typically fluorophores bound to dextran) are entrapped. The polymer matrix is porous, allowing diffusion of analytes to interact with the entrapped fluorophores, resulting in a fluorescent response which is captured with an optical system [96-99]. By minimising the chemical and physical effects of free dyes and bulky optodes one can investigate the intracellular environment in a more natural state [100].

A problem faced when using free dye is the likely hood that the dye will itself be toxic to the cell [54], this will similarly lead to abnormal cellular responses however in this instance through chemical disturbance (toxicity) rather than physical perturbation. Through the use of an inert bio-compatible matrix chemical sensors offered the considerable benefit of reduced chemical interference between the sensing components and the cellular sample. This is entirely replicated in nanosensors technology offering a great benefit over free dye without a significant size increase. Without the protective physical barrier the sensing molecules are susceptible to random protein binding and or protein / organelle sequestration, additionally the fluorescent intensities of the dyes are often affected by protein binding [90] - consequently any measurements taken will be affected. The protective nature of the matrix also allows for enhanced longevity of the

sensing components (through the prevention of damage to the dye by protein binding) enabling fully reversible sensors to be produced [87]. The bio-compatible matrix of the sensor is a separate domain / environment to that of the sample matrix, within this closed system it is possible to secure several components making up a more complex sensing regime, not possible when using a free dye technique. This allows for the development of more highly selective sensors incorporating ratiometric sensing regimes using more than one dye [88], or electron transfer regimes using valuable optically silent ionophores in conjunction with fluorophore partners; as indicated, the use of a sensor matrix immediately increases the scope of analysis. This can quite easily be enhanced further with slight alterations to the method by which the sensors are fabricated, e.g. by altering pore size (allowing entrapment of different sensing constituents, dyes / enzymes) [53] or final nanosensor size [101]. Finally, the nanosensors technology retains the other major advantage of using free dye in that one can simultaneously observe and measure over a greater spatial area rather than in the immediate vicinity of an optode sensing tip. Because of the introduction of many free-dye molecules across the intracellular environment it is possible to achieve a cell-wide picture simultaneously, essential if the experimenter wishes to observe, say, ion flux across the cell.

2.1.2 The nanosensor fabrication process

The fabrication of nanosensors is relatively simple. There are no specialist chemicals, conditions, or equipment required and with a small amount of care and attention one can synthesise a batch of nanosensors from start to finish in an eight hour day. Subsequent functionalisation of the fundamental nanosensor may be carried out for particular project if so required, and could extend the process beyond a single day, although it is possible to stop at one of many points along the fabrication route and store the partially made nanosensors for completion at a more convenient time. In essence, to make a nanosensor, an aqueous phase sphere of nanometre proportions is defined by forming a water micelle in an oil phase of hexane; the nanosensor is created by polymerising monomer units dissolved within this aqueous sphere. In this case the micelle is formed through the use of two surfactants, namely Dioctyl sodium sulfosuccinate and Polyoxyethylene (4) lauryl ether (Brij 30®). Detailed work has been carried out

previously optimising the relative quantities of water, hexane, and surfactant to create defined micelles of a required size (typically 50 – 200 nm ∅) [101, 102]. Once an aqueous 50 nm sphere has been defined in space it is possible to locate to and dissolve a combination of monomers and fluorophores into this sphere prior to polymerisation to form the structurally sound nanosensor. The matrix chosen for all nanosensors used during this research was polyacrylamide, formed from Acrylamide and N,N'-methylenebisacrylamide (a vinyl addition polymerisation initiated by a free-radical generating system).

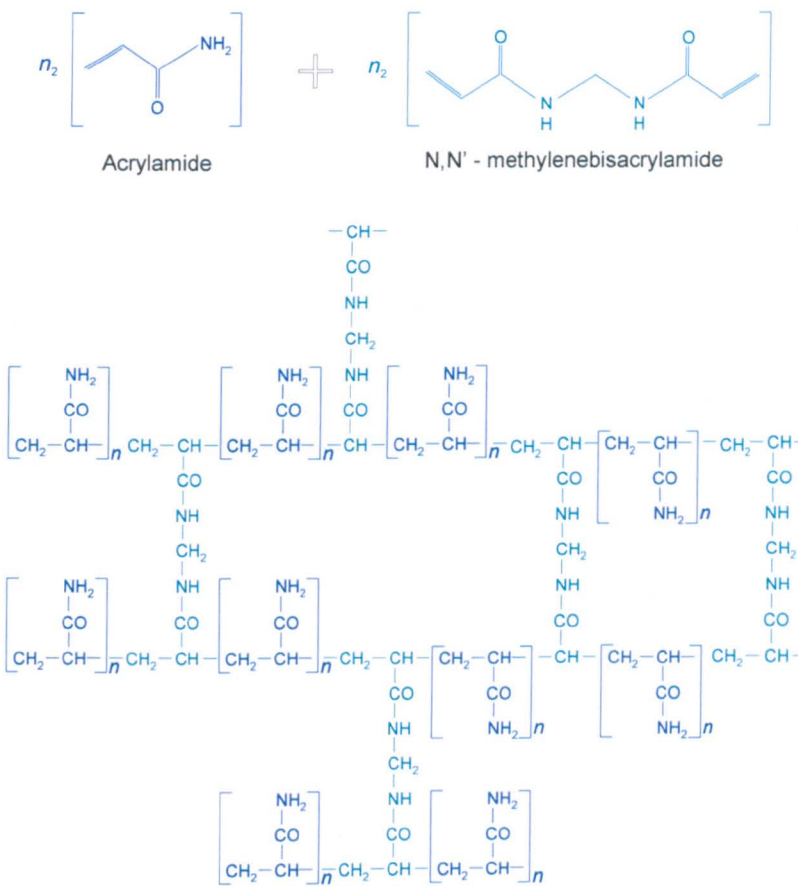

Figure 18 Schematic of the basic polyacrylamide matrix. This polymer backbone can be altered with the addition of small quantities of functionalised acrylamide monomers providing chemical moieties for further modification at a later stage, e.g. the attachment of peptides or lipids.

Free-radical mediated polymerisation of the monomers was typically initiated by the addition of ammonium persulfate (APS) and N,N,N',N'-Tetramethylethylethylenediamine (TEMED) although sodium metabisulphite (SMBS)

was evaluated as a possible alternative due to the detrimental interference of the APS / TEMED with some fluorophores. TEMED accelerates the rate of formation of free radicals from persulfate and it is these free radicals which catalyse polymerisation. The persulfate free radicals convert acrylamide monomers into acrylamide free radicals which in turn react with un-activated acrylamide monomers to begin the polymerisation chain reaction, detailed reaction mechanisms and kinetics can be found in the literature [103, 104]. As explained later this free radical polymerisation can be practically halted by the presence of oxygen. After polymerisation the nanosensors were washed repeatedly in ethanol to remove residual surfactants still adhering to the nanosensor surface. Finally the nanosensors were collected with filtration and allowed to dry.

2.1.3 Tailoring of surface chemistry

The surface of the nanosensor is an important aspect of the nanosensor technology as it provides an anchorage which can be utilised for interactions with other chemical moieties or cell membranes during delivery. The tailoring of the nanosensor surface for a specific function will be important for the successful application to different cell types and environments. The tailoring of a particular surface chemistry therefore is as important, if not more so, than the fabrication of the nanosensor itself. During this research the polyacrylamide matrix was modified to provide surface groups which were available for further 'post-fabrication' modification. This was achieved by the incorporation of an amine modified acrylamide into the matrix at the fabrication stage providing primary amines on the nanosensor surface for latter modification.

2.1.4 Characterisation techniques

When developing something on the nano-scale it is obviously important to have reliable characterisation methods for confirmation of fabrication techniques. Dynamic Light Scattering (DLS) was a valuable tool for assessing the size and size uniformity of a batch of nanosensors. It is worth noting that the fabrication process produces a bimodal distribution of size; the two populations will, in general, be approximately 50 nm and

200 nm in diameter respectively. The number of larger particles is a great deal less than that of the smaller counterpart, and can be easily removed with an appropriately sized syringe filter as part of the fabrication process (typically immediately prior to use as part of an experimental preparation). DLS apparatus is a form of Photon Correlation Spectroscopy but at a fixed angle. This enables the cost of the equipment to be reduced and thus makes it more accessible for applications which don't require anything other than 90° analysis (i.e. sub 250 nm particles). DLS measures the scattering intensity of a laser light source from particles suspended in solution; laser light is used as it is both coherent and monochromatic (i.e. consistent intensity of a single colour / wavelength (λ)). Light scatters in all directions (Rayleigh scattering) when the particles are small relative to the wavelength (hence the fixed angle detection being feasible for small particle analysis) and so it is possible to observe temporal fluctuations in the light scattering intensity due to Brownian motion. Using a coherent light source makes it possible to detect subsequent constructive / destructive interference which provides information about the movement of the surrounding particles in suspension. This autocorrelation data combined with the known variables such as temperature, density, and solution viscosity allow for particle size estimation.

Further to the physical characterisation obtained with DLS it was necessary to obtain information regarding the surface chemistry. This showed that the specific tailoring of the polymer matrix had been accomplished and the surface functional groups were present and available for modification.

Two methods were employed for surface analysis. Firstly Zeta potential data was acquired which could be used to infer the presence of functional groups on the surface as expected, i.e. primary amines on the surface which would increase the nett surface charge of the nanosensor; nanosensors with charged surface moieties could then be distinguished from standard nanosensors on a charge basis. Negatively charged, carboxylated nanosensors could be identified using the same principle. Zeta potential is a measure of the effective charge associated with particles in solution and not a direct measurement of the surface charge. It is usually, but not necessarily, of the same sign as the potential actually at the particle surface [105]. The nett charge that arises at the particle surface affects the distribution of ions in the interfacial region leading to an

increased concentration of counter-ions adjacent to the particle surface, referred to as the Stern planar. The Stern planar makes up the inner part of a double layer of ions surrounding each particle, the outer part consists of a diffuse layer of ions which are less firmly associated and are affected by a balance of electrostatic forces and random thermal motion (see Figure 19). Therefore as the distance increases away from the particle the potential drops until it reaches the value of the bulk solution, which is generally taken to be zero. As a particle moves, either through Brownian motion or upon the application of an electric field, the particle moves through the solution with its most closely associated ions with it, as a single entity. The notional boundary between those ions which are attracted to the particle enough to move with it and those that are not is referred to as either the slipping plane or surface of shear; it is at this point that the Zeta potential is taken and quoted. The Zeta potential value lies between the potential of the surface and the bulk solution and is affected by the properties of the solution, both concentration and type of ions present, which is why Zeta potential values stated without reference to the pH and ionic strength of the bulk solution are meaningless [106]. There are many identifiable points between the surface and the bulk solution which will have a unique potential (obviously there will be an infinite number as the distance from the particle increases) namely the surface potential, the Stern planar potential, and the Zeta potential, experimentally however the Zeta potential is the most readily accessible.

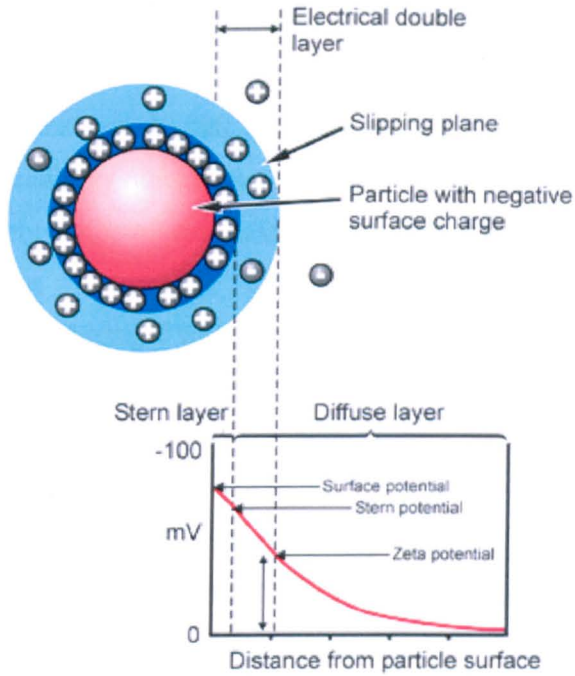

Figure 19 Zeta potential schematic from Malvern Instruments [107].

Secondly, and more directly, fluorophores (of a different wavelength to that of the internalised fluorophore) were attached to the surface groups of the nanosensor. This meant that an additional fluorescence signal coming from the nanosensor after the attachment process indicated the presence of available functional groups. This combined approach of electrostatic and fluorescent assessment clearly revealed the presence of surface group availability.

2.1.5 Nanosensor development

As with all technologies, further development and trying to make improvements to existing protocols should proceed as a matter of course. Increasing the brightness of nanosensors is an ongoing research theme for all involved. Developing different strategies for attaching / entrapping fluorophores is regular and some successes have been achieved. At present the accepted procedure for the introduction of fluorophores into the polymer matrix is to purchase ones already attached to dextran, which is very water soluble (at <5 million MW) [108], and physically entrap them within the polymer matrix; the matrix grows around each dextran molecule during fabrication. This

approach does however limit the number of fluorophores one can successfully pack into the nanosensor, increasing the number of dextran molecules or buying bigger dextrans (e.g. 250,000 MW rather than 10,000 MW) surpasses the upper packing limit of the nano-sized droplets relatively quickly and leads to a breakdown of the micro-emulsion. As it is possible to only entrap several dextrans into each nanosensor there are relatively few fluorophores per nanosensor, especially when, for some dextran-bound fluorophores (e.g. FITC-dextran) with a labelling frequency of 0.003 – 0.02 mols of FITC per mol of Glucose, there is on average only 1 - 3 fluorophores per 10,000 MW dextran [109].

One solution is to attach greater numbers of fluorophore to dextrans in-house, using these rather than the examples available for purchase. This approach has been initially successful and is currently under development by researchers. Further to this, an altogether different approach, where the fluorophores were attached directly to functional groups present in the backbone of the polymer matrix, was investigated. This negates the requirement of dextran altogether and potentially allows for the incorporation of increased numbers of fluorophores by several orders of magnitude. This approach has proven to offer the potential of much brighter nanosensors; as the fluorophores attach to all available functional groups however, this includes those on the nanosensor surface; additional procedures need to be implemented to remove or mask these surface located fluorophores to prevent interaction with the external environment, when internalised a cell for example.

2.2 Materials and Methods

2.2.1 Reagents

Materials: Acrylamide, N,N'-Methylenebisacrylamide, Ammonium Persulphate (APS), N,N,N',N'-Tetramethylethylethylenediamine (TEMED), Brij 30, Dioctyl sulfosuccinate sodium salt (98 %), Fluorescein isothiocyanate-Dextran 10,000 MW (FITC-Dextran), Tetramethyl Rhodamine isothiocyanate-Dextran 10,000 MW (TRITC-Dextran) and Fluorescein isothiocyanate Isomer I were purchased from Sigma-Alrdrich. N-(3-Aminopropyl) methacrylamide hydrochloride was purchased from Polysciences Inc., Warrington, PA. Hexane was purchased from Fisher Scientific. Pureshield Argon was supplied by BOC. Sulfosuccincinimidyl -4- (N-maleidimidomethyl)- cyclohexane -1-carboxylate (sulfo-SMCC) was purchased from Calbiochem, Darmstadt, Germany. Tat peptide (CRRRQRRKKRG) was synthesised by the University of Nottingham Biomedical School peptide synthesis service with standard F-moc chemistry.

2.2.2 Nanosensor fabrication

Nanosensors were prepared by the free radical polymerisation of acrylamide in a reverse-phase micro emulsion. Chemical sensing elements (dextran bound fluorophores) dissolved in the aqueous phase along with all acrylamide monomers, became physically entrapped within the polymer matrix during the polymerisation step. 3.08 g of Brij 30 and 1.59 g of Dioctyl sulfosuccinate were weighed into a 100 ml glass round bottomed flask, the vessel was flushed with argon, sealed, and set aside. Into a glass scintillation vial 540 mg acrylamide and 160 mg of N,N'-Methylenebisacrylamide were dissolved in 2 ml of deionised water with sonication (Fisher Brand, FB11021). Meanwhile, hexane was purged with argon to displace oxygen (~ 1 h). To the surfactants, 42 ml of de-oxygenated hexane was added as well as a 25 mm magnetic stirrer bar. Care was taken to minimise oxygen contamination by providing a flow of argon into the round bottom flask as the hexane was added. The surfactants were allowed to fully dissolve in the

hexane (~ 20 min); the flask was clamped and stirred over a stirrer plate (Stuart, SB 161-3). Aliquots of the required fluorophores were added to the dissolved acrylamides from stock solutions (e.g. 20 μl of a 5 mg ml^{-1} solution of FITC-Dextran plus 20 μl of a 5 mg ml^{-1} solution of TRITC-Dextran) then 2 ml of this solution was added to the surfactants in hexane in a drop-wise manner. With all the components now brought together the reverse-phase micro-emulsion was left to form (~ 20 min) in a sealed argon environment. Polymerisation was initiated by the addition of 30 μl 10 % w/v APS in water and 15 μl TEMED and allowed to proceed for 2 h. Hexane was removed by rotary evaporation (Buchi Rotavapor R-200). To the remaining viscous solution 80 ml of ethanol was added and split between two centrifuge tubes then spun at 6000 rpm on a centrifuge (Hermle Z300) for 4 min to pellet the nanosensors. This process was repeated six times to remove the surfactants. Finally the nanosensors were re-suspended in approximately 10 ml ethanol which was removed with vacuum filtration through a 0.02 μm filter (Whatman, Anodisc 25, 0.02 μm) allowing the nanosensors to be collected, which were subsequently dried and stored at -18 °C.

2.2.3 The importance of deoxygenation

It is of paramount importance to remove all trace oxygen from the hexane prior to using it for nanosensor fabrication. This is solely because of the free-radical polymerisation employed during fabrication. A free-radical polymerisation reaction is inhibited by any molecule or element which acts as a free radical scavenger of which oxygen is a prime example. Most unsuccessful attempts to fabricate nanosensors can be attributed to a lack of degassing and as a matter of course one should generally assume this is the case before investigation into more complex matters which may be believed to be the root of the problem.

2.2.4 Nanosensor fabrication schematics

The following series of images help to visualise the nanosensor fabrication process. The blue box is representative of the Hexane oil phase. Figure 20, surfactants are dissolved

in hexane. Figure 21, the formation of a micro-emulsion creates nano-sized aqueous spheres; the size of these spheres ultimately dictates the size and shape of the final nanosensor. Figure 22, after the addition of APS and TEMED, the dissolved monomers polymerise and entrap the dextran bound fluorophores.

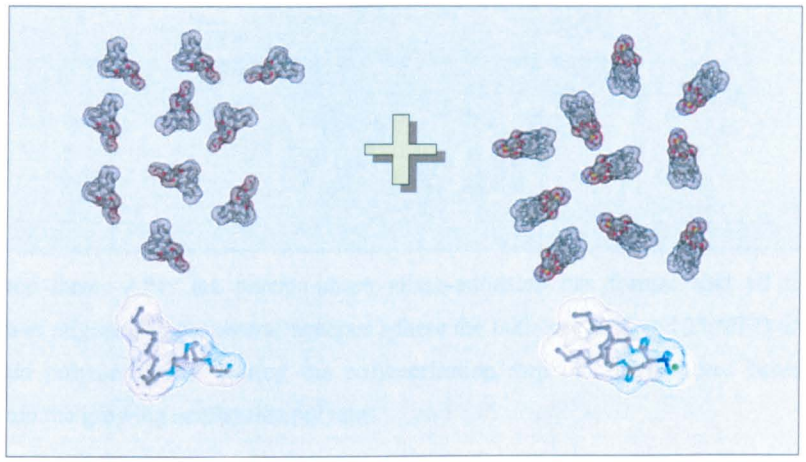

Figure 20 Step one: Surfactant addition to oil phase. The two surfactants are weighed into a round bottomed flask and 42 ml of degassed hexane is added. The mixture is stirred until the two surfactants have completely dissolved before the aqueous phase is added.

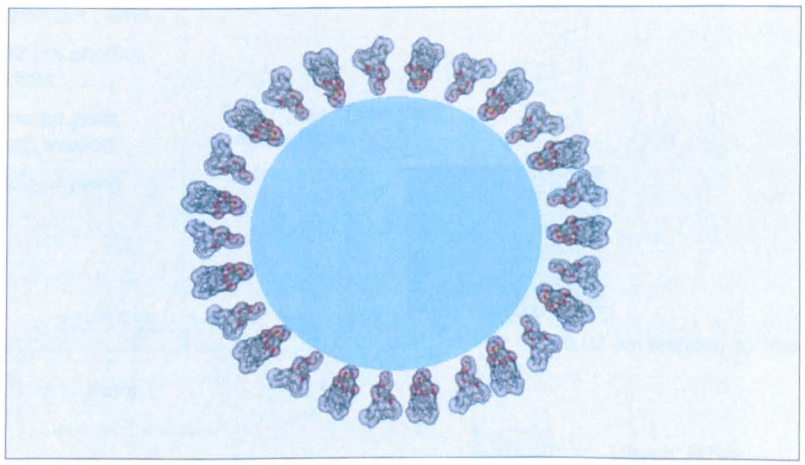

Figure 21 Step two: The aqueous phase (containing acrylamide monomers and fluorophores) is added to the hexane in a drop-wise manner. If the temperature of the hexane / surfactant solution is too low this addition step can cause the Brij 30 component to drop out of solution. This is clearly observed by the formation of translucent debris which may take on the colour of the fluorophores as they adhere to the surfactant. An easy remedy is to gently heat the flask with hot water until full dissolution is achieved once more.

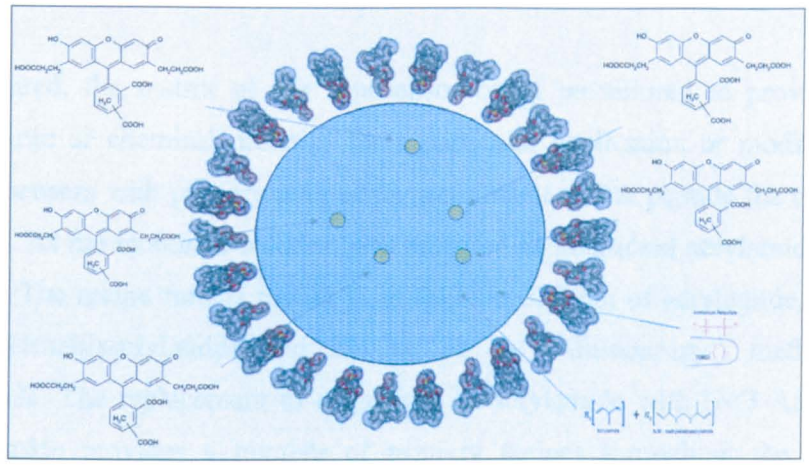

Figure 22 Step three: After the reverse-phase micro-emulsion has formed and all the nanosensor constituents have migrated to the central aqueous sphere the initiators APS and TEMED are added to the flask to initiate polymerisation. During the polymerisation step the fluorophores become physically entrapped within the growing acrylamide polymer.

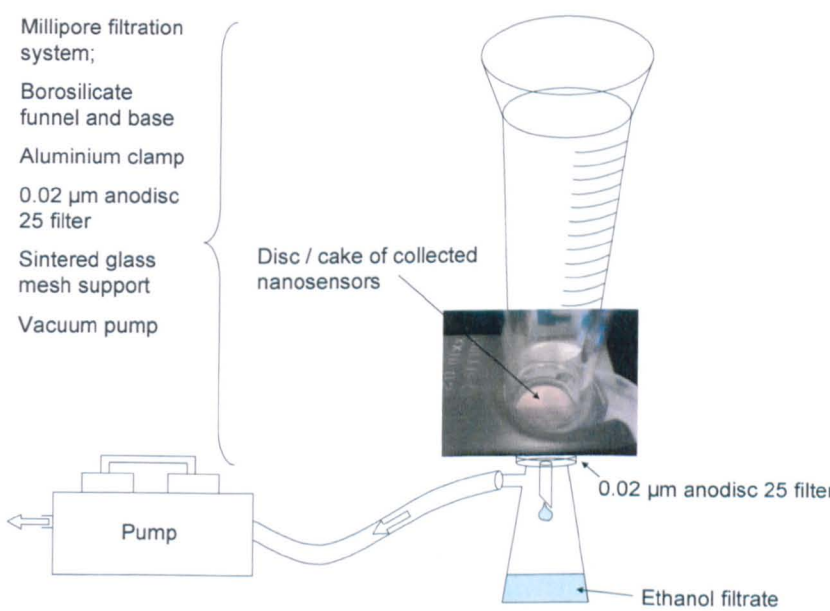

Figure 23 Step Four: The ultrafiltration set up. After rotary evaporation to remove the hexane and several centrifuge washing steps in ethanol the nanosensors are collected from the ethanol cleaning solution with filtration to produce a dried disc of nanosensors. The glassware is connected to the vacuum pump via an additional solvent trap on ice (not shown) to protect the inner workings of the pump from the ethanol filtrate. The final product: a cake of dried nanosensors containing $Ru([dpp(SO_3Na)_2]_3)$ in this example is the final point of the fabrication process; the nanosensors are collected and weighed to assess yield before being packed in glass vials for storage.

2.2.5 Alternative polymer matrices

When required, the matrix of the nanosensor could be tailored to provide specific surface charge or chemical moieties for a particular application or modification. To make nanosensors with primary amines for attachment of Tat peptide the modification was simple. As the monomer solution was prepared an additional acrylamide monomer was added. The recipe for the matrix is as follows, 529 mg of acrylamide, 160 mg of N,N'-Methylenebisacrylamide and 21 mg of N-(3-Aminopropyl) methacrylamide hydrochloride. The replacement of a quantity of acrylamide with N-(3-Aminopropyl) methacrylamide provides a number of primary amines throughout the nanosensor matrix. Figure 24 shows the amine functionalised acrylamide utilised to provide the polymer matrix with primary amines; the NH_2 groups present in acrylamide being bonded to a carbonyl group, thus amides, were not applicable to the modification chemistries used in this research.

Figure 24 N-(3-Aminopropyl) methacrylamide hydrochloride (left).

To achieve a nett negative surface charge, if required, an acrylamide monomer was synthesised in-house which, upon disassociation in water, provided a negatively charged surface. Succinic anhydride was first reacted with N-(3-Aminopropyl) methacrylamide hydrochloride in toluene for 10 h under reflux condensation, to give a carboxylated acrylamide with a negative charge as shown in Figure 25. This newly formed monomer was then incorporated into the monomer solution in the same manner as previously described for nanosensor synthesis.

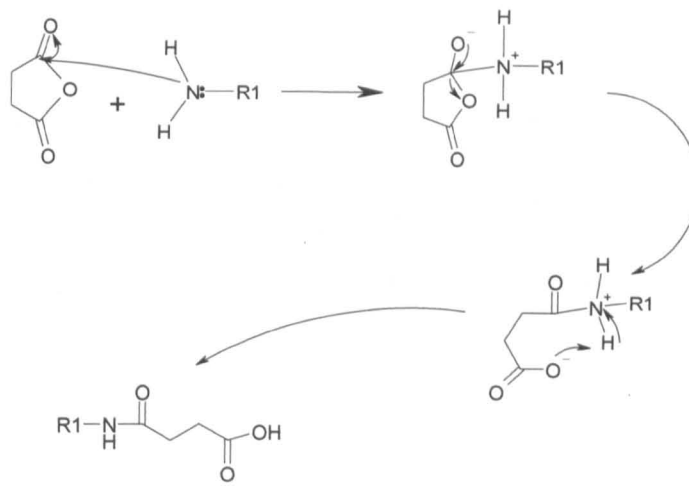

Figure 25 Succinic anhydride reaction with a primary amine providing a carboxylic acid group.

2.2.6 Synthesis of the metal ligand complex Ruthenium 4,7-diphenyl-1,10-phenanthroline / $Ru([dpp(SO_3Na)_2]_3)$

The synthesis of an oxygen sensitive fluorophore was carried out in house with reference to the literature [110, 111] to be used during the development of nanosensor synthesis techniques and fluorescence spectrophotometry. Historically this fluorochrome has been used for cellular oxygen concentration measurements, in this instance however its primary function was to be a stock fluorochrome that was cheap to produce and easily manipulated to effect a change in fluorescence for quick assessment of nanosensor functionality. In this manner it was possible to synthesise and experiment on numerous batches of nanosensors to understand fluorescence and polymer synthesis without the cost implications of fluorescent probes sourced commercially. With only minor modification to previous methods this dye was synthesised according to the following method:

$RuCl_3$ was refluxed for 48 h in deionised water with stirring with 3.5 molar equivalents of 4,7-diphenyl-1,10-phenanthrolinedisulfonic acid disodium salt. During this reflux the solution changed colour from dark green to very dark red, noticeable when swirling the flask. After cooling to room temperature and filtration the solution was concentrated on

a rotary evaporator to approximately 5 ml and loaded onto a Sephadex G25 column, eluted with deionised water. The red fraction was collected, all other coloured bands, ranging from purple through brown to green, as seen in Figure 26, were discarded. The collected fraction was removed and evaporated to a powder. As can be seen from the structure in Figure 26 the product of this synthesis will be a range of isomers and no determination was made regarding the position of the SO_3Na groups on the phenyl rings as Anderson *et al* state that the mixture of isomers gives no evidence of heterogeneous fluorescent lifetimes [110].

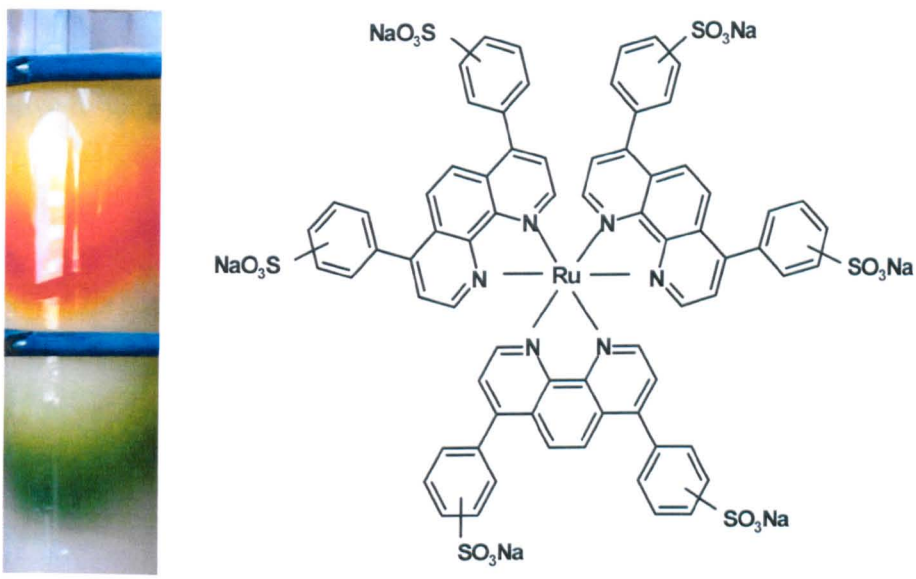

Figure 26 Photograph of the column showing the appearance of differently coloured bands during the separation of $Ru([dpp(SO_3Na)_2]_3)$ (orange / red band) through Sephadex G25.

2.2.7 Effect of initiator scheme APS / TEMED upon fluorophore function

To gauge the effect of free-radical production, during polymerisation, upon the dissolved fluorophores in the polymer solution, their peak emissions were monitored as APS and TEMED were added to a cuvette of solution. In a manner simulating nanosensor fabrication, selected fluorophores, at concentrations identical to fabrication, were dissolved in 2 ml of deionised water in a cuvette. Fluorescence data was then collected every 10 min with spectrofluorometry at an appropriate wavelength for 2 h.

This identified whether or not the fluorophores would be photo-bleached during a 2 h simulation; if the fluorophores became photo-bleached this would invalidate the result. After confirmation that the data collection method did not photo-bleach the fluorophores to any measurable extent APS was added to the solution and the 10 min fluorescent assessment continued. After an initial reading TEMED was also added to the solution providing the catalyst for free radical production and the fluorescence of the solution was further monitored for another 2 h, i.e. the same length of time as the polymerisation step during fabrication. Admittedly the presence of acrylamide monomers would have probably served to 'use up' the free radicals; however the forming polyacrylamide gel would interfere with the fluorescent signal collected. This experiment allowed for the direct comparison of different fluorophores and presented a relative result regarding the effect of the initiation scheme upon the functionality of the fluorophores.

2.2.8 Physical characterisation

DLS measurements were carried out on a Viscotek DLS 802 in filtered deionised water at room temperature. 100 µl of the suspended nanosensors were aliquoted into a black quartz cuvette with two small windows located at 90° as per the light path for this type of measurement. It was important to flush the cuvette with filtered water and dry with pressurised air prior to analysis as dust particles can severely impair the results obtained. Measurements were taken in ambient conditions and each analysis was made up of 10 correlation analyses lasting 10 seconds each. The intensity count was adjusted with sample dilution and laser intensity control (software manipulated), until a steady level between 500 and 1000 k Counts was achieved. The software used for analysis was onmiSIZE which calculated the experiment correlation functions for each analysis of the sample. Using the sum and calc option provided it was possible to generate a hydrodynamic radius for each sample and omit correlations which seemed to be impaired by dust debris. The resulting data was described showing the calculated population distribution of particle size and relevant peak analysis of the population.

2.2.9 Surface chemistry characterisation

Zeta potential measurements were carried out on a Zetasizer2000 from Malvern Instruments in pH 7.2 phosphate buffer with an ionic strength of 10 mM. Different samples of nanosensors were suspended in buffer at approximately 1 mg ml^{-1} and filtered with a 0.02 μm syringe filter. The solution was then diluted with filtered buffer as necessary to achieve a stable count of around 300 indicated with the instrument software. Analysis does not require an accurate concentration of particles between samples. The instrument was always flushed with fresh filtered buffer prior to use to ensure no foreign matter interfered with the analyses.

2.2.10 Functional characterisation

A series of simple experiments were performed which showed that nanosensors responded to differing concentrations of analyte with a measurable, visual fluorescent change. A suspension of nanosensors in appropriate buffer, typically at 5 mg ml^{-1}, were placed in a cuvette and assessed with spectrofluorometry. Subsequently a change was effected to the solution, for example by the addition of HCl, NaOH, or EDTA altering the concentration of analyte to which the selected nanosensors were responsive. This change was monitored and measured using the Kinetics software of the Cary Varian Eclipse spectrofluorometer. The simultaneous monitoring of dual emission wavelengths was performed (coming from dual wavelength excitation). This function was particularly useful to demonstrate the ratiometric nature of some fluorescent sensing schemes. Calibrations were obtained of the nanosensor response to, for example, pH or [free Ca^{2+}] by making up several independent suspensions in buffers with a pre-determined pH or analyte concentration. Subsequent calibration graphs were plotted using Microsoft Excel from the peak emission values for each buffer solution. For measurements of oxygen concentration in solution the level of oxygen was affected through the means of an argon purge which displaced the oxygen molecules. After an initial measurement was taken, an argon line was placed into the solution which was purged for several minutes before another reading was taken. This provided a quick

response showing that nanosensors could provide data on the relative oxygen concentration in solution.

2.2.11 Nanosensor development: SuperBrights

Creating potentially brighter nanosensors with additional fluorophores was achieved by omitting the dextran carrier to which fluorophores have conventionally been attached and conjugating fluorophore molecules directly to the polymer backbone of the nanosensor matrix. The fabrication procedure was identical to that described in section 2.1.2 though no fluorophores were added to the aqueous phase prior to polymerisation. Briefly 529 mg of acrylamide, 160 mg of N,N'-Methylenebisacrylamide and 21 mg of N-(3-Aminopropyl) methacrylamide hydrochloride make up the constituent parts of the polymer matrix and nanosensor fabrication proceeded to completion, i.e. dried (blank) nanosensors were stored at -18 °C. Subsequently 100 mg of nanosensors were suspended in 4 ml 2 mM FITC in deionised water and stirred at room temperature for approximately 2 h, then left at 4 °C overnight. The labelled nanosensors were then precipitated with ethanol as described previously and collected with filtration.

2.3 Results and Discussion

This chapter deals with fabrication and characterisation of the tools utilised during this research, namely nanosensors (with or without surface modification) and fluorophores. It was important to spend time ensuring the variables of nanosensor fabrication for this project were considered, controlled, and reproducible. As such the fabrication techniques ensured that the results obtained through the use of nanosensors would be free from the artefacts of batch to batch variation.

2.3.1 Nanosensor fabrication

One of the primary results to be observed during the fabrication of nanosensors was the effect of the initiator scheme upon nanosensor batch yield, and fluorophore activity. The effect upon yield is clearly illustrated in the two tubes in Figure 27, showing typical examples of nanosensor batches initiated with SMBS and APS / TEMED respectively. The constituent parts of each batch were identical yet SMBS initiation led to a much lower final yield of nanosensors. It appears that SMBS initiated nanosensors were also much brighter i.e. had more fluorophores per part polyacrylamide than APS / TEMED initiated examples. This evidenced by the more concentrated colour of the SMBS initiated batch.

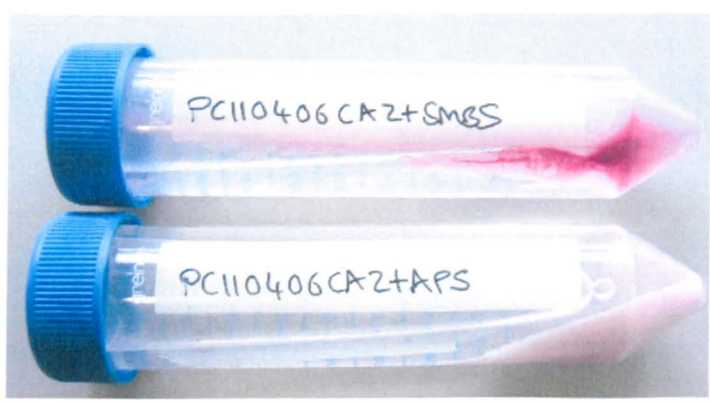

Figure 27 The comparative yields of nanosensors after initiation with SMBS (top tube) and APS / TEMED (bottom tube) respectively.

It was speculated however that the darker colouration was not only a concentration effect but evidence that SMBS initiation did not damage the Fluo-4 fluorophore. It is shown in Figure 28 that the combined APS / TEMED scheme clearly did affect Fluo-4 reducing its fluorescent emission by approximately 60 %. On the assumption that during SMBS polymerisation, lower numbers of free radicals are produced, it seems logical that a fluorophore damaged by free radicals will fair better than with APS / TEMED initiation. Therefore SMBS polymerisation is also likely to be less effective, due to the lower number of free-radicals produced – perhaps being more susceptible to the effects of dissolved oxygen. This effect will lead to small chain lengths of polymer and probably result in quantities of un-reacted monomers remaining. These factors will undoubtedly reduce the number of fully formed nanosensors and therefore final yield. For these reasons the SMBS initiation scheme was abandoned in favour of the more reproducible APS / TEMED free radical production, even though the damage to some fluorophores remained a point of concern. It may be the case that fluorophores which do not interact with free radicals are acceptable candidates for SMBS initiation, however as certain fluorophores are necessary for particular applications (such as Fluo-4 for calcium measurements) the wish for consistent nanosensor fabrication was most important. The successful calibration of Fluo-4 calcium nanosensors reinforced the choice of APS / TEMED (results in section 3.3.3).

The transient increase in FITC fluorescence is attributed to an increase in pH affected by the addition of APS, and a subsequent reduction in pH with the addition of TEMED.

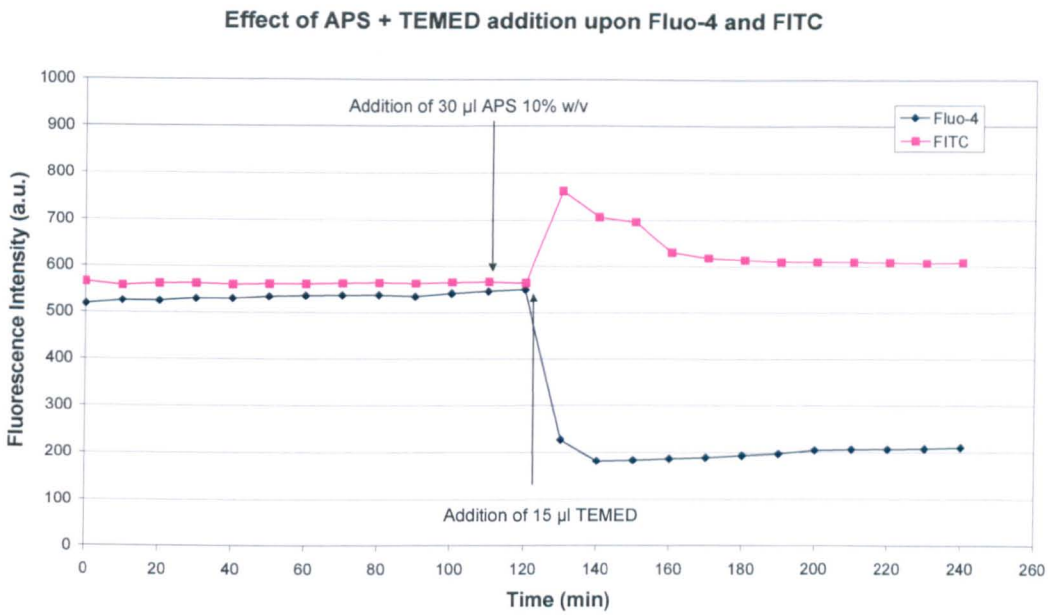

Figure 28 This figure represents the effect of free radical polymerisation upon fluorophores during fabrication (see materials and methods section for a full description). The increasing base line drift of the Fluo-4 signal is attributed to the deionised water gradually attaining Ca^{2+} ions from the atmosphere during the 4 h experiment. It is well know that the ion concentration of deionised water will steadily increase as it absorbs ions from its surrounding environment and the atmosphere.

2.3.2 Physical characterisation

The use of DLS to physically characterise the size of nanosensors was to show that the fabrication process produced results as expected. The technique was very simple and easily accessible requiring special care only over the quality of the water used. The Viscotek DLS 802 OmniSIZE interface allowed for fast experimental set up and is shown in Figure 29.

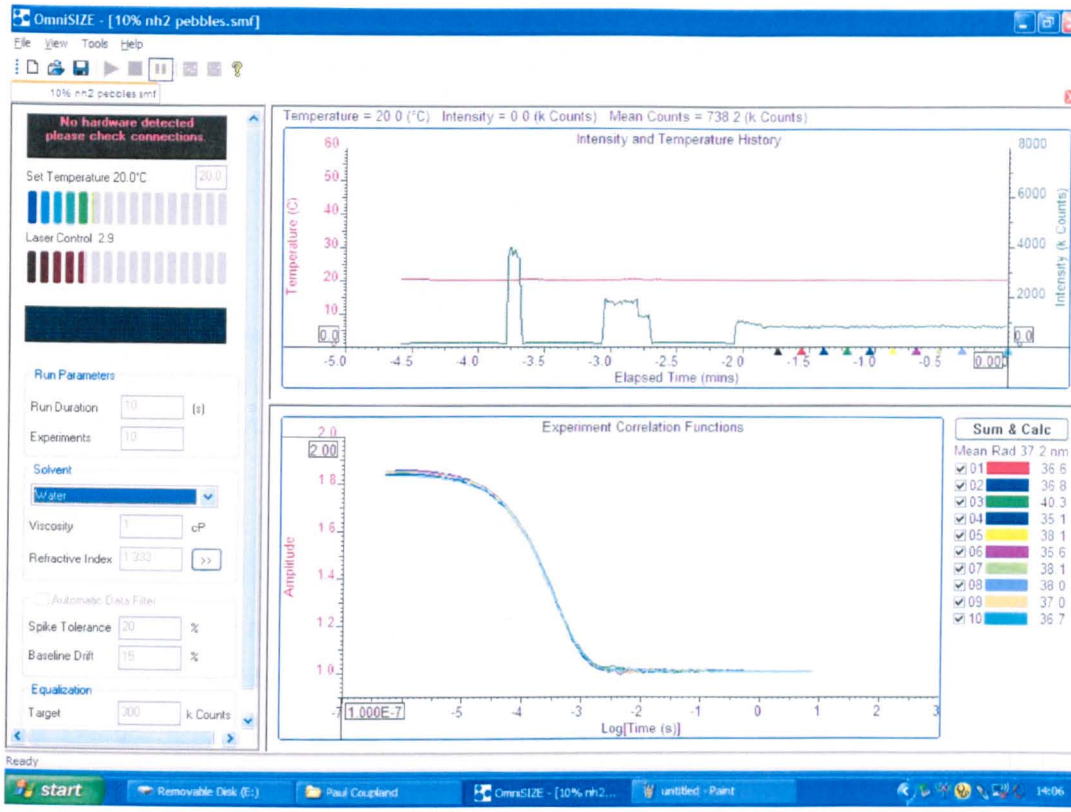

Figure 29 Viscotek DLS 802 OmniSIZE interface providing control over experimental parameters including laser intensity, temperature, run number and duration, and solvent choice.

As shown the left hand panel of the interface allowed one to input all experimental parameters and provided control over laser intensity to fine tune the count intensity of events. These events i.e. particle laser scatter, can be seen as the green trace in the upper right panel. As can be seen in this experiment the initial sample concentration was too high at approximately 4000 k Counts so was removed for dilution a couple of times before being fine tuned with the laser intensity to reach the target count of just under 1000 k Counts. Once the target count was achieved and remained steady the analysis was triggered and 10 individual 10 second captures were taken, marked by coloured triangles and grey and white columns. The lower right panel shows the correlation functions for each run colour coded to match the key on the right hand side. This function allowed any errant results, usually from dust debris, to be omitted if required. Finally the sum & calc button performed population analysis and provided peak data on the experimental sample, Figure 30.

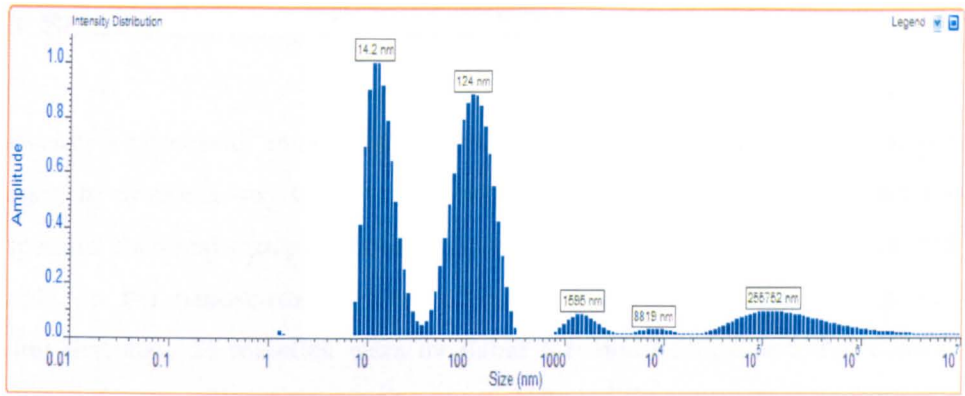

Figure 30 PC030406CA2+ DLS before filtering showing bimodal distribution and dust / debris.

Evidently there is a bimodal distribution of size as expected, with radii of 14.2 and 124 nm respectively. Evidence from DLS data confirmed the success of nanosensor fabrication relating to physical size and uniformity and was a quick and easy technique. Finally, Figure 31 shows a sample of nanosensors that have been filtered with a 0.02 µm syringe filter. The larger population of the bimodal sample has been removed providing a uniform population for experiment as well as the removal of all foreign matter and debris picked up during fabrication.

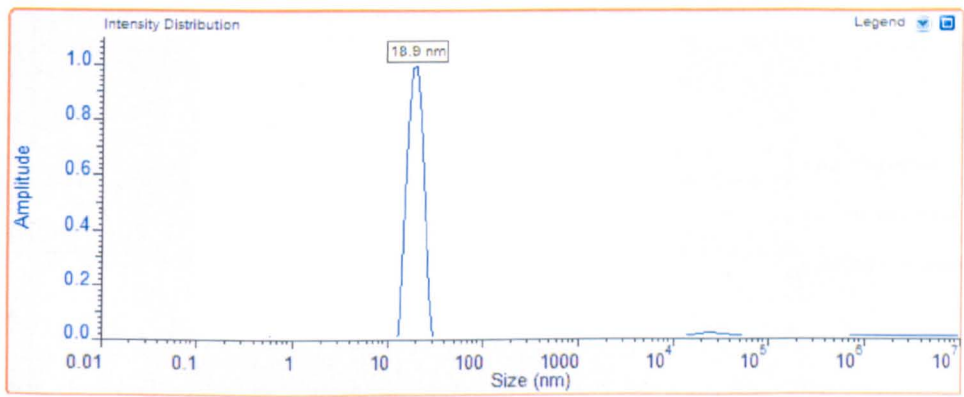

Figure 31 Calcium green batch of nanosensors representative of a typical batch shown after filtration which removes the larger sized particles.

This DLS result shows that a nanosensor suspension can be prepared for use with a syringe filter, and is therefore a valid method for sterilisation as the smaller population easily passes through the 200 nm pores. DLS proved to be a very useful tool which was very quick, requiring only minimal sample preparation and provided some key insights into nanosensor fabrication and manipulation.

2.3.3 Surface chemistry characterisation

To develop a successful modification protocol of the nanosensor surface, it was also necessary to devise a way to assess the surface chemistry of the nanosensor showing that specific chemical groups had been incorporated into the polymer matrix and were available on the nanosensor surface. Characterisation of the surface was useful in showing that specific moieties were available for modification and that unsuccessful attempts to functionalise the nanosensors could be attributed to other variables. As the groups incorporated into the polymer matrix during this research would provide a nett surface charge different to the standard acrylamide polymer matrix it was possible to use charge assessment as a means for inferring the presence of both primary amine and carboxylic acid groups. Figure 32 shows Zeta potential data collected for standard nanosensors (amide), and those with primary amine, and carboxylic acid surface groups respectively.

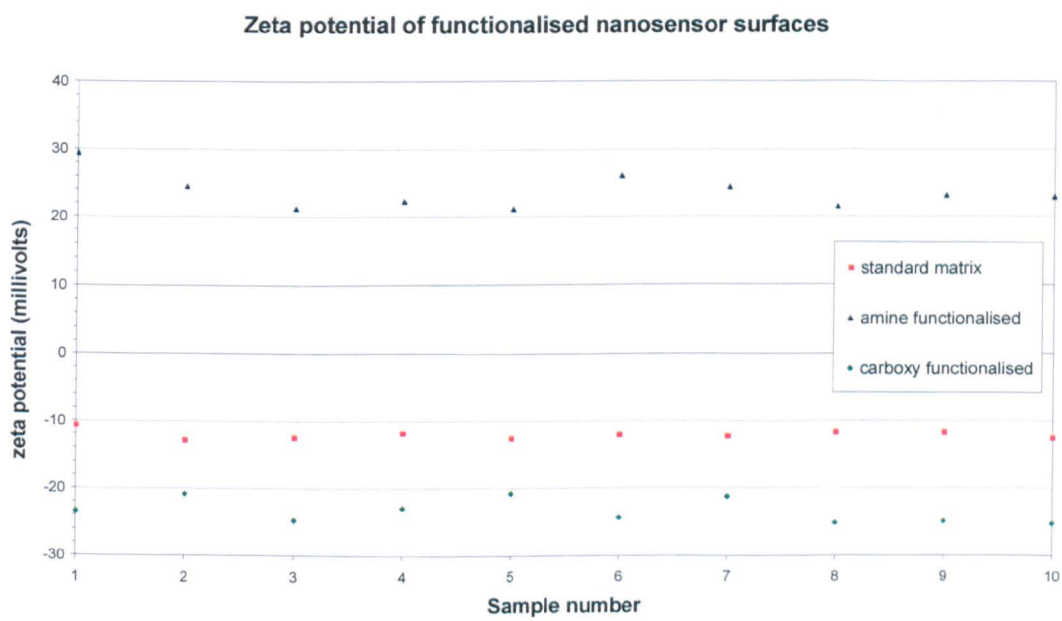

Figure 32 Zeta potential measurement data of three sets of nanosensors with different surface chemistries. 10 samples of each type were analysed in 10 mM pH 7.2 phosphate buffer.

These data show that there was a significant difference between the types of nanosensor in terms of Zeta potential. On the understanding that the different surface chemistries

would affect the distribution of ions in the interfacial region, and consequently the Zeta potential, it was taken that differences in these sample sets corresponded to respective surface chemistry.

Although the charge data suggested different surface chemistries it did not show that there were in fact available groups for attachment. To prove this for the primary amine-functionalised nanosensors an additional basic experiment was created. A molecule was attached to the nanosensor via the primary amine groups to give the nanosensor an additional, measurable characteristic. The most straightforward way was to add an aliquot of fluorophore with an isothiocyanate group to utilise the spontaneous conjugation between isothiocyanates and primary amines. FITC, Figure 33, was readily available and thus chosen as the fluorophore to label $Ru([dpp(SO_3Na)_2]_3)$ ($\lambda_{emission}$ = 610 nm) containing nanosensors providing an additional fluorescent peak at 520 nm when illuminated at 488 nm.

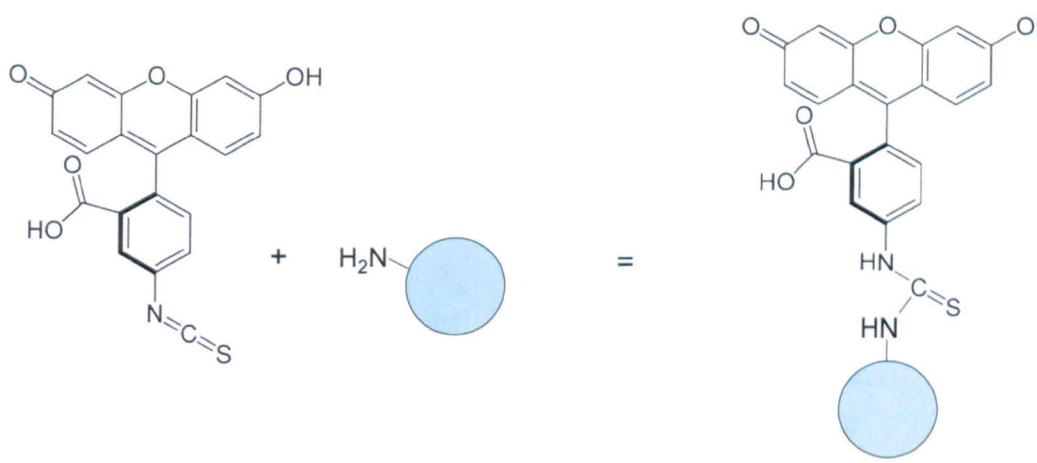

Figure 33 FITC reacting with primary amine group of N-(3-Aminopropyl) methacrylamide in polymer matrix.

Two aliquots of $Ru([dpp(SO_3Na)_2]_3)$ nanosensors were suspended in water and left overnight at 4 °C, a small amount of FITC was added to only one aliquot of nanosensors. Subsequent precipitation with ethanol, and centrifugation, repeated several times, washed away any FITC that remained unbound. An additional fluorescent peak would therefore provide evidence for the presence of primary amines. The result from this experiment is shown in Figure 34, clearly the blue trace, showing data for the amine

functionalised nanosensors, shows that they have attained an additional fluorescent emission, attributable to FITC.

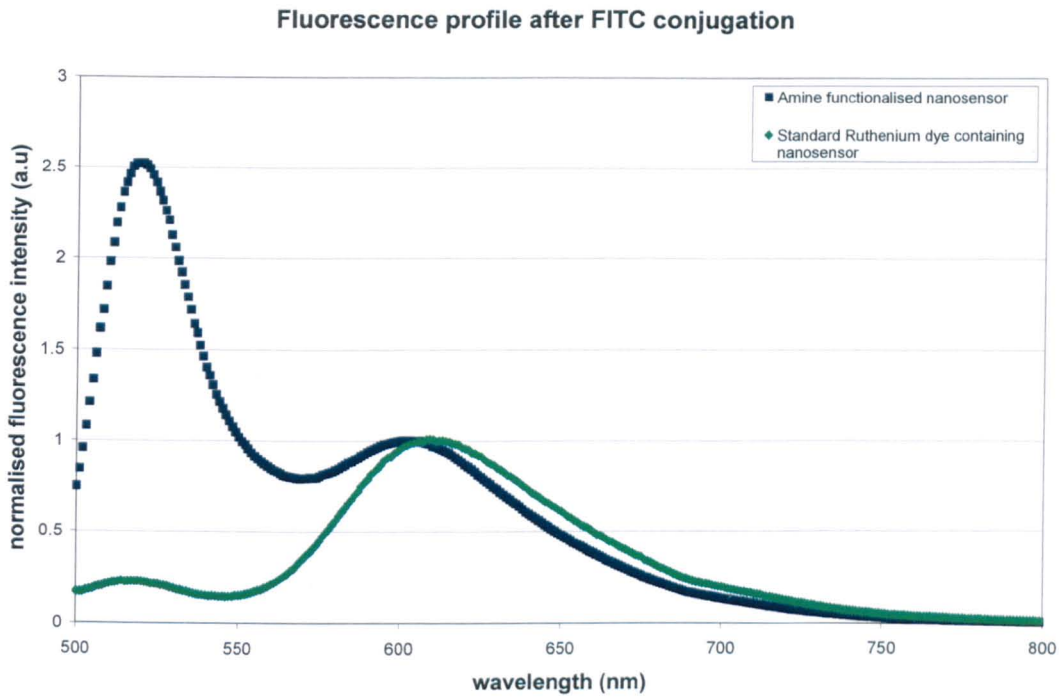

Figure 34 Fluorescent assessment of standard and primary amine Ru([dpp($SO_3Na)_2]_3$) nanosensors after labelling with FITC. The small amount of FITC fluorescence in the standard nanosensors represents residual FITC residing in the polymer which could not be removed with several washing steps.

The combination of Zeta potential characterisation and demonstration of FITC conjugation provides strong evidence for surface bound primary amines.

2.3.4 Functional characterisation

Regardless of all the different aspects of characterisation that can be carried out on the nanosensor and its component parts, the only true representation of function was to actually use them as intended. Many tests were carried out to gain assurance that the nanosensors could measure the concentration of analytes to the magnitude required for 'real world' examples of their intended use. Experiments investigating the effects of random protein binding (encountered in the intracellular environment) and photo-

bleaching were not carried out as they have been covered elsewhere [95]. Primarily the function of a nanosensor is to sense, i.e. if a change in concentration occurs in the factor the nanosensor is designed to measure then it needs to be able to report this change to the user. One of the earliest experiments was to immerse oxygen sensitive nanosensors in water and subsequently alter the concentration of dissolved oxygen whilst monitoring the fluorescent intensity change of the entrapped fluorophore. Figure 35 shows the data collected for the effect of oxygen concentration in solution upon $Ru([dpp(SO_3Na)_2]_3)$ based nanosensors. Oxygen acts to quench the level of fluorescence from $Ru([dpp(SO_3Na)_2]_3)$ meaning that in a minimal oxygen environment the fluorescent signal would be stronger than in an oxygen rich environment. This is exactly the effect seen when argon was purged through a solution of $Ru([dpp(SO_3Na)_2]_3)$ nanosensors in water.

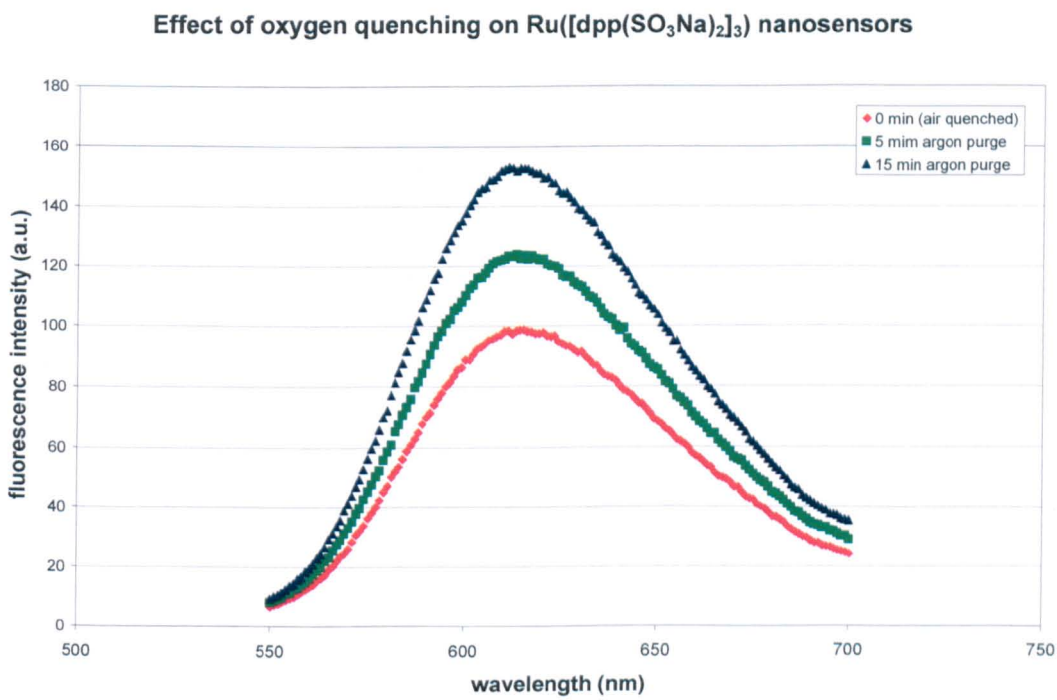

Figure 35 The effect of dissolved oxygen upon $Ru([dpp(SO_3Na)_2]_3)$ nanosensors. Purging argon through the solution displaced oxygen which was evidenced by an increase in fluorescence. $\lambda_{excitation} = 488$ nm.

To illustrate the ratiometric nature of nanosensors containing an additional reference fluorophore, the same experiment was carried out on nanosensors containing both $Ru([dpp(SO_3Na)_2]_3)$ and Oregon Green, an oxygen insensitive fluorophore with a lower

emission wavelength of 525 nm but readily excited with a 488 nm wavelength similar to Ru([dpp($SO_3Na)_2]_3$). The data shown in Figure 36 is normalised around Oregon Green peak emission which clearly shows the usefulness of ratiometric schemes. Due to the insensitivity of Oregon Green to oxygen, and the consistent concentration of both dyes in each nanosensor, fluctuations in signal intensity do not influence the ratio between the two reporter dyes. This means that variations in nanosensor concentration or numbers of photons getting to or from a nanosensor in a non-uniform environment such as a cell will not invalidate the results obtained.

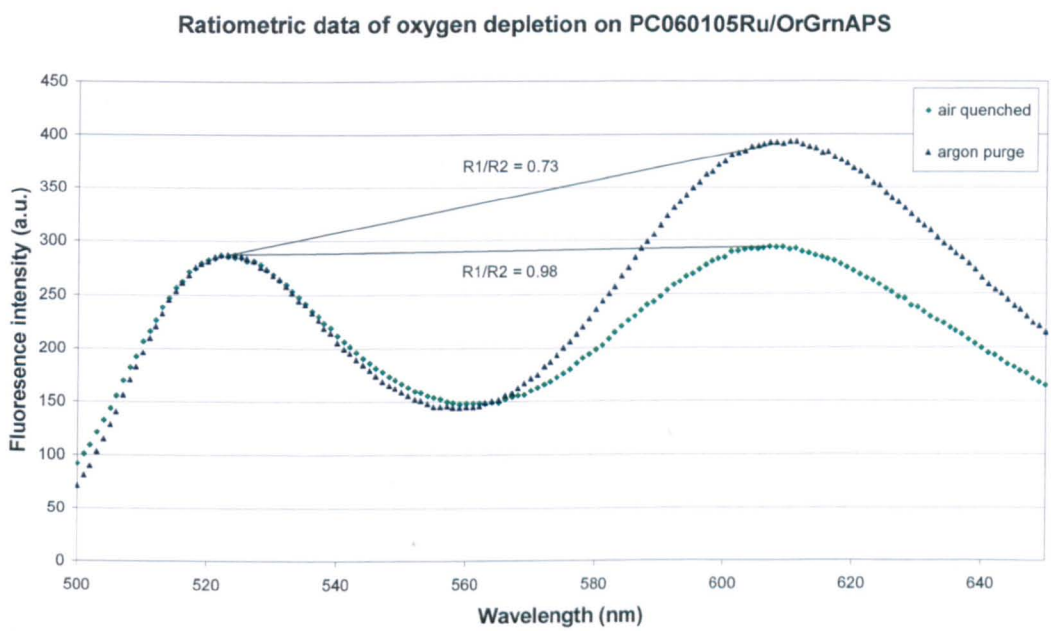

Figure 36 Ratiometric data analysis of oxygen levels using nanosensors. The ratio between the two reporter dyes is independent of both nanosensor concentration and fluctuations in signal intensity; this allows non-uniform environments to be addressed. $\lambda_{excitation} = 488$ nm.

Investigation into the function of pH sensors carried out with real-time monitoring of sequential pH change, Figure 37 provided clear insight into the roles of each reporter fluorophore. The addition of HCl and NaOH aliquots create pH fluctuations in the buffered system (phosphate buffer). HCl addition lowers the pH which is evidenced by a drop in FITC fluorescence, and conversely FITC fluorescence intensity increases upon the addition of NaOH. Throughout the experiment however the fluorescence from Alexa568 remains constant providing a continuous reference for ratiometric analysis.

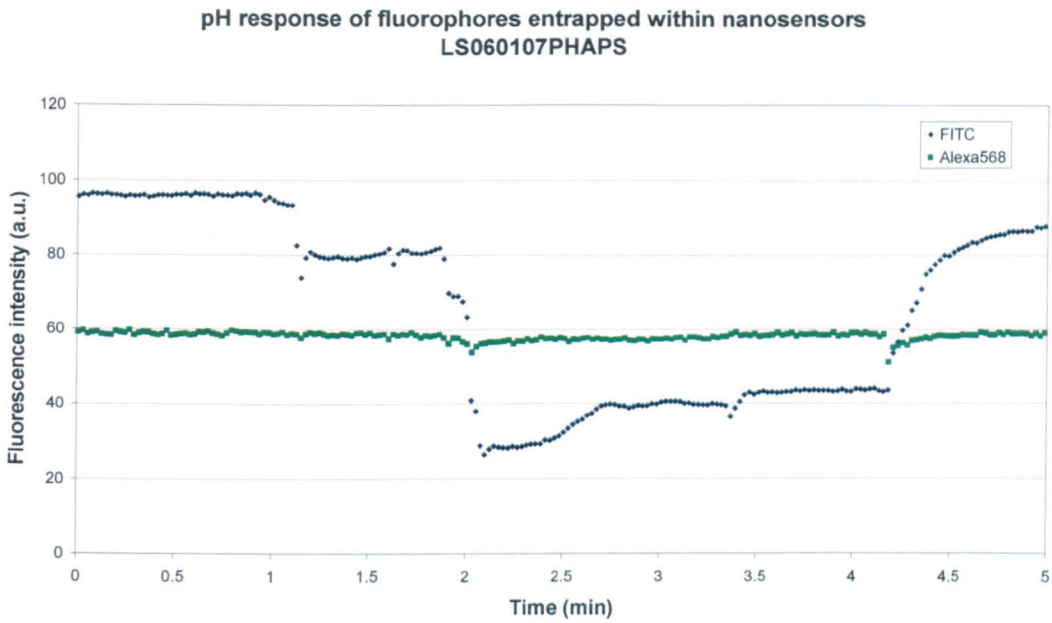

Figure 37 Clear illustration of the role a reference dye plays in a ratiometric sensing scheme.

Calibration experiments were carried out in appropriate buffers, Figure 38 shows a typical example of a pH calibration of FITC nanosensors. As illustrated the response is a classical shape with an approximate pK_a close to that given for FITC, 6.4 [112]. This shows that the characteristics of the entrapped fluorophore are not affected, either by the fabrication procedure or ultimate location, and that nanosensors are capable of measuring pH across a physiological range. More detailed analysis of the function of pH and [free Ca^{2+}] nanosensors is described chapters three and four.

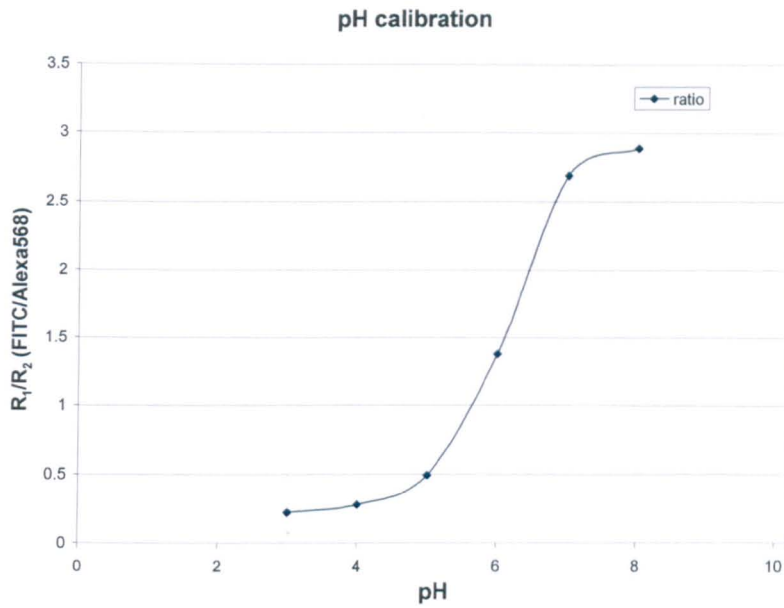

Figure 38 pH calibration of FITC nanosensors in citrate buffer solutions.

2.3.5 SuperBrights

The idea of attaching fluorophores directly to the polymer backbone of the nanosensor matrix to create brighter sensors stemmed from the experiments which demonstrated primary amine availability, in an almost identical way that was reported latterly [113]. When FITC was used as a visual label to prove that primary amines were available throughout the nanosensor matrix the first SuperBright nanosensors had been fabricated. The process of developing these brighter nanosensors is formative but hopefully future work will realise these ideas. Attaching fluorophores to functional groups throughout the polymer matrix will be random; therefore fluorophores will be present on the nanosensor surface. This of course allows interaction between the fluorophores and the environment into which they are submerged which undermines the reasoning behind nanosensors. At present no schemes have been trialled to solve this problem but there will likely be several solutions. One solution is to remove the surface fluorophores through a process known as enzyme-shaving. If the fluorophores are attached to the matrix via a cleavable linker, one which can be cleaved by a readily available enzyme, then suspending the nanosensors in a solution containing appropriate enzyme will begin

to cleave the linkers and remove the fluorophores. As enzymes are sizeable entities they will migrate into the matrix through pores on the polymer at a particular rate (diffusion rate) which may be calculated or establish through experiment. The known diffusion rate of the enzyme through the polymer will then allow 'shaving' of the fluorophore to a particular depth, creating an elementary, reverse engineered core-shell nanosensor from a single polymer. If the difficulties of this approach undermine its usefulness perhaps a less creative suggestion may be to simply mask the surface bound fluorophores with an additional layer of bio-compatible material such as polyethylene glycol (PEG). A chain length will be chosen which will be long enough to physically protrude away from the nanosensor surface more than the fluorophore molecule preventing interaction with random proteins but allowing free diffusion of analytes.

The relative fluorescence, or brightness, of the SuperBright nanosensors was significantly greater than those made with standard methods of fluorophore entrapment. Although fluorophores were present on the surface it was still possible to assess their relative merits using confocal microscopy. SuperBrights, when added to the culture media of growing CHO-K1 cells localised to the extra cellular membrane due to an electrostatic attraction. An image of this is shown in Figure 39.

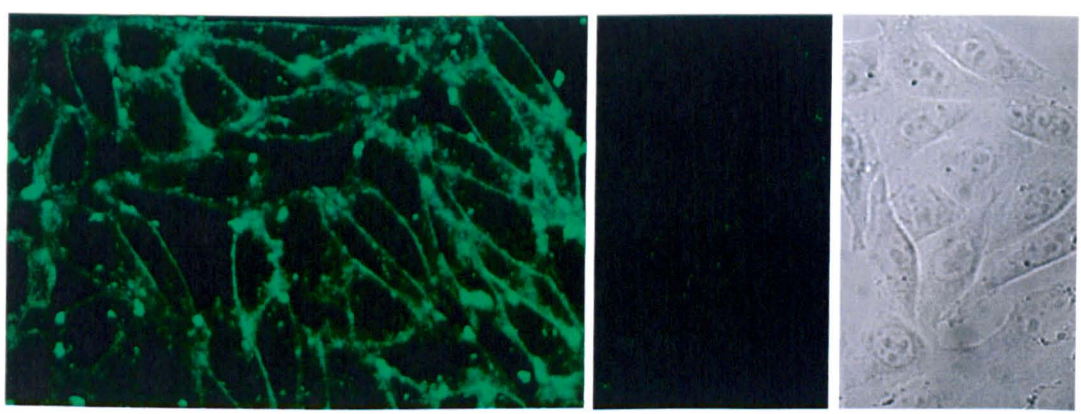

Figure 39 Comparison of SuperBright FITC nanosensors (left) with standard nanosensors (middle) when incubated with CHO K1 cells (example of confluency, right) at the same concentration when viewed with confocal microscopy with similar settings (laser power and gain) for each sample. Highly visible labelling of the membrane is achieved with both lower laser power, and gain on the confocal microscope x63 magnification. This correlates to an increased number of FITC molecules per nanosensor.

2.4 Conclusions

Nanosensor technology provides a platform and a means to place reporter dyes inside a bio-compatible matrix in order to minimise detrimental interaction between the dye and the environment in which it is located. Examples have been fabricated capable of measuring a range of analytes and provide a fluorescent response which can be monitored with a variety of optical methods. Complex sensing schemes can be implemented due to the containment aspect provided by the polymer matrix such that reference dyes allow for the curtailment of problems associated with fluctuations in concentration or signal intensity. We have shown that the polymer matrix can be tailored to suit particular applications in terms of nett charge, or provide functional groups for subsequent modification broadening the scope of their practicality and providing an avenue for further developments. There are many techniques available to address the nanosensors and characterise both their physical and chemical attributes allowing prompt confirmation of a successful fabrication or addition to the standard nanosensor assembly. Development of the nanosensor as a sensing technology is ongoing and there are several issues which are being resolved to improve the applicability and ease of use of the technology. As an improvement in terms of minimising sensor / cell interaction and achieving the ultimate aim of silent observation nanosensors provide a firm basis from which to achieve this objective, they are a vast improvement over free-dye based methods.

3 Chapter 3 – Measuring intracellular calcium flux in CHO-K1 cells as a model system for nanosensor development

3.1 Introduction

"Ja, Kalzium das ist alles" ("Yes. Calcium that's everything") [114]

3.1.1 The importance and ubiquity of calcium throughout biology

No better sentence describes the prevalence and importance of calcium than that found in the abstract of Whitfield and Chakravarthy's 2001 book entitled 'Calcium: The Grand Master Cell Signaler'[115].

"...exciting story to tell about Ca^{2+}, the versatile Master Cell Signaler whose influence reaches into all corners of the cell and controls cell proliferation, differentiation, cell functions to numerous to mention here, and even cell death."

To a certain extent, all cellular, physiological, and pathological phenomena that occur in cells are accompanied by ionic changes [116]. Calcium is a very important ion in biological systems playing an active role in a high number of cellular processes and pathways. The concentration of calcium changes dramatically in very short periods of time during normal cellular activity, calcium concentration can fluctuate over a full micromole (e.g. 0.1 – 1.2 μM) between pre- and post-activation. The calcium ion is a universal intracellular secondary messenger in cell physiology playing a part in many plant and animal signal transduction pathways [115, 117, 118]. Secondary messengers are intracellular chemical compounds (commonly calcium or cyclic adenosine monophosphate (cAMP)) which transfer a hormonal or drug activated message from the outer cell membrane to intracellular organelles, the cytoplasm or nucleus. Arguably calcium is the most widespread and diverse of all intracellular secondary messengers playing a key role in signal transduction, and involved heavily in cellular biochemistry, physiology, and pathology. Along with cAMP a variety of intracellular processes are controlled by Ca^{2+} and the fluctuation of Ca^{2+} concentration in response to an external stimulus, that being chemical, physical, or electrical, is a much investigated field. The actions of many drugs trigger a shift in the concentration of intracellular free-calcium ([free Ca^{2+}]), this fluctuation can be used as a signal that the administered drug has had

an effect, often signal intensity can directly relate to the degree of effect. Silver [119] specifically states that calcium signals are used in a large proportion of regulatory pathways and are thus considered ubiquitous in cell biology, yet they are also selective and specific in the control exerted among myriad functions within a common cytoplasm. Table 1 shows some common roles of calcium in biology.

Event Type	Example	Primary Stimulus
Cell Movement	Muscle contraction Chemotaxis	Neurotransmitter Chemical stimulus
Secretion	Neurotransmitter release Endocrine hormone release Exocrine secretion	Action potential Hormone Neurotransmitter
Cell division	Cell transformation Egg fertilisation	Chemical stimulus Sperm
Intermediary metabolism	Glycogen / lipid degradation	Hormone
Membrane permeability	Substrate uptake Cation uptake Cell communication	Hormone Action potential Paracrinal agent
Vision	Retinal Rod	Light

Table 1 A non-exclusive list of cellular events regulated by intracellular concentration flux of Ca^{2+}. Adapted from Intracellular Calcium: It's Universal Role As Regulator, Campbell [117].

There is a large body of evidence showing that the majority of uni- and multicellular organisms require calcium for normal growth and function [115, 117, 118, 120-122]. Ringer showed at the end of the 19th Century that Ca^{2+} was necessary for the normal contraction of the frog heart, the development of fertilized eggs and tadpoles, and that calcium was important in the adhesion of cells to each other, the latter also being demonstrated by Herbst [123]. and since then many phenomena have been shown to be abolished or inhibited by the removal of extracellular Ca^{2+} [120, 121]. Plants also require calcium to maintain cell structure and function; the necessity of calcium has also been shown in bacterial growth [124], and is vital in the formation of viable bacterial spores [125]. The structure and function of all eukaryotic cell tissues are maintained by Ca^{2+} bound to phospholipids, protein and nucleic acids and other membrane components [126,

[127] as well as the crucial role of precipitates of calcium phosphate and carbonate as the major inorganic components in animal skeletons. Ca^{2+} also plays a significant electrical role in cells in conjunction with sodium, potassium, chlorine and magnesium ions; particularly, Ca^{2+} carries a significant quantity of current in vertebrates and invertebrates during an action potential [128, 129]. The role of Ca^{2+} as a cofactor for extracellular enzymes and proteins is well established, for example in blood clotting, whilst some regulatory cell surface proteins and extracellular proteins require Ca^{2+} for stability and activity. The classical complement pathway, from an antibody-antigen complex is also inhibited if Ca^{2+} is removed [130]. The role of Ca^{2+} in these events was often alluded to through the use of Ca^{2+} chelating agents such as EDTA or EGTA and, as will become clear later, these agents proved useful when calibrating the fluorescence response of Ca^{2+} nanosensors. How complex messaging is achieved through a single ion remains unsolved illustrating that investigation into the various functions of $[Ca^{2+}]$ remains an important research field. For that reason calcium has been chosen as a model intracellular ion; research into which will likely benefit from the advance of nanosensor technology.

3.1.2 Current intracellular calcium measurement

At present the most common method for analysing intracellular calcium concentration is through the use of fluorochromes such as fura-2, indo-1, fluo-3 and fluo-4, and calcium green [131], and techniques based upon fluorescent or luminescent probes are the most effective; these types of measurements are central to almost all work on cellular Ca^{2+} transport [132]. Two types of intracellular Ca^{2+} indicators have become widely used: probes that change their fluorescent emission when Ca^{2+} binds, and probes that emit light when Ca^{2+} is bound. Dyes commonly used differ in excitation / emission spectra or their affinity for Ca^{2+}. Ratiometric dyes change their emission spectra upon binding Ca^{2+} which can occur with or without a change in peak excitation wavelength. The evaluation of the accurate intracellular $[Ca^{2+}]$ concentration is achieved by calculating the ratio of the emission values at two different excitation wavelengths (for dual excitation dyes, for example fura-2) or by taking the ratio of the fluorescence signals at two different emission wavelengths (for dual emission dyes, for example indo-1). These

dyes bind Ca^{2+} with a ratio of 1:1, so calibration simply consists of determining fluorescence ratios at various known concentrations. Non-ratiometric dyes however do not change their emission spectra when binding Ca^{2+}; binding merely results in a change in fluorescence intensity. Calibration of responses measured using non-ratiometric dyes is hardly possible as fluorescence intensity is a function not only of Ca^{2+} concentration but also of the dye concentration which may not be uniform in a particular preparation and may also vary with time owing to, for example, changes in cell volume. The most notable drawback of using free-dyes within live cells is the possibility of interaction between the dye and the surrounding environment. As referred to in chapter two the issues here are that cytotoxicity of the dye may affect the cell biology being measured and that the cell biology itself affects the dye response. The encapsulation of the dye within a polymer body allows the diverse array of dyes to be used whilst negating the associated weaknesses.

3.1.3 Purinoceptor of CHO-K1 cells

It was necessary to prove that a reliable method for increasing $[Ca^{2+}]$ in mammalian cells could be established in order to firstly assess the functionality of Ca^{2+} sensitive nanosensors when internalised in cells. This would allow subsequent experiments into particular biochemical pathways, processes or events, which ultimately lead to $[Ca^{2+}]$ fluctuation, to be planned on the basis of an established method for $\Delta[Ca^{2+}]$ measurement with nanosensors. The chosen approach was to induce an increase in intracellular calcium in cultured Chinese Hamster ovary (CHO) K1 cells via activation of an endogenous purinoceptor. Purinoceptors are a class of cell surface receptors that can be activated with adenosine and other endogenous purines and pyrimidines e.g. ATP, UTP, caffeine, and are widespread in the body including the cardiovascular, respiratory, immune, and nervous systems [133]. CHO cells contain very few endogenous receptors which makes them ideal transfection recipients which is why they are often chosen as a model cell line for research. The plan was to activate this purinoceptor and induce a $[Ca^{2+}]$ flux through the administration of ATP or UTP to the extracellular environment as described previously [134, 135].

3.2 Materials and Methods

3.2.1 Reagents

Calcium sensitive dyes, Fluo-4 dextran 10,000 MW and Fluo-4 acetoxymethyl (AM) ester as well as the reference dye AlexaFluor-568 dextran 10,000 MW were all purchased from Invitrogen. Pluronic® F-127 20 % solution in dimethyl sulfoxide (DMSO), a non-ionic surfactant polyol (polymers or monomers with multiple hydroxyl functional groups) approximately 12,500 daltons, used to help disperse the Fluo-4 AM ester, and probenecid, a blocker of organic anion transporters, reducing Fluo-4 expulsion from the cell, and DMSO solvent were purchased from Sigma-Aldrich.

For cell culture DMEM F12+ phenol red free (i.e. without pH indicator, ideal for low level fluorescence work), phosphate buffered saline, foetal calf serum, trypsin EDTA and L-glutamine were all purchased from Sigma-Aldrich. NaOH, for dissolving probenicid and adjusting pH as well as HCl were also purchased from Sigma-Aldrich.

Calcium buffer constituents, NaCl, KCl, HEPES, $MgSO_4$, $NaHCO_3$, $CaCl_2$, and glucose were all purchased from Sigma-Aldrich.

3.2.2 Cell culture

CHO-K1 cells were cultured using standard culture methods and grown in DMEM F12 with 10 % FCS and 5 mM L-glutamine (DMEM F12+). No antibiotics were used. Cells were always incubated at 37 °C with 5 % CO_2.

Thawing and reanimating cell culture – Prepared cell culture (DMEM F12+) media was pre-warmed to 37 °C in a water bath. Cells to be reanimated were removed from liquid nitrogen and thawed quickly in water bath. A plastic 30 ml universal tube was prepared by the addition of 10 ml warmed DMEM F12+. Cells were transferred into the same

universal tube and washed with centrifugation for 5 min at 1000 rpm. Supernatant was decanted and cells were re-suspended in 1 ml warmed DMEM F12+ before being transferred to plastic 30 ml universal tube with ~15 ml warmed DMEM F12+. The cell solution was then transferred to T-75 tissue culture flask and placed in an incubator.

Incubation of cells – Cells were incubated until confluency reached desired level for passaging, if necessary fresh DMEM F12+ was added every 2 – 3 days.

Passaging of cell population – When growing cells reached a confluency of 100 % they were ready for passaging. DMEM F12+ in flasks was aspirated with vacuum line and ~5 ml PBS was poured into flask. The flask was swirled gently before the liquid was aspirated once again. This process was repeated twice. The adherent cell layer was removed from the flask surface with the addition of 1 ml Trypsin/EDTA which was allowed to cover the cells for 3 – 5 min. The flask was tapped gently in the hand to fully dislodge the cells before 10 ml of DMEM F12+ was added to the flask. The cell solution was drawn up into a pipette several times to break up any clumps before being transferred to a plastic 30 ml universal tube. The cells were collected with centrifugation for 5 min at 1000 rpm and re-suspended in 1 ml DMEM F12+, they were drawn up and down with a 1000 µl pipette approximately 20 times to separate cells and ensure cell population uniformity. The cell solution was added to 10 ml DMEM F12+ in a plastic 30 ml universal tube. Cells were split 1/40 for continued culture. 250 µl of the cell solution was mixed with ~15 ml DMEM F12+ for each new T-75 tissue culture flask and transferred to an incubator.

Preparing cells for experiment – Typically for experiments populations of CHO-K1 cells were plated out 48 h to prior to experiment in 35 mm Ø plastic dishes at a confluency of approximately 60 % providing roughly uniform adherent and well spread groups of around 10 - 15 cells. This format was preserved for all confocal laser scanning microscopy and only in a small number of experiments were the cells grown in T-25 / T-75 flasks for cell suspension work with spectrofluorometry.

Freezing down cells for stock – When necessary flasks of cells were prepared to supplement the stock of cells maintained for this research. Cells in T-75 flasks were

grown to 100 % confluency, washed, trypsinised, and collected with centrifugation as normal. Each flask worth of cells was then re-suspended in 3 ml of freezing mix (FCS with 10 % DMSO). This was separated into three cryovials which transferred to a -80 °C freezer. After 24 h the cryovials were then transferred to liquid nitrogen for long term storage.

3.2.3 Fabrication of calcium nanosensors

Nanosensors were fabricated as described in chapter two, using dextran bound Fluo-4 and Alexa568 as the Ca^{2+} sensitive, and reference dyes, respectively. Fluo-4 is a derivative of Fluo-3 with two chlorine substituents replaced by fluorine [136]. This structural change allowed greater excitation at 488 nm hence lower concentrations of the dye could be used *in-situ*. The dissociation constant (K_d) of each batch of dye was given and could vary, however all experiments described here used Fluo-4 with a K_d of 600 nM meaning at 600 nM [free-Ca^{2+}] approximately 50 % of possible associations between Fluo-4 and Ca^{2+} are complete. An ideal response of Fluo-4 to increasing calcium and the relative increase in fluorescence is depicted in Figure 40.

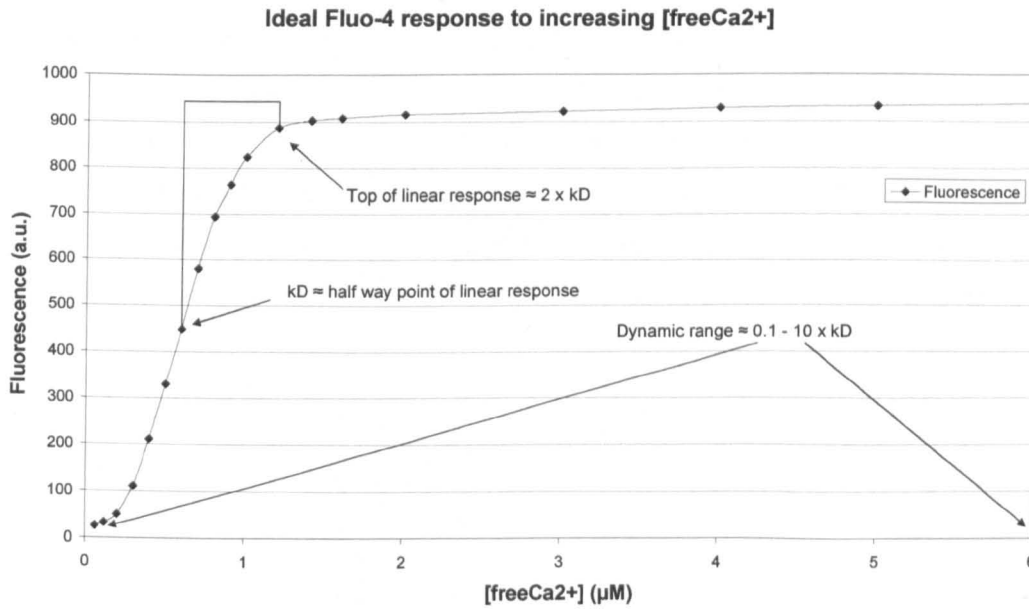

Figure 40 An ideal response of Fluo-4 to increasing [Ca^{2+}].

The dissociation constant also describes the dynamic range of a dye, dynamic range ≈ 0.1 – 10 times the K_d. The Fluo-4 therefore used in this instance has a dynamic range roughly equal to 60 nM – 6 μM.

3.2.4 Functional proof of nanosensor response with EGTA mopping

To achieve an initial response to changing [Ca^{2+}], 20 mg of nanosensors were suspended in 4 ml 5 mM $CaCl_2$. This suspension was placed in a cuvette and monitored on a fluorescence spectrophotometer whilst a small amount (approximately 10 mg) of EGTA was added to the cuvette directly. The solution was agitated with a pipette several times to promote dissolution of the EGTA whilst the fluorescence of Fluo-4 was measured constantly for four minutes.

3.2.5 Formulation of calcium calibration buffers

When investigating intracellular calcium the calibrations of devices for these measurements are normally carried out in EGTA calcium buffers. A do-it-yourself guide to the preparation of EGTA calcium buffer solutions was found in the literature which gave clear instruction on how to formulate a series of calcium buffers ideal for these experiments [137]. The buffers were made up without alteration from the method described giving buffer solutions numbered 1 – 10 with the free-Ca^{2+} concentrations as shown in Table 2. The ratio of each part of the buffer (EGTA / Calcium-EGTA) is shown as is the corresponding concentration of free-Ca^{2+} in each buffer, numbers 1 – 10.

Buffer Solution	Free-Ca^{2+} (μmol / L)	Bound-Ca^{2+} (mmol /L)
1	9.005	3.591
2	6.714	3.549
3	4.927	3.495
4	3.340	3.425

5	2.471	3.331
6	1.729	3.198
7	1.259	2.999
8	0.814	2.666
9	0.414	1.999
10	0.249	1.333

Table 2 Free-Ca^{2+} buffer solutions with relative concentrations of free- and bound-Ca^{2+}.

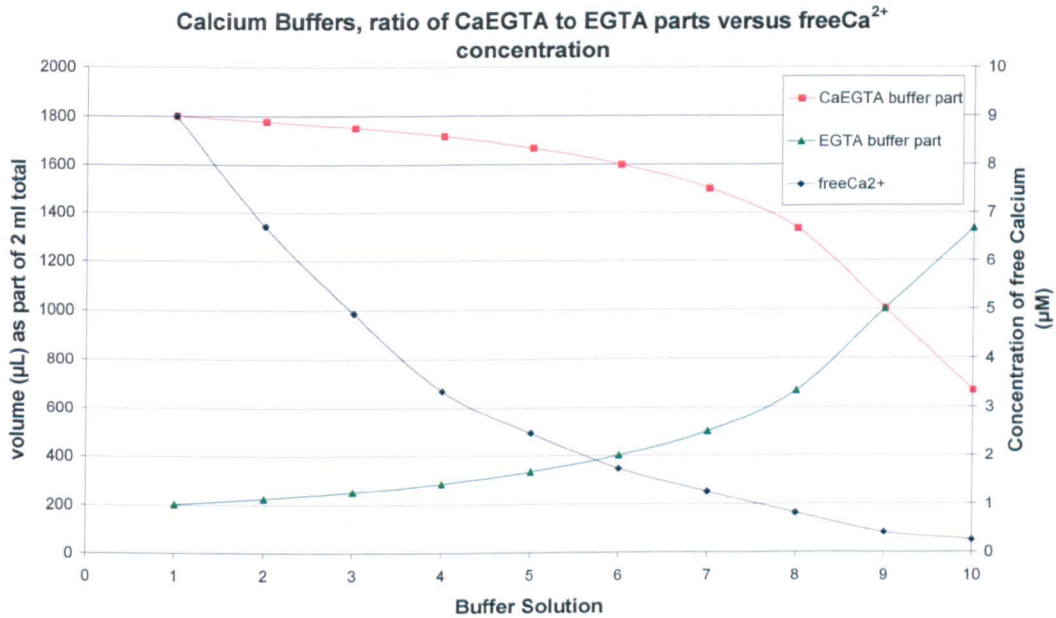

Figure 41 EGTA Calcium buffers with corresponding [Ca^{2+}].

3.2.6 Calibrating nanosensors with spectrofluorometry

The calcium nanosensors were calibrated using spectrofluorometry on a Varian, Cary Eclipse fluorescence spectrophotometer. 4 ml of 5 mg ml^{-1} calcium nanosensors in the appropriate buffer solution were placed in a cuvette and the fluorescence of the solution was measured. Several samples of buffer of each calcium concentration were measured and the resulting calibration was compiled by dividing the peak intensity of Fluo-4 with the peak intensity of reference dye Alexa568 (R_1/R_2). The R_1/R_2 value of each sample was then plotted to obtain a calibration graph of the nanosensors.

3.2.7 Calibrating nanosensors with confocal microscopy

In a similar manner as described in 3.2.6 nanosensors were suspended in solutions of appropriate buffer. These samples were then transferred into 35 mm plastic cell culture discs and viewed with a Leica DM-LFS confocal microscope with a Leica TCS SP scanning head using a water immersion 63 x, 0.9 NA lens. Using an immersion lens required one to first focus on the bottom of the cell culture dish and subsequently raise the focal plane ensuring the entire voxel was positioned within the buffer solution. Image analysis was carried out using Leica Microsystems Confocal software (LCS, version 2.5). Each channel of fluorescence, green (Fluo-4) and red (reference dye Alex568), was analysed using the software and the average pixel intensity was taken. The average intensities were used to calculate a R_1/R_2 for each sample as described previously and were plotted similarly.

3.2.8 Formulation of HBSS+ Ca^{2+} buffer used for experiments

For experiments aiming to induce a calcium flux in CHO-K1 cells a buffered saline solution was prepared based on Hanks Buffered Saline Solution with additional calcium. The addition of $CaCl_2$ to the buffer solution supplied a reservoir of free calcium outside the cell which acted to enhance the calcium flux initiated through ATP, UTP, or ionomycin. The simple idea was that freely available calcium outside of the cell would allow a prolonged response after the activator was administered. A stock solution of HBSS+ Ca^{2+} may be made up in distilled water (omitting 10 mM (90 µg per 50 ml) glucose as it breaks down quickly during storage) adjusted to pH 7.4 and autoclaved. This may be stored at 4 °C for up to one month. The components of the HBSS+ Ca^{2+} are shown in Table 3.

Compound	Concentration (mM)
NaCl	147
KCl	24
$MgSO_4$	1
HEPES	10
$NaHCO_3$	1
$CaCl_2$	1.3
Glucose	10 (added to HBSS immediately prior to experimental use)

Table 3 Components of HBSS buffer solution with added calcium. Glucose must only be added on the day that the buffer is to be used as it breaks down when stored; excess buffer containing glucose should be discarded.

3.2.9 Loading of CHO-K1 cells with Fluo-4 AM ester fluorescent dye

A fluorescent loading solution was prepared of 4.56 µl 1 mM Fluo-4 AM in DMSO mixed with 4.56 µl 20 % Pluronic, this mixture was subsequently added to 1 mL DMEM F12+ (DMEM F12 supplemented with 10 % FCS, 2 mM Glutamine) and 2.5 mM Probenecid. Probenecid stock solution (250 mM) was prepared directly before use; 0.355 g in 2.5 ml 1 M NaOH plus 2.5 ml HBSS+ Ca^{2+}. Cells were washed with DMEM F12+ and 100 µl of Fluo-4 solution was applied to each 35 mm cell culture dish. After one hour at room temperature the cells were washed three times with HBSS+ Ca^{2+} then left to rest for a further 30 minutes. If the washing step is found to remove the cells from the plate it may be necessary to alter the loading protocol. Satisfactory loading was also achievable with the following method. After applying the 100 µl of Fluo-4 solution the cell populations were left at RT for approximately 15 min, before being returned to the incubator (37°C, 5 % CO_2) for 20 min to speed up the process of dye loading. The loading solution was then diluted 10 fold with HBSS+ Ca^{2+} (rather than the harsher process of three separate washing steps) and held at RT prior to stimulation approximately 10 minutes later.

3.2.10 Loading of CHO-K1 cells with nanosensors

All cell experiments were performed on live cells which had been cultured with standard techniques at 37 °C with 5 % CO_2. Cells were cultured in 35 mm plastic petri dishes from IWAKI and seeded 48 h prior to experimentation so that the cells were approximately 60 % confluent at the time of the experiment. If so, required cells were cultured in tissue culture flasks so a large population was available. The larger populations were required for work with spectrofluorometry when cells were trypsinised and collected with centrifugation prior to measurements. For the calcium work cells were incubated with Tat- functionalised nanosensors (prepared as described in section 4.2.5) for 3 h. Cells were then washed at least twice with warmed PBS or DMEM+ before DMEM PRF was applied before imaging.

3.2.11 Initiating intracellular calcium flux in CHO-K1 cells

An elevation in CHO-K1 [Ca^{2+}] was created by the administration of either UTP or ionomycin from a stock solution. An aliquot was added to the cell culture plate or cuvette directly, depending upon format of experiment. The resulting fluorescence response was monitored against time. For stimulation the amount of HBSS+ Ca^{2+} per dish was adjusted to 900 µl; 100 µl of stimulant solution was added at a concentration 10 times that of the final concentration required.

Solution (a) – UTP - Uridine triphosphate is a pyrimidine nucleotide formed with the organic base, Uracil. It is ubiquitous in nature as a substrate during transcription for the synthesis of RNA; it also acts as a source of energy like ATP during metabolic reactions but is more specific. In this instance the key factor of UTP is that it binds with surface purinoceptors of CHO-K1 cells ultimately leading to a transient intracellular increase of [Ca^{2+}]. A 100 µM stock of UTP was made up in HBSS+ Ca^{2+} and added at a ten-fold dilution to experimental populations of CHO-K1 to initiate [Ca^{2+}] increase.

Solution (b) – Ionomycin - Ionomycin is a naturally occurring compound synthesised and released by *Streptomyces conglobatus* and acts as a narrow spectrum antibiotic

against Gram-positive bacteria. In mammalian cell lines ionomycin has been found to act as a selective Ca^{2+} ionophore, more effective than the well known and much used A23187. Ca^{2+} influx by ionomycin does not act directly at the plasma membrane but stimulates store-regulated cation entry. 200 μM stock was made up, firstly at 50 mM in DMSO then diluted with HBSS+ Ca^{2+} to 200 μM. Sonication was needed in order to fully dissolve the ionomycin calcium salt.

3.2.12 Image capture and processing

With confocal microscopy a series of images were collected over several minutes, approximately one every 1.5 seconds, during which an increase of $[Ca^{2+}]_i$ was initiated through the administration of either UTP or ionomycin. Fluo-4 was excited with an argon laser at 488 nm and emitted light was captured between 500 and 540 nm, Alexa568 was excited with a krypton laser at 568 nm and emitted light was collected from 600 – 650 nm. An aliquot of stimulation stock solution was administered with a glass pipette directly to the culture media as close to the objective lens as possible by placing the tip of the pipette against the ceramic body of the immersion lens and allowing the solution to flow into the culture media. The series of images captured were then analysed using Leica Confocal Software 2.5. Regions of interest (ROI) were chosen in the captured image representing several individual cells, as well as the entire image as a whole, from which a response could be presented graphically as fluorescence intensity against time.

Similar experiments carried out with a fluorescence spectrophotometer differed slightly. The cells were in suspension in a cuvette rather than adherent as was necessary for the *en masse* data collection format of spectrofluorometry, therefore cells had to be trypsinised after loading of nanosensors or Fluo-4 and collected with centrifugation prior to suspension in HBSS+ Ca^{2+} for the experiments. Fluorescence emission, initiated with a pulsed xenon arc lamp source, was captured at a single wavelength (520 nm) approximately five times per second for several minutes.

3.3.1 Fluo-4 free dye calibration against calcium buffer solutions

An initial confirmation of much of the experimental set up was achieved with a simple assessment of a free dye fluorescence response to two calcium buffers, one low in [free Ca^{2+}] and the other with a high [free Ca^{2+}]. This trial showed that the buffers, fluorescent reporter dye, and fluorescence response all acted as expected and provided confidence in several experimental variables. Figure 42 shows the fluorescence spectrum attained for the dye in each of the two buffered environments, normalised around the peak intensity of the reference dye and that the response was as expected. The reference dye remained unaffected by the varying concentration of [free Ca^{2+}] in solution and ratiometric data could be obtained. Further to this, a calibration of a series of [free Ca^{2+}] buffers was attained and an example is given in Figure 43. The shape of the graph is similar to that of the perceived 'ideal' response; importantly an approximate K_d can be estimated close to that given for this particular batch of Fluo-4.

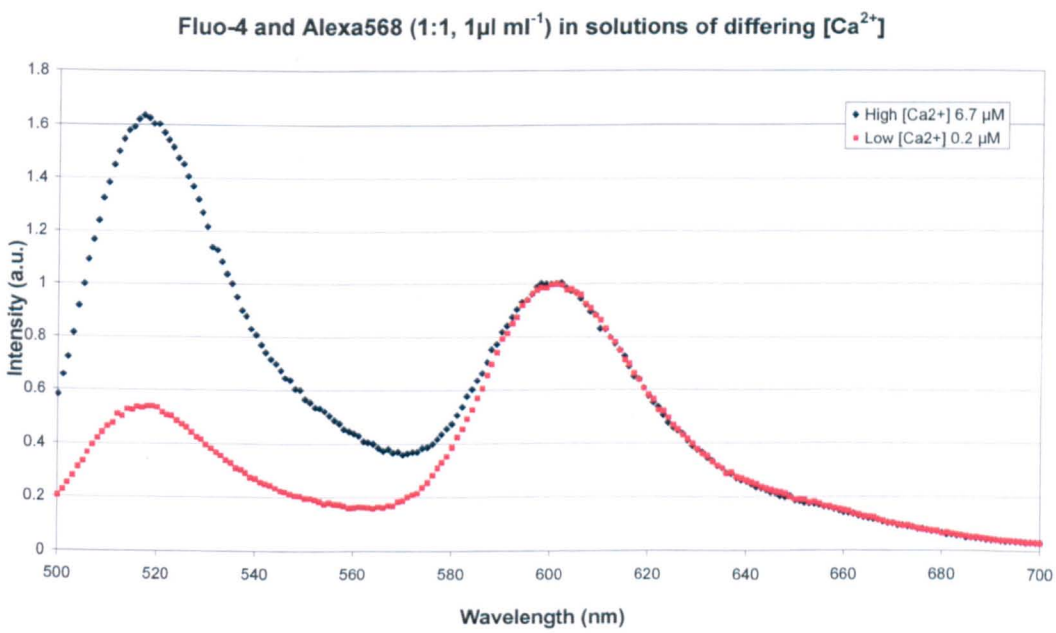

Figure 42 Fluorescent response of free dyes to solutions of high and low [free Ca^{2+}].

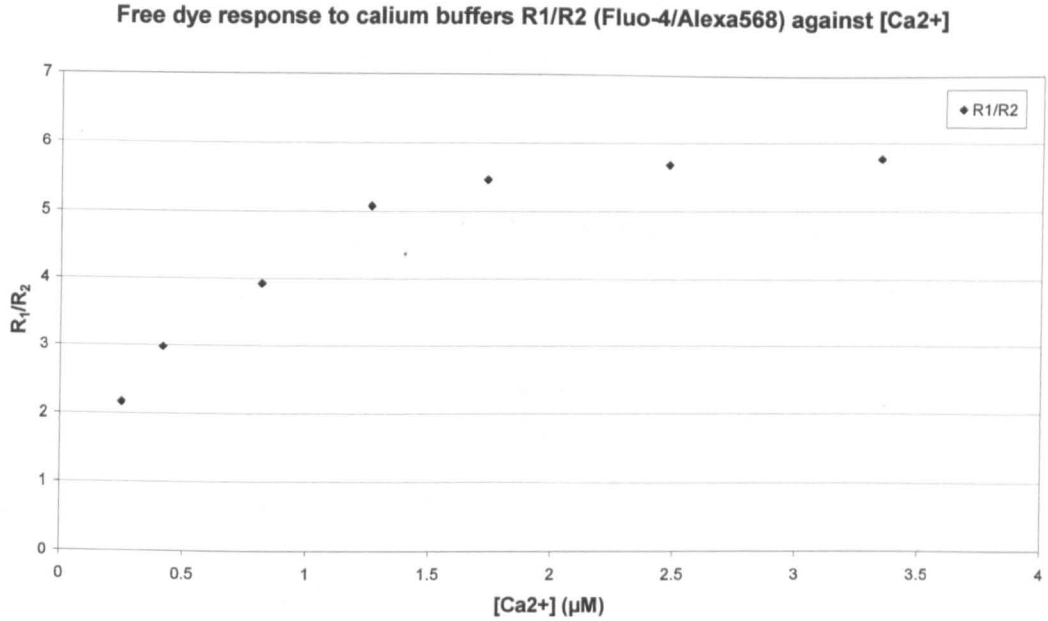

Figure 43 Free dye response calibratied against Ca^{2+} buffers.

The estimation of K_d from this graph is achieved by taking the top of the linear part of the response to be about the fourth data point (1.259 μM free Ca^{2+}) which is twice the K_d. The calculated K_d therefore is approximated to half of 1.259 = 629.5 nM close to the given K_d of 600 nM. Calculation of exact dissociation constant for any dye is extremely difficult as a large number of variables play a part. The exact figure of K_d is dictated by the conditions in which the dye is located, and this will therefore differ between different solutions, i.e. in different cells or parts of a cell. Being able to calculate a figure which was within 10 % of that given by the manufacturer was taken to be more than satisfactory for showing the buffer solutions and ratiometric dye system was accurate enough for this feasibility investigation.

3.3.2 Calcium nanosensor response to EGTA mopping

As a first indication of the response of nanosensors to differing [free Ca^{2+}] a very simple experiment was carried out utilising the calcium chelating properties of EGTA. It was clear to see the effect the addition of EGTA had upon the fluorescence being monitored. Figure 44 shows how the presence of EGTA immediately reduced the availability of

Ca^{2+} to the entrapped Fluo-4 within the nanosensor. This clearly indicates the functionality of the reporter dye is unaffected by its entrapment within a polyacrylamide matrix.

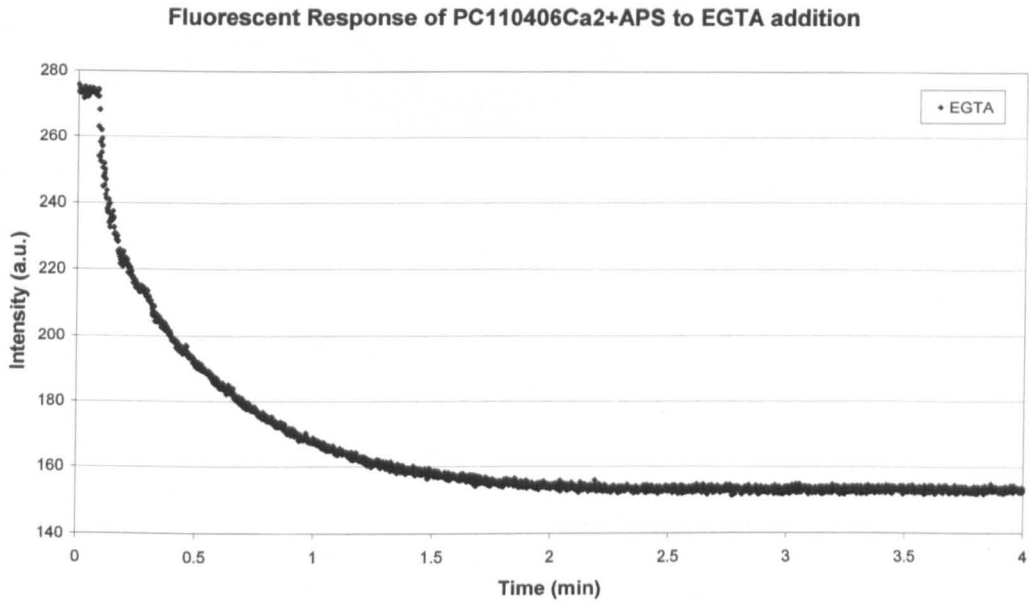

Figure 44 Calcium sensitive nanosensors at 5 mg ml^{-1} in 5 mM $CaCl_2$ responding to the addition of approximately 10 mg EGTA after 0.1 min.

3.3.3 Calibration of calcium nanosensors with spectrofluorometry

Fabricated nanosensors containing Fluo-4 and Alexa568 were calibrated against calcium buffers in a similar manner to the free dye proving that the encapsulation within a polyacrylamide matrix did not significantly alter the functionality of the ratiometric sensing scheme. Figure 45 shows the fluorescence data obtained for each of the six buffers used and has been normalised around the peak intensity of the reference dye.

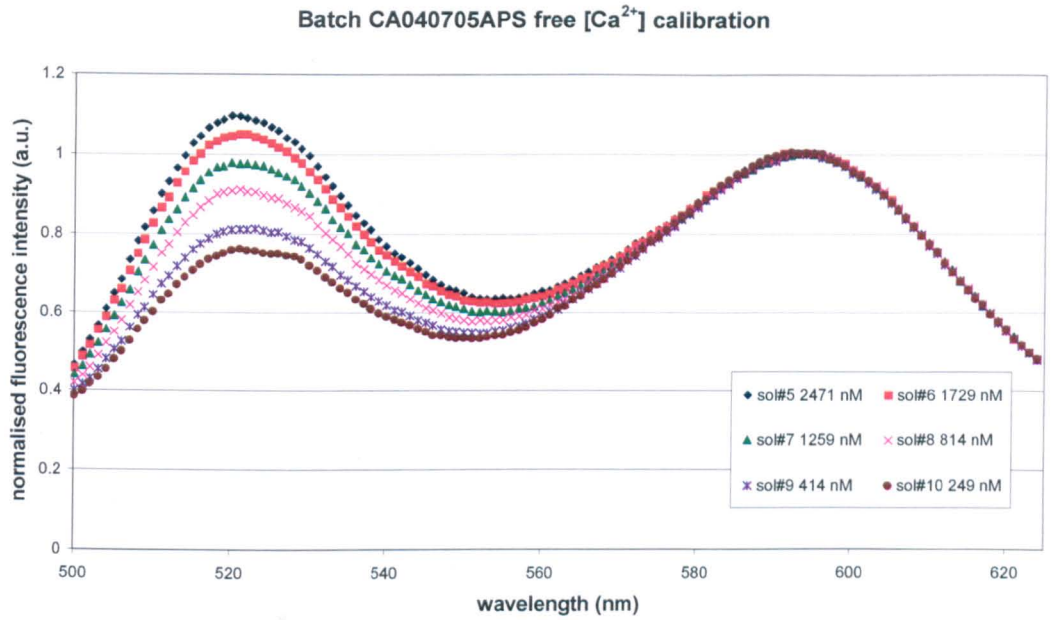

Figure 45 Calibration of nanosensors against Ca^{2+} buffers.

The ratiometric data calculated from Figure 45, shown in Figure 46, shows similar shape to that of the free dye calibration in Figure 43 although differs slightly at the higher concentrations.

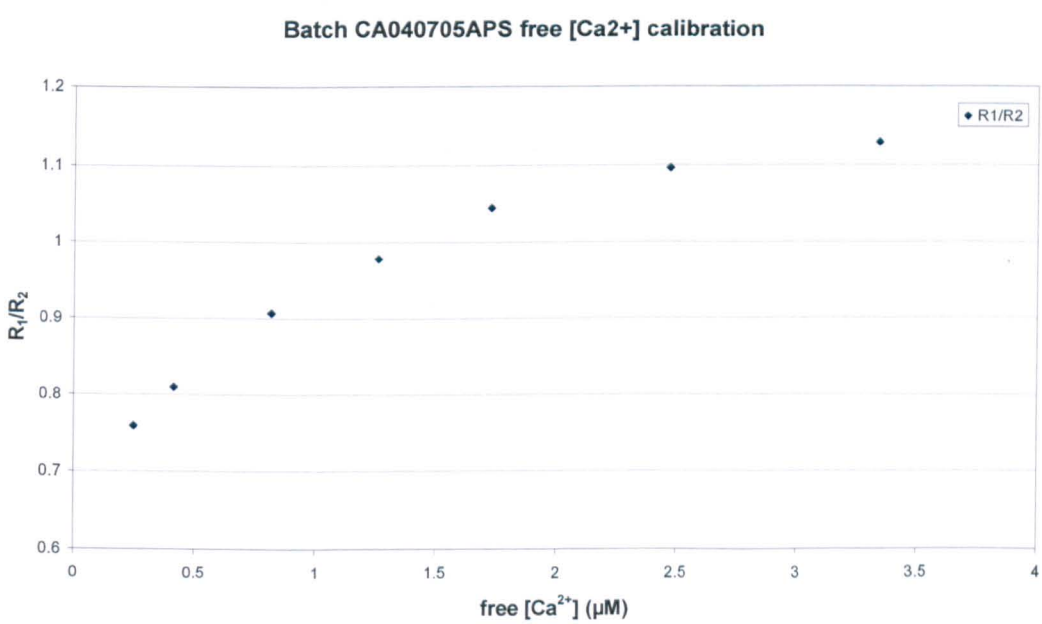

Figure 46 Ratiometric data for calcium nanosensors calibrated against Ca^{2+} buffers.

This difference could be attributable to the attenuated light path which includes a body of polyacrylamide although it is much more likely that the differences lie within experimental errors highlighting most probably the variation between different solutions of buffer. Significantly, the response of the nanosensors to increasing [free Ca^{2+}] was found to be reproducible and each batch of nanosensors could be calibrated prior to experiments showing their functionality as [free Ca^{2+}] sensors. The only way one could get an exact calibration of [free Ca^{2+}] would be to calibrate the nanosensors in the exact same conditions on which they are to be used, in this way the K_d of the dye would remain constant. This would ideally mean inside a CHO-K1 cell, or at least in a solution identical to the intracellular environment, however as the intracellular environment is a dynamic system it can never be truly replicated so extracellular calibrations of any dye are only ever approximations. The nanosensor calibration does show the same response shape with a roughly equivalent K_d and can be said to differentiate between [free Ca^{2+}] of at least 0.2 μM. The difference between basal and activated [free Ca^{2+}] in CHO-K1 cells is approximately 1.0 μM (~ 0.1 – ~ 1.0 μM) [134] which, according to these calibrations, is well within the sensitivity of the nanosensors.

As a method of verifying the techniques for [free Ca^{2+}] monitoring the results achieved were compared directly with published calibrations. Figure 47 shows a calibration presented by Biotek who utilised a Molecular Probes calibration kit designed for the exact purpose of calibration of Fluo-4 and other calcium indicators against [free Ca^{2+}]. As can be seen the fluorescence response looks similar to all those obtained using the buffers and nanosensors prepared for this investigation.

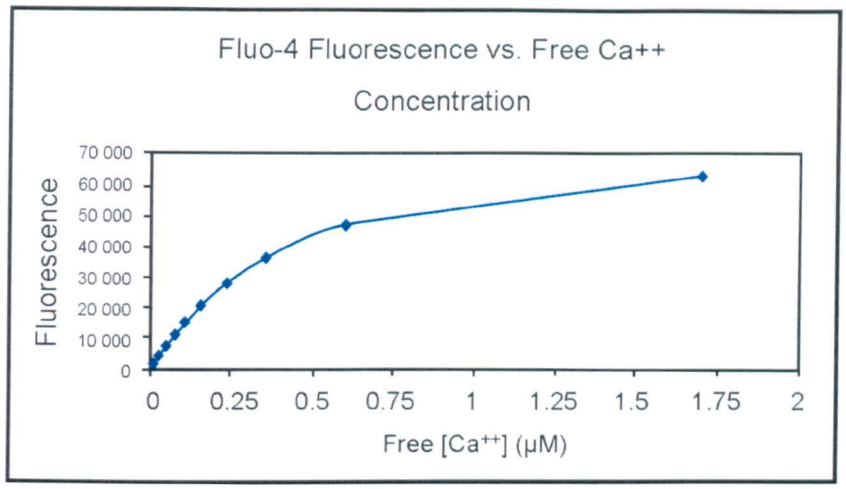

Figure 47 Using a Calcium Calibration kit from Molecular Probes (Invitrogen) various concentrations of free Calcium ion are reacted with a constant concentration of Fluo-4 indicator dye. The fluorescence was measured from the top using an FLx800 fluorescence reader with a 485/20 Excitation and a 530/25 Emission filters. When constant amounts of indicator dye are incubated with increasing amounts of free Ca^{2+}, an increase in fluorescent signal is observed. Free calcium can be tightly controlled in experimental situations using $K_2EGTA/CaEGTA$ buffering system, which utilises the K_d of CaEGTA as a means to provide free calcium ion. When the free calcium ion concentration increases from 0 to approximately 0.6 μM, the increase in fluorescent signal from Fluo-4 is virtually linear. Levels of free calcium above 0.6 μM result in greater fluorescence, but the increase is no longer linear. Free Calcium Concentration Curve produced by Biotek [138].

3.3.4 Calibration of calcium nanosensors with confocal microscopy

Experiments investigating nanosensor response to intracellular [free Ca^{2+}] flux were designed to be carried out with confocal microscopy, therefore it was necessary to show the same level of sensitivity when using this optical technique when compared to spectrofluorometry which had been used initially. The set up was very similar, aliquots of nanosensors were suspended in several solutions of [free Ca^{2+}] buffer and the fluorescence intensity was measured. Figure 48 shows typical data sets for both techniques ranging from 0.5 – 2.5 μM [free Ca^{2+}]. Fitting of a trend line as a visual guide to each set shows the similarity in shape between the methods and indicates that spectrofluorometry showed a smoother more classical response which perhaps enabled greater accuracy in this instance.

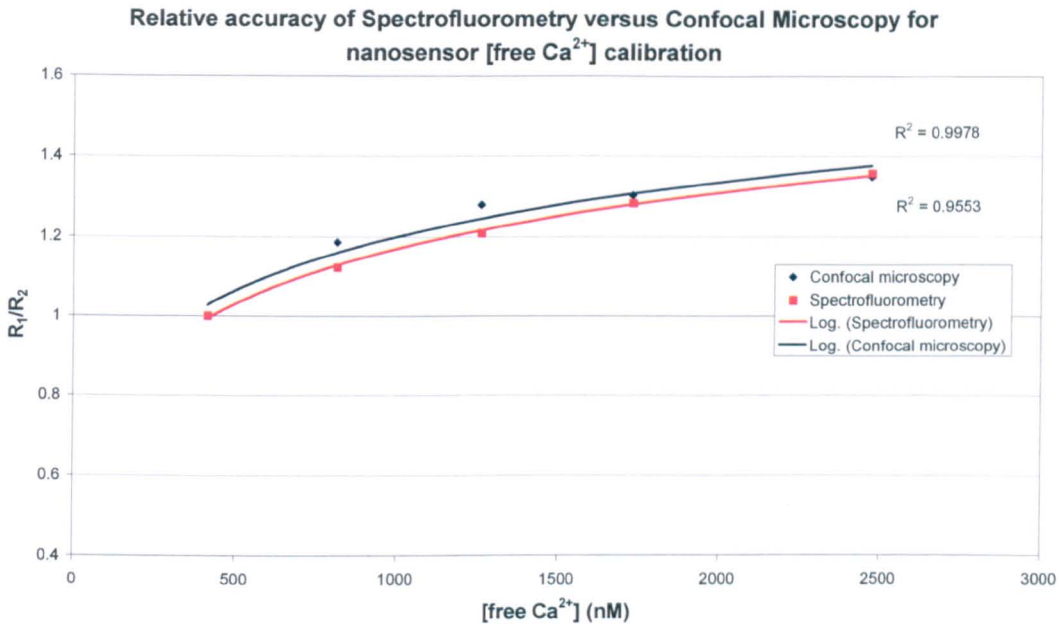

Figure 48 Ratio of fluorescence from Fluo-4 and Alexa568 nanosensors (R_1/R_2).

It was possible to differentiate between [free Ca^{2+}] in the range of basal to activated levels of [free Ca^{2+}] in CHO-K1 cells with nanosensors and confocal microscopy. Thus *in situ* monitoring with confocal microscopy was determined to be a valid technique.

3.4 Results and Discussion: Intracellular calcium flux

3.4.1 The initiation of intracellular Ca^{2+} flux

The study into the feasibility of using nanosensors to monitor intracellular Ca^{2+} was essentially split into two distinct parts. Firstly it was necessary to show that the nanosensors to be used could sense an increase in [free Ca^{2+}] which is why such attention was paid to making calcium buffers and establishing a reproducible response with a number of techniques and comparing this with standardised results. The previous sections show reasonably that any calcium flux within the range of 0.1 – 1.0 μM could be detected with nanosensors located within CHO-K1 cells and therefore the activation of particular pathways involving Ca^{2+} can be monitored. The second part of this study was to achieve a method which could reproducibly create the necessary calcium flux to be monitored. These next sections describe the relative successes of achieving this goal before the combination of both creating an intracellular calcium flux and monitoring its progression with nanosensors is discussed.

3.4.2 Loading of CHO-K1 cells with Fluo-4 AM ester

Using acetoxymethyl (AM) ester derivatives of fluorescent dyes is the most common technique for loading cells with indicator dyes. These derivatives are non-polar and cell permeant, freely able to diffuse across the cell membrane. Synthesis is achieved by derivatising carboxylate groups on the dye to acetomethyl esters (Figure 49 – Fluo-4 AM ester), which also renders the indicator insensitive to ions. Once inside the cell however intracellular esterases hydrolyse the AM esters rendering a polyanionic dye sensitive to ions, as shown in the schematic representation in Figure 50; the now polar dye is cell impermeant which minimises leakage. In practice AM ester derivatives are often mixed with one of the Pluronic® block co-polymers which helps dispersion in the loading medium [139].

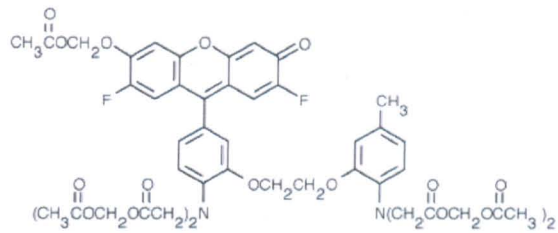

Figure 49 Fluo-4 AM ester, each carboxylate of the dye has been derivatised with an acetoxymethyl ester.

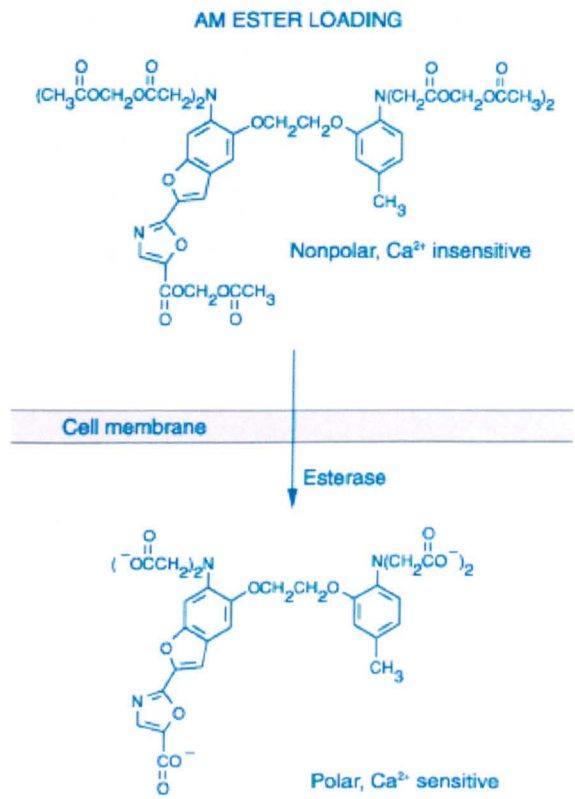

Figure 50 Schematic diagram of the processes involved in loading cells using membrane-permeant acetoxymethyl (AM) ester derivatives of fluorescent indicators, in this case fura-2 (taken directly from the Invitrogen, Molecular Probes Handbook [140].

Cells loaded at 37 °C remained adherent, well spread, and were clearly labelled with Fluo-4 (Figure 51). It was only clear that levels of fluorescence were adequate for calcium monitoring after stimulation as the very low basal level of $[Ca^{2+}]$ during the normal resting state of the cells meant that the Fluo-4 molecule was essentially 'off'.

However upon stimulation it was obvious that Fluo-4 loading had been successful as an increase in fluorescence was detected with this dye in elevated [free Ca^{2+}] of approximately 1 μM [136].

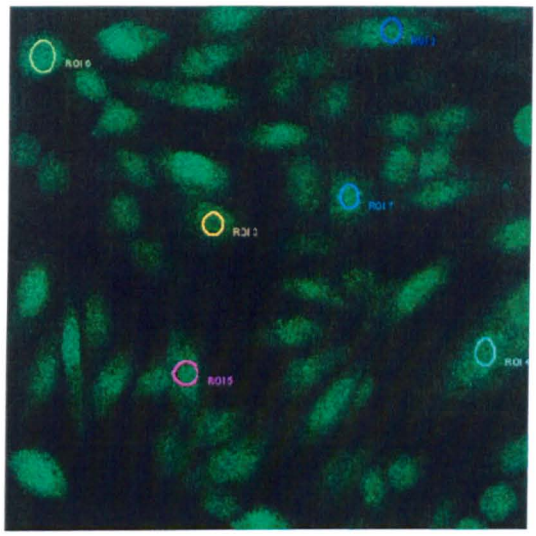

Figure 51 Populations of CHO-K1 loaded with Fluo-4 AM ester viewed after stimulation with 10 μM UTP, x63 magnification. Several regions of interest (ROI) are marked representing individual cells from which responses were measured and plotted using the inbuilt confocal software.

3.4.3 Measuring ionomycin-induced calcium elevations in CHO-K1 cell cultures loaded with Fluo-4 AM fluorescent reporter dye

As described previously ionomycin is a calcium ionophore which binds and chaperones calcium ions into the intracellular environment. Upon addition to the cell culture media of growing CHO-K1 cells it causes a prolonged increase in [Ca^{2+}], this was monitored with both confocal microscopy and spectrofluorometry. Figure 52 shows a typical response to the addition of 20 μM ionomycin to a 35 mm cell culture dish of CHO-K1 cells at approximately 60 % confluency. A standard trace is shown in Figure 53 calculated from the averages of several separate populations. The addition of ionomycin elicited an almost immediate effect. This led to an initial fluctuation in signal before a steady and gradual increase in fluorescence, and therefore [Ca^{2+}]. The fluctuation of the signal and general noise was thought to be an artefact of the manner in which the aliquot of ionomycin was applied with the pipette, as essentially the addition was taking

place directly in the optical path and was known to cause some turbulence as shown in Figure 54. The same experiment was carried out with spectrofluorometry in order to produce a response with less noise to create a clear picture of ionomycin elicited response. In Figure 52 the top six traces represent chosen regions of interest. The bottom line represents the whole image, including darker areas between cells – the average intensity is therefore significantly lower and although there is a clear response it is not as marked as the set of data is skewed towards a lower intensity. The right panel represents the transmitted light confirming that the response is an increase in fluorescence only.

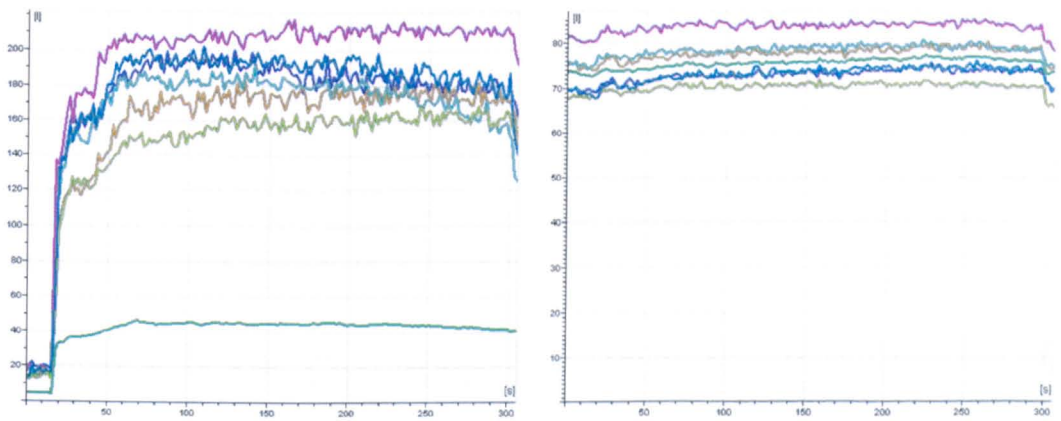

Figure 52 Confocal measured response of ionomycin addition to CHO-K1 cells. The left panel represents Fluo-4 fluorescence excited at 488 nm.

A series of confocal images captured during the experiment can be seen in Figure 55 depicting clearly the effect of ionomycin addition and visualises the increase in Fluo-4 fluorescence.

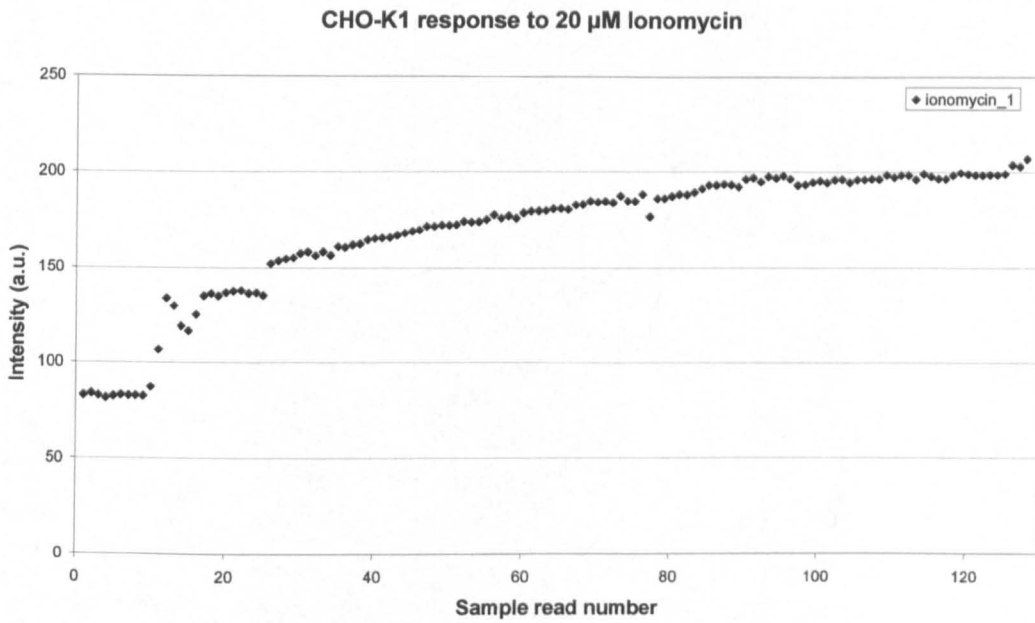

Figure 53 Ionomycin induced elevation in [free Ca^{2+}] produced from several sets of confocal data for response of ionomycin addition to adherent CHO-K1 cells. Each sample read number, that is each scan of the sample taken by the scanning head of the confocal microscope, took approximately 1.8 seconds.

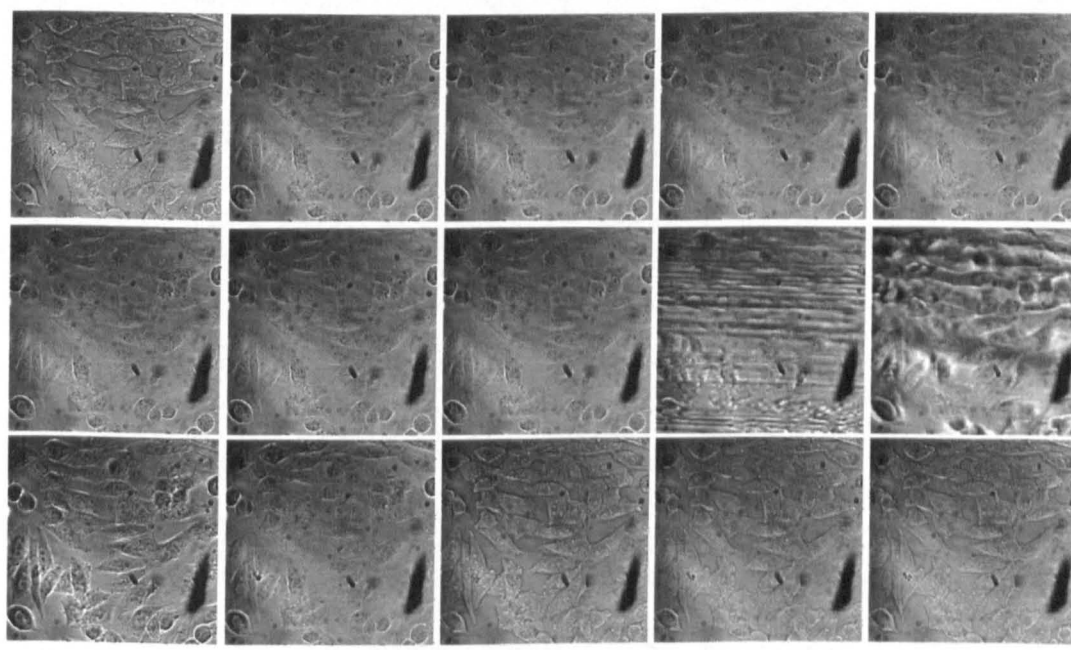

Figure 54 15 frames of a time series capturing the addition of 100 µl ionomycin, x63 magnification. The addition after frame eight causing distortion to the captured image subsidising five frames later. This also decreases the amount of detected fluorescence which is why it was thought the initial fluctuations in fluorescence signal after ionomycin addition may be attributed to this turbulence effect.

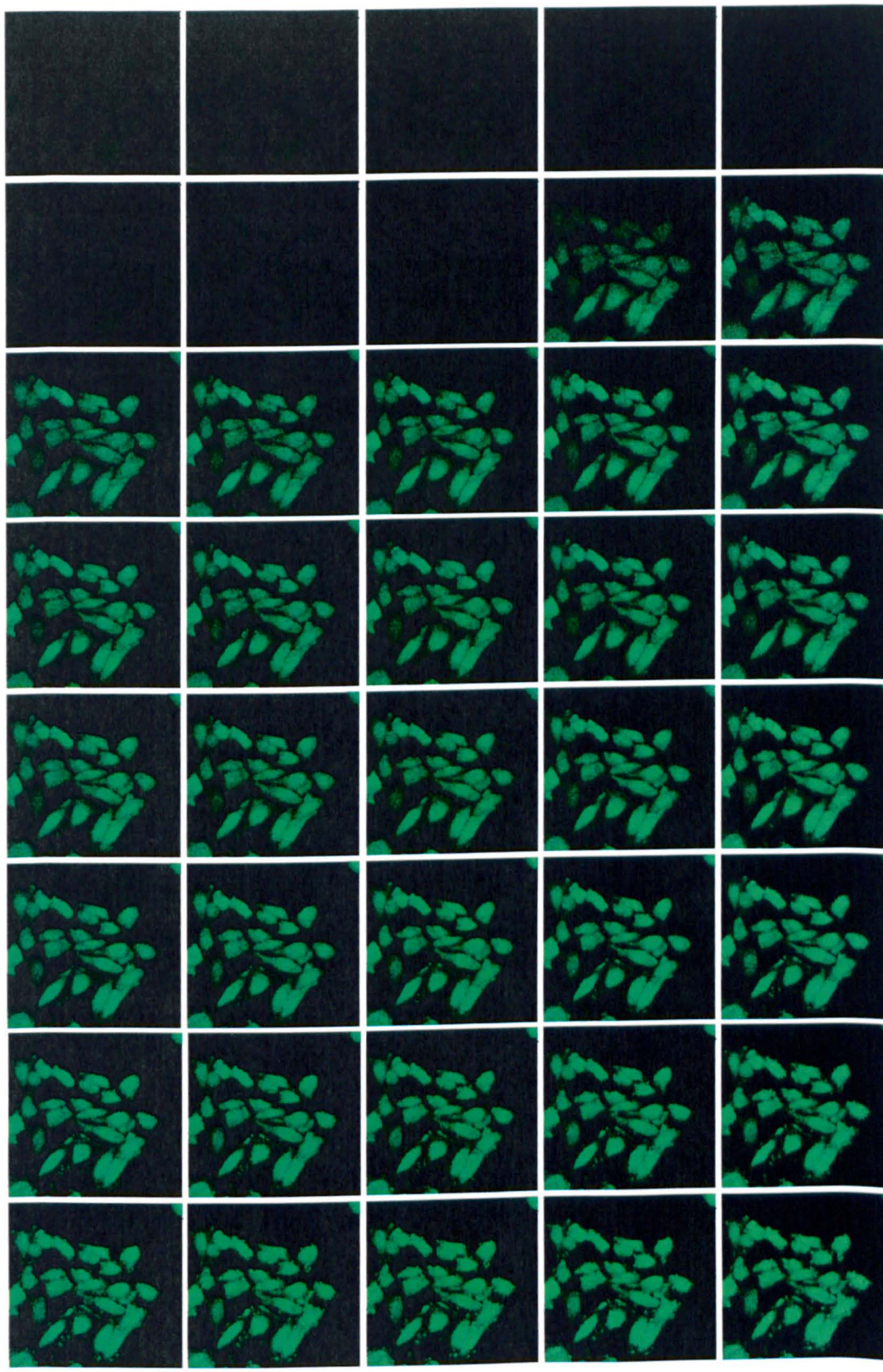

Figure 55 Temporal image series of ionomycin induced [Ca^{2+}] elevation, x63 magnification.

Using a suspension of CHO-K1 in a cuvette it was possible to reproduce an ionomycin addition whilst monitoring the response with spectrofluorometry. The benefits of this method were two-fold. Firstly, capture rate was significantly increased as this technique does not scan the sample and therefore no time was lost waiting for the scanning head to track transversely as in confocal microscopy. The increased capture rate produced a more detailed picture of the response. Secondly the effects of turbulence no longer affect the amount of light captured by the detector, and the effect of turbulence thought to be affecting the results obtained with confocal microscopy could be assessed. Figure 56 shows the response captured with spectrofluorometry over five minutes with one capture every 0.5 seconds, it is clear to see the enhanced detail and reduction in noise.

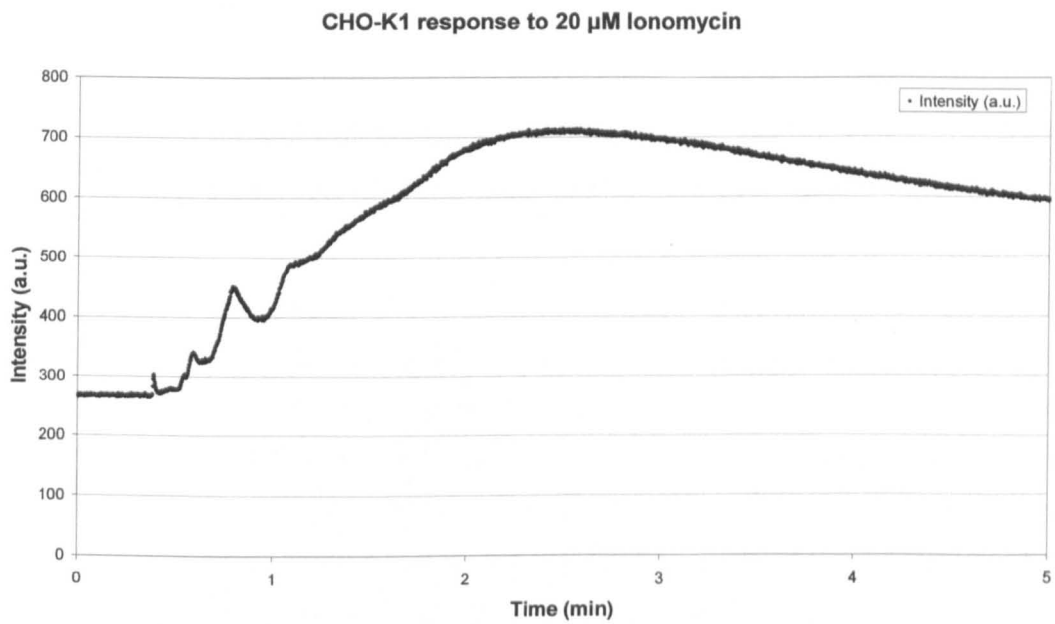

Figure 56 Spectrofluorometry measured response to ionomycin addition.

The data obtained with confocal microscopy is taken from a small number of cells, typically 15 – 30 cells, however when in suspension the captured fluorescence comes from a significantly larger number of cells attributing to the smoother more averaged data set. From the additional clarity it was deduced that the original speculation, inferring the method employed during confocal microscopy affected the results, seems to have been incorrect. Fluctuations in signal after the addition of ionomycin are not

attributable to turbulence even though turbulence may disrupt the signal for approximately 5 – 8 scans.

Ionomycin is thought to work by producing ion permeable pores within the cell membrane, thus flooding the inside of the cell with calcium, which flows down its concentration gradient into the cell. In a personal communication, Briddon suggests that low doses of ionomycin can selectively permeabilise intracellular calcium stores (mechanism unknown) and that the initial oscillating response may be explained by this theory. There are ways in which this could be tested, for example by depleting the intracellular stores, removing extracellular calcium etc. For the purposes of this work however, these questions can remain – the fact that we can monitor the oscillations is encouraging in itself.

3.4.4 Measuring UTP-induced transient calcium elevations in CHO-K1 cell cultures loaded with Fluo-4 AM fluorescent reporter dye.

The response to the addition of UTP occurred within approximately 10 seconds; this may have been faster but turbulence caused by the addition caused a temporary interference of the image capture. As shown in Figure 57 the response was transient and typically the level of $[Ca^{2+}]$ returned to basal level after approximately 170 seconds. The response was different from each cell, and assuming similar loading efficiencies of Fluo-4 across the population, it may be possible in this instance that the dosing level of 10 μM UTP created a less than maximum dose response; however there is a reported EC_{50} of UTP in CHO-K1 of 2.8 ± 0.6 μM [134]. Figure 58 shows captured confocal images of the fluorescence response to UTP addition and Figure 59 shows confocal microscope captured data.

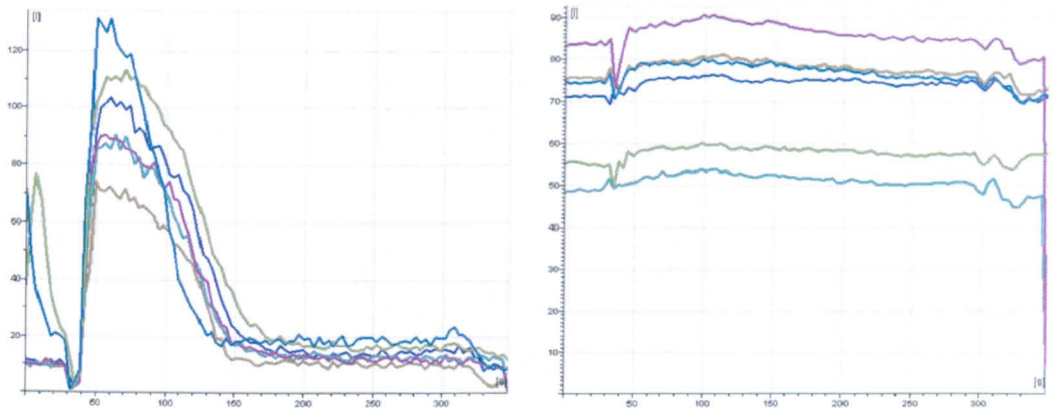

Figure 57 Confocal measured response of UTP addition to CHO-K1 cells. The left panel represents Fluo-4 fluorescence excited at 488 nm. Each of the six traces represent regions of interest (ROI) chosen with the integrated confocal microscope's software, an example of which can be seen in Figure 51. The right panel represents the transmitted light (grey channel) confirming the response is an increase in fluorescence and not input laser intensity. It is noteworthy in this example that the effects of turbulence can be clearly seen in both channels immediately after addition at scan 30. It is also possible to see $[Ca^{2+}]$ spikes prior to UTP addition occurring due to various stresses the individual cells are experiencing.

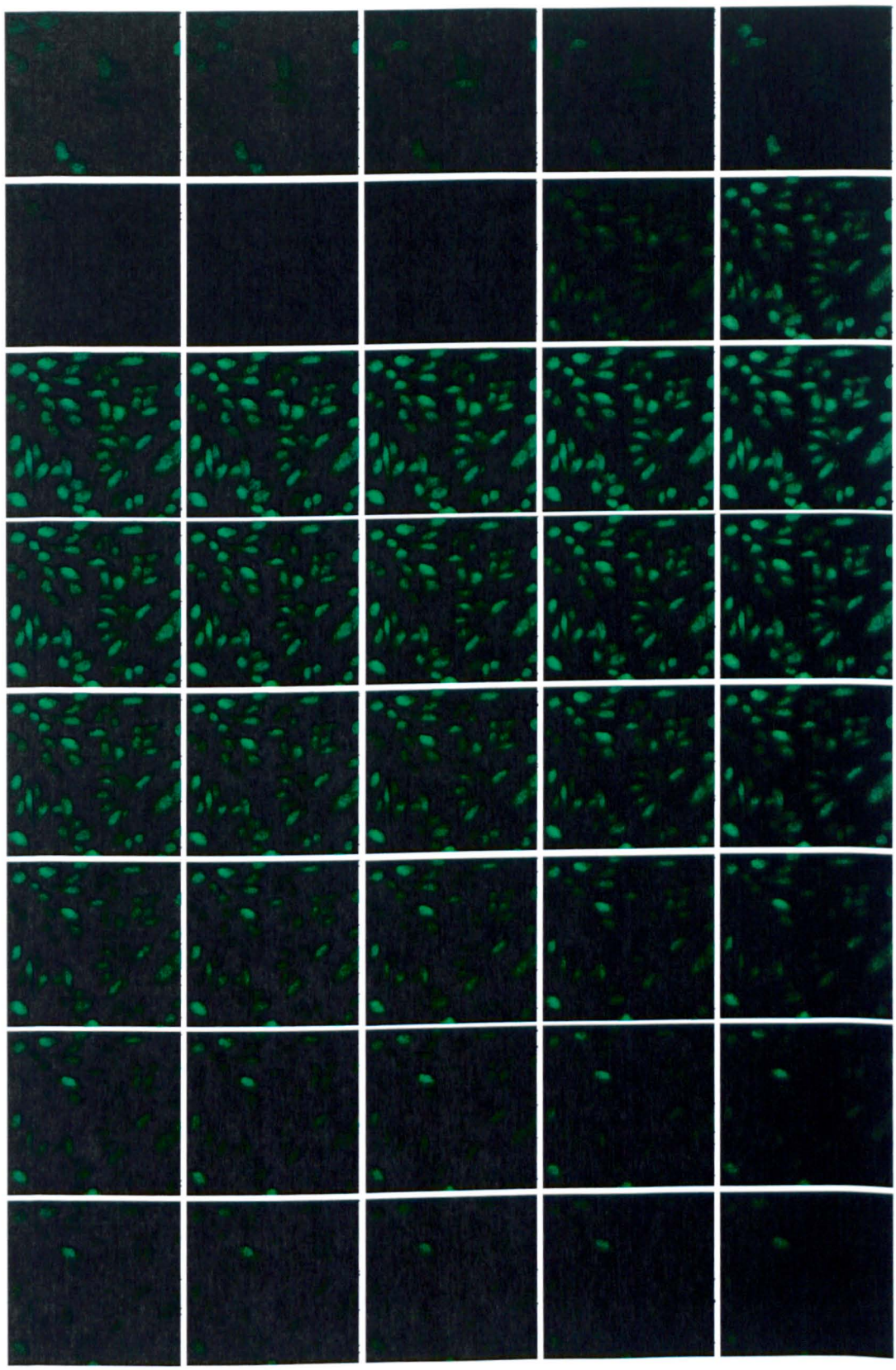

Figure 58 Temporal image series of UTP induced [Ca^{2+}] elevation, x63 magnification.

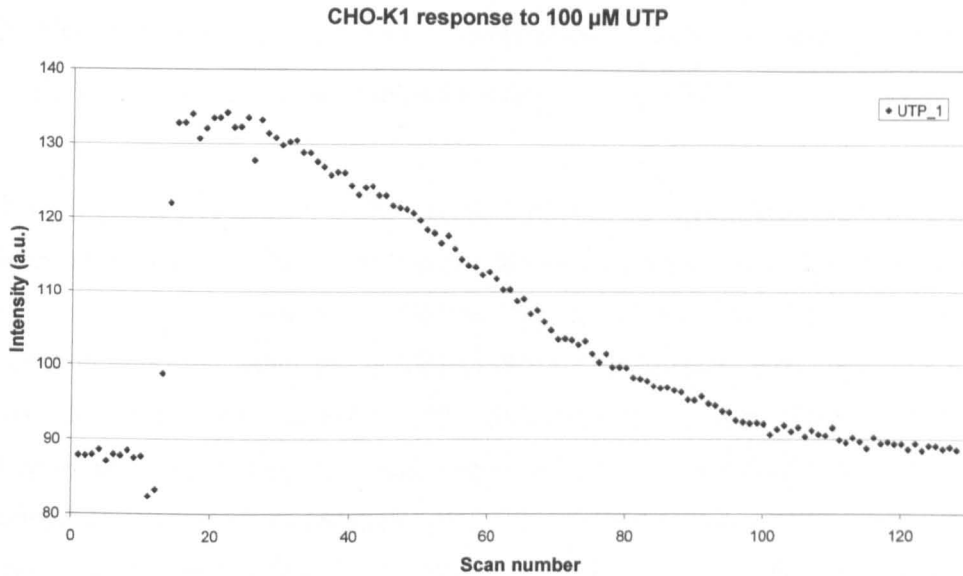

Figure 59 Induced elevation in $[Ca^{2+}]$ as determined from confocal data for response of UTP addition to adherent CHO-K1 cells.

The data shown in Figure 59 was validated when the same response was monitored with a spectrofluorometer shown in Figure 60.

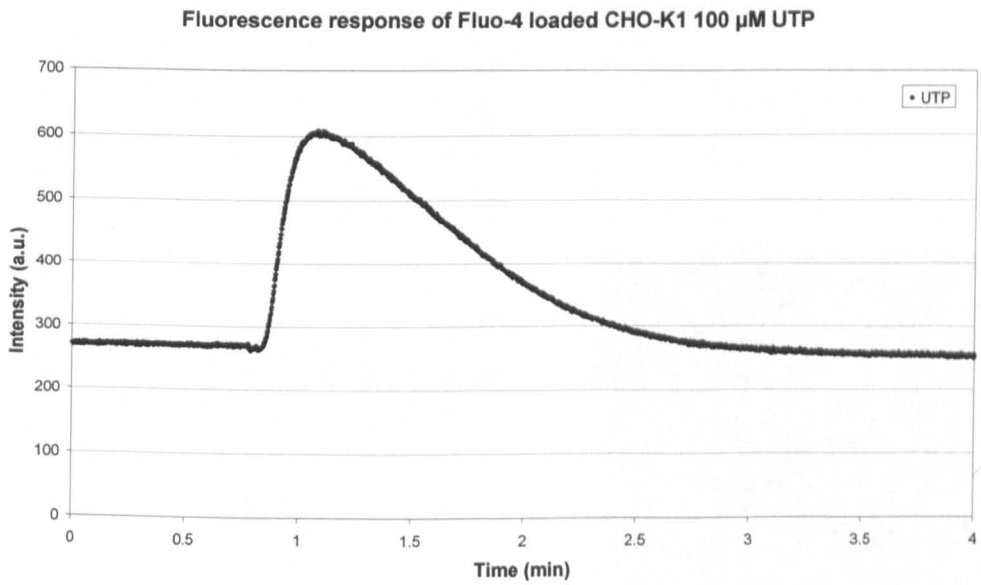

Figure 60 UTP addition to CHO-K1 cells as monitored with spectrofluorometry, with reference to the work by Iredale and Hill [134], a classic transient increase in $[Ca^{2+}]$ was observed.

3.5 *Results and Discussion: Intracellular measurements of calcium flux in CHO-K1 cell cultures using nanosensors*

Utilising nanosensors to monitor flux of intracellular [Ca^{2+}] did not proceed as had been anticipated. One factor that seemed to be hindering progress was the lower levels of reporter dye loading compared with the free-dye Fluo-4 AM ester. This became apparent as a greater input power of excitation light coupled with increased voltage across the PMT for detection was necessary to observe basal fluorescence comparatively with the free dye. Upon the addition of ionomycin or UTP as previously described no increase in fluorescence was observed with confocal microscopy. Figure 61 shows a response typical to both ionomycin and UTP from confocal microscopy, the extra channel is that from the reference dye Alexa568 which should stay at a constant fluorescence signal.

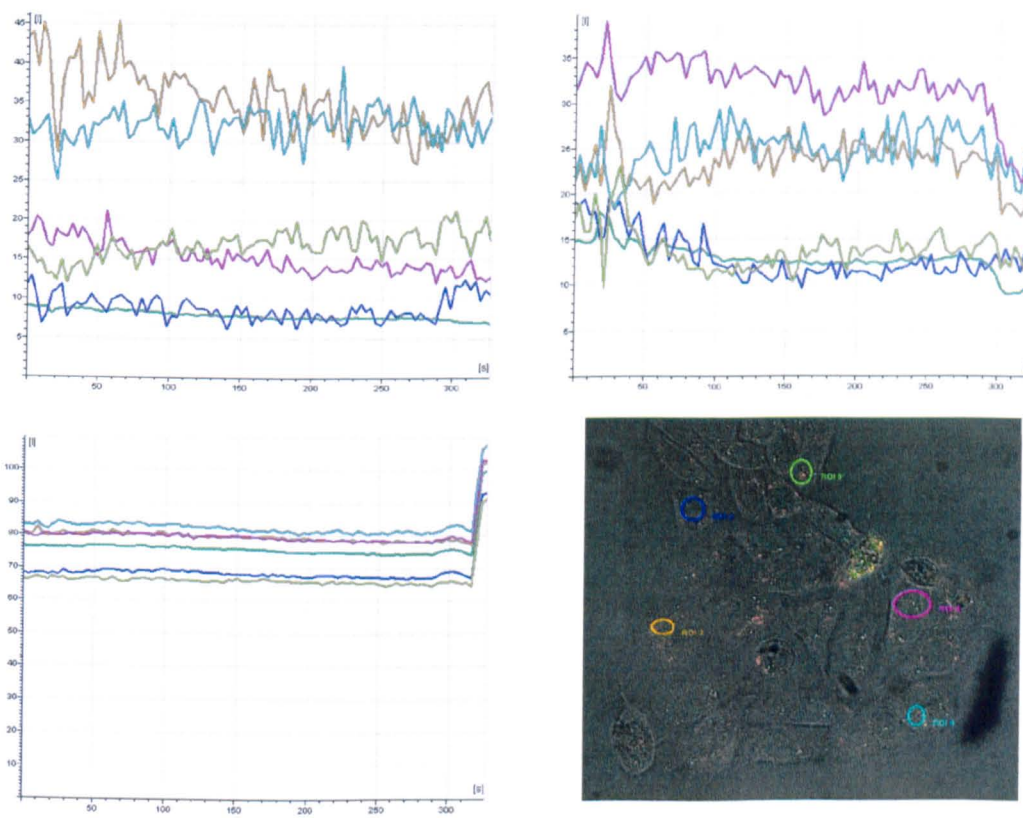

Figure 61 Ionomycin response in CHO-K1 cells as measured with calcium nanosensors. Addition of ionomycin did not yield a fluorescent response as had been seen previously with Fluo-4 AM ester.

With confidence in both the capacity of nanosensors to measure an calcium flux and the experimental aptitude to produce increased [free Ca^{2+}] it was not immediately clear as to why the expected fluorescent response was not observed. The batch of nanosensors being used for these particular experiments had been calibrated (Figures 45 and 46) and control plates of CHO-K1 responded to addition of both stimulants (Figures 55 and 58). If the level of fluorescence in the nanosensor loaded CHO-K1 cells was so low, was it possible the background noise of the experimental set up was masking the true response? The level of noise seemed similar to previous experiments with free Fluo-4 at around 5 – 10 intensity units (Figures 52 and 57). However it seemed prudent to carry out similar experiments with spectrofluorometry so many more fluorophores could be addressed at once which may have enabled a response to be observed.

The response measured with spectrofluorometry can be seen in Figure 62, and it is clear that no classical, transient [free Ca^{2+}] increase was achieved. Experimental noise is greater than experienced with free reporter dye and it was necessary to increase the PMT voltage to achieve a signal comparable with free dye experiments. However, the responses previously measured with free dye would still be easily observed above the noise inherent with the lower numbers of actual fluorophores present. With the addition of an aliquot of UTP there is a drop in fluorescence. This is attributable to the dilution effect of adding a non-fluorescent volume to a sample being addressed in this manner. The evidence is clear however that, unfortunately, it was not possible to replicate the measurements of [free Ca^{2+}] flux achieved with Fluo-4. Obviously the question is, why?

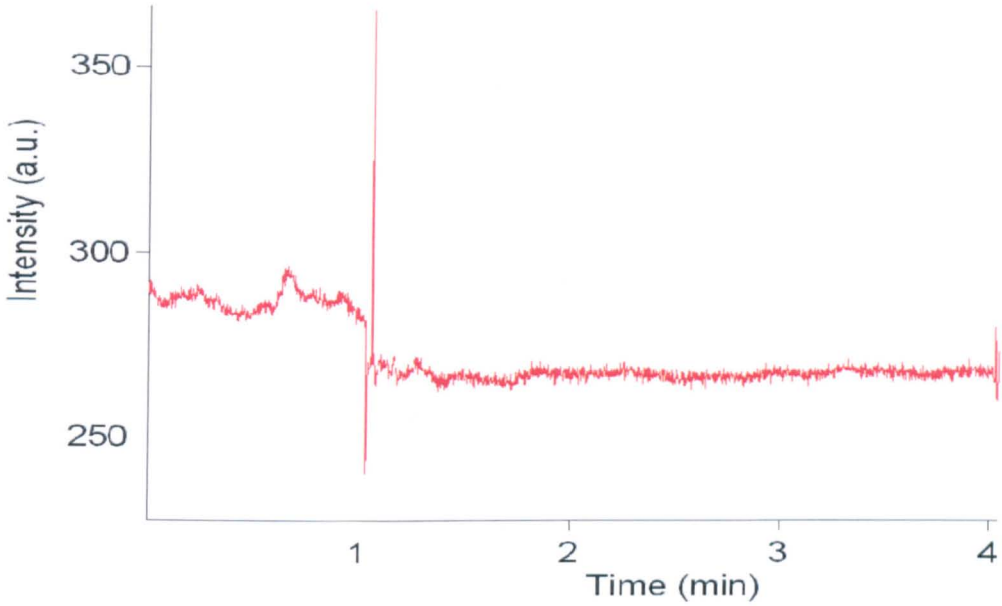

Figure 62 Spectrofluorometry measurement of UTP addition to calcium nanosensor loaded CHO-K1 cells. Addition of 200 µl UTP aliquot providing extracellular concentration of 10 µM similar to previous experiment with free Fluo-4.

It is suggested that the nanosensors, albeit localised inside each CHO-K1 cell (as reported in chapter four section 4.3.3), are unable to monitor [Ca^{2+}] flux. There is no doubt however, from the work reported in section 3.4.1, that [Ca^{2+}] flux is occurring. Although there is lower fluorescence intensity due to the lower numbers of individual fluorophores per cell, a response similar to those previously reported could still be observed with nanosensors and a classic response curve would be greater than the background noise. It remains then that the [free Ca^{2+}] flux and the nanosensors do not interact with one another inside the cell. The reasons why this scenario occurs will be discussed in greater detail in the chapter four.

3.6 Conclusions

It has been possible to show that [free Ca^{2+}] can be manipulated within CHO-K1 cells as measured using a standard method of Fluo-4 and confocal microscopy. This allows future research into intracellular calcium measurements to be carried out knowing that a reproducible [free Ca^{2+}] flux can be produced as required which eliminates a significant variable during experiments using calcium sensitive nanosensors. Additionally a method of measuring [Ca^{2+}] flux with Fluo-4 has been incorporated into nanosensor technology research as a standard to which measurements using nanosensors can be compared and contrasted. This has created a goal to which nanosensor development can proceed to prove their applicability.

3.6.1 Future Ideas

Intracellular Fluo-4 AM loading versus nanosensor loading efficiency could be assessed, possibly with flow cytometry, to develop techniques to benefit from the greater signal gained from increased numbers of fluorophores whilst still retaining the inherent bio-compatibility of the nanosensor polymer body. Equally, spectrofluorometry could be used to draw comparison between Fluo-4 AM ester loaded CHO-K1 cells and nanosensor loaded cells. The same number of cells in the same volume (e.g. one T75 flask ~60 % confluency removed to 3 ml), will show the order of magnitude in difference of fluorescence achieved from each loading technique and may begin to show how many nanosensors must be successfully loaded per cell to attain an adequate signal. The assumption here is that the number of individual molecules of reporter dye will be much greater when free dye is used rather than the nanosensors.

4 Chapter 4 – The development of a Tat mediated transport system for intracellular nanosensor delivery

4.1 Introduction

4.1.1 Cell penetrating peptides

Cell-penetrating peptides (CPPs) are a class of peptides which have been studied extensively over the past 15 or so years primarily because of their ability to enhance the uptake of various cargoes into living mammalian cells. Emerging techniques of using these peptides for cellular delivery are beginning to provide a means by which silent delivery is possible via a non-mechanical approach contrasting electroporation, gene gun bombardment [53], and pico-injection [56]. There are numerous reviews on the possibilities and advantages of using CPPs as delivery vectors, in particular therapeutic agents for human treatment [141-146]. For example Gariepy and Kawamura illustrate how the functional efficacy of therapeutic agents would be greatly enhanced through the controlled import and intracellular targeting to specific organelles [144]. The value of using CPPs as delivery agents became ever more apparent as it emerged CPPs could offer this significant ability (targeted delivery) and the short peptide structure of CPPs could be tailored easily to enhance delivery strategies.

The effect of CPPs was observed prior to the isolation of an individual example, this is because native CPPs (peptide sequences found in nature rather than those latterly synthesised) in their truest form are part of a larger protein. It was the observation that some proteins were able to translocate across cellular membranes by a process known as protein transduction which initiated the search for the element of the protein responsible for this process. Several proteins are well know for this behaviour such as Human Immunodeficiency virus (HIV-1) Tat protein [147], Herpes Simplex virus (HSV-1) VP22 protein [148], and *Drosophila* Antennapedia homeoprotein [149]. Although these proteins traverse the membrane they themselves are not CPPs, the portion of the protein responsible for membrane translocation is the 'protein-transduction domain' (PTD). CPPs are often referred to as protein transduction domains; however a PTD remains a part of the protein for which the PTD sequence aids membrane translocation. Only when the domain has been removed from its natural location is it classed as a CPP,

indeed this also holds if the peptide was not originally derived from a native protein; it is this domain which when removed from the protein forms the CPP [150]. It is useful to understand this distinction as when one explores the literature on CPPs and protein-transduction technology a misunderstanding of the nomenclature can be frustrating. In the literature peptides which cross cell membranes are sometimes referred to as Membrane Translocation Sequences (MTS) [145, 151], though this terminology is used less frequently and will not be used during this discussion. Discovering the protein-transduction domains was a relatively straightforward process whereby proteins exhibiting CPP behaviour were isolated and cleavage or site directed mutagenesis led to the eventual identification of amino acids not involved in membrane translocation; removal of necessary amino acids decreased or halted the cellular localisation of the peptides. This trial and error approach revealed PTDs which translocated the entire protein and also retained their activity in isolation when removed from the native protein. Derossi *et al* [152] working on the *Drosophila* Antennapedia homeoprotein discovered the PTD through site directed mutagenesis and discovered the driving force behind the internalisation of this protein; the third helix was essential for membrane translocation. Importantly though it was observed that the third helix was also sufficient for membrane translocation alone; from this work it was possible was to develop a 16 amino acid long CPP referred to as penetratin (pAntp) [149, 153].

CPPs are defined as peptides with a maximum of 30 amino acids, which are able to enter cells in a seemingly energy-independent manner, thus being able to translocate across membranes in a non-endocytotic fashion [154]. Initially it was discovered by Green and Loewenstein in 1988 that an 86 long amino acid section of the HIV-1 Tat protein was internalised readily by viable cells [155]. Even though CPPs have subsequently been used to successfully deliver different types of cargo to viable cells the exact mechanisms of entry and membrane translocation have not yet been fully established. In recent years several different and contradictory explanations have been proposed. Notably whether or not the mechanism is one of endocytosis is highly debated. Initially it was thought that endocytosis did not play a part due to the evidence that peptide internalisation occurred at 4 °C, a temperature at which all active transport mechanisms involving endocytosis cannot occur. Additionally CPPs being taken up by many different cells and tissue types suggests a common internalisation method which

suggests binding to conserved cell membrane determinants [156]. However recent data from several groups now argues for an energy-dependant process of entry [157]. One thing that is certain and is conserved between all examples of CPPs and PTDs is the higher than average concentration of cationic amino acids (e.g. arginine) [158]. This singular fact has been taken into consideration and suggests that in some way at least the initiation of cellular uptake comes from ionic interactions between the cationic nature of all CPPs and the anionic nature of the lipid membrane. The mechanisms involved following this primary ionic interaction are still debated; they may consist of currently unknown mechanisms or simply endocytosis [159]. It is also feasible, taking into account the physico-chemical diversity of the different CCPs, that diverse mechanisms of uptake are present and account for cellular uptake of different peptides.

It seems well established that there is a consistent cationic nature of CPPs and the likelihood that this plays a major role in cell penetration; though charge alone is not a sufficient driving force to induce translocation [143]. Reiterated throughout recent literature is the principal role that arginine plays in the CPPs [145, 159]. For a fuller review see Lundberg and Langel [145]. Studies into the various permutations of Tat and poly-R-PTDs (arginine rich) suggested an essential role of the guanidinium head-groups of the arginine residues for cellular uptake and that only a subset of residues is necessary within the peptide backbone [160]. CPPs have been previously explored as a delivery method for molecules and nano-sized particles, and reports show successful internalisation when CPPs have been conjugated to the surface of different particles [161-164].

4.1.2 HIV-1 Trans activating transcription factor

Historically the most extensively studied CPP is generally accepted to be Tat and this is most likely as protein transduction was first seen in the HIV model in 1988 [147, 165] when the full length HIV-1 Tat protein internalised within mammalian cells acting as an activator of transcription. Tat is so called as it *Trans*-activates, that is it affects transcription at a different site to where it is located on the HIV genome. It is also likely that because HIV has such a severe impact upon man that research into this virus and all

underlying mechanisms are of great importance which automatically created a great deal of enthusiasm and interest. HIV has several exclusive regulatory proteins in addition to the usual retroviral structural and transcription proteins, e.g. viral capsid, reverse transcriptase, and envelope proteins depicted in Figure 63 [166] and the Tat protein is one of these novel regulatory proteins. As mentioned previously Tat is a *Trans*-activator of transcription – it serves to up-regulate the transcription of viral or host cell genes in order to promote a consistent high-level state of HIV infection and the formation of new immature virions.

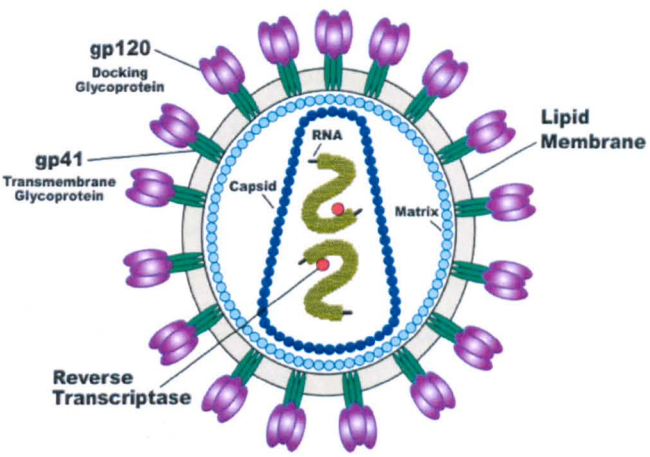

Figure 63 Structural schematic of the HIV-1 particle [166].

The Tat gene itself is made up of two exons (a sequence of gene which is retained in mRNA prior to transcription into a protein, there are other portions of the genome which do not make proteins (introns) [167]) of 72 and 14 amino acids which make up an 86 amino acid protein with several distinct regions including a highly basic region containing two lysine and six arginine residues. Investigation allowed the Tat gene to be characterised into several regions (Regions I – V plus Exon 2) and the functionally of these regions to be proposed. The first exon, amino acids 1 – 72, is sufficient for complete Tat activity and the significance of the 14 amino acid second exon is poorly understood [168]. However it was found that a very important section within Region IV, amino acids 48 – 52 (GRKKR), was essential for a functional Tat protein and mutations in this highly basic region prevented Tat-led *trans*-activational transcription [169]. In order to gain access to the eukaryotic nucleus, proteins which are larger than 45 kDa must have targeting signals and with continued investigation into the multiple functional

sites of the Tat gene it was established that the highly basic region of amino acids 49 – 58 acted as a nuclear localisation signal (NLS) responsible for nuclear import and is similar to other conventional NLS [170, 171] – more significantly, with regards to this work, the observation that Tat protein is secreted from and then taken up by live cells [172] suggested an ability from membrane translocation which may be harnessed for the delivery of various cargo to live mammalian cells. Many groups investigated which specific region of the Tat protein that could cross cellular membranes, Fawell *et al* delivered heterologous proteins into several different mammalian cell lines and showed that Exon 2 was unnecessary for this activity [141, 142]. It is now demonstrated that the very well conserved basic region constituting amino acids 48 – 57 of HIV-1 Tat containing lysine and arginine is capable of delivering various cargo from fluorophores to nanoparticles into many different cell types [157].

In summary, a CPP can be defined roughly as a short, cationic, helical peptide derived from native PTDs or synthesised directly, for example, homo-arginine peptides which exhibit similar, sometimes enhanced translocation properties [151]. These peptides can be used to deliver various cargoes into various cell lines as they confer their ability to cross cellular membranes onto the cargo to which they are attached. Attachment of the cargo is typically through covalent bond between an additional residue incorporated at one end of the peptide to the surface of the nano-particle or therapeutic agent being delivered, CPP-cargo constructs are added to the cell culture media in a simple incubation step for intracellular delivery. To date the process of membrane translocation is debated and controversial with a great deal evidence for both endocytosis and energy-independent pathways available [150, 156-158, 173-176]. Though the current status of understanding is not ideal regarding internalisation mechanisms, one can still utilise these peptides if successful, controlled, and consistent intracellular delivery can be shown, ultimately with undetectable cell perturbation and alteration.

4.2 Materials and Methods

4.2.1 Cell culture

Throughout this chapter the cells used for all experiments were cultured using standard techniques as described previously, 3.2.2.

4.2.2 Synthesis of Tat peptide

Tat peptide used in this study was synthesised by John Keyte at the Biomedical School of the University of Nottingham using standard techniques of peptide synthesis based on Fmoc chemistry, for information on the methods employed the reader is referred to the title, Fmoc Solid Phase Peptide Synthesis: A Practical Approach, Volume 222 from the series A Practical Approach [177]. The custom 11 amino acid residue sequence of the peptide was CRRRQRRKKRG, molecular weight 1499.83. In addition to the Tat sequence a cystein residue was incorporated onto the N-terminus for attachment to the nanosensor surface. Table 4 lists the amino acids incorporated into the peptide.

Arginine	Arg	R	Polar	Strongly basic
Cystein	Cys	C	Polar	Neutral
Lysine	Lys	K	Polar	Basic
Glutamine	Gln	Q	Polar	Neutral
Glycine	Gly	G	Non-polar	Neutral

Table 4 Constituent amino acids of the Tat based peptide.

4.2.3 Fluorescent labelling of Tat

Utilising the spontaneous reaction between primary amines and isothiocyanate as described in section 2.3.3 a sample of Tat peptide was fluorescently labelled so optical

assessment of cellular internalisation was possible. Fluorescein Isothiocyante (FITC) was dissolved in anhydrous DMSO at 1 mg ml^{-1}. 5 x 50 µl aliquots of this FITC stock solution were added drop wise to a solution of 10 mg Tat peptide in 5 ml PBS solution. This solution was incubated in the dark at 4 °C for 8 h before washing in ethanol and collecting with centrifugation. The FITC-Tat conjugate was allowed to dry before being stored at -18 °C.

4.2.4 Incubation of FITC-Tat conjugate with mammalian cell lines

To assess the ability of Tat peptide to cross mammalian cell membranes aliquots of FITC-Tat conjugate were incubated with cells for 1 h prior to washing and optical assessment with confocal microscopy. A stock solution of FITC-Tat conjugate at 10 mg ml^{-1} was made up in PBS and stored frozen. For experimentation the FITC-Tat conjugate stock solution was thawed and 1 – 5 µl ml^{-1} was added to the cell culture media of cells prior to incubation. Cells were washed after incubation twice with fresh cell culture media to remove any excess or non-internalised conjugate before imaging in fresh, phenol red-free culture media.

4.2.5 Surface functionalisation of nanosensors with Tat peptide

The surface of amine functionalised nanosensors was functionalised with Tat peptide, CRRRQRRKKRG. Covalent attachment of the peptide to the sensor was accomplished using a modified method originally described by Shriver-Lake [178] via the hetero-bi-functional cross-linker Sulfosuccinimidyl 4-N-maleimidomethyl cyclohexane-1-carboxylate (sulfo-SMCC). 50 mg of the amine functionalised nanosensors were immersed in 2 mM sulfo-SMCC in phosphate buffered saline pH 7.2 with agitation for 1 h. Excess sulfo-SMCC was removed by washing in ethanol; subsequently the nanosensors were collected with centrifugation. 5 mg synthetic peptide was dissolved in 5 ml of PBS and this solution was added to the sulfo-SMCC functionalised sensors and agitated for 2 h at room temperature, then overnight at 4 °C. Unbound peptide was

removed by washing in ethanol and the Tat nanosensors were collected by centrifugation, filtered with ethanol to dryness and stored at -18 °C.

4.2.6 Mixed population studies of FITC-Tat conjugate loaded CHO-K1 cells with control population

To achieve enhanced imaging of FITC-Tat conjugate loaded cells they were seeded with control cells allowing simultaneous side-by-side observation. A T75 flask of CHO-K1 cells at 60 % confluency was doped with FITC-Tat conjugate at 2 $\mu l\ ml^{-1}$. After a 1 h incubation under standard conditions the cells were washed with fresh culture media and removed from the flask with trypsin / EDTA. Cells were collected with centrifugation at 1000 rpm for 5 min and re-suspended in fresh culture media. A control flask of cells having no treatment was collected in the same manner. These two populations of cells were combined and plated out in 35 mm diameter cell culture dishes and allowed to rest for 24 h prior observation with confocal microscopy.

4.2.7 Incubation of Tat nanosensors with mammalian cell lines

Tat nanosensors were incubated with various mammalian cell lines at concentrations ranging from 1 – 5 $mg\ ml^{-1}$. Depending upon specific experimental protocol incubation times varied from 1 to 90 h although typically incubation for intracellular delivery lasted for 3 h. Tat nanosensors were initially suspended in an aliquot of fresh culture media (e.g. 300 µl) before addition to the cell culture dish to make a final volume of 2 ml, when working with 35 mm diameter cell culture dishes. Cells were always washed twice with PBS or fresh culture media prior imaging in phenol red-free culture media.

4.2.8 Staining of human mesenchymal stem (hMSC) cells with CD 105: FITC, mouse IgG monoclonal antibody

CD marker (for a description of CD markers see section 5.1.3) CD 105: FITC antibody obtained from Serotec (product code MCA 1557F) was used to counter stain the membranes of hMSC cells which had been loaded with nanosensors containing rhodamine in order to prove nanosensors did not locate exclusively to cellular membranes. After incubation with nanosensors the cells were washed and replenished with fresh culture media. The culture media was then doped with 200 µl CD 105: FITC antibody as supplied and incubated in complete darkness at room temperature for 40 min. The cells were washed once again prior to imaging.

4.2.9 Confocal microscopy Z-stack profiling of internalised nanosensors

Optical sections of individual cells loaded with nanosensors were taken through the *z*-axis of the cell using confocal microscopy to reveal the intracellular localisation of nanosensors. This imaging technique, utilising a mechanical stage and integrated software, allowed optical sectioning of individual cells and $x - z$ or $y - z$ images to be rendered. Subsequent analysis of the rendered images yielded information to the three dimensional intracellular localisation of nanosensors.

4.2.10 Inducing calcium flux in CHO-K1 cells as a model system for intracellular measurement

UTP or ionomycin when added to CHO-K1 cells induces a distinctive calcium flux and was used to assess the functionality of internalised calcium responsive nanosensors (sections 3.4.1). CHO-K1 cells grown in 35 mm cell culture dishes to 60 % confluency were used for confocal microscopy. Cells grown to 60 % confluency in T25 cell culture flasks were removed to 2 ml cell culture media in UV grade disposable plastic cuvettes for work with spectrofluorometry. To induce calcium flux or a sustained high level of intracellular calcium UTP or ionomycin were added to the cells respectively.

Experiments were carried out in a modified Hanks Buffered Saline Solution (HBSS) high in calcium (1.3 mM $CaCl_2$) to provide an extracellular environment high in [free Ca^{2+}], this increased the chances of successful intracellular calcium flux upon stimulation [179].

4.2.11 Calibration of calcium responsive nanosensors

Carefully controlled calcium buffers were made up without modification from McGuigan *et* al [137], each buffer had a specific concentration of free calcium ranging from 0.25 – 5 μM. 5 mg ml^{-1} solutions of calcium responsive nanosensors were made up of each buffer and the corresponding fluorescence was measured using spectrofluorometry. Additionally calibrations were carried out using confocal microscopy as described in section 3.2.7. Ratiometric data analysis was possible due to the digital nature of the images taken with confocal microscopy and their suitability to processing. Both techniques for calibration of nanosensors were subsequently evaluated using free Fluo-4 dye in similar buffer solutions.

4.2.12 Lysing of CHO-K1 cells with tween20

CHO-K1 cells were incubated for 3 h with aliquots of calcium responsive nanosensors. Non-internalised nanosensors were removed with a PBS wash, prior to detaching cells with Trypsin / EGTA; cells were then centrifuged and resuspended in 1.3 mM $CaCl_2$ HBSS. The cuvette was placed in the spectrofluorometer and the baseline monitored for several minutes before 100 μl 5 mM tween 20 was added to the cuvette.

4.2.13 Endosomal identification with LysoTrackerRED®

CHO-K1 cells were incubated with either nanosensors or FITC-Tat conjugate and subsequently washed to remove all surplus or non-internalised synthetic fluorescent nanosensors or peptide conjugates. LysoTrackerRED® (Invitrogen, UK) was incubated

with the cells as per the protocol provided (Invitrogen, MP 07525) with slight modification. 2 µl of the provided solution was added to each 35 mm cell culture dish which was subsequently kept in the dark for 30 min prior to imaging, no additional washing step was required.

4.2.14 Calibration of pH responsive nanosensors

Citrate buffers were made up ranging from pH 3 – 8 and solutions of pH responsive nanosensors (described in section 2.3.4) were made up in each buffer at 5 mg ml^{-1}. Corresponding fluorescence measurements were taken using spectrofluorometry. Additionally calibrations were carried out with confocal microscopy and ratiometric data analysis was as described in section 4.2.11.

4.2.15 Measuring intracellular pH with nanosensors

CHO-K1 cells incubated with pH responsive nanosensors were imaged using confocal microscopy and ratiometric analysis of fluorescence from the FITC: TRITC fluorophore pair entrapped within the nanosensor was analysed and compared with the pH calibrations acquired in section 4.2.14. Direct comparison between calibration solutions and pH nanosensors located in the intracellular domain was possible as all microscope settings were stringently preserved between experiments. In order to acquire the most accurate measurements possible the average fluorescent intensity was taken for the entire 512 x 512 pixel image for every image taken in both FITC (green) and TRITC (red) channels. The ratio of the average fluorescence intensity was used to calculate pH measurements in the cell in conjunction with similarly expressed pH measurements of the calibration solutions.

4.3 Results and Discussion

4.3.1 Proof of Tat function with FITC fluorophore conjugates

It was expected that the Tat peptide synthesised in-house would act as described in the literature, that it would internalise within cells after crossing the cellular membrane when added to the cell culture media and incubated at 37 °C. To test this however the Tat peptide would have to effect a change upon the cell which could be observed. It is colourless in liquid and does not generate a known biochemical event which could be measured easily; therefore simply incubating the Tat peptide with a plate of cells would not give an observable result even if internalisation was successful. The simplest change which could be achieved was one of colour, this could be observed with confocal microscopy and to this end it was decided to conjugate fluorophore(s) to each Tat in the hope of creating a fluorescently labelled molecule which could be viewed upon intracellular localisation.

Figure 64 Schematic representation of FITC-Tat conjugate (not relative scale or fluorophore position). There are 8 sites (Arg and Lys) on the Tat peptide for isothiocyanate reaction, the N-terminus may also allow for an additional attachment.

Initial experiments were carried out using CHO-K1 cells, several cell cultures were observed after being incubated for one hour with increasing concentrations of FITC-Tat conjugate in the culture media. The results from these experiments illustrated in Figure 65 showed that increased concentration of FITC-Tat conjugate in the culture media led to an increase in cellular fluorescence at 500 – 540 nm as expected for fluorescein with a peak of emission at 520 nm. In order to provide a representative control, the concentration of FITC molecules in the control cell culture was maintained at an equal level to the 5 μl ml^{-1} FITC-Tat conjugate. This was assessed by spectrofluorometry and

an example of a sample of culture media from each plate prior to incubation is shown in Figure 66.

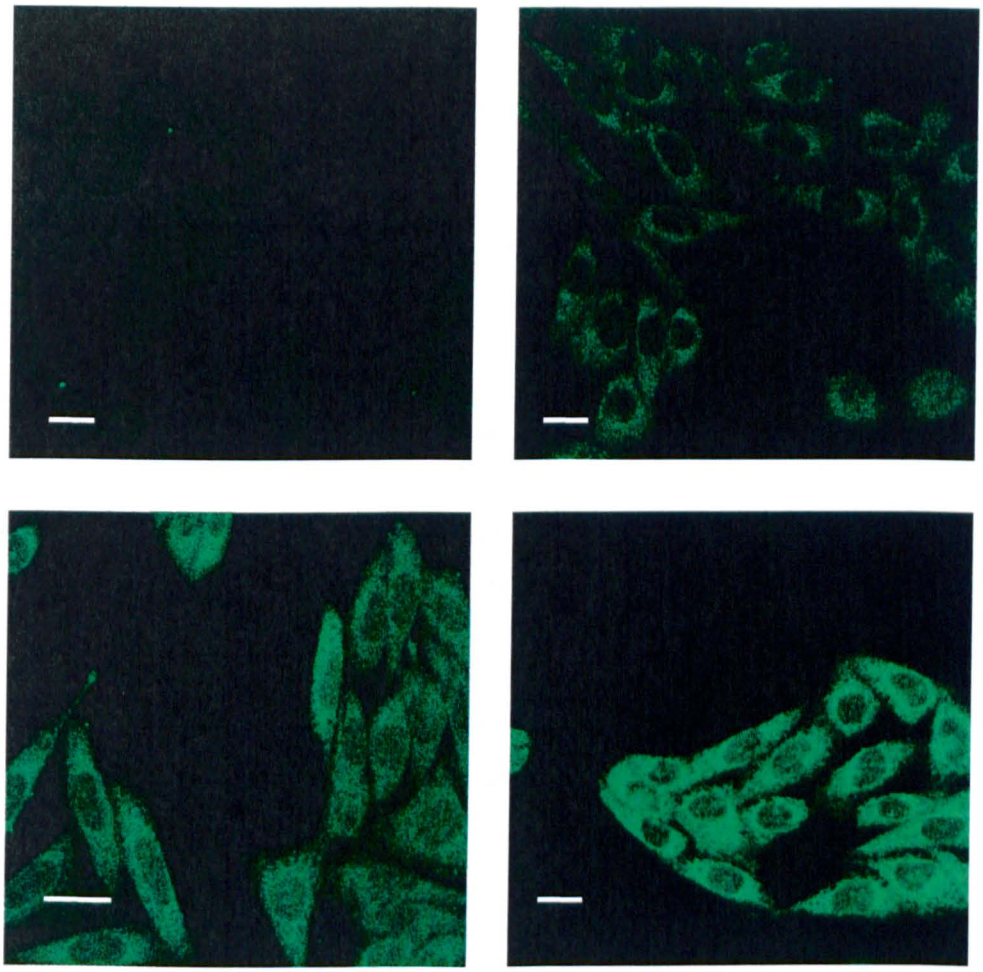

Figure 65 Incubation of fluorescein labelled Tat with CHO cells. In the free FITC control, FITC was dissolved in the culture medium so that the fluorescence of that medium equalled the 0.005 % (v/v) concentration of FITC-Tat conjugate. Free FITC control (top left) 0.001 % (v/v) FITC-Tat conjugate (top right) 0.002 % (v/v) FITC-Tat conjugate (bottom left) 0.005 % (v/v) FITC-Tat conjugate (bottom right). x63 magnification, scale bar = 30 μm.

The control shows very slight fluorescence comparatively suggesting that very little or no free FITC passively diffused into the cells within the one hour incubation. These experiments showed that the synthesised Tat peptide enhances the uptake of FITC into CHO-K1 cells and is therefore exhibiting the same properties as CPPs described in the literature.

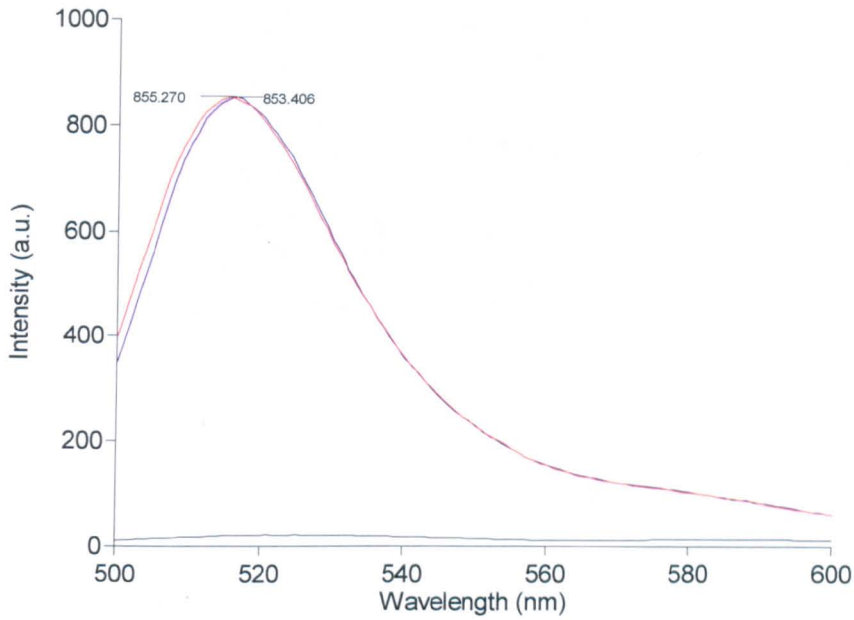

Figure 66 Graph showing equivalent fluorescence of cell culture media loaded with FITC-Tat conjugate (red trace) and free FITC dye (purple trace). The background fluorescence of DMEM F12 cell culture media (phenol red is present as a pH indicator) is shown as the black trace.

A sample of FITC-Tat conjugate was sent to collaborators at The University of Newcastle who carried out an incubation experiment with A172 human glioblastoma cells. The reasoning behind this was two-fold; primarily to investigate whether the Tat mediated delivery system was applicable to another cell line other than CHO-K1, but also to assess the ease with which Tat based system could be used by a different group with no specialist knowledge in intracellular delivery. As seen in Figure 67, the difference between the passive diffusion of free FITC into the cells and that of Tat conjugated FITC is striking. Again an adequate control representative of FITC concentration was in place.

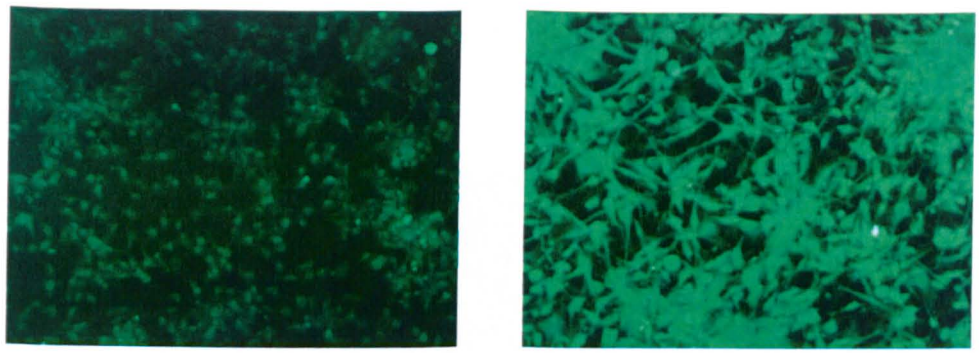

Figure 67 Control of free FITC (left panel) compared with an equal amount of FITC conjugated to Tat peptide (right panel), x10 magnification.

Being absolutely certain of differences between control and treated cells can sometimes be tricky especially when working with very low levels of fluorescence. Further to this the images presented are of different plates imaged separately, the reader is only told that the manner in which the images were taken remained constant. Simple changes in the conditions of image capture, even ambient room temperature can affect the image. For example it would be very easy to produce the same images in Figure 65 and Figure 67 by simply altering the source laser power or PMT voltage when viewing the same plate of cells. With this in mind it was thought that a clear and indisputable image could be produced by means of having treated and control cells alongside each other in the same culture dish and imaging them jointly. To do this it was necessary to take two flasks of cells, one as a control, one incubated with FITC-Tat conjugate, and subsequently mix the two populations prior to imaging. This would provide a population of cells having both fluorescent and non-fluorescent contributions if Tat had truly enhanced the uptake of FITC.

As shown in Figure 68 it was possible to obtain this image and to further assure that the Tat peptide synthesised in-house acts as a functional CPP. Though it cannot be 100 % verified it is most likely that a difference in fluorescence between cells indicates they are from the different populations respectively. This experiment was also the first indication that FITC-Tat conjugate remained in live cells after 24 h – the cells were allowed 24 h to settle after trypsinisation. This suggests that the cells do not completely eliminate the FITC-Tat conjugate within 24 h and that internalised Tat does not reduce cellular viability, as the cells had adhered to the cell culture dish and although CHO-K1

cells tend to take 48 h to become fully spread and attain the characteristic morphology of healthy CHO-K1 cells.

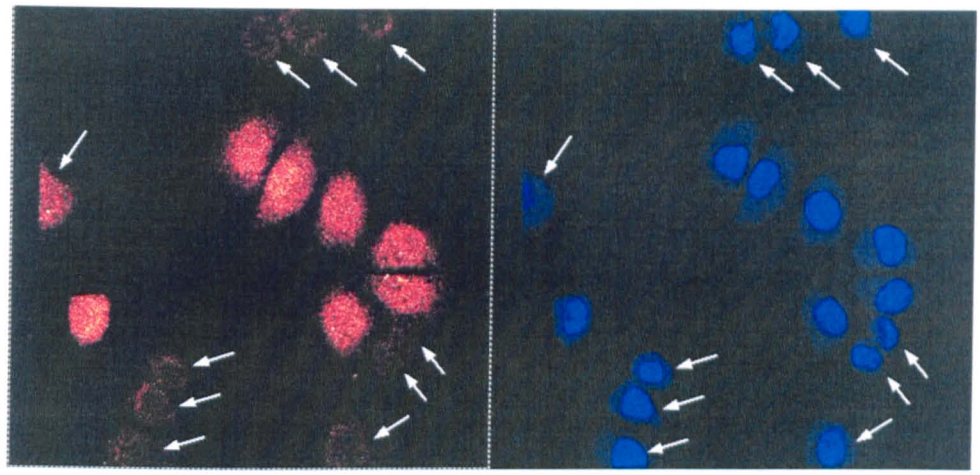

Figure 68 Mixed population of CHO-K1 cells showing cells incubated with free FITC only (white arrows) and those incubated with FITC-Tat conjugate (fluorescent cells), x63 magnification, fluorescence from FITC is shown in the left panel; additionally cells were stained with DRAQ5 nuclear stain to illuminate each cell's location improving image clarity (right).

4.3.2 Tat delivery of nanosensors

After establishing the functionality of the Tat peptide, investigation into the possibility of delivering a much larger cargo into the cells was investigated. Similar experiments to those described for FITC-Tat conjugate (section 4.3.1) were carried out substituting the FITC-Tat conjugate with Tat functionalised nanosensors containing fluorescein (FITC-Tat nanosensors (fabrication reported in section 4.2.5)). The true potential of CPPs as a tool for delivering nanosensors was ascertained by delivering FITC-Tat nanosensors into CHO-K1 cells during a short incubation. Figure 69 shows a single CHO-K1 cell in which nanosensors have localised within its cytoplasm. The focal plane of the image dissects the nucleus of the cell at its mid point relative to the *z* axis.

The image definitely appears to show clear localisation of nanosensors in the cytoplasmic region of the cell; it could be concluded that the delivery was successful from this image alone. It was not expected that the nanosensors would locate to the

nucleus as the size exclusion properties of the nuclear membrane would prevent nuclear membrane translocation. It was a concern however that the imaging technique may be misleading when using a single fluorophore in this manner.

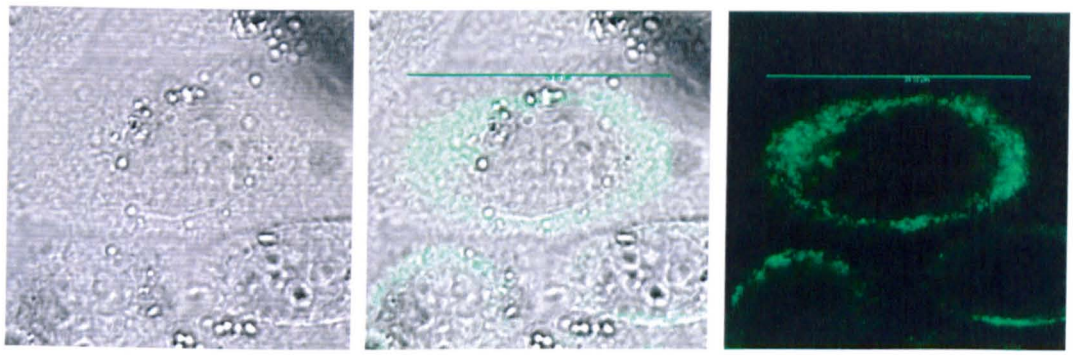

Figure 69 1.25 mg ml^{-1} FITC-Tat nanosensors, 2 h incubation delivery, assessed and imaged with confocal microscopy, x63 magnification. Bright field (left) overlay (middle) and FITC fluorescence (right).

From this image it is certainly possible to say there is a substantial amount of fluorescence associated with what appears to be the cytoplasmic area of the cell but this image itself is not definitive. If one considers the way in which the confocal microscope works, particularly the point spread function (also known as the voxel) and how the image forms as this point is scanned across the sample, it is possible to describe a scenario where the nanosensors are only located on the extracellular surface but the same image as seen in Figure 69 is formed. Figure 70 is illustrated to represent a three dimensional volume from which information is gathered to form the image; this is a cross sectional area or slice, an individual *z* stack. Regardless of where a fluorophore lies in the *z* axis of this volume it will be represented in the two dimensional image produced from the scanning across the sample of the point spread function.

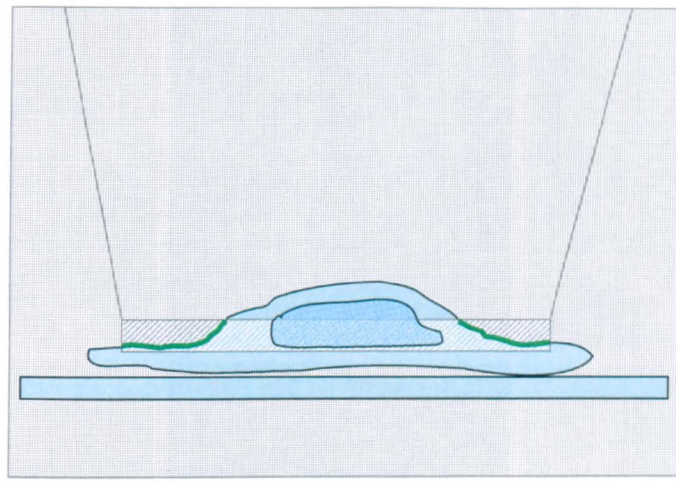

Figure 70 Schematic of confocal scanning area.

If the fluorescence is located only on the membrane as depicted and the pin-hole is such that the point spread function is thin enough to capture the upper surface then a top down two-dimensional representation of this volume would look like a concentric circle of fluorescence against a dark background, Figure 71, which shows a striking resemblance to the image of the CHO-K1 cell in Figure 69.

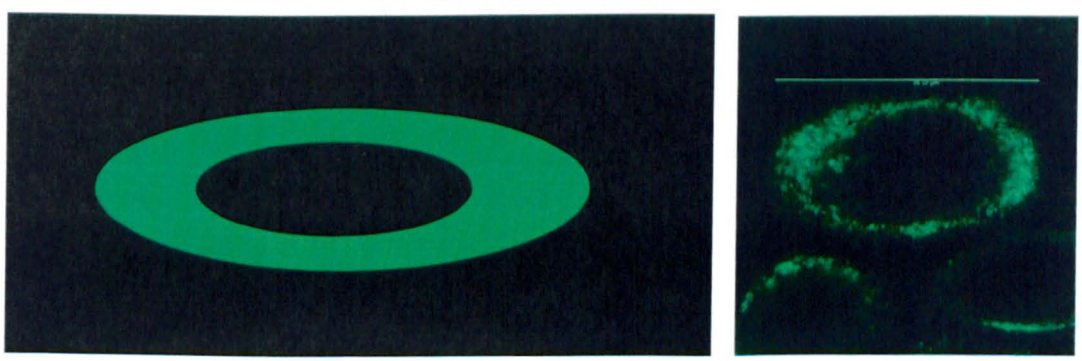

Figure 71 Schematic of a confocal image of a scanned area compared with the fluorescence image of a CHO-K1 cell loaded with FITC-Tat nanosensors.

Similar images were collected for A172 human glioblastoma cells as shown in Figure 72.

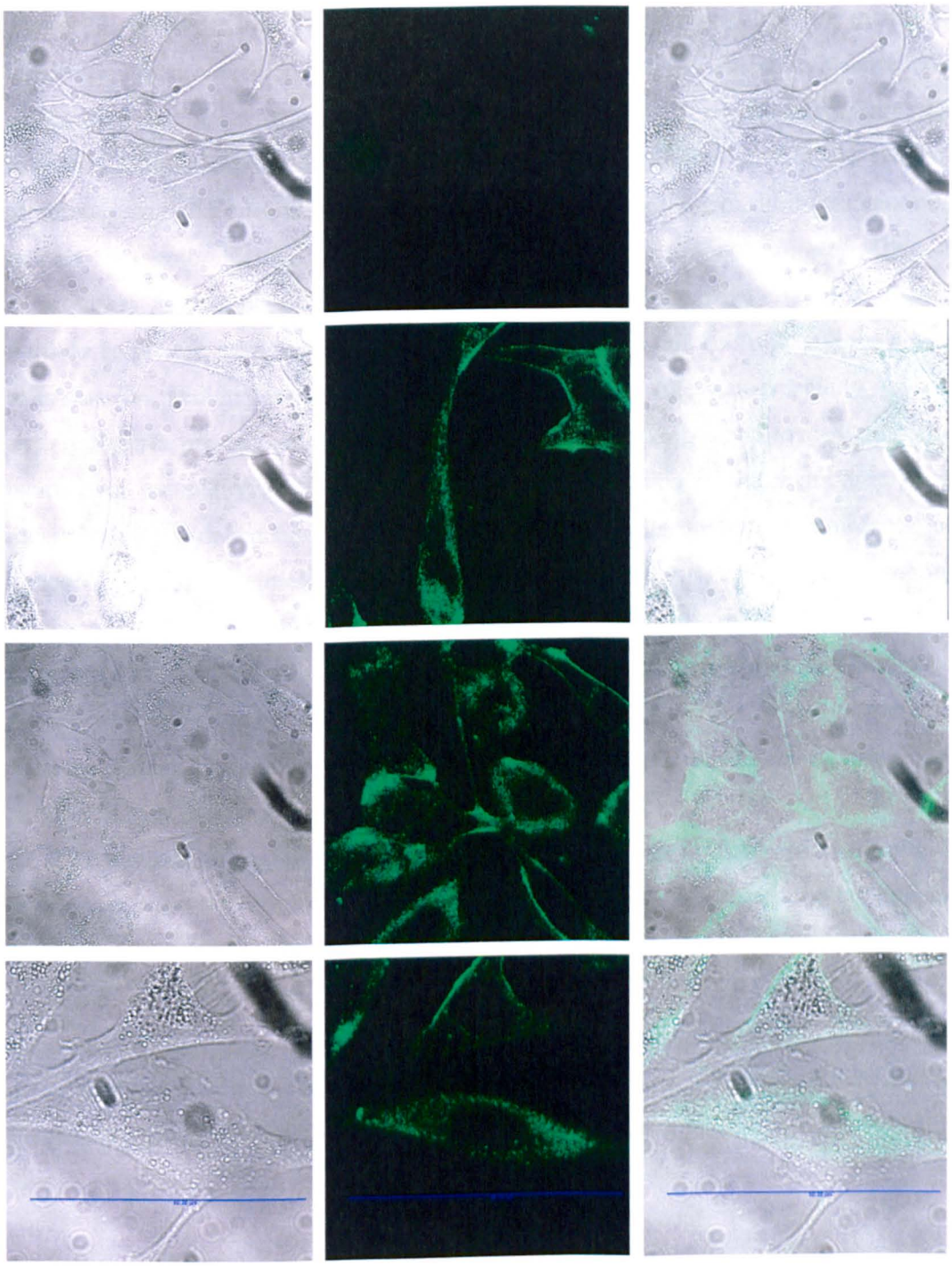

Figure 72 A172 human glioblastoma cells loaded with FITC nanosensors, x63 magnification with individual image digital zoom. The top panel of images show control cells (incubated with FITC nanosensors which had not been Tat functionalised) demonstrating no fluorescence as expected, thus confirming both that the cells do not exhibit auto-fluorescence at a level which could affect interpretation and that nanosensors do not internalise into these cells unless tailored to do so.

Again this gives the impression of successful delivery but the possibility of membrane localisation is not excluded by these images. Thus a means to elucidate a more exact localisation at least with regards to intra / extracellular delivery was necessary. The relatively simple way to do this was to use florescent dyes that specifically stain the membrane and allow for clear identification when imaging. Obviously it was necessary to stain the membrane with a fluorophore of different colour to that entrapped within the nanosensors. It was possible utilise human mesenchymal stem cells (hMSC) for this purpose as the use of membrane markers was routine with this cell line, and the chance to assess Tat mediated nanosensor delivery with this cell line was especially valuable considering the present and great interest in stem cell based regenerative medicine. Thus nanosensor incubations with hMSC and subsequent staining of the membrane would ideally show independent localisation of the two fluorophores (membrane and nanosensor) proving intracellular delivery of nanosensors. The chosen membrane marker was mouse anti-human CD 105: FITC antibody which necessitated an alternative fluorophore to be entrapped in the nanosensors. The alternative fluorophore chosen was rhodamine B due to its spectral characteristics, in that it could be excited with the 568 nm krypton laser of the confocal microscope and distinguished from FITC, and that it was readily available in a dextran conjugated form of 10,000 MW, identical to the previously used FITC-dextran. The incubation conditions were similar to previous experiments but included an additional incubation of CD marker after the wash stage (for removing nanosensors which had not been internalised). As shown in Figure 73 the initial images were similar to those taken of CHO-K1 cells loaded with FITC nanosensors, again there appears to be clear cytoplasmic localisation. This is significant as the similarity in behaviour with a different dye argues that the entrapment method within the nanosensor matrix is robust, however the same argument remains regarding possible membrane location.

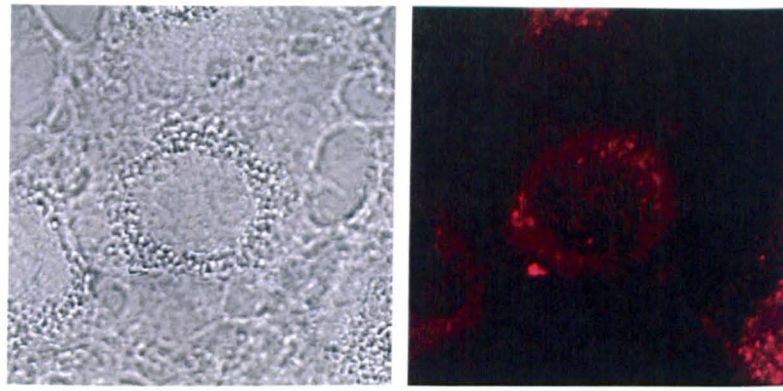

Figure 73 hMSC cell loaded with rhodamine B nanosensors, x63 magnification with x2.54 digital zoom.

The additional incubation with CD 105: FITC antibody made it possible to clearly identify cellular membranes shown in the green channel after 488 nm excitation and emission collection for FITC. Figure 74 gives a clear indication that the nanosensors are not localised on the membranes as feared but have passed through the cellular membranes and located within the cytoplasmic region of each cell. Had the nanosensors located upon the cell membrane then the pattern of fluorescence would be identical for each colour and in the overlay image the predominant colour would be the sum of each channel – yellow in this instance.

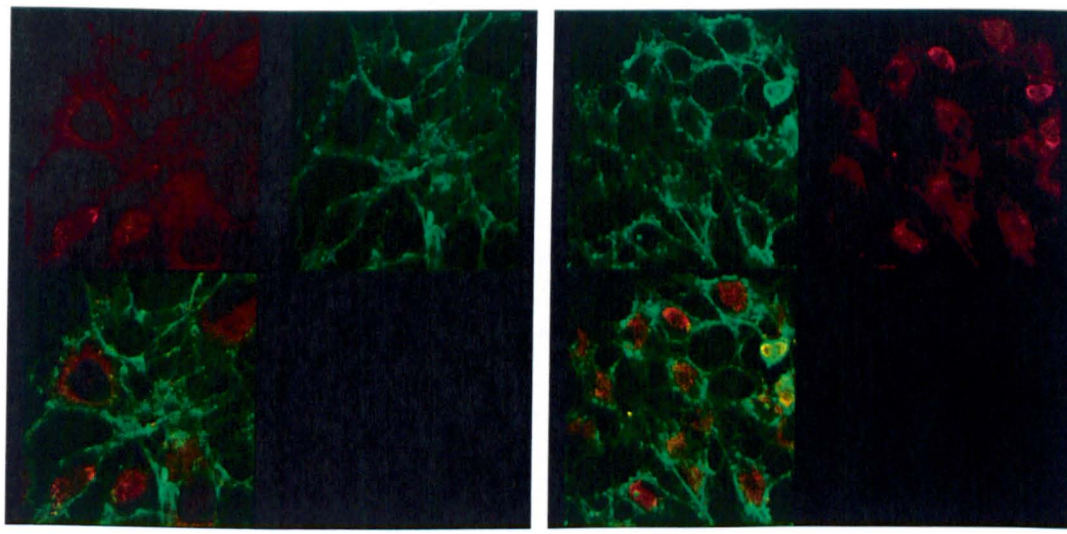

Figure 74 hMSC cells loaded with rhodamine B nanosensors (red) and counter stained with mouse anti-human CD 105: FITC antibody (green), x63 magnification.

4.3.3 Post-delivery intracellular nanosensor localisation

As the development of this delivery method continued and the protocols of fabrication, delivery, washing, and imaging became more refined it began to appear that the nanosensors may not have been uniformly distributed throughout the cytoplasm. It was expected that if the cell had no recognition of nanosensor presence then they would be distributed throughout the cytoplasm in a random, yet consistent, fashion. However, as depicted in Figure 75, enhanced imaging allowed better insight into the sub-cellular distribution of the nanosensors and it was shown that areas of punctate fluorescence existed within the cell suggesting a non-uniform distribution of nanosensors. In addition, being able to see clear areas of fluorescence in this way suggests the nanosensors are congregated into a defined space rather than diffuse throughout the cytoplasm. Individual nanosensors are much smaller than the resolution of the optical system and can therefore not be represented by these fluorescent areas.

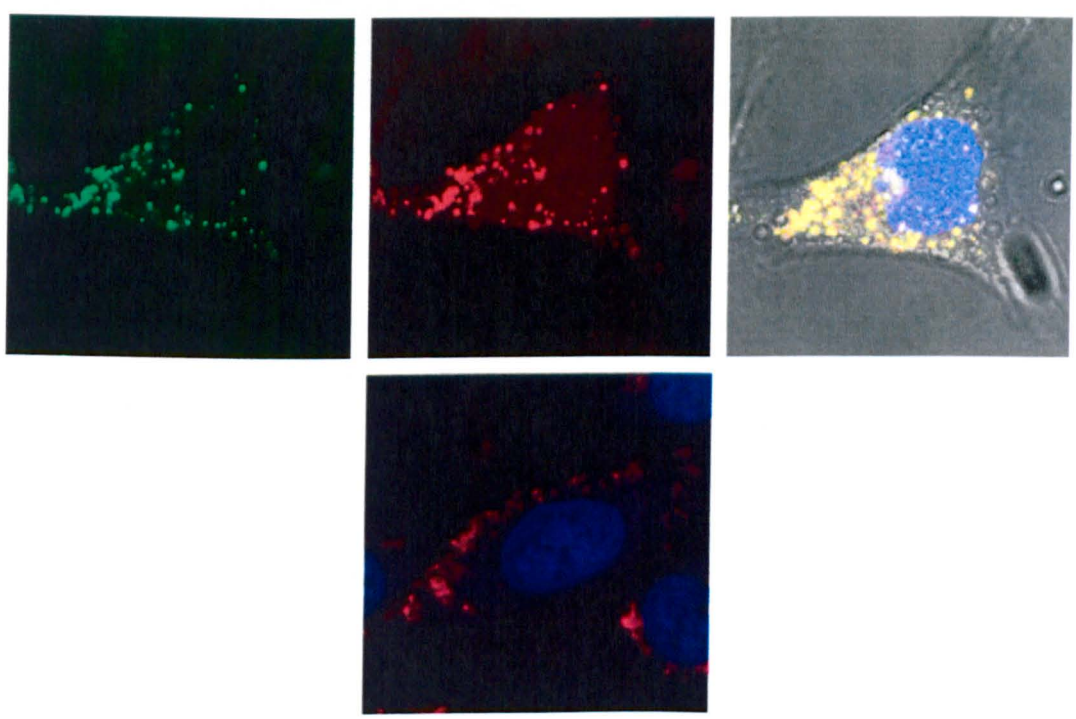

Figure 75 Punctate fluorescence seen in A172 human glioblastoma cells loaded with FITC: TRITC nanosensors (top panels) and CHO-K1 cells after loading with rhodamine B nanosensors, x63 magnification. Cells were counter stained with DRAQ5 nuclear stain.

z-stack profiles were captured for individual cells (a series of two dimensional images are collected whilst altering the position of the *z*-axis) to improve the image detail of the three dimensional position of nanosensors. Microscope software renders the stack of two dimensional images into a three dimensional volume and enables the user to look through the stack of images from an *x-z* or *y-z* perspective. This perspective gives more information into the localisation of fluorescence in the cell as seen in Figure 76.

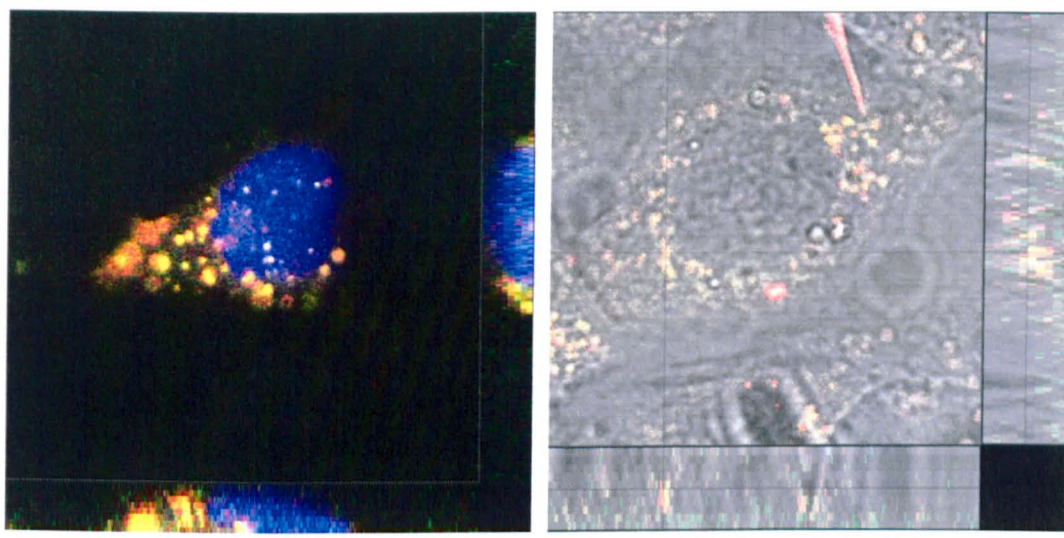

Figure 76 Individual *x-y* sections of image series of an A172 human glioblastoma cell (left, bright field omitted, x63 magnification x2.68 digital zoom) and CHO-K1 (right, x63 magnification, x3.22 digital zoom) loaded with FITC: TRITC nanosensors with corresponding *x-z* and *y-z* renditions of the cell.

The panels to the right and bottom of each image reveal the internal fluorescence of the cell if viewed from an *x-z* or *y-z* perspective respectively at a particular dissection (i.e. if one were to take an infinitely small slice of the cell and view this side on). Not only is it clear to see that the discrete areas of fluorescence are located between the nucleus and the cell wall in an *x-y* plane but also in *x-z* and *y-z* planes (i.e. within the cytoplasmic domain). This further qualifies intracellular delivery with a second technique (the other being based on counter staining the membrane as shown previously) and provides more information on the size and shape of the observed punctuate fluorescence. The information presented in the images obtained led to an overall suspicion that the cell was actively involved in recognition and ultimately the cellular distribution of Tat functionalised nanosensors under the incubation conditions used. It was not known

however if this would have any impact upon the functionality of the nanosensors after intracellular delivery.

4.3.4 Intracellular measurements with functional nanosensors

The ultimate objective of a Tat based delivery system would be to measure a real-time response of nanosensors to a specific analyte after successful intracellular delivery - this being the most comprehensive assessment of the ability of Tat to deliver a nanosensor cargo into a cell whilst allowing the nanosensor to retain its ability to sense the environment around it. Not only does this mean the delivery process must not induce any biochemical changes or cellular functions, but means Tat must also deliver the nanosensor to the cytoplasm (or chosen micro domain) without impairing the function of the nanosensor through, for example, protein adsorption or vesicle entrapment. The analyte chosen for this assay was calcium. Primarily this was because calcium plays such an important role in cellular biochemistry, as a secondary messenger for example, but also because a reliable method for generating a free Ca^{2+} flux was in place for CHO-K1 cells through the simple addition of UTP or ionomycin to the culture media, as explained in more detail in chapter 3.

After loading CHO-K1 cells with nanosensors which contain Fluo-4 (a calcium sensitive fluorophore with a K_d around 600 nM) and Alexafluor568 (acting as a reference dye) a time series of images was taken with confocal microscopy whilst an aliquot of UTP or ionomycin was added to the culture media and the subsequent increase in fluorescence monitored. Control cells loaded with Fluo-4 AM ester free dye throughout the cell gave a classical response after the addition of both UTP and ionomycin, Figure 77 comparative to reports in the literature [134].

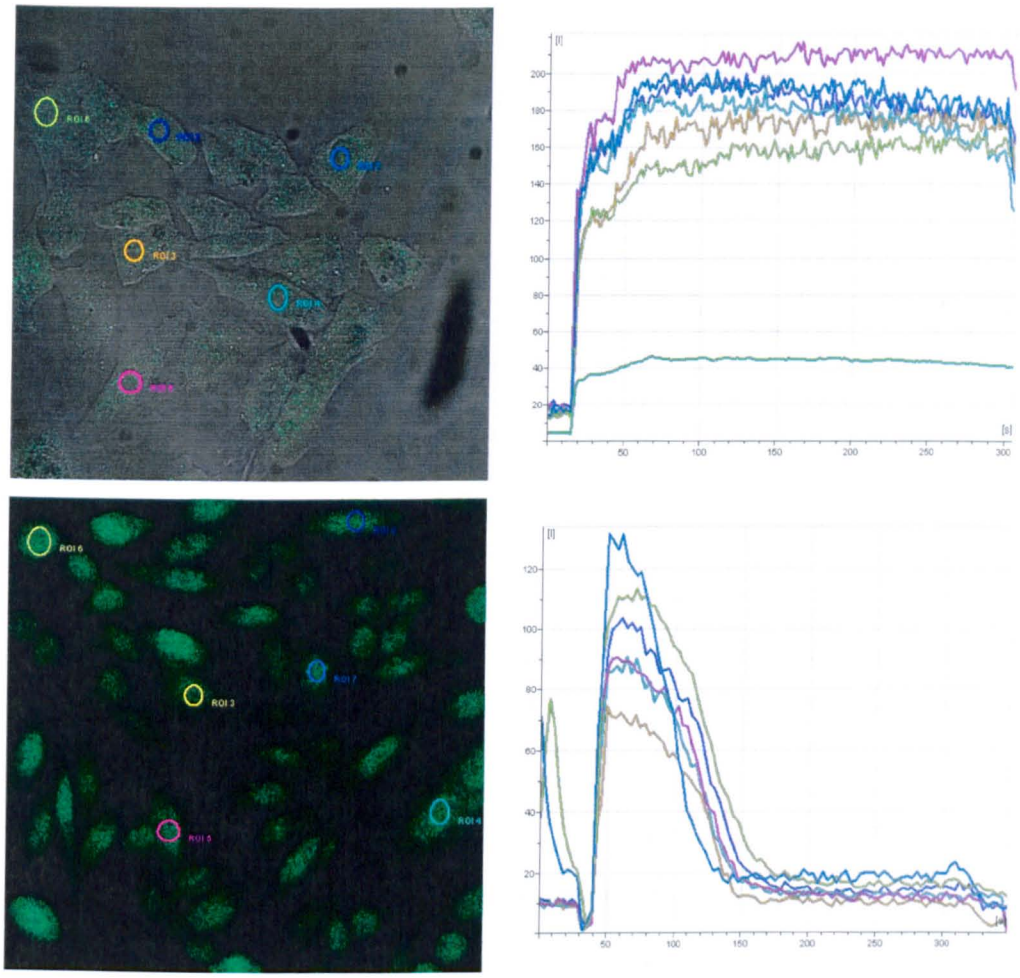

Figure 77 Control response of free dye to ionomycin (top) and UTP (bottom). A UTP response gives a transient calcium flux whilst ionomycin addition leads to a consistently elevated calcium level.

No increase in fluorescence was observed when cells loaded with calcium sensitive nanosensors were activated with ionomycin (Figure 78). UTP addition similarly appeared not to stimulate a response when measured with similar nanosensors.

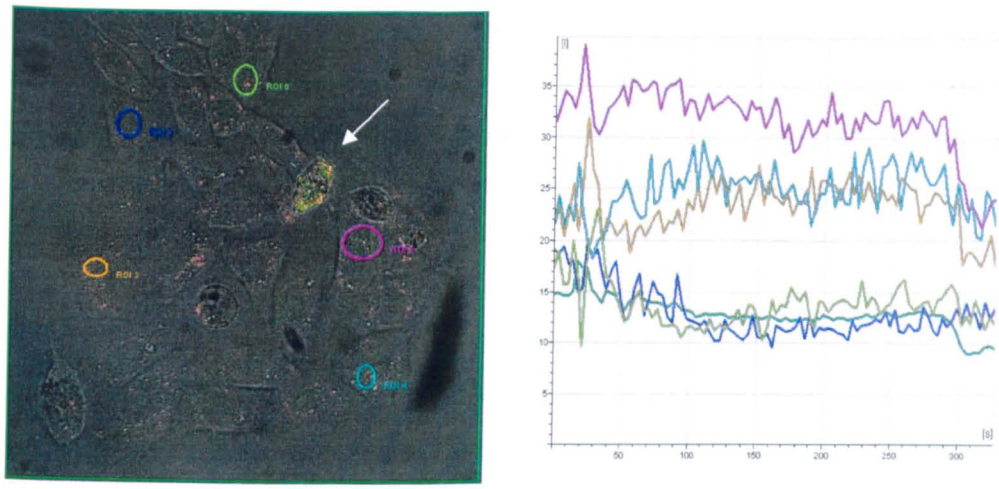

Figure 78 Nanosensor response to the addition of ionomycin (the cell highlighted with an arrow is explained later).

This was significant because the sensors used had been calibrated with calcium buffers (in the range of basal to activated free-calcium levels (100 nM - 1200 nM) of CHO-K1 cells) and responded accordingly, Figure 79.

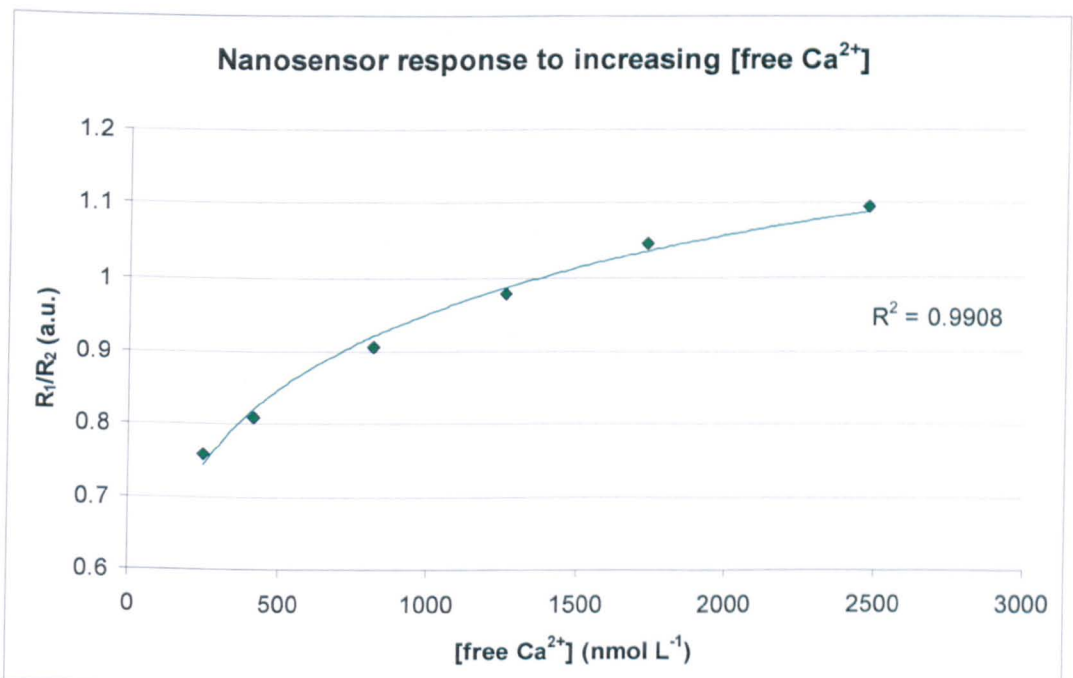

Figure 79 Nanosensor response to buffers increasing in free Ca^{2+} concentration.

Knowing that the nanosensors used were responsive to calcium flux, the calcium concentration could be characteristically elevated in CHO-K1 cells, and that intracellular nanosensor delivery was an established technique, the absence of calcium flux measurements could suggest one of two things. Firstly, there was simply not enough fluorescence signal coming from the sensors to allow for an increase in fluorescence to be distinguished from background noise. Or, secondly, that the sensors were not in an environment where they were able to detect an increase in free-calcium. This may have been due to random protein binding at the nanosensor surface, although many protein adsorption studies have been carried out showing that the fluorophores entrapped within nanosensors are unaffected and retain functionality in a protein rich environment [95]. The other seemingly logical possibility was the entrapment of the nanosensors within a micro environment of the cell which did not experience any calcium flux during the experiments albeit the rest of the cell did experience an elevated level of free Ca^{2+}.

It was necessary to distinguish which factor prevented the induced free Ca^{2+} flux from being detected and a way of increasing the overall signal was sought. With confocal microscopy it is possible, as mentioned previously, to increase both laser power and the voltage of the PMT detectors in order to induce and amplify the fluorescence respectively. However these were both already at a high level and it did not seem sensible to force a signal from a low number of cells experiencing the perturbation associated with a high powered laser. With this in mind it seemed logical to look at a greater number of cells simultaneously; to this end a fluorescence spectrophotometer was employed to look at a cell suspension of CHO-K1 whilst previously described UTP / ionomycin additions were performed. The same controls were carried out to ensure a calcium flux could be monitored and as shown in Figure 80 the response of CHO-K1 cells containing free Fluo-4 in suspension was faultless.

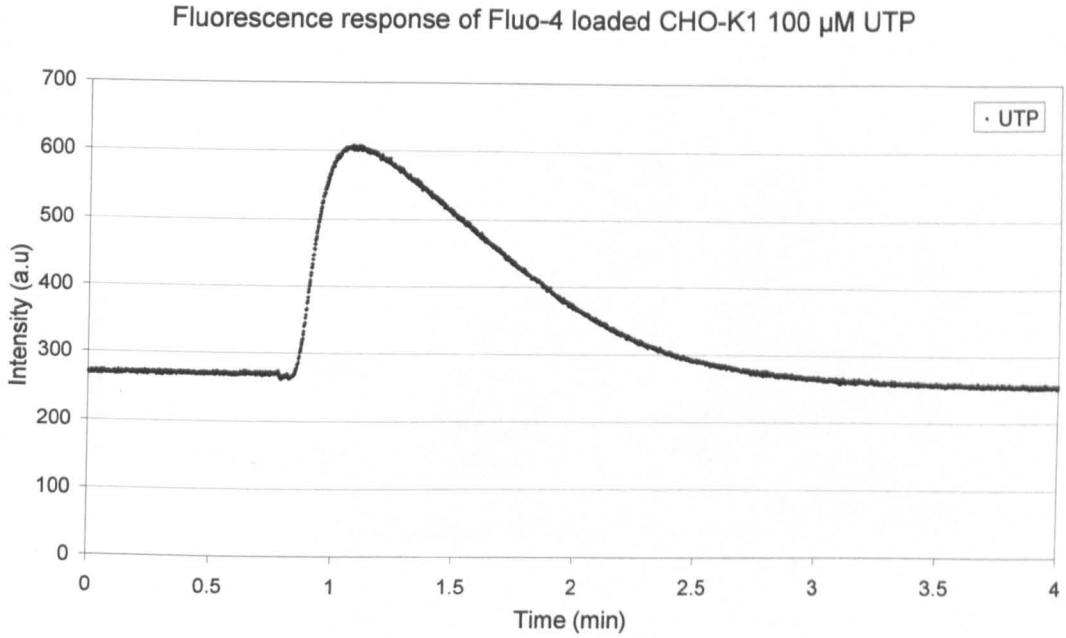

Figure 80 Fluorescence response of CHO-K1 cells in suspension loaded with Fluo-4 free dye to UTP addition.

The same experiment carried out on CHO-K1 cells loaded with nanosensors did not produce the same response. As shown in Figure 81 there was no classical UTP response. The trace in Figure 81 is somewhat noisier than the control Figure 77; this is because there is less fluorescence per cell, purely because there are fewer fluorophores per cell than when loaded with free dye. However the signal was amplified by increasing the PMT voltage so the base line was of a similar level to that of the control and had a classical UTP response been observed the fluorescence should have increased which, although with a little noise, would still have been evident.

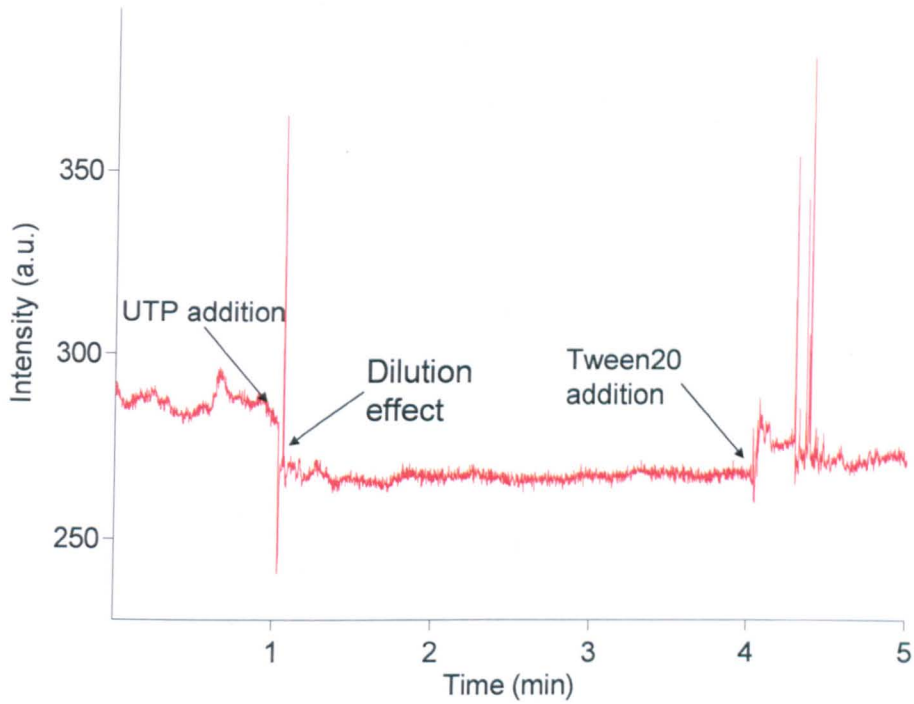

Figure 81 Fluorescence response of CHO-K1 cells in suspension loaded with Fluo-4 nanosensors to UTP addition.

As can be seen the addition of an aliquot of UTP at one minute did not induce the increase in fluorescence but in fact led to an overall decrease in fluorescence in stark contrast to the response as hoped. This can be explained in terms of dilution, as the addition of a non-fluorescent volume has reduced the concentration of fluorophores in the cuvette suggesting the Fluo-4 did not experience any increase in calcium. After this addition a stable level of fluorescence was monitored and at four minutes the cells were lysed with 10 mM tween20. A subsequent small increase in fluorescence was observed which at first may seem somewhat puzzling. It implies however that nanosensors were inside the cell yet only when the cell was lysed did they come into contact with a higher concentration of free-calcium. Had they experienced a higher concentration of free-calcium whilst still in the cell an increase in fluorescence would have been observed after the addition of UTP. An interesting artefact of Figure 78 helps explain this theory. A single cell (highlighted) located top right in the cluster of cells appears brighter than all the rest in the same image. It is assumed that this cell is no longer viable and that

dead cells fluoresce more because cellular membranes are one of the first structures to lose integrity after cell death allowing fluorophores to freely diffuse into the cell. However in this scenario one would expect the cell to fluoresce more strongly in the same colour to the cells around it as it is only a concentration effect. This is not the case here as it is clearly yellow in contrast to the red cells in the same image. Considering the pair of fluorophores entrapped in the nanosensors, free Ca^{2+} sensitive Fluo-4 (green) and free Ca^{2+} insensitive Alex568 (red) reference dye, it is logical to assume that in a low [free Ca^{2+}] environment the Fluo-4 would essentially be 'off' and only red light emitted from Alexa568 would be observed. In a high [free Ca^{2+}] environment however Fluo-4 would be 'on' and the combination of green and red light would be imaged as patches of yellow. Therefore, with membranes which have lost integrity, this cell has allowed higher than normal levels of free Ca^{2+} to enter intracellular compartments which the nanosensors respond to with an increase in Fluo-4 fluorescence. Fluo-4 emission plus Alex568 emission produces a yellow signal.

Combining the evidence from the initial experiments developing Tat delivery, when pictures showing punctate patterns of fluorescence in the cytoplasmic region were observed, and the latter experiments assessing a functional response to a know analyte flux it is suggested that the nanosensors locate into endosomes / lysosomes upon entry to the cells and are essentially sheltered from the cytoplasm.

4.3.5 Illuminating intracellular nanosensor locale with LysoTrackerRED®

To this point only circumstantial evidence was available for endosomal localisation so it was deemed worthwhile investing in a scheme to identify endosomal position in the cytoplasm and confirm that this co-localised with the fluorescence attributed to nanosensors. For this an endosome dye was chosen, LysoTrackerRED®, which produced a strong red colour when the dye located in the acidic environment of an endosome. This could then be used in conjunction with green (FITC) nanosensors in order to produce yellow fluorescence when nanosensors associated with endosomes were imaged. Figure 82 shows endosomal location in CHO-K1 cells after incubation with LysoTrackerRED®.

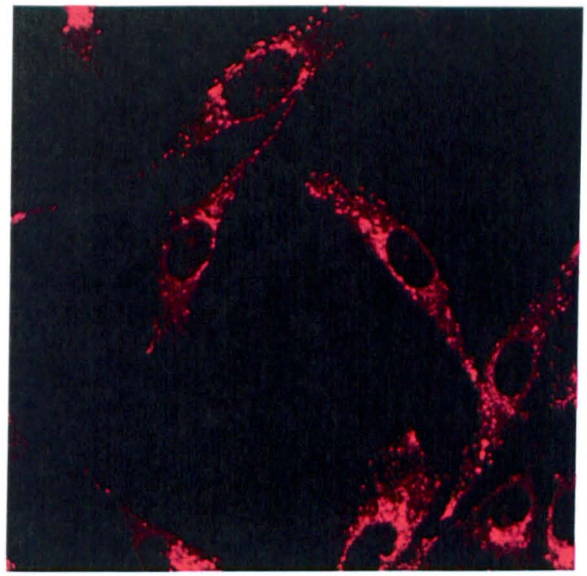

Figure 82 Endosome identification with LysoTrackerRED®, x63 magnification with x1.72 digital zoom.

The cells in Figure 83 show the punctate pattern of fluorescence illustrating the position of endosomal bodies in CHO-K1 cells. In contrast, the distribution of FITC-Tat conjugate is shown in the cell in Figure 84; there is no evidence of co-localised fluorescence between FITC-Tat conjugate and endosomes which would have been indicated with yellow fluorescence.

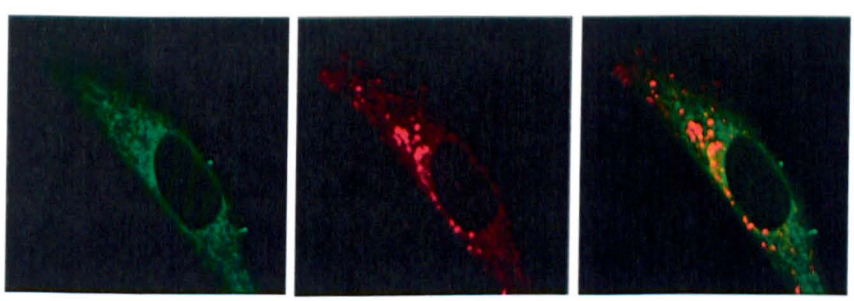

Figure 83 FITC-Tat conjugate and endosomes do not show co-localised fluorescence, x63 magnification with x3.00 digital zoom.

Visualising endosomes with LysoTrackerRED® allowed for investigation into the localisation of Tat-functionalised nanosensors after delivery, Figure 84 and Figure 85 provide evidence for endosomal localisation as punctate yellow fluorescence.

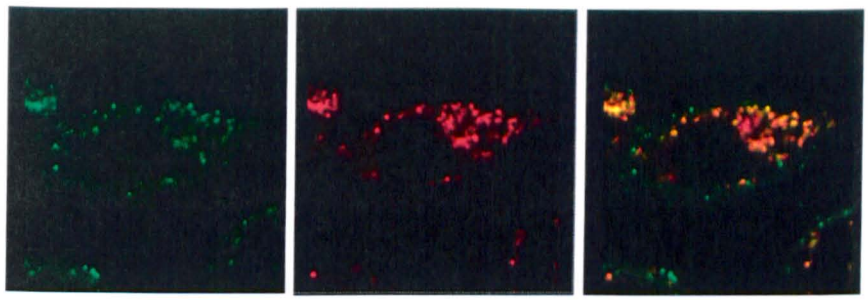

Figure 84 Co-localisation of fluorescence of LysoTrackerRED® and FITC nanosensors, x63 magnification with x3.42 digital zoom, gives an apparent yellow colour when imaged with confocal laser scanning microscopy.

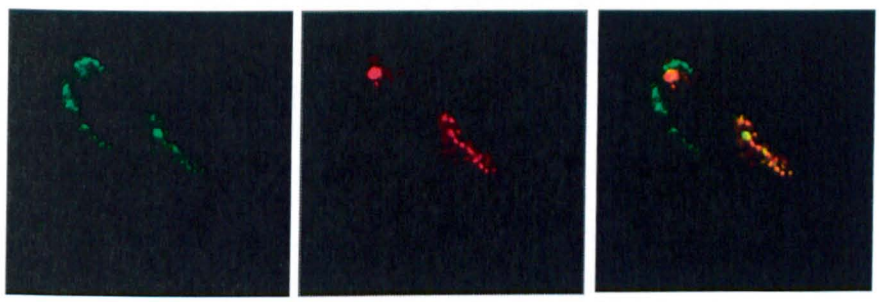

Figure 85 Interaction of Tat-functionalised nanosensors with the cellular membrane may initiate the formation of endosomes, x63 magnification with x3.28 digital zoom.

The fluorescent pattern shows FITC nanosensors both on the surface of the cell and located within endosome / lysosomes within the cytoplasm. It seems to indicate that all endosome / lysosomes have nanosensors entrapped within them, the distinction between green and yellow fluorescence helping to demonstrate that combined green and red fluorescence, giving yellow, only occurs when they are packed together. It is known from the control incubation of FITC-Tat conjugate (Figure 82) that LysoTrackerRED® fluorescence is strongly red in isolation so it can be concluded the nanosensors are closely associated with endosomes after Tat mediated delivery. Figure 85 is particularly interesting as it seems to show greater numbers of endosomes in the area of the cell where nanosensor internalisation has occurred. This coincides with little to no green fluorescence on the cellular membrane in the same area of the cell. This scenario is vice versa towards the left of the cell where there is greater membrane bound fluorescence and little endosomal fluorescence. Does this suggest that the formation of endosomes is triggered through the internalisation process of Tat-functionalised nanosensors to a higher number than the normal levels generally found in control state CHO-K1 cells?

To answer this, CHO-K1 cells incubated with FITC-Tat conjugate were contrasted with CHO-K1 cells incubated with Tat functionalised FITC nanosensors, both were counter stained with LysoTrackerRED® and the relative numbers of endosomes were assessed in images from each population, Figure 86. It does appear that the presence of Tat-coated nanosensors triggers the formation of a greater number of endosomes compared with the presence of FITC-Tat conjugate within CHO-K1 cells. This is most likely due to the difference in size between FITC, having a hydrodynamic diameter of approximately 1 nm, and nanosensors, typically 40 – 60 nm in diameter.

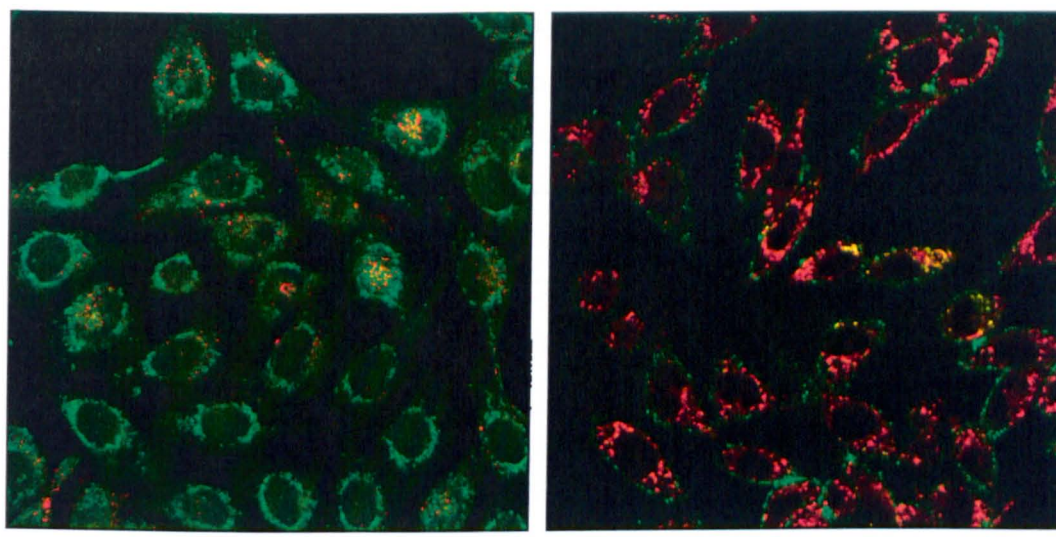

Figure 86 CHO-K1 cells incubated with FITC-Tat conjugate (left) and FITC-Tat nanosensors (right) both stained with LysoTrackerRED®, x63 magnification. Seemingly incubation with nanosensors leads to the formation of more endosomes than with FITC-Tat conjugate.

4.3.6 Measuring intracellular pH with nanosensors as proof of endosomal / lysosomal localisation

The results reported up to this point indicated that endocytosis or endocytosis-like mechanisms were implicated in the localisation of Tat delivered nanosensors within the cell. To test this proposition, nanosensors capable of measuring pH were delivered to the cell so that the post-delivery environment could be evaluated and compared with literature values for endosomes, late endosomes, and lysosomes. It was hypothesised that if Tat mediated delivery of nanosensors triggers endocytosis, and the nanosensors

become subsequently located within these structures, it would be possible to use the pH response of nanosensors to measure the pH of the endosome / lysosome and thus prove endosomal localisation. Although lysosomal pH can vary between individual cells and cell types it is generally accepted that the lysosomal pH is approximately 5.0 [180]. The pH of the cell culture media was approximately 7.0 – 7.2 (all experiments were carried out in fresh culture media) and accordingly the cytoplasmic pH would also be expected to be in this range [181, 182].

The calibration of pH sensitive nanosensors was performed immediately prior to experimentation and the settings of the confocal laser power output, PMT voltage etc remained exactly the same for calibration and experimentation, these steps ensured accuracy of the data collected. Had a single parameter differed then the validity of the pH measurement could not be verified. In practice it was difficult to measure the pH from an individual endosome as the concentrated fluorescence in that region saturated the detectors which had been previously set for measuring the fluorescence of calibration solutions with much more disperse fluorophores. Strategies to make the calibration more similar to that of the real measurement (spherical endosomal bodies) included forming liposomal vesicles containing nanosensors from Lipofectamine2000® and although they formed similar sized and bright bodies, Brownian motion prevented reliable images to be taken. During image capture the movement of the liposomes caused streaking across the image and consequently the fluorescence for each data point was not representative. It was not possible to dry the solution so that the nanosensor containing liposomes were stationary as this would have necessitated a different objective to that of the 63x immersion lens used for cell imaging creating a dissimilar optical set up between calibration and experiment, not to mention the fact that calibration of pH after drying the citrate buffers would have been impossible. It may have been possible to stick the liposomes to the cell plate surface through an electrostatic or chemical force. It seemed most readily achievable however to simply take an average ratio of fluorescence between channels over the entire image for both calibration solution and cell imaging (512 x 512 pixels = 262144). As well as initially reducing the intensity of detected fluorescence for the calibration solutions it was possible to capture images which could be directly compared as they were taken with the same instrumental parameters.

The data in Figure 87 and Figure 88 are of the fluorescence ratios taken for the calibration solutions and internalised nanosensors respectively and Figure 89 illustrates how the intracellular pH measurements fit with the calibration (red triangles).

pH	Calibration ratio (R_1/R_2)
3	0.55
4	1.09
5	2.55
6	4.78
7	5.72
8	6.53

Figure 87 pH calibration data for citrate buffers.

Intracellular pH measurement	Measured fluorescence ratio (R_1/R_2)	Calculated pH
A	2.30	4.88
B	2.58	5.03
C	2.73	5.10
D	2.30	4.88
E	2.31	4.89

Figure 88 Fluorescence ratio data for nanosensors internalised in CHO-K1 cells and the calculated pH as given from the calibration.

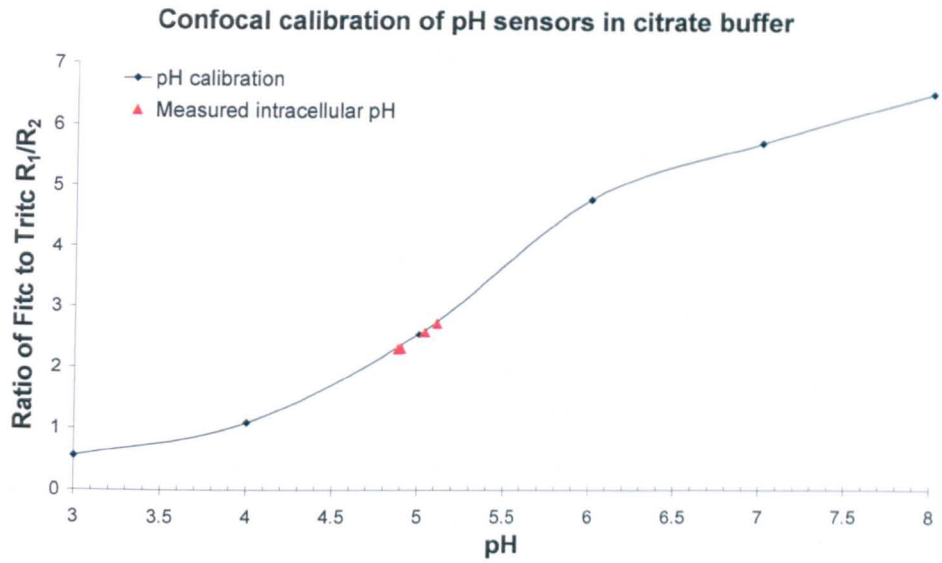

Figure 89 pH calibration of nanosensors and calculated intracellular pH (red triangles).

The pH values approximated lie within the range of values the literature describes for late endosomes to lysosomes. Although it would be prudent not to rely on this method for exact pH measurement it is evidence enough to propose that the pH is close to 5 and therefore conclude that the nanosensors are in an acidic environment close to the literature value for a lysosome.

This final piece of evidence strongly suggests that Tat-mediated delivery of nanosensors induces endocytosis within the mammalian cell lines tested and that this leads to the entrapment of the nanosensors in endosomal / lysosomal vesicles. This entrapment prevents the nanosensor from sensing and responding to changes within the cytoplasmic domain which accounts for the unsuccessful measurement of intracellular Ca^{2+} flux with this delivery method to date.

4.3.7 Internalisation and intracellular trafficking

With the evidence that endocytosis represents the major pathway for Tat-mediated nanosensor entry into mammalian cell lines the question arose as to whether the nanosensors naturally broke out of the endosome after internalisation. This question

now seemed to be the most important in terms of feasibility for Tat-mediated delivery as prolonged endosomal entrapment would prevent useful cytoplasmic measurements being taken. If nanosensors remained in endosomes after delivery then a scheme must be devised to ensure endosomal escape. To date no information was available on the long term fate of nanoparticles after Tat-mediated delivery so a simple experiment was devised to image nanosensor location several days after delivery. Figure 90 shows images of CHO-K1 cells loaded with nanosensors immediately after the delivery incubation period of 3 h and after a prolonged rest period of approximately 90 h. Several plates were loaded in parallel as the imaging process led to bacterial infection which could not be remedied and hence these plates could not be further evaluated after the 90 h rest period. However it was deemed that the exact same conditions each plate under went maintained consistency throughout the experiment and viable results could be drawn.

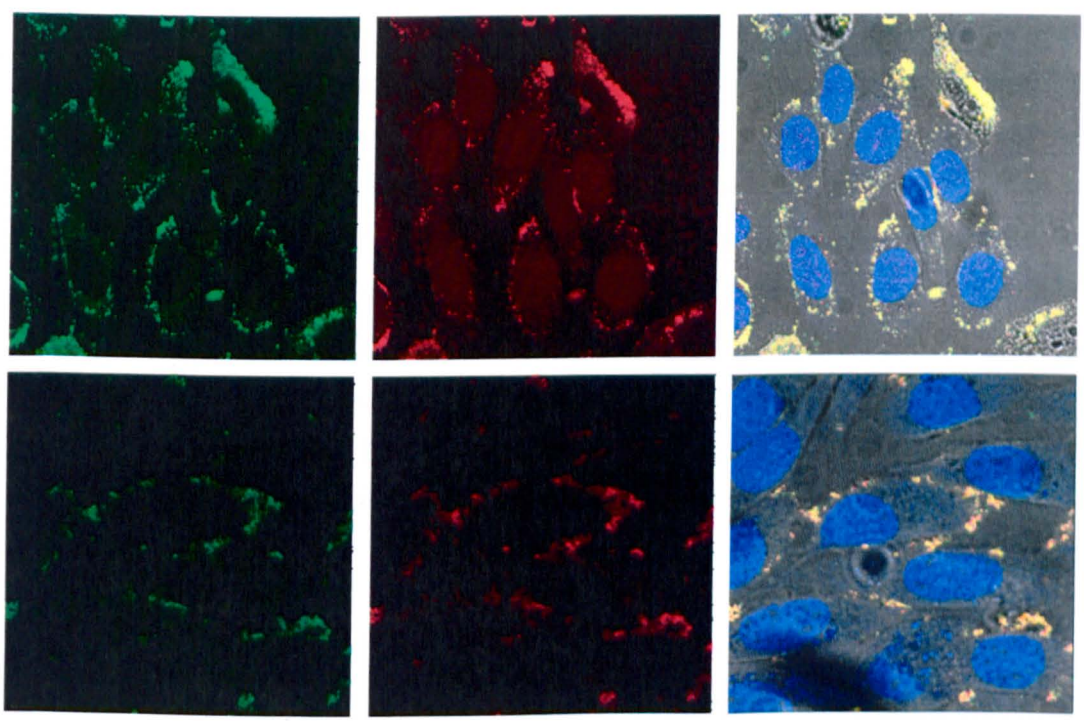

Figure 90 CHO-K1 cells loaded with FITC:TRITC nanosensors imaged immediately after a 3 h delivery incubation period (top) and after 90 h (bottom) x63 magnification. Cells were washed twice with PBS prior imaging and fresh culture media was replenished.

From these images it is apparent that nanosensors which were initially associated with the cytoplasmic region are more exclusively associated with the outer membrane region of the cells and are no longer located inside the cell. The possibility therefore is that CHO-K1 cells have recycled the nanosensors through the cytoplasm and out of the cell in a manner that deals with unwanted foreign bodies that have entered the cell. Importantly also is the seemingly non-cytotoxic nature of Tat-mediated nanosensor delivery suggested by the healthy morphology of the cells 90 h after delivery. Overall confluency of the cell plates increased accordingly showing that the presence of nanosensors had no major detrimental effect upon cellular growth and metabolism. It must be noted that this is a simple observation and a true picture may only be completed through proper cytological assay.

The results demonstrating Tat internalisation are not as clear cut as this discussion may have led one to believe so far. Regarding initial experiments with FITC-Tat conjugate no attention has yet been paid to more detailed observation of the intracellular localisation of these conjugates. It is well known that Tat is a potent nuclear localisation signal [170, 183] and as such one would expect to see nuclear associated fluorescence. This has not been observed in experiments carried out in this research and is assumed to be due to the limiting size and specificity of nuclear pores preventing Tat nanosensors crossing the nuclear membrane. For FITC-Tat conjugate however it was unexpected that little or no nuclear fluorescence occurred after incubation. Latterly, detailed confocal images taken in conjunction with counter-stained nanosensors (i.e. red as opposed to the green FITC-Tat conjugate) or LysoTrackerRED® highlighted a reproducible fluorescent pattern emerging after FITC-Tat conjugate delivery. Resultant fluorescence is dissimilar to diffuse cell-wide fluorescence observed after incubation with fluorophore-AM esters or other cell permeable dyes. This pattern was originally seen in human embryonic stem (hES) cells during a cell applicability study, and subsequently repeated in CHO-K1 cells as shown in Figure 91. This experiment shows that FITC-Tat conjugate crosses CHO-K1 cellular membrane within 20 min but more importantly that the pattern of fluorescence in the cytoplasm shows an uneven distribution of fluorescence which alludes to an association with sub-cellular organelles or compartments.

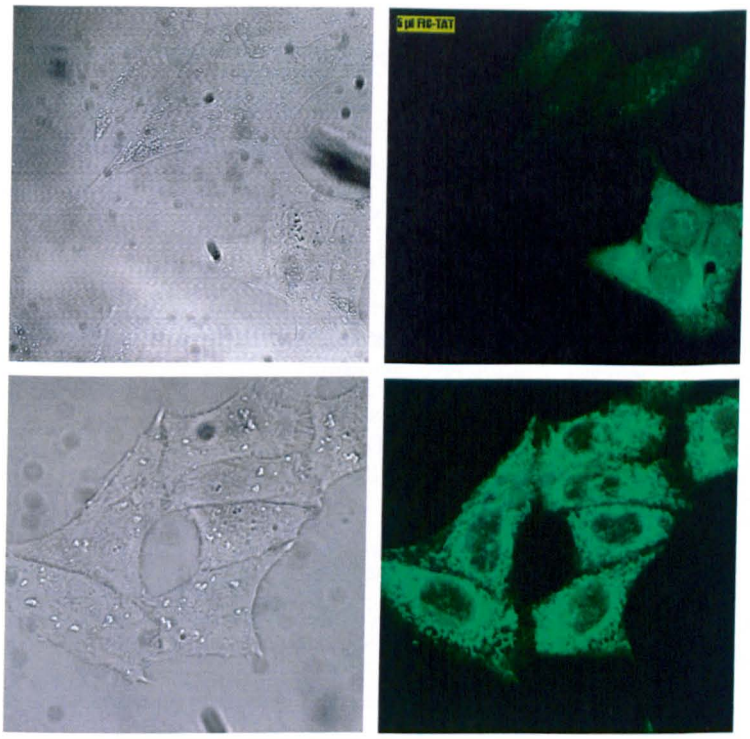

Figure 91 FITC-Tat conjugate incubated with hES cells (top, x63 magnification) 2.5 µl ml^{-1}, 2 h incubation, and CHO-K1 cells (bottom, x63 magnification with x2.58 digital zoom) 2.5 µl ml^{-1}, 20 min incubation. Cells were washed twice with PBS prior imaging, control cells incubated with equivalent amount of FITC showed no fluorescence.

Further information on the nature of sub-cellular location was gained by loading cells with FITC-Tat conjugate simultaneously with rhodamine B nanosensors or the endosomal stain LysoTrackerRED®. Figure 92 and Figure 93 show images from these respective incubations and, interestingly, the images look identical; i.e. whether FITC-Tat conjugate were loaded in conjunction with rhodamine B nanosensors *or* LysoTrackerRED®. This reinforces the argument for endosomal location of nanosensors after Tat-mediated delivery but also highlights the non-endosomal / lysosomal location of FITC-Tat conjugate after delivery. There is clearly an interaction with sub-cellular organelle(s) and or the induction of an endocytosis-like cellular process but dissimilar to nanosensor intracellular recognition.

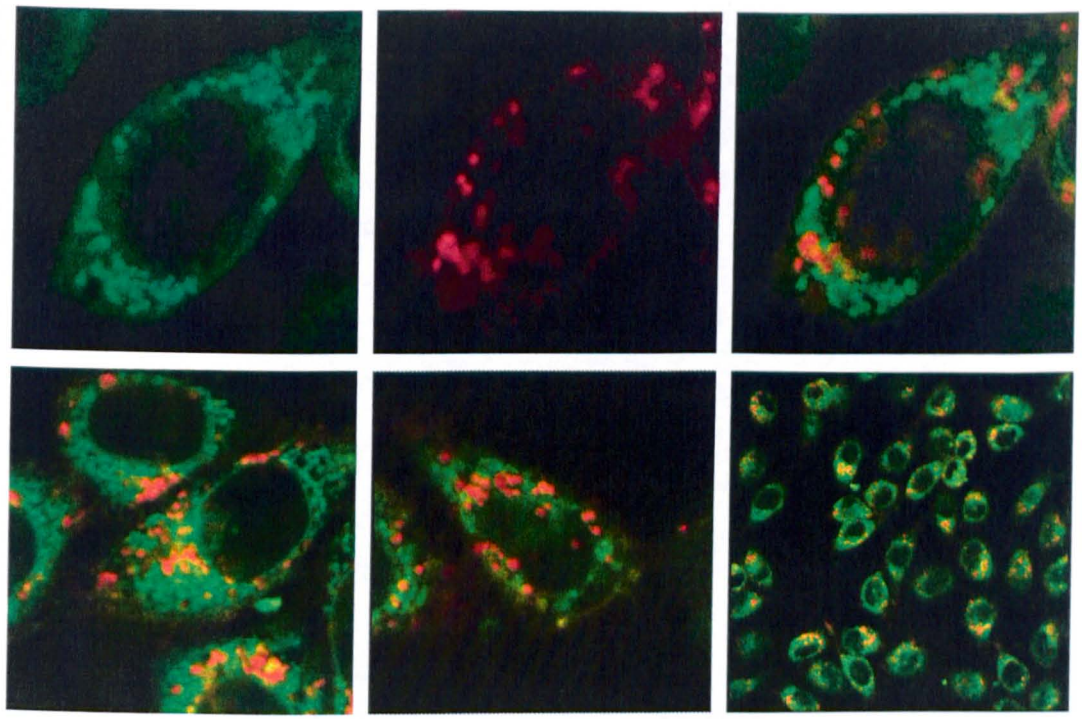

Figure 92 Several examples of CHO-K1 cells loaded with FITC-Tat conjugate and rhodamine B nanosensors.

Figure 93 shows a population of CHO-K1 loaded with FITC-Tat conjugate in which endosomal position has been identified with LysoTrackerRED®. Using a lower magnification can often obscure detail such as punctate fluorescence of FITC-Tat conjugate although it can still be observed when contrasted with an example such as Figure 77 (CHO-K1 cells loaded with Fluo-4 AM ester). Both FITC-Tat conjugate and endosomal position are further qualified with a cross section of relative fluorescence for each channel taken across x and y planes. Fluorescence fluctuation across the traces for each plane coincides with cellular nuclei and the extracellular spaces. Additionally, regarding FITC-Tat conjugate localisation, the fluorescence for each channel is not equivalent showing that fluorescent species are not co-localised. Similar trends in the traces just represent the location of both FITC-Tat conjugate and endosomes in cytoplasmic regions.

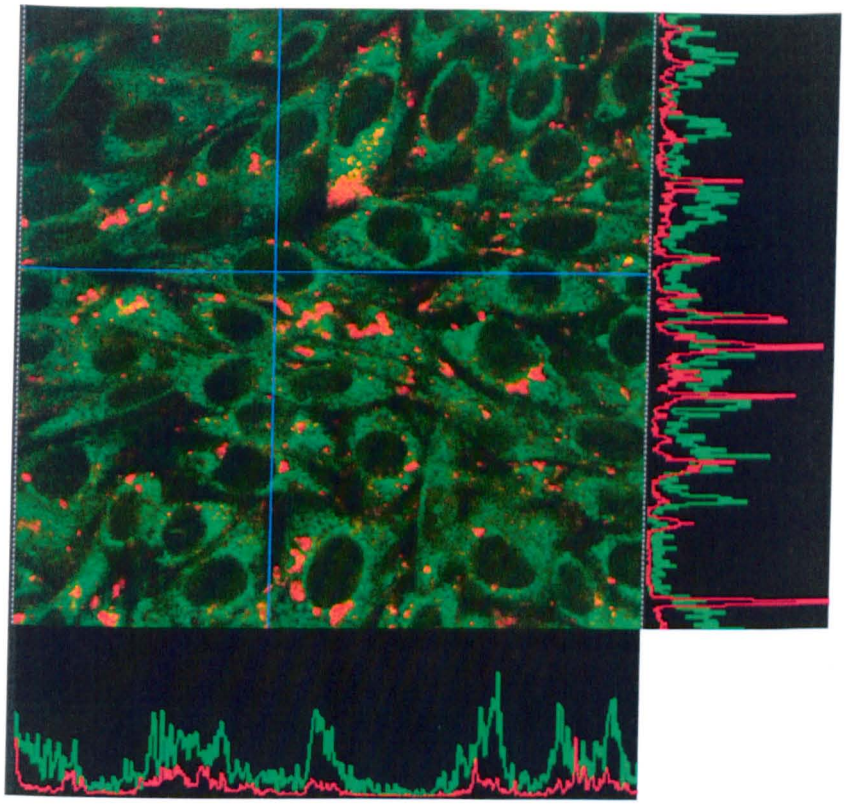

Figure 93 CHO-K1 population loaded with FITC-Tat conjugate and counter stained with LysoTrackerRED®, x63 magnification, showing endosomal position. Bottom and right panels show fluorescence intensity for each channel along a cross section of the image.

Several endocytotic pathways operate in eukaryotic cells for particle uptake including both clathrin-dependent and independent pathways the latter including macropinocytosis, phagocytosis and caveolae-mediated internalisation. It is suggested that in this instance different pathways lead to the internalisation of Tat nanosensors and Tat conjugate. This may be solely attributable to the difference in size between the two bodies or there may be more complicated biological, chemical or electrostatic forces playing a part. The most substantial evidence for this difference may well be that LysoTrackerRED® does not co-localise with the punctate regions of intracellular FITC-Tat conjugate fluorescence in the cytoplasm yet does co-localise with FITC-Tat nanosensors. An explanation of this result could be that FITC-Tat conjugate internalisation is via a predominantly caveolae-mediated trafficking mechanism which proceeds along a non-acidic and non-digestive pathway [184]. Therefore it would not be possible to use LysoTrackerRED®, which only provides information on the location of

intracellular acidified vesicles (e.g. endosomes / lysosomes), to reveal the location of caveosomes where FITC-Tat conjugate may be located.

4.4 Conclusions

Utilising cell penetrating peptides for the delivery of nano-sized cargoes was a technology that was easily accessed requiring already well established standard chemistry and cellular techniques. This was initially shown by the in-house synthesis of a fully functional Tat analogue peptide which was proven to exhibit cellular penetration through fluorescent labelling. The applicability of the Tat peptide-mediated delivery system was shown to be broad with successful internalisation shown in several mammalian cell lines including both human embryonic and mesenchymal stem cells. The obvious promise of CPP delivery does not need to be reiterated here but the usefulness of this technique is certainly becoming increasingly accepted throughout the scientific community and the results obtained here only serve to add to the interest that CPPs have generated.

The processes involved in fabrication of Tat-functionalised nanosensors and of cellular delivery have been standardised and only a short incubation is now required which may prove to be shorter in the future; the time course of Tat-mediated internalisation is an obvious point of attention which remains to be studied in full. Achievement of a standard delivery method utilised several microscopy based techniques from simple observation to *z*-stack confocal profiling and counter-staining with membrane markers. The result of these efforts was to show that Tat-functionalised nanosensors can internalise within mammalian cell lines and locate to the cytoplasmic region without particular association with either the nucleus or cellular membrane.

By establishing reproducible internalisation, and improved cellular imaging, it became increasingly obvious that the distribution of the nanosensors was not uniform which led to the central question: Does the cell play a part in internalisation and direct the process of intracellular localisation?

If this scenario was true it was likely to negatively impact on the distribution of nanosensors throughout the cell in a uniform and unimpeded manner as required. It was clearly shown that nanosensors did not reach the nucleus attributed to the size exclusion

properties of nuclear pores, but evidence mounted for a biological pathway which presented a more significant reason than simple size exclusion. The requirement to prove or disprove a cell guided process affecting internalisation, distribution, and ultimately the functionality of internalised nanosensors was required. Evidence and counter evidence was abound in the literature regarding the possible mechanisms of Tat peptide entry, however a consistent theme of endocytosis, at least in some form prevailed, and thus it became the focus of this work to show whether endocytosis was responsible for the ultimate distribution of internalised nanosensors.

Means to prove free cytoplasmic distribution were established which included the use of a commercially available dye which accumulated in acidic bodies in the cell, i.e. late endosomes or lysosomes. LysoTrackerRED® was used to show that fluorescence from nanosensors and endosomes / lysosomes co-localised when Tat-mediated delivery was used to deliver nanosensors. The evidence for co-localisation of fluorescence was obtained and as such it was concluded this directly represented the co-localisation of the fluorescent species involved, namely lysosomal dye and fluorophores entrapped within nanosensors. It was also possible to utilise a method based on intracellular analyte flux, developed primarily to show the positive function of sensors upon delivery, but alluding to the entrapment of nanosensors in intracellular vesicles. Methods such as this are well established and depend on measuring secondary messenger evolution after the initiation of receptor agonism i.e. a cellular response after a drug molecule has been administered. With little modification a method was developed by which an intracellular calcium flux could be instigated in CHO-K1 cells through a simple addition of UTP, or ionomycin. The key observation was that nanosensors known to respond to fluctuations in the appropriate concentration range of intracellular [free Ca^{2+}] (0.1 – 1.2 μM), did not show a similar response when internalised in cells via Tat-mediated delivery. It was also important to show that cells loaded with Fluo-4 AM ester, the same calcium sensitive dye as entrapped in the nanosensors, did exhibit a classical response when the same agonist was administered. From these experiments it was possible to conclude that the nanosensors were encapsulated in areas of the cell which did not experience cytoplasmic Ca^{2+} flux and cannot therefore be freely distributed in the cytoplasm.

Utilising the very function that nanosensors are designed to provide, pH measurements were taken of the immediate environment in which the nanosensors were located. Literature values for late endosomes / lysosomes range from pH 4.8 – 6 and FITC: TRITC pH responsive nanosensors were used to make comparative measurements. In combination with the circumstantial evidence gathered these measurements could help elucidate the mechanism(s) of cellular entry for Tat-functionalised cargo. Appropriate calibration of the pH nanosensors with the confocal microscope system used revealed that the environment in to which the nanosensors localised had a pH of approximately 5. This value fitted very well with those published for lysosomes and a strong case for endocytotic internalisation proceeding along an acidic and digestive pathway was presented. In summary Tat-mediated delivery of nanosensors has been established as being endocytotic in nature as evidenced by images of punctate cytoplasmic fluorescence, proof of encapsulation within an area discrete from the cytoplasm itself, and the measurement of a pH of approximately 5 – equal to that of lysosomes.

It was observed that the location of FITC-Tat conjugate had a specific pattern, dissimilar to that of free dye. Punctate fluorescence after FITC-Tat conjugate loading likewise suggested the role of an independent cellular pathway although it was shown to be different to the one associated with nanosensor internalisation. This was exhibited with co-localisation studies using both nanosensors and LysoTrackerRED® to show endosomal / lysosomal position distinct from FITC-Tat conjugate position. The finding that Tat peptide progresses along different internalisation pathways depending upon the cargo to which it is attached presents a very interesting question about the internalisation processes involved. It may be possible to tailor nanosensors in order that different pathways are initiated and successful cytoplasmic delivery is achieved without the need to investigate schemes and mechanisms for endosomal escape.

Methods are now in place to assess nanosensor location after delivery which will allow for more focussed investigations in the future. Regarding the future course of research and experimentation it is suggested that the time course of Tat-mediated internalisation is elucidated; it is known that FITC-Tat conjugate internalises within minutes yet only satisfactory levels of loading of Tat-nanosensor incubation were found after 3 h. This in itself suggests different internalisation pathways but it would be beneficial to know a

more exact time line involved. Also it would be prudent to investigate the possibilities of multiple nanosensor surface functional moieties with a means to direct the mechanisms of cellular internalisation after the initial function of the CPP has been utilised. Various polymeric based systems are currently being investigated in the drug / gene delivery fields to aid endosomal break down and escape as well as fusion lipids; the utilisation of these or other suitable candidates could enhance the already proven track record of Tat as a vector of cellular internalisation.

5 Chapter 5 – Analysis of the internalisation of nanosensors in mesenchymal stem cells

5.1 Introduction

This chapter describes the investigation of the effect of internalising nanosensors within mesenchymal stem cells (MSCs). The aims of the investigation were two-fold, firstly to conclude that nanosensors could be viewed as a 'silent technique' not instigating the differentiation of MSCs down a particular lineage, and secondly, to validate flow cytometry as a method for the continued research into advancements within the nanosensor technology and as a means to monitor the nanosensors in cells *en masse*, something unobtainable with the more traditional method of confocal microscopy.

5.1.1 Mesenchymal stem cells

Various adult tissues have a reservoir of stem cells which enable tissue renewal after the effects of disease, ageing, or trauma have had an effect upon the structure and health of the tissue. Watt and Hogan [185] define stem cells as having the capacity for extensive self-renewal and for originating at least one type of highly differentiated descendant. Mesenchymal stem cells (MSCs) are an example of these multipotent cells and are found in adult marrow. Clonogenic fibroblast precursor cells, or colony forming unit-fibroblasts (CFU-F) as they were initially termed were isolated by Friedenstein *et al* [186] in a ground-breaking study from whole bone marrow in which it was shown the cells were capable of forming both bone- and cartilage-like colonies. Now it is shown they have a differentiation potential to become one of many lineages of mesenchymal tissue, including marrow stroma, bone, muscle, cartilage, tendon, and adipose [187] as well as ectodermal [188] and endodermal [189] lineages. This multi lineage characteristic has lead to the proposition of renaming the cells as 'marrow stroma cells'; although this name equally fails to encompass all roles the cells can perform, such as tissue repair. Most recently the name 'multipotent stromal cell' has been proposed as a more appropriate replacement. However this type of cell is ultimately referred to, for the purpose of this thesis, they will simply be referred to as MSCs. MSCs have been shown to acquire characteristics specific to the tissue with which they are co-cultured [190-192] and have generated a great deal of promise and interest as a source of cells for cell-based

therapeutic strategies due to this intrinsic ability [193]. They are becoming increasingly accepted as a readily available source of stem cells and are found in virtually all post-natal organs and tissues, although not peripheral blood [194]. Currently bone marrow is thought to be the most readily available and enriched source of MSCs and may offer a common pool of multipotent MSCs; i.e. before they gain access to the circulating blood system and take on the characteristics (to meet specific requirements of repair and maintenance) of the tissue they ultimately reside in [195]. It is proposed that once released from the bone marrow to reside in other tissues, even though they are morphologically similar and display similarity in the expression of main marker genes [196], their true multi-potency is lost, yielding cells with only tri- bi- or uni-potency [193, 197]. It has been shown that cells isolated even by density-gradient fractionation remain a heterogeneous population with differing proliferation and differentiation characteristics [198]. The ability to harvest stem cells from the host, therefore negating the confounding allogenic immune response to cell implants coming from other sources, and without the moral and legal implications of embryonic stem cells has enormous potential as therapeutic cell-based tissue engineering. The scope for MSC based medicine is growing all the time with examples already for cardiovascular therapy [199-201], diabetes [191], immunoregulation [202], Parkinsons disease [203], and cystic fibrosis [204].

5.1.2 MSCs as model stem cell line for nanosensor development

The great potential of MSCs for tissue engineering is being researched enthusiastically, yet certain, rather large questions, remain. The central dogma of MSC research is whether in fact MSCs exist at all. This is due to the lack of a true identity, and agreeable determination of what a MSC is. There remains to be a marker specific distinction which says "Yes, that is a mesenchymal stem cell". The question is: Are bone marrow isolations a proviso of a diverse mixture of lineage-specific progenitors and not true stem cells? [195] Referring to this argument is simply a way of showing that research into MSC is a very popular area and provides a perfect ground for showing the research potential of nanosensors. In particular a study by Altman *et al* [205] which showed that mechanical stress alone can cause the differentiation of MSCs down a specific lineage into ligament cells, allows a demonstration that the internalisation process of

nanosensors and their continued presence will not lead to the differentiation a cell down a particular line. This published study was over a period of several days but nonetheless shows that a physical / mechanical stress can affect the differentiation potential of multi-lineage MSCs. With this in mind the effects of nanosensor internalisation upon MSCs has been investigated with flow cytometry using currently accepted surface markers, CD 105^+ / CD 29^+ / CD 34^- / CD 45^- acting as indicators of undifferentiated MSCs [206].

5.1.3 CD antibodies (markers)

CD stands for Cluster of Differentiation and defines a protocol used for the identification of cell surface molecules. Originally the CD protocol was established to bring together into an organised catalogue the large number of monoclonal antibodies produced by numerous laboratories against epitopes (part of a macromolecule recognised by the immune system) on the surface molecules of leukocytes (white blood cells) [207]. Since then the use of the CD marker system has been extended to cells other than leukocytes, such as stem cells, and allows the presence of cell surface molecules to be used for the definition of a cell type. Frequently the absence of a specific surface molecule is key to identification and cells are characterised as, for example, CD34+ and CD31-, i.e. these cells express CD34 but not CD31. Finally, observing the binding of the CD antibodies is necessary so the attachment of fluorophores is regularly utilised to make sure that the CD marker is visible when bound to the cell surface molecules. For identification of the mesenchymal stem cells reported here four CD markers are used, the cells are positive for CD 29 and CD 105 and negative for CD 34 and CD 45.

CD 29 (Integrin β1) – present on lymphocytes, monocytes, granulocytes, platelets, mast cells, fibroblasts and endothelial cells. Receptor for VCAM-1 (vascular cell adhesion molecule-1).

CD 105 (Endoglin) – present on endothelial cells, bone marrow subset, activated macrophages, smooth muscle cells. Participates in cellular response to TGF - β1 (transforming growth factor).

CD 34 – present on haematopoietic precursors, capillary endothelial cells, embryonic fibroblasts. 'Stem cell marker', participates in cell-cell adhesion.

CD 45 (Leukocyte Common Antigen) – present on haematopoietic cells. This is a tyrosine phosphatase which has a role in signal transduction.

Lack of availability of a conjugated anti CD 29 required the use of a second antibody (with an attached fluorophore) specific for CD 29 antibody. Schematically, as shown in Figure 94, the attachment of CD 29 2nd antibody with PE fluorophore is necessary for fluorescence detection.

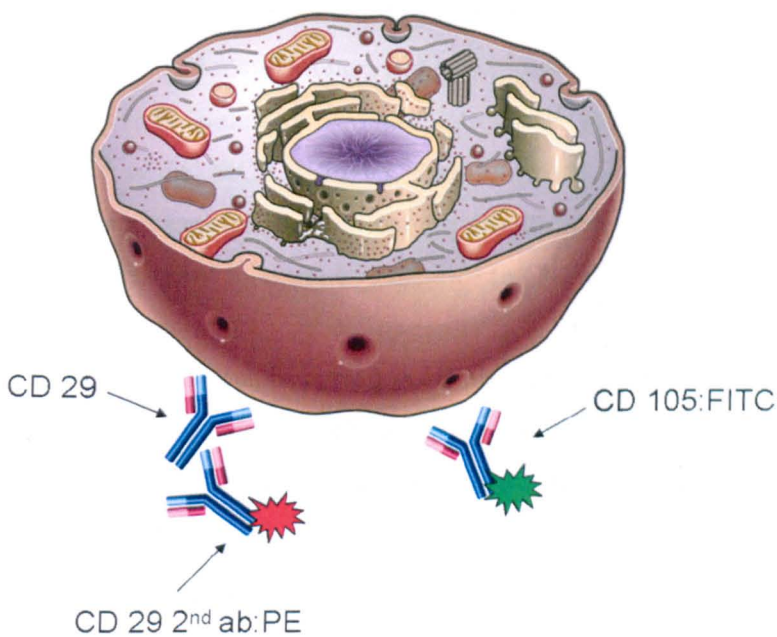

Figure 94 Schematic representation of CD marker binding to a mesenchymal stem cell (not to scale, picture of generic animal cell).

Controls are generally required to account for fluorescent signal coming from random binding of the antibodies to the cell surface. Isotype controls, CD markers with no specificity for the cell type being investigated, are employed for this purpose; additionally in this scenario using CD 29 2nd ab:PE alone determines the amount of background fluorescence, if any, from non-specific binding of this antibody.

5.2 Materials and Methods

5.2.1 Reagents

Cell culture media consisting of DMEM+ 10 % FCS 20 mM L-glutamine with penicillin and streptomycin, phosphate buffered saline (PBS), trypsin / EDTA and trypan blue were all purchased from Sigma and cell fixation solution (FACS fix) made up with 0.5% formalin in Isoton particle-free PBS, was purchased from Immunotech, (Beckman-Coulter). OptiCLONE isotype control antibody solution IgG1-FITC / IgG1-PE / IgG1-PE-Cy5 (cat number IM1672) and human CD antibodies CD 34:FITC (cat number IM1870) CD 45:PE* (cat number IM2078U) and CD 29 (cat number IM1598) were all obtained from Beckman Coulter. Rat anti-mouse IgG1-PE* (cat number 1145-09) was purchased from Southern Biotech Associates and mouse anti-human CD 105:FITC (product code MCA 1557F) was obtained from Serotec. FITC-Tat nanosensors, blank nanosensors (no fluorophore, no surface functionality), and FITC-Tat conjugate were fabricated in house as described in Chapter 2.

*Phycoerythrin (PE) has a large absorption coefficient and quantum efficiency close to one. *In vivo*, it functions to transfer light energy to chlorophyll during photosynthesis and is one of the brightest dyes used today, it emits in the yellow/orange at about 570 nm. PE is not generally known by those accustomed only with fluorescent microscopy as it photobleaches rather quickly.

5.2.2 Cell culture and preparation

Human fetal liver tissue was obtained from legal terminations of pregnancy during the first and early trimesters with informed written consent. All patients were over 18 years of age, spoke English and had no known history of inherited disease. The research group had no contact with the patient and were not in any way involved in the clinical decision to terminate the pregnancy. Local Research Ethics Committee approval was

granted before commencement of the project and UK Department of Health guidelines incorporating recommendations in the Polkinghorne Code of Practice were meticulously followed. Pure cultures of MSCs were identified using FACS with the appropriate surface marker fluorescent antibodies. The requirement of certain techniques associated with stem cell culture is not necessary for MSC culture, e.g. the inclusion of a feeder layer or the use of leukaemia inhibitory factor (LIF). The use of both these factors is often associated with stem cell culture, for example to maintain embryonic stem cells (ESCs) with a normal karyotype and the ability to fully differentiate into functional cells a feeder layer is employed consisting of mouse embryonic fibroblasts. In addition to supplying as-yet-unidentified growth factors, the feeder layer provides LIF, which prevents embryonic stem cell differentiation. Once LIF is withdrawn from the culture, ESCs begin to differentiate [208, 209]. Some culture techniques negate the use of a feeder layer by adding LIF directly to the growth medium, and through the use of conditioned culture media combined with extracellular matrix proteins allowing for adhesion of cells to the culture flask and for the binding of cellular growth factors [210]. For MSC culture however the use of a feeder layer or conditioned media is not necessary as the cells can be cultured readily in DMEM with 10% foetal calf serum (FCS) 20 mM L-glutamine (DMEM+). Cell culture of MSCs was as described previously for CHO-K1 cells (3.2.2), in T75 tissue culture flasks which were passaged when confluency reached 100 %.

Cell preparation for flow cytometry experiments was performed on the afternoon prior to flow cytometry analysis and the cells were fixed and stored overnight in FACS tubes in darkness. Each flask of cells, loaded with nanosensors (or controls) were washed twice with PBS, trypsinised, and pelleted with centrifugation. They were then re-suspended in 1 ml of DMEM+. A 60 µl aliquot of each cell suspension was mixed with 40 µl of fresh DMEM+ plus 100 µl of trypan blue (200 µl total volume) in order to count the cells and to prepare suspensions with enough cells for flow cytometry. Cells were counted with a standard haemocytometer and the 1 ml suspensions were diluted accordingly to provide 10^6 cells ml^{-1}. A 100 µl aliquot of this suspension was removed to a 15 ml centrifuge tube and pelleted with centrifugation. The supernatant was removed and 5 µl of the appropriate antibody or isotype control was added to the cells. The cells were drawn up several times with the pipette to ensure proper mixing; once the cap was replaced the cells were gently vortexed then incubated for 30 min in the

dark at room temperature. Subsequently the cells were washed in 2 ml DMEM+, vortexed, and pelleted once more. In the case of CD 29 an additional incubation is required as the fluorogenic molecule used was the 2nd antibody rat anti-mouse IgG1-RPE. To maintain consistency, all cell samples were subjected to the same number of washing and incubation steps using a 5 µl aliquot of DMEM+ in place of antibody. Once antibody attachment was complete and the cells had been washed, 500 µl of FACS fix (0.5% formalin in Isoton) was added to each cell pellet and the whole vortexed. Each sample was removed to a FACS tube, capped, and stored overnight in the dark.

5.2.3 Flow cytometry

Using a Beckmann Coulter Flow cytometer each sample of cells were analysed with 488 nm (for FITC) and 568 nm (for PE) laser illumination. Data for each plot was gathered from 50,000 cells.

5.2.4 Data analysis

The detected events were analysed using Walter and Eliza Analysis Software: Electrical and Lucid (WEASEL) version 2.4, flow cytometry analysis software. WEASEL software was used to generate plots showing chosen parameters of the data and to colour the plots for enhanced clarity (using the colour on dot density function).

5.3 Results and Discussion

The key questions at the beginning of this study where as follows:

- Is it possible to use flow cytometry to assess cell morphology and cell viability after nanosensor loading?
- If so is it possible to identify loading limits to a cell population before the onset of cell damage or death?
- Does the loading process or presence of internalised nanosensors affect surface markers representative of mesenchymal stem cell identification?
- Can flow cytometry be used to show the presence of fluorescent nanosensors internalised within cells?
- Is it possible to analyse internalised nanosensors and cell surface bound antibody simultaneously?
- Is it possible to use flow cytometry as a measure of numbers of internalised nanosensors? (i.e. show differences in relative fluorescence intensity)
- Would it be possible to measure the relative fluorescence of two different fluorophores within the nanosensors and therefore monitor the internal environment? (e.g. for pH monitoring with ratiometric FITC: TRITC sensors)

In order to answer these questions the two features investigated were forward and side scatter (FS/SS) as a measure of cell viability and the presence and relative intensity of fluorophores on the surface of, or internalised within MSCs.

5.3.1 Flow cytometry cell morphology of healthy MSCs

Initial information was gathered which determined what healthy MSCs looked like when assessed with flow cytometry. This information provided a central picture to which other experimental populations were compared. Figure 95 shows cell population plots, each is made up of two chosen parameters. In this instance the *x* axis shows forward scatter and side scatter is shown on the *y* axis. The position of each event (dot), which represents a single cell, is dictated by the combination of both parameters. Each

plot is coloured using the 'colour on dot density' function available in the software, i.e. red to blue colouration shows an increase in localised cell numbers on the plot and therefore where the majority of the population lies. The data can be selected (gated) to remove cells which do not fit certain criteria; this is useful for various FACS techniques for example when counting numbers of specific cell types in blood samples. However none of the data presented here has been gated and is presented 'as seen' by the flow cytometer. The key result and the most obvious from the figure is the similarity between each plot. This indicates the cell morphology and viability remains similar for cells which were incubated with Tat nanosensors compared to the total control population and the population incubated with nanosensors which had no surface Tat peptides. This condition acted as a 'nanosensor presence control' showing that just the presence of nanosensors in the cell culture media had no effect on cell morphology or viability. Should the internalised nanosensors have affected the cells this control would have served to show it was the process or presence of internalised nanosensors affecting morphology.

The plot provides information on the cell culture in general, which is why FS/SS controls are assessed for each experiment. To the lower left of the plot it is often likely to find a small population of events which generally represent dead cells or cell debris. Possibly in the case of these experiments this section of the plot may show nanosensor debris or aggregations too. If necessary, the data can be gated to remove these data from the plots to add clarity to the results. From Figure 95 it was found that the MSCs were healthy examples (not too much side scatter) and remained so after incubation with Tat nanosensors at these loading concentrations. The small debris / dead cell populations are not un-expected and are not an indication of problems arising from the loading of nanosensors.

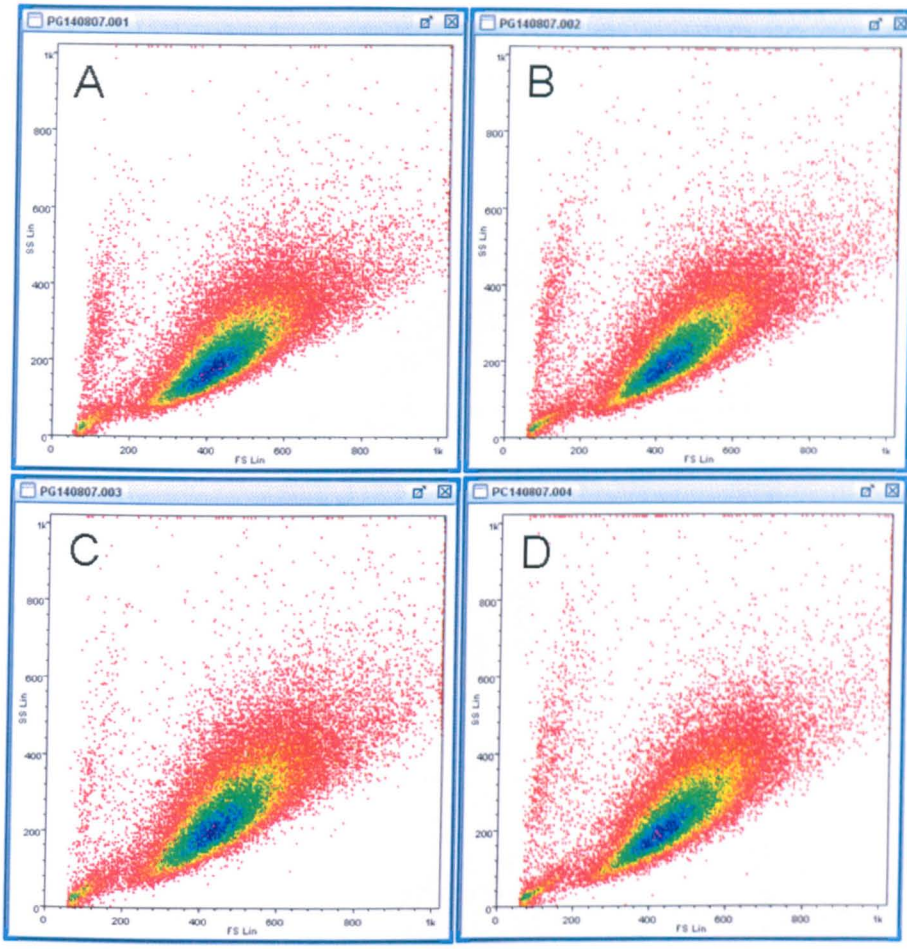

Figure 95 Forward and side scatter plots of MSCs after Tat nanosensor loading; no fluorophores in nanosensors. A: Total control population T75 flask 100 % confluent, no treatment showing healthy plot of cells. B: T75 flask treated with 24 mg of control nanosensors without Tat surface peptides i.e. cells without internalised nanosensors. C: T75 flask incubated with 12 mg of Tat nanosensors. D: T75 flask incubated with 24 mg of Tat nanosensors.

5.3.2 Cell death through overloading

To identify loading limits to a cell population before the onset of cell damage or death the confluency of the experimental T75 cell populations was reduced to approximately 25 – 30 % whilst maintaining the addition amount of nanosensors. This would likely induce overloading as the relative amount of nanosensors per cell was greatly increased. Figure 96 shows the flow cytometry data obtained.

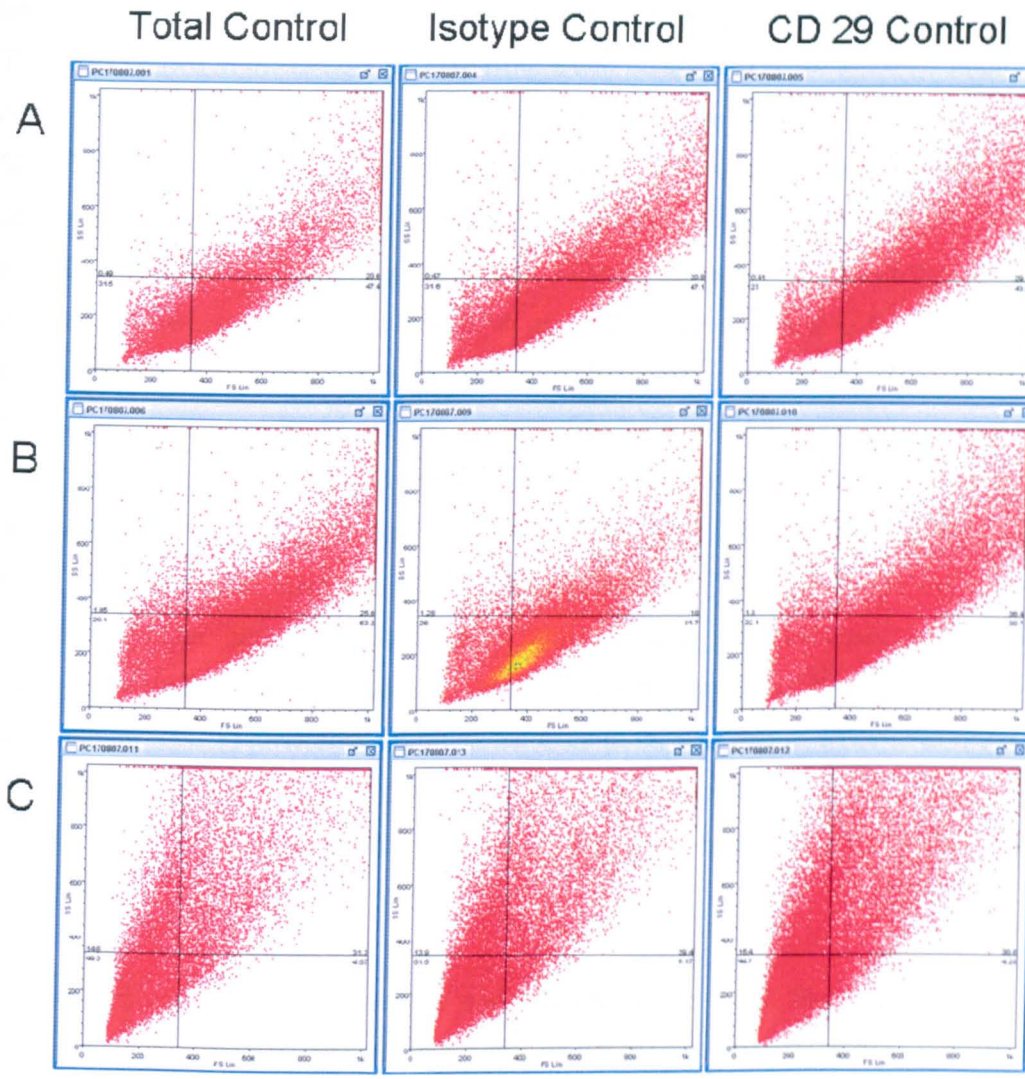

Figure 96 Forward and side scatter plots of MSCs after loading with Tat nanosensors with no fluorophore. T75 flasks approximately 25 – 30 % confluent. A: control cells. B: T75 flask treated with 12 mg Tat nanosensors. C: T75 flask treated with 24 mg Tat nanosensors. Left Column: total control, no antibody labelling. Middle column: Irrelevant antibody Isotype control, labelling with OptiCLONE. Right column: CD 29 2nd antibody control labelling. More side scatter reveals an increase in granular content of the cells which is an indication of poor cell health and possible cell death.

The middle and right panels in each row represent a sub-population taken from the original experimental flask and labelled with specific antibodies; the populations in the left panel have no antibody labelling. The initial point to observe in this figure is the difference in scatter between the three conditions (rows). Each of the plots on the top row comes from a population of control cells which were not incubated with nanosensors of any type. Acting as a total control these plots represent a true picture of

how these cells appear when addressed with flow cytometry, and their FS/SS measured. The plots shown in the middle row are from a cell population (with a similar number of cells) which has been incubated with 12 mg of nanosensors for three hours. Each plot of 50,000 cells shows a similar shape distribution to the control cells. One difference is the density of the population on the second column, the Isotype control populations labelled with OptiCLONE. The labelling with OptiCLONE will not have caused this apparent difference between populations. It is much more likely the tightness of the population is a difference in cell preparation technique, possibly better pipette trituration or vortexing. The other populations in this experiment are distributed over a much greater area than other experiments which may be representative of the low confluency, and consequent immaturity, within the cell culture flask. The difference in individual cell size is greater within immature (low confluence) populations; which is likely being portrayed here. For conformation, future experiments with flow cytometry should include assessment of a range of populations of different maturity and confluency (e.g. 10, 20, 30, 40 ... 100 % confluent MSCs) providing adequate controls to answer this question. However the epicentre of the population in this panel remains in the same position as that of the control cell populations and provides enough evidence for the cells being morphologically similar.

It is understood, when internalising nanosensors within cells, that there will be an overload limit, which, when breached will cause severe physical perturbation to the cells. This appears to have occurred with the 24 mg per ~ 25 % confluent T75 of MSCs experiment (Figure 96). All the panels in the bottom row show the same scatter distribution which is shifted along the axis of side scatter relative to the control and 12 mg populations. This indicates an increase in the degree of granulation within the cells which is likely attributed to the onset of cell death. It is believed there will also be increased numbers of nanosensor-containing lysosomes which may contribute to the increased side scatter signal; however a degree of increased side scatter from lysosome presence may have been expected with the 12 mg populations yet none was observed, thus it is possible to say the side scatter is not simply due to the presence of lysosomes. This experiment shows that overloading of cells with nanosensors can be assessed with flow cytometry and a series of future experiments could easily be carried out to find out

at which loading point (relative amount of nanosensors per cell) morphological changes / reduced cell viability occurs; essentially a LC_{50} or LD_{50} calculation.

5.3.3 Do internalised nanosensors affect expression of surface markers representative of mesenchymal stem cell identification?

As described previously the labels chosen to show the presence of particular markers for MSC identification were: negative for CD 34 and CD 45 (showing the cells were different from the haematopoietic lineage of bone marrow cells) and positive for CD 29 and CD 105 (showing undifferentiated MSCs) [206]. Assessment of the presence and absence of these markers was carried out with appropriate antibodies labelled with fluorophores. The following figures show the parameters of PE and FITC for the same cellular populations as shown in Figure 95 and Figure 96, as well as plots showing double negative and double positive staining of the labelled antibody markers. Initially the staining of the total control population was performed and these results are shown in Figure 97. The cluster of the population is much tighter in these plots due to the auto-fluorescence of each cell being very similar across the population.

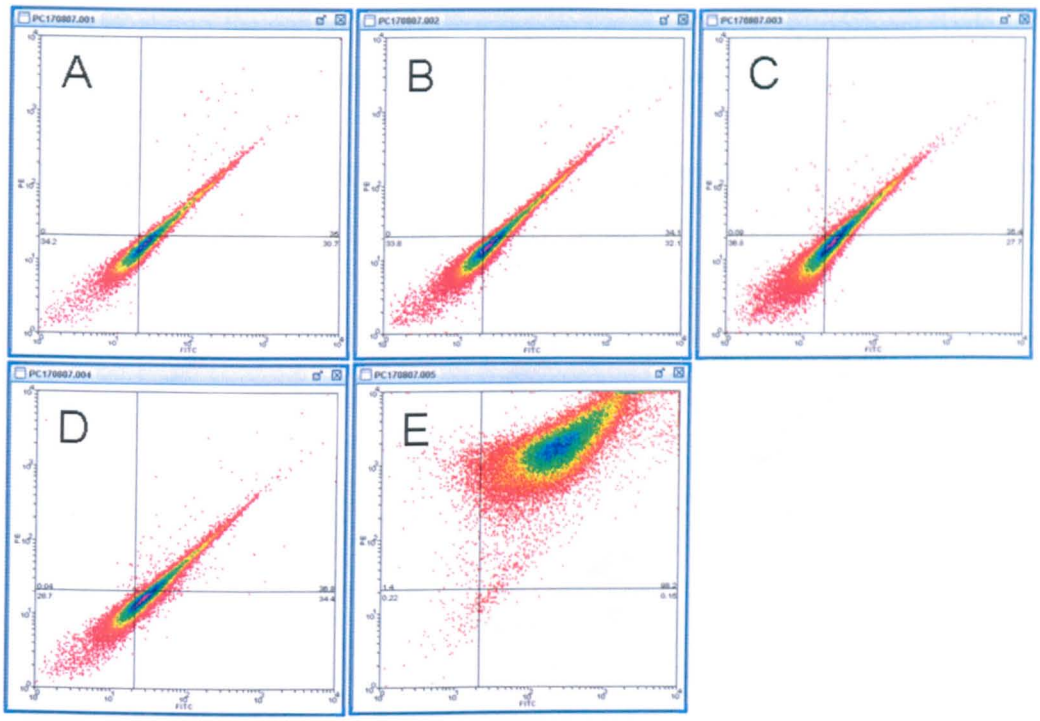

Figure 97 Total control cells, no nanosensor incubation. A: No labelling. B: Isotype control: C: CD 29 2nd antibody control: D: CD 34 and CD 45 double negative. E: CD 105 and CD 29 double positive.

As previously, the panels in the top row from left to right are as follows: left – total control, no labelling: middle – irrelevant antibody isotype control: right – CD 29 2nd antibody control. The bottom two panels represent the CD marker data as follows: left – CD 34 and CD 45 negative: right – CD 29 and CD 105 positive. The results show that in the control population there is no labelling of the cells with either OptiCLONE (no random antibody binding or leaky membranes) or with the CD 29 2nd antibody (no non-specific binding). The results for CD 34 and CD 45 are identical to the controls affirming that no labelling has occurred. This is contrasted by the double positive labelling seen in the plot of CD 29 and CD 105. The population is situated as such because it has shifted across the *x* axis, indicating the presence of FITC (from CD 105), and shifted up the *y* axis, indicating the presence of PE (from CD 29). Had only one antibody attached then the population would be shifted along the axis of that parameter only. The increase in cluster size is representative of the relative distribution of labelling across the population. These plots act as a standard for control cells to which others can be compared.

Figure 98 shows the antibody labelling results for the 25 – 30 % confluent flask of cells incubated with 12 mg of nanosensors – scatter plots shown previously in Figure 96.

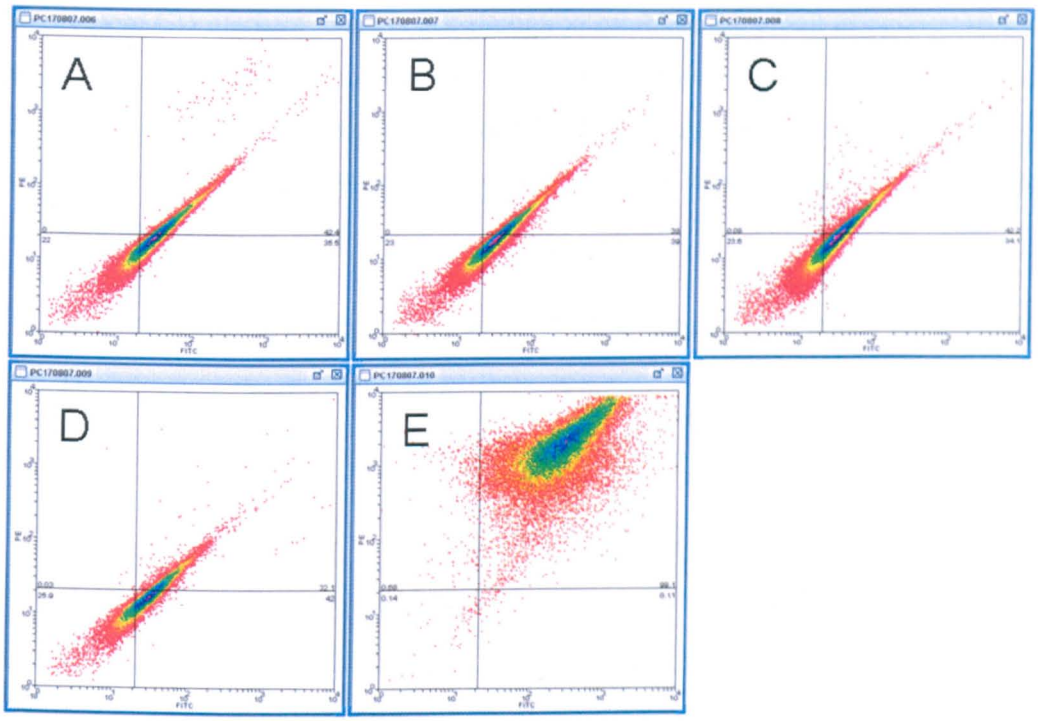

Figure 98 Cells incubated with 12 mg Tat nanosensors per T75 flask. A: No labelling. B: Isotype control. C: CD 29 2nd antibody control. D: CD 34 and CD 45 double negative. E: CD 105 and CD 29 double positive.

Most evident is that the fluorescent profile for each plot is the same as the control cells, showing that the presence of internalised nanosensors has not affected the relative presence or absence of the chosen CD markers.

Incubating 24 mg nanosensors with a 25-30 % confluent T75 flask of MSCs caused a majority of the cells to detach from the plate (as seen when counting the cell populations during experimental preparation) those that remained were considerably rolled up and spiculated i.e. cellular processes were still visible suggesting they had shrunken quickly. Bearing this in mind it was assumed the cells were no longer viable so using CD antibody markers for cell identification on these cells was ruled out. However an isotype and CD 29 2nd antibody control was carried out to establish whether the membranes had become leaky. As seen in Figure 99 the membranes appear

to remain intact even though the cells looked morphologically non-viable and this observation was backed up with the FS/SS data indicating the cells were dead or dying. It shows that assessment of flow cytometry data based on the presence / absence of fluorescent CD markers alone is not enough to establish the effect of nanosensors upon cell health or viability. A combination of (confocal) microscopy, and more quantitative flow cytometry FS/SS data could be used to address cell health more specifically. Flow cytometry therefore is a powerful tool which can be used to establish upper loading limits of nanosensors.

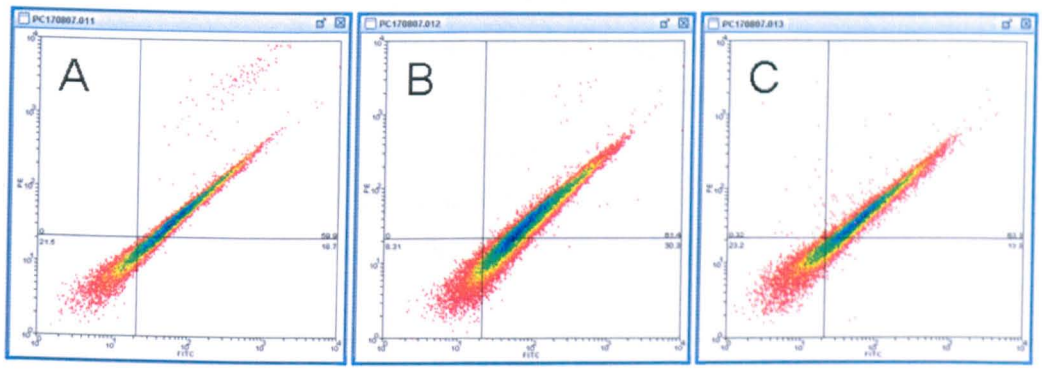

Figure 99 Suspected unviable cells after 24 mg Tat nanosensor incubation although these plots are very similar to the plots for control cells. A: No labelling control. B: Isotype control. C: CD 29 2nd antibody control.

The question of how long it takes for surface marker changes to occur after internalisation is important for these experiments because, to be detected, the changes must occur within the time-frame of the experiment. For these experiments the nanosensors were loaded over a three hour period and subsequent resting times were only 2 – 20 h before they were labelled and fixed. If changes in surface markers take a number of days, or even several passages, to become apparent then it would seem this approach will not pick them up. Future work utilising flow cytometry must take this into consideration.

5.3.4 Investigation of internalised fluorescent nanosensors using flow cytometry

Assessing the feasibility of using flow cytometry to observe internalised nanosensors was based on a simple experimental design of monitoring the FITC parameter, as for CD 105, after loading MSCs with FITC-Tat nanosensors. Controls of FITC-nanosensors with no surface Tat peptides and FITC-Tat conjugates were carried out to act as negative and positive controls respectively. Initially each population used during these experiments was assessed using trypan blue as a marker for cell viability, an example of which is shown in Table 4. The trypan blue assay data would normally be used to determine loading amounts at which unacceptable morphological alterations within the cells deem further experimentation invalid. Hopefully it will become apparent how much more information is available when using flow cytometry and FACS analysis regarding cell health compared to this basic cell viability test.

Trypan Blue Cell Viability Data				
		FITC-nanosensors		
		No. Viable cells	No. Non-viable cells	Percentage viability
Low	6 mg	160	3	98.1
Medium	12 mg	167	2	98.8
High	24 mg	169	1	99.4
		FITC-TAT-conjugate		
		No. Viable cells	No. Non-viable cells	Percentage viability
Low	0.143 mg	95	9	90.5
Medium	0.286 mg	122	7	94.2
High	0.571 mg	70	4	94.3
		FITC-TAT-nanosensors		
		No. Viable cells	No. Non-viable cells	Percentage viability
Low	6 mg	206	2	99.0
Medium	12 mg	217	1	99.5
High	24 mg	169	1	99.4

Table 4 Typical qualitative data available during assessment of cell viability after loading.

Figure 100 shows two negative controls of 12 mg and 24 mg of FITC-nanosensors per 100 % confluent T75 of MSCs, as expected there has been no detectable internalisation or binding of nanosensors to the surface. This further substantiates the observations that an active delivery method is required for the internalisation of nanosensors into non phagocytic mammalian cells.

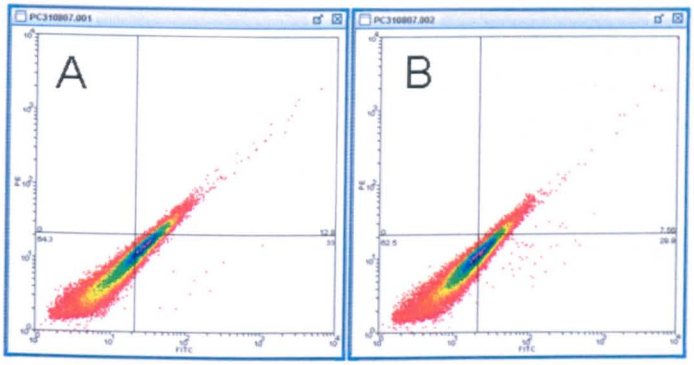

Figure 100 Control cells incubated with FITC nanosensors without Tat surface peptides. A: T75 flask loaded with 12 mg FITC-nanosensors. B: T75 flask loaded with 24 mg FITC-nanosensors. No binding is seen providing more evidence for the necessity of an active precursor of internalisation.

Results obtained for the positive control of FITC-Tat conjugate loading are shown in Figure 101. Loading amounts of 0.143, 0.286, and 0.571 mg FITC-Tat conjugate are shown from left to right. It is clear the addition has caused a shift along the *x* axis, the FITC parameter, in each MSC population. There is no shift along the *y* axis as seen previously as PE is not present, only a single fluorophore was used in these experiments. Additionally these data can be directly compared to the loading of CHO-K1 cells with FITC-Tat conjugate which were assessed with confocal microscopy previously (section 4.3.6) showing that two independent methods and independent cell lines have yielded the same results. Figure 102 shows the same experiment substituting FITC-Tat conjugate for FITC-Tat nanosensors. Again it was possible to observe internalised nanosensors indicated by a positive shift in the FITC parameter.

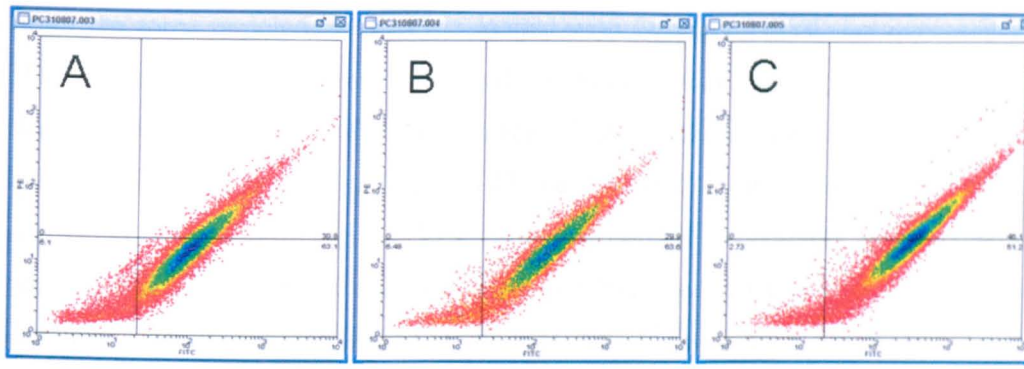

Figure 101 Positive control cells loaded with FITC-Tat conjugate. A: T75 flask loaded with 0.143 mg FITC-Tat conjugate. B: T75 flask loaded with 0.286 mg FITC-Tat conjugate. C: T75 flask loaded with 0.571 mg FITC-Tat conjugate.

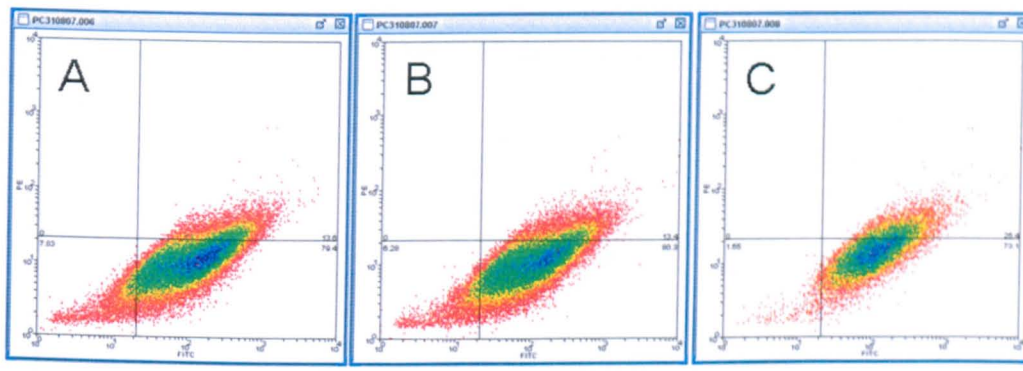

Figure 102 Cells loaded with FITC-Tat nanosensors. A: T75 flask loaded with 6 mg FITC-Tat nanosensors. B: T75 flask loaded with 12 mg FITC-Tat nanosensors. C: T75 flask loaded with 24 mg FITC-Tat nanosensors.

These experiments also help to resolve any question as to whether Tat nanosensors simply attach to the cellular surface of cells as opposed to becoming internalised after passing through the cellular membrane. The cell preparation protocol requires that the cells are removed from the T75 flask surface, which is achieved with a trypsin / EDTA solution. Trypsin is an endopeptidase which specifically cleaves at the carboxylic side of lysine and arginine [211]; Tat peptide has several of each residue and will be quickly cleaved by trypsin. Cleavage of Tat peptide and centrifugation / washing steps will ensure that any cargo attached to the cell via Tat will be certainly stripped from the cell surface – any subsequent fluorescent signal therefore can only originate from inside the cell.

From the same population of MSCs loaded with 24 mg of FITC-Tat nanosensors per 100 % confluent T75 (shown previously in Figure 102) it was possible to show the simultaneous detection of fluorescence from surface attached antibodies and internalised nanosensors. In Figure 103 the left and middle panels show irrelevant antibody isotype control and CD 29 2nd antibody control respectively and the final result portrayed in the right panel shows a sub-population loaded with FITC-Tat nanosensors and subsequently labelled with CD 29 plus the 2nd antibody. This shows that future experiments requiring the simultaneous observation of internalised nanosensors and surface bound antibodies is possible; as long as the fluorophores are chosen carefully so that their spectral properties do not significantly overlap.

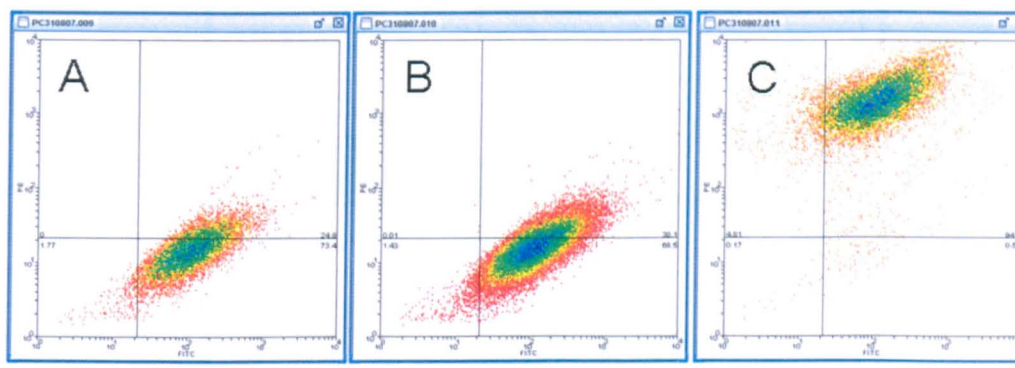

Figure 103 Antibody labelling controls for MSCs loaded with FITC-Tat nanosensors, 24 mg per T75 flask, same population as Figure 102. A: Isotype control showing only FITC fluorescence coming from internalised nanosensors. B: CD 29 2nd antibody control showing only FITC fluorescence coming from internalised nanosensors. C: CD 29 positive labelling control showing both FITC and PE fluorescence coming from internalised nanosensors and surface bound CD 29 antibody respectively.

Finally it was shown that the relative intensity of fluorescence within cells can be monitored with flow cytometry, Figure 104. The data presented is of the MSCs loaded with FITC-Tat conjugate. The top section shows a histogram for the forward scatter from these cells, the middle section the side scatter, and the bottom section the FITC intensity for each cell. Arbitrary units are used in each case. The *y* axis represents cell number and differences between cell populations show different cell number counts during flow cytometry and do not imply differences between cell morphology or fluorescence. Information regarding the intensity of fluorescence from each cell is found on the *x* axis of the bottom section which is displayed on a logarithmic scale. The

data on FS/SS is linear. The main points from these histograms are that the FS/SS intensity does not increase as the amount of FITC-Tat conjugate added to the cells was increased, indicating that there is no morphological change. However there is a coincidence of increase in average cell population fluorescence with increased FITC-Tat conjugate loading.

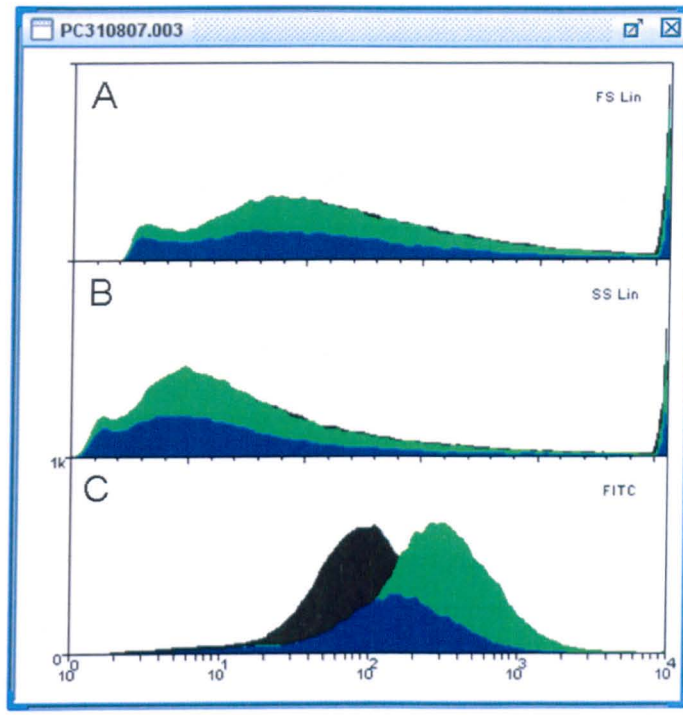

Figure 104 Histogram plot showing data from FITC-Tat conjugate loaded MSCs. Black filled line: T75 flask loaded with 0.143 mg FITC-Tat conjugate. Blue filled line: T75 flask loaded with 0.286 mg FITC-Tat conjugate. Green filled line: T75 flask loaded with 0.571 mg FITC-Tat conjugate. The key result is the position of the peaks on the *x* axis. Panel A: Linear forward scatter data. Panel B: Linear side scatter data. Panel C: Log FITC fluorescence data. Both forward and side scatter remain constant for the three populations indicating no change in cellular morphology. A shift in peak position from left to right indicates an increase in the number of cells showing an increase in FITC associated fluorescence. This coincides with increasing concentrations of FITC-Tat conjugate during the incubation.

The shift from left to right, in the distribution of each cell population, along the FITC parameter *x* axis shows that it is possible to measure a difference in fluorescence between populations. It would therefore be possible to have a heterogeneous population (e.g. these three flasks of cells mixed together) and still separate them out accordingly.

When the histogram plots of FITC-Tat nanosensors are compared it was not possible to see an increase in fluorescence as was observed with the FITC-Tat conjugate. Shown side by side in Figure 105, with the fill of each plot removed for clarity, one can see that the distribution of fluorescence within the different populations (6, 12, and 24 mg per 100 % confluent T75) of FITC-Tat nanosensor loaded MSCs stays constant about the 10^2 mark. This suggests the average number of nanosensors per cell remains constant even though the initial number of nanosensors incubated with the cells doubles between each of the three populations.

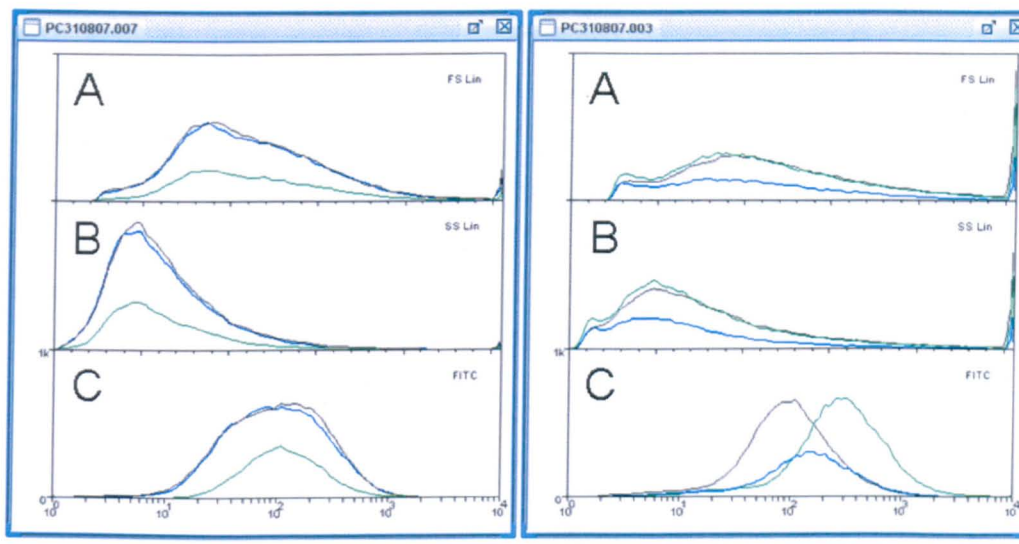

Figure 105 Left: Histogram plot showing data from FITC-Tat nanosensor loaded MSCs. Right: Histogram plot showing data from FITC-Tat conjugate loaded MSCs (as in figure 105). Panel A: Linear forward scatter data. Panel B: Linear side scatter data. Panel C: Log FITC fluorescence data. Fills removed for clarity. An increase in the amount of nanosensors incubated with the cells has not led to an increase in fluorescence as seen with FITC-Tat conjugate.

Reasons behind this are speculative at present. One could argue that the cells only allow a certain number of nanosensors to internalise until a point at which the cell becomes 'full' and surplus extracellular nanosensors are prevented from crossing the cellular membrane. However this seems not be the case as overloading of the cells is a major concern, and can easily be detected through morphological or FS/SS assessment with flow cytometry.

The results may be described using the assumption that each cell takes up nanosensors at a constant rate. If, after the incubation period, there are still surplus nanosensors in the 6 mg (lowest) loading condition then there will be no difference in numbers of nanosensors per cell across all conditions as additional nanosensors are washed away after the incubation period. For example, if there is just a single cell that can take up five nanosensors in three hours, then the conditions of 6, 12, and 24 nanosensors will all give the same result, one cell with five nanosensors. However if the cell can take up 25 nanosensors in the incubation period then ultimately there will be three different cells with 6, 12, and 24 nanosensors respectively yielding a difference in fluorescence between them. Again though, results have been obtained which suggest the three hour incubation period is long enough for overloading of the cells, this was clearly seen when 24 mg of nanosensors were incubated with the ~ 25 % confluent T75 flask. Assuming the pH environment in which the FITC-Tat nanosensors locate to after internalisation is the same between each cell population the result can only mean there is the same average number of nanosensors per cell in each population. However this is unlikely since the initial loading amounts were different – and differences were seen with the FITC-Tat conjugate.

Whatever the cause for this unexpected similarity in numbers of nanosensors internalised it is encouraging that flow cytometry is such a useful and accessible technique which can be utilised when answering these questions.

5.3.5 Confocal microscopy assessment of internalised nanosensors in MSCs

To fully substantiate the results from flow cytometry analysis, intracellular analysis of nanosensors was assessed with confocal microscopy as described in Chapter 4. Utilising rhodamine B nanosensors, which emitted red light, to contrast CD 105:FITC (green) located on the cell's surface confocal images were captured which could be directly comparable to the results reported here (Figure 103). Illustrated in Figure 106 surface labelling of cells with CD 105:FITC can be differentiated from intracellular fluorescence signal originating from rhodamine B nanosensors.

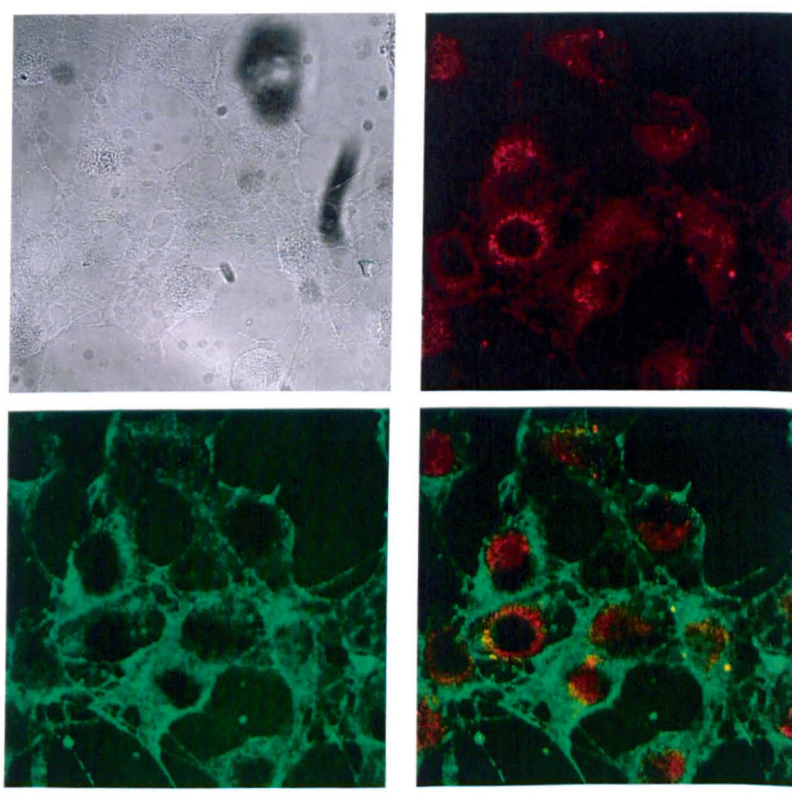

Figure 106 hMSC cells loaded with rhodamine B nanosensors (red) and counter stained with mouse anti-human CD105:FITC antibody (green).

An image is produced (bottom right) which overlays the two fluorescence channels enabling visualisation of nanosensors and CD marker simultaneously much like the flow cytometry data in Figure 103, in which internalised FITC nanosensors are viewed

simultaneously with surface bound CD 29:PE. Analysis of surface bound fluorescence at the same time as the interrogation of intracellular nanosensors is thus possible with two different techniques which yield comparable results. Confocal microscopy enables very detailed images to be taken with information in the locale of internalised nanosensors and is essential for the development of intracellular delivery methods. In contrast flow cytometry provides *en masse* data analysis of nanosensors equalling whole populations of cells which can number in the hundreds of thousands and is essential for gathering qualitative and robust data. The suitability of these techniques to nanosensor examination therefore provides a very powerful means by which to gather relevant data for nanosensor development and application; realised by utilising the combined strengths of each technique.

5.4 Conclusions

Flow cytometry provides the ability to look at entire cellular populations rather than other currently utilised techniques such as confocal laser scanning microscopy and trypan blue cell viability studies which look at far fewer cells in each experiment. Also, the population plots produced with flow cytometry measuring the forward and side scatter give a much clearer and more detailed insight into the population's health in general. This is far better than the 'yes or no' results on cell viability achieved with trypan blue staining or the far more arbitrary information gathered whilst viewing the cells with microscopy. These experiments have also shown that the CD markers accepted to identify pluripotent mesenchymal stem cells are not affected during or immediately after incubation with and subsequent internalisation of Tat delivered nanosensors. As previously mentioned a possible flaw in these experiments is that the amount of time it takes for surface markers to alter after MSCs come into contact with nanosensors is not addressed. If it takes considerably longer than the length of time allowed between incubation and flow cytometry analysis then any changes would have been missed; future experimental controls will have to take this into account. The incubation of nanosensors with MSCs was not assumed to initiate differentiation, if simply incubating MSCs with polyacrylamide particles initiates stem cell differentiation this will be an altogether different, exciting avenue of research. As well as showing that the mechanical interaction of nanosensors and MSCs does not cause any detectable change in cell lineage, flow cytometry was found to be an ideal technique for the assessment of intracellular nanosensors and fluorophore conjugates. It was possible to provide data on both FITC-Tat conjugates and FITC-Tat nanosensors within the cells and in the case of the conjugate a relative increase of fluorescence could be monitored. Even though some unanswered questions remain around the way in which nanosensors accumulate inside the cells and how the numbers of nanosensors outside the cells ultimately leads to the numbers internalised, it is apparent that flow cytometry could be used to measure the fluorescent response of ratiometric nanosensors to an analyte or pH fluctuation within the cell. Calibration of each batch of nanosensors is always carried out prior to experiment, so a way of calibrating the nanosensors with flow cytometry must be devised so the full potential of flow cytometry for nanosensors research can be

realised; perhaps internalising nanosensors in synthetic liposomes and flowing through the cytometer with specific buffers would suffice. This research has shown that flow cytometry in general is a valuable tool in the continuous development of nanosensor technology. Further to this it was possible to measure fluorophores both located on the cell surface and internalised within the cell, thus opening the door for experiments using nanosensor / surface markers in conjunction.

Interestingly it will be possible to trace the movement of nanosensors after internalisation with flow cytometry in terms of mother to daughter cell lineage and answer a major question of whether daughter cells end up with equal numbers of nanosensors during proliferation of nanosensor loaded cells. One scenario is that daughter cells retain equal numbers of nanosensors; comparatively proliferation may yield cells without any nanosensors whatsoever. FACS could determine and separate out these cells on the basis of nanosensor presence ultimately helping to elucidate the different pathways engaged in intracellular nanosensor movement and localisation. Additionally flow cytometry would seem invaluable in determining whether nanosensors are recycled out of the cell altogether by intracellular digestive processes and how long this takes. The overall conclusion from this work is that flow cytometry should be considered without doubt as a key tool during future research of nanosensor development and application.

6 Chapter 6 – Conclusions and Future Direction

6.1 In conclusion

It is without doubt that using a bio-compatible polymer matrix, to serve as a physical and chemical barrier between sensing element and cellular environment, remains a sound proposition as a means to get closer to silent biological observation. This ultimate goal is not yet achieved but the nanosensor technology investigated here forms a strong platform for further development and design iteration. Highlighted through the experiments carried out in this research, the two major areas which need to be addressed are, firstly, the intensity of fluorescent signal coming from a single nanosensor, and secondly, the techniques in which the nanosensors are introduced into the intracellular environment. Prior to this research the theoretical use of cell penetrating peptides as a delivery vector was a valid idea with reference to the literature at that time and the results found here do not denote that CPPs will not serve as efficient delivery vectors in the future. With an emphasis of research attention on post-delivery escape from intracellular vesicles the realisation of CPP delivery vehicles may be soon to come.

6.2 Increasing nanosensor fluorescent signal

A solution to this problem has been proposed and initially investigated experimentally as shown in section 2.3.5. The so-called SuperBright nanosensors built on the current platform but looked at another method of introducing the fluorophores into the polymer matrix which allowed a far greater density of fluorophores per volume of polyacrylamide. The results were initially promising but further work is necessary to realise the idea. By attaching fluorophores to the polymer directly they locate indiscriminately throughout the matrix – this means on the surface of the nanosensor also. Obviously in this surface location they will come into contact with the environment which contradicts the idea of the protective capacity of a nanosensor. However, although not investigated yet, there are foreseeable solutions to this problem which appear realistic.

6.2.1 Enzyme-shaving

This technique is simple, and relies on the diffusional characteristics of an enzyme moving through the polymer matrix. The idea is this: the fluorophores are attached to the polymer backbone of the nanosensor via a cleavable linker, one that a specific enzyme is able to cleave when the nanosensors are dispersed in solution. After confirming the diffusion rate of the enzyme through the polymer it will be possible to allow enzyme activity to reach a certain depth, e.g. 2 nm, at which point the enzyme activity will be halted, perhaps by precipitation of both enzyme and nanosensor in ethanol. Denaturing of the enzyme may be possible with heat for example before the nanosensors are re-suspended so that the redundant enzymes can be washed out of the polymer matrix, Figure 107. Essentially it is analogous to producing core-shell nanoparticles but from a homogeneous matrix. A perhaps significantly simpler way would be to tune polymer pore size and linker length so that enzymes just remove the available surface bound fluorophores.

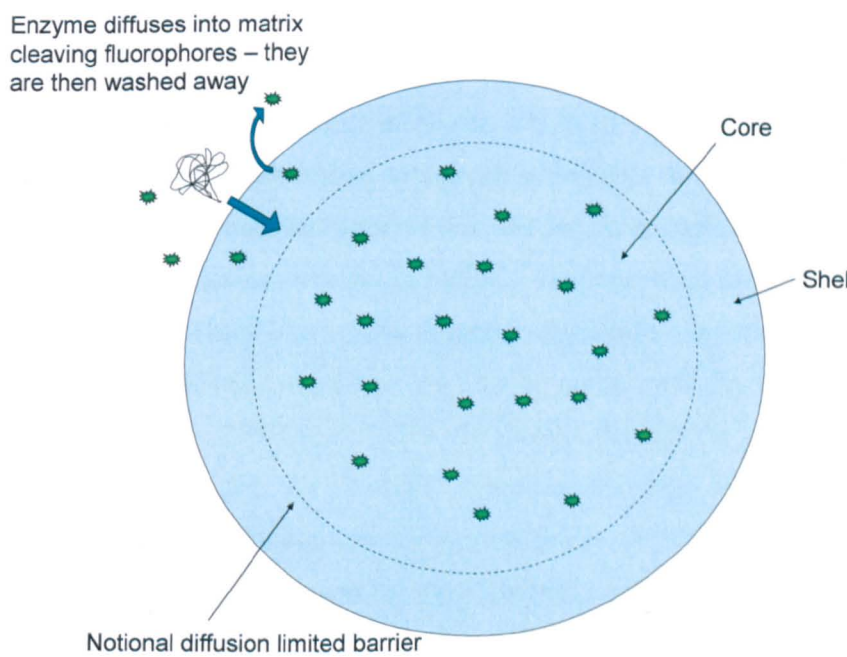

Figure 107 Enzyme-shaving to produce core-shell nanosensors.

6.2.2 Surface fluorophore shielding (molecular shielding)

One could feasibly prevent interaction between surface bound fluorophores and the intracellular environment by attaching a surface molecule which physically protruded further from the surface of the nanosensor than the fluorophore molecule. The molecular shield would be packed to a density so that larger protein species, for example, were prevented from interaction with the fluorophores, but analyte diffusion into the nanosensor was not inhibited. One candidate molecule for this shield could be polyethylene glycol (PEG) which is biologically compatible and readily dissolves in biological aqueous environments. Obviously this solution, as well enzyme-shaving, requires that discrete polymer functional groups are incorporated into the polymer matrix for attachment of the various moieties, if Tat for example is still required as a delivery vector. There are however multiple chemistries which can be investigated to effect this requirement.

6.3 CPP mediated delivery

Understanding the translocation mechanisms by which CPPs enter cells will aid in the coalescence of CPPs and nanosensors to provide a valuable silent delivery technique. These translocation mechanisms however are not yet fully explained so nanosensor research must look to devise suitable techniques for benefiting from the features of CPPs which are useful whilst overcoming the more detrimental aspects like intracellular localisation. These mediatory steps will need to be taken until the full extent of the mechanisms involved in CPP translocation are understood; maybe then the design of custom CPPs which do not, for example, trigger endocytotic mechanisms will be possible. Tat delivery – although proven successful for the delivery of nanosensors across the cell plasma membrane evidence reported here suggests that the nanosensors actually become entrapped within cytoplasmic vesicles (most likely lysosomes). This presents a problem for analyte measurements as the nanosensors, without access to the cytoplasm, are unable to respond to cellular analyte flux as required.

6.3.1 The use of Tat functionalised liposomes as a combinatorial delivery vehicle

Liposomal delivery for oligonucleotides is used routinely for host cell transfection and other cargoes have been delivered using liposomes. The delivery of nanosensors has been explored using liposomes within the scope of this research although is not reported here. The main problem of liposomal delivery is the low rates of uptake, often attributed to the low number of liposome – cell interactions. Combining liposomal delivery with CPP based translocation may offer a route to internalising nanosensors without leading to endocytosis pathways and localisation in intracellular vesicles. The suggestion is to conjugate a Tat peptide to the head group of a portion of lipids making up the liposome. Notionally the Tat peptide will encourage liposome – cell interaction whereupon nanosensors entrapped within the liposome are ejected into the cytoplasm as the liposome fuses with the cellular membrane. To achieve this, a lipid available from Avanti® Polar Lipids Inc. (P/N 880128) may be applicable, Figure 108. This lipid, DSPE-PEG(2000)Amine, having an amine group on the hydrophilic head group will allow the attachment of Tat in a manner comparable to that already explored for the attachment of Tat directly to amine functionalised nanosensors using sulfo-SMCC (Figure 109).

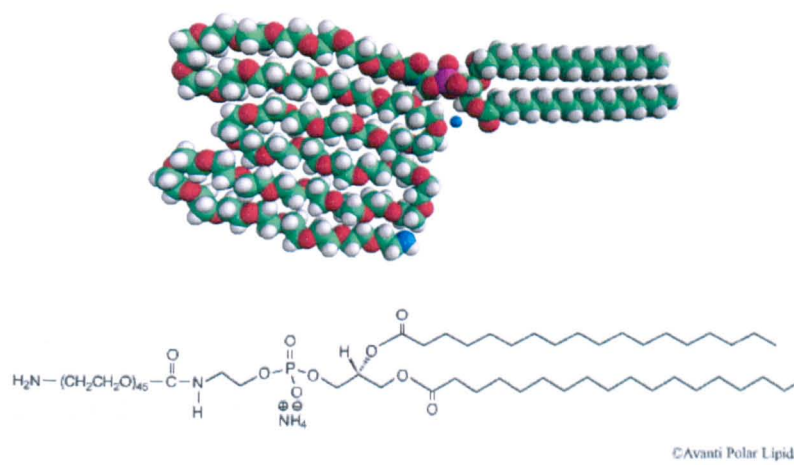

Figure 108 Structures for Avanti Product Number: 880128 DSPE-PEG(2000)Amine 1,2-Distearoyl-sn-Glycero-3-Phosphoethanolamine-N-[Amino(Polyethylene Glycol)2000] (Ammonium Salt).

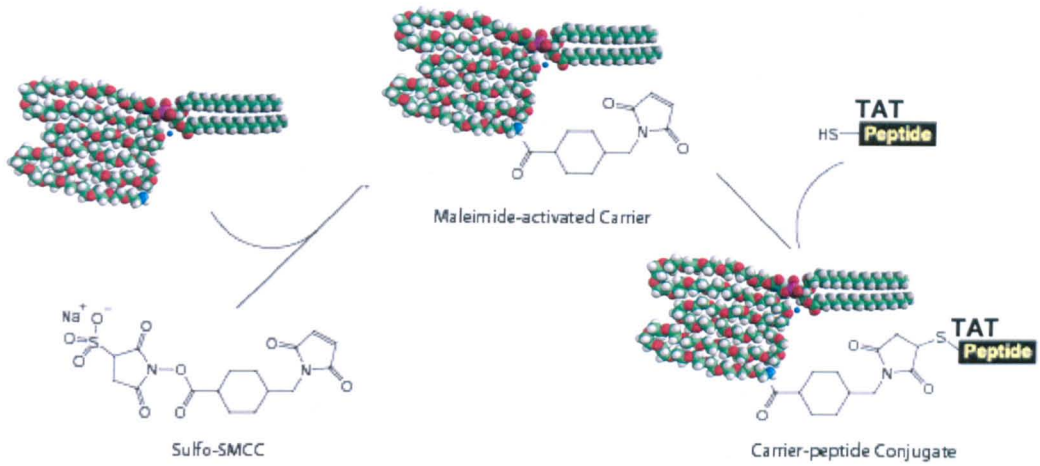

Figure 109 Schematic of one route to Tat attachment to a lipid molecule.

Subsequently liposomes may be produced from 50:50 DOTAP:DOPE (a readily available mixture specifically for transfection) plus a portion of DSPE-PEG(2000)Amine-Tat in an aqueous solution of nanosensors (acrylamide and *bis*-Acrylamide only). With reference to the schematics illustrated here it is apparent that the Tat may be sterically hindered from interacting with the cell membrane; this is because it seems the primary amine group necessary for conjugation faces towards the liposome and away from the cell. It is not known at this time how flexible the PEG(2000) component will be (or if this image correctly portrays DSPE-PEG(2000)Amine) and whether this will allow for Tat – cell interaction. It is estimated that the length of Tat will be at least that of the entire lipid if not twice the length, even in its alpha helical conformation. The flexibility of the PEG and the relative size of Tat would probably favour Tat – cell interaction, however alternatives are possible. With reference to Avanti® Polar Lipids Inc. it would seem that a PEG chain MW close to 350 yields a straight PEG component presenting the end group directly (Figure 110).

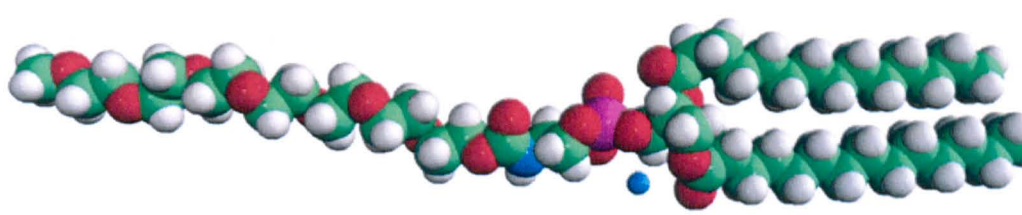

Figure 110 An example of a PEG(350) lipid providing a linear PEG backbone.

Unfortunately the lowest PEG MW offered for a primary amine end group lipid is 2000, the 350 PEG MW having methyl groups exclusively. The ordering of custom lipids is offered by Avanti® Polar Lipids Inc. but the costs incurred will no doubt be substantial. Investigation into alternative chemistries for Tat attachment may find methyl group an acceptable linker group. There may also be a route to using sulfo-SMCC with a PEG spacer as an alternative.

6.3.2 Nanosensor endosomal breakout

A route of investigation may be to accept the inevitability of endocytosis and concentrate on devising mechanisms for breaking out of the endosome once inside the cell. Again, utilising the fusion of nanosensor bound lipids with the endosomal membrane which can then be cleaved by cellular enzymes may provide a means for cytoplasmic localisation.

6.3.3 Multi-functionalised multi-layered nanosensor constructs

One final suggestion is the synthesis of a multi-functional polymer matrix allowing the attachment of multiple functional groups. These groups could also be conjugated to the polymer matrix via cleavable linkers which are cleaved by indigenous cytoplasmic enzymes removing the functional group once its use has been exhausted. In this manner a multi-functional multi-layered coat could be built up around the nanosensor. For example, an ultimate nanosensor construct could contain a relatively greater number of fluorophores attached to the polymer backbone directly; have an outer layer of Tat peptide, lipids, and PEG molecules enhancing cellular interaction, and fusion, whilst remaining inherently biologically compatible. There are evidently several routes which may possibly provide better nanosensors that are a few steps closer to true silent observation.

7 References

1. Lambeck, P.V., *Integrated optical sensors for the chemical domain.* Measurement Science & Technology, 2006. **17**(8): p. R93-R116.
2. Udd, E., *An Overview of Fiberoptic Sensors.* Review of Scientific Instruments, 1995. **66**(8): p. 4015-4030.
3. Gauglitz, G., *Direct optical sensors: principles and selected applications.* Analytical and Bioanalytical Chemistry, 2005. **381**(1): p. 141-155.
4. Brogan, K.L. and D.R. Walt, *Optical fiber-based sensors: application to chemical biology.* Current Opinion in Chemical Biology, 2005. **9**(5): p. 494-500.
5. Biran, I. and D.R. Walt, *Optical Imaging fiber-based single live cell arrays: A high- density cell assay platform.* Analytical Chemistry, 2002. **74**(13): p. 3046-3054.
6. Lin, J., *Recent development and applications of optical and fiber-optic pH sensors.* Trac-Trends in Analytical Chemistry, 2000. **19**(9): p. 541-552.
7. Song, A., S. Parus, and R. Kopelman, *High-performance fiber optic pH microsensors for practical physiological measurements using a dual-emission sensitive dye.* Analytical Chemistry, 1997. **69**(5): p. 863-867.
8. Bosch, M.E., et al., *Recent development in optical fiber biosensors.* Sensors, 2007. **7**(6): p. 797-859.
9. Leung, A., P.M. Shankar, and R. Mutharasan, *A review of fiber-optic biosensors.* Sensors and Actuators B-Chemical, 2007. **125**(2): p. 688-703.
10. Passaro, V.M.N., et al., *Guided-wave optical biosensors.* Sensors, 2007. **7**(4): p. 508-536.
11. Kovacs, B., et al., *Optical biosensor for urea with improved response time.* Biosensors & Bioelectronics, 2003. **18**(2-3): p. 111-118.
12. Bhunia, A.K., et al., *Light scattering, fiber optic- and cell-based sensors for sensitive detection of foodborne pathogens.* Journal of Rapid Methods and Automation in Microbiology, 2007. **15**(2): p. 121-145.
13. Jeronimo, P.C.A., A.N. Araujo, and M. Montenegro, *Optical sensors and biosensors based on sol-gel films.* Talanta, 2007. **72**(1): p. 13-27.
14. Castillo, J., et al., *Biosensors for life quality - Design, development and applications.* Sensors and Actuators B-Chemical, 2004. **102**(2): p. 179-194.
15. Fricker, M.D. and A.J. Meyer, *Confocal imaging of metabolism in vivo: pitfalls and possibilities.* Journal Of Experimental Botany, 2001. **52**(356): p. 631-640.
16. Hutzler, P., et al., *Tissue localization of phenolic compounds in plants by confocal laser scanning microscopy.* Journal of Experimental Botany, 1998. **49**(323): p. 953-965.
17. Johnsson, N. and K. Johnsson, *Chemical tools for biomolecular imaging.* Acs Chemical Biology, 2007. **2**(1): p. 31-38.
18. Tsien, R.Y., *Building and breeding molecules to spy on cells and tumors.* Febs Letters, 2005. **579**(4): p. 927-932.
19. Zhang, J., et al., *Creating new fluorescent probes for cell biology.* Nature Reviews Molecular Cell Biology, 2002. **3**(12): p. 906-918.
20. Petty, H.R., *Fluorescence microscopy: Established and emerging methods, experimental strategies, and applications in immunology.* Microscopy Research and Technique, 2007. **70**(8): p. 687-709.
21. Weiss, S., *Fluorescence spectroscopy of single biomolecules.* Science, 1999. **283**(5408): p. 1676-1683.
22. Hell, S.W., *Toward fluorescence nanoscopy.* Nature Biotechnology, 2003. **21**(11): p. 1347-1355.
23. Garini, Y., B.J. Vermolen, and I.T. Young, *From micro to nano: recent advances in high-resolution microscopy.* Current Opinion in Biotechnology, 2005. **16**(1): p. 3-12.
24. Bui, J.D., et al., *Probing intracellular dynamics in living cells with near-field optics.* Journal of Neuroscience Methods, 1999. **89**(1): p. 9-15.
25. Pickup, J.C., et al., *Fluorescence-based glucose sensors.* Biosensors & Bioelectronics, 2005. **20**(12): p. 2555-2565.
26. Koschinsky, T. and L. Heinemann, *Sensors for glucose monitoring: technical and clinical aspects.* Diabetes-Metabolism Research And Reviews, 2001. **17**(2): p. 113-123.

27. Koschwanez, H.E. and W.M. Reichert, *In vitro, in vivo and post explanTation testing of glucose-detecting biosensors: Current methods and recommendations.* Biomaterials, 2007. **28**(25): p. 3687-3703.
28. Voldman, J., M.L. Gray, and M.A. Schmidt, *Microfabrication in biology and medicine.* Annual Review of Biomedical Engineering, 1999. **1**: p. 401-425.
29. Cote, G.L., R.M. Lec, and M.V. Pishko, *Emerging biomedical sensing technologies and their applications.* Ieee Sensors Journal, 2003. **3**(3): p. 251-266.
30. Vojinovic, V., J.M.S. Cabral, and L.P. Fonseca, *Real-time bioprocess monitoring Part I: In situ sensors.* Sensors and Actuators B-Chemical, 2006. **114**(2): p. 1083-1091.
31. Rodriguez-Mozaz, S., M.J.L. de Alda, and D. Barcelo, *Biosensors as useful tools for environmental analysis and monitoring.* Analytical and Bioanalytical Chemistry, 2006. **386**(4): p. 1025-1041.
32. James, D., et al., *Chemical sensors for electronic nose systems.* Microchimica Acta, 2005. **149**(1-2): p. 1-17.
33. Veetil, J.V. and K.M. Ye, *Development of immunosensors using carbon nanotubes.* Biotechnology Progress, 2007. **23**(3): p. 517-531.
34. Kim, K.Y., *Nanotechnology platforms and physiological challenges for cancer therapeutics.* Nanomedicine-Nanotechnology Biology and Medicine, 2007. **3**(2): p. 103-110.
35. Levy, L., et al., *Nanochemistry: Synthesis and characterization of multifunctional nanoclinics for biological applications.* Chemistry Of Materials, 2002. **14**(9): p. 3715-3721.
36. Wu, Y.H. and S.S. Hu, *Biosensors based on direct electron transfer in redox proteins.* Microchimica Acta, 2007. **159**(1-2): p. 1-17.
37. Yotter, R.A., L.A. Lee, and D.M. Wilson, *Sensor technologies for monitoring metabolic activity in single cells - Part I: Optical, methods.* Ieee Sensors Journal, 2004. **4**(4): p. 395-411.
38. Yotter, R.A. and D.M. Wilson, *Sensor technologies for monitoring metabolic activity in single cells - Part II: Nonoptical methods and applications.* Ieee Sensors Journal, 2004. **4**(4): p. 412-429.
39. Pumera, M., et al., *Electrochemical nanobiosensors.* Sensors and Actuators B-Chemical, 2007. **123**(2): p. 1195-1205.
40. Tan, W.H., Z.Y. Shi, and R. Kopelman, *Miniaturized Fiber-optic Chemical Sensors with Fluorescent Dye-Doped Polymers.* Sensors and Actuators B-Chemical, 1995. **28**(2): p. 157-163.
41. Vo-Dinh, T., *Nanobiosensors: Probing the sanctuary of individual living cells.* Journal Of Cellular Biochemistry, 2002: p. 154-161.
42. Vo-Dinh, T., et al., *Antibody-based nanoprobe for measurement of a fluorescent analyte in a single cell.* Nature Biotechnology, 2000. **18**(7): p. 764-767.
43. Vo-Dinh, T., B.M. Cullum, and D.L. Stokes, *Nanosensors and biochips: frontiers in biomolecular diagnostics.* Sensors And Actuators B-Chemical, 2001. **74**(1-3): p. 2-11.
44. Vo-Dinh, T. and P. Kasili, *Fiber-optic nanosensors for single-cell monitoring.* Analytical and Bioanalytical Chemistry, 2005. **382**(4): p. 918-925.
45. Tan, W.H., et al., *Ultrasmall for cellular.* Analytical Chemistry, 1999. **71**(17): p. 606A-612A.
46. Tan, W.H., Z.Y. Shi, and R. Kopelman, *Development of Submicron Chemical Fiber Optic Sensors.* Analytical Chemistry, 1992. **64**(23): p. 2985-2990.
47. Mohr, G.J., et al., *Application of potential-sensitive fluorescent dyes in anion- and cation-sensitive polymer membranes.* Sensors and Actuators B-Chemical, 1997. **39**(1-3): p. 239-245.
48. Wroblewski, W., et al., *Towards advanced chemical microsensors - an overview.* Talanta, 2004. **63**(1): p. 33-39.
49. Clark, H.A., et al., *Subcellular optochemical nanobiosensors: probes encapsulated by biologically localised embedding (PEBBLEs).* Sensors And Actuators B-Chemical, 1998. **51**(1-3): p. 12-16.
50. Singh, A. and K.P. Gopinathan, *Confocal microscopy: A powerful technique for biological research.* Current Science, 1998. **74**(10): p. 841-851.
51. Williams, D.A., D.N. Bowser, and S. Petrou, *Confocal Ca2+ imaging of organelles, cells, tissues, and organs,* in *Confocal Microscopy.* 1999. p. 441-469.
52. Stubbs, S. and N. Thomas, *Dynamic green fluorescent protein sensors for high-content analysis of the cell cycle,* in *Measuring Biological Responses with Automated Microscopy.* 2006. p. 1-21.
53. Clark, H.A., et al., *Optical nanosensors for chemical analysis inside single living cells. 1. Fabrication, characterization, and methods for intracellular delivery of PEBBLE sensors.* Analytical Chemistry, 1999. **71**(21): p. 4831-4836.

54. Xu, H., et al., *A real-time ratiometric method for the determination of molecular oxygen inside living cells using sol-gel-based spherical optical nanosensors with applications to rat C6 glioma.* Analytical Chemistry, 2001. **73**(17): p. 4124-4133.
55. Buck, S.M., et al., *Nanoscale probes encapsulated by biologically localized embedding (PEBBLEs) for ion sensing and imaging in live cells.* Talanta, 2004. **63**(1): p. 41-59.
56. Clark, H.A., et al., *Optochemical nanosensors and subcellular applications in living cells.* Mikrochimica Acta, 1999. **131**(1-2): p. 121-128.
57. Lakowicz, J.R., *Principles of Fluorescence Spectroscopy.* 1999, New York: Kluwer Academic / Plenum Publishers.
58. Kasha, M., *Characterization of Electronic Transitions in Complex Molecules.* Discussions of the Faraday Society, 1950(9): p. 14-19.
59. Wilson, T. and B.R. Masters, *Confocal Microscopy - Introduction.* Applied Optics, 1994. **33**(4): p. 565-566.
60. Minsky, M., *Memoir On Inventing The Confocal Scanning Microscope.* Scanning, 1988. **10**(4): p. 128-138.
61. Minsky, M., *Microscopy Apparatus*, U.S.P. Office, Editor. 1957: United States of America. p. 1-5.
62. Johnson, B., *Image is everything - Confocal microscopy in focus.* Scientist, 1999. **13**(3): p. 22-24.
63. Ribbe, A.E., *Laser scanning confocal microscopy in polymer science.* Trends in Polymer Science, 1997. **5**(10): p. 333-337.
64. Paddock, S.W., Fellers, T.J, and Davidson, M.W *Introduction to confocal microscopy.* Microscopy U 2000 [cited.
65. Webb, R.H., *Theoretical basis of confocal microscopy*, in *Confocal Microscopy*. 1999. p. 3-20.
66. Born, M.a.W., Emil, *Principles of Optics: Electromagnetic Theory of Propagation, Interference and Diffraction of Light.* 2000, Cambridge: Cambridge University Press.
67. Sheppard, C.a.S., D, *Confocal Laser Scanning Microscopy.* Royal Microscopical Society Microscopy Handbooks. 1997, Oxford: Bios Scientific Publishers Ltd. 120.
68. Zucker, R.M. and O.T. Price, *Practical confocal microscopy and the evaluation of system performance.* Methods-a Companion to Methods in Enzymology, 1999. **18**(4): p. 447-458.
69. Babcock, G.F., *QuantiTation of phagocytosis by confocal microscopy*, in *Confocal Microscopy*. 1999. p. 319-328.
70. Bkaily, G., D. Jacques, and P. Pothier, *Use of confocal microscopy to investigate cell structure and function*, in *Confocal Microscopy*. 1999. p. 119-135.
71. Dailey, M., et al., *Concepts in imaging and microscopy exploring biological structure and function with confocal microscopy.* Biological Bulletin, 1999. **197**(2): p. 115-122.
72. Kong, S.K., et al., *Practical considerations in acquiring biological signals from confocal microscope*, in *Confocal Microscopy*. 1999. p. 20-26.
73. Ohata, H., et al., *Confocal imaging analysis of intracellular ions in mixed cellular systems or in situ using two types of confocal microscopic systems*, in *Confocal Microscopy*. 1999. p. 425-441.
74. Ribbe, A.E., et al., *Identification of the morphology of a thin film by fluorescence laser-scanning confocal microscopy.* Polymer, 1998. **39**(26): p. 7149-7151.
75. Leica-Microsystems, L. *http://www.leica-microsystems.com/Confocal_Microscopes*. 2007.
76. Hamamatsu, P.K.K. *Photomultiplier Tubes Construction and OperTating Characteristics Connections to External Circuits.* 1998.
77. Serway, R.A., *Physics for Scientists and Engineers.* 1990: Saunders College Publishers. 1200.
78. Henel, G. and J.L. Schmitz, *Basic theory and clinical applications of flow cytometry.* Labmedicine, 2007. **38**(7): p. 428-436.
79. Marti, G.E., et al., *Introduction to flow cytometry.* Seminars in Hematology, 2001. **38**(2): p. 93-99.
80. Rahman, M., *Introduction to Flow Cytometry.* 2005, Kidlington: Serotec. 33.
81. Watson, J.V., *Introduction to Flow Cytometry, First Paperback Edition.* 2004, Cambridge: Cambridge University Press.
82. Herzenberg, L.A., S.C. De Rosa, and L.A. Herzenberg, *Monoclonal antibodies and the FACS: complementary tools for immunobiology and medicine.* Immunology Today, 2000. **21**(8): p. 383-390.
83. Bakke, A.C., *Clinical applications of flow cytometry.* Laboratory Medicine, 2000. **31**(2): p. 97-102.

84. Bene, M.C., *Clinical applications of flow cytometry outside HIV monitoring.* Cytometry Part A, 2004. **59A**(1): p. 109-109.
85. Schmidt, M., et al., *FACS technology used in a new rapid bacterial detection method.* Transfusion Medicine, 2006. **16**(5): p. 355-361.
86. O'Toole, P., *Cell Sorting - The Basics RMS Flow Cytometer Course 2005.* 2005, University of York: York.
87. Clark, H.A., et al., *Optical nanosensors for chemical analysis inside single living cells. 2. Sensors for pH and calcium and the intracellular application of PEBBLE sensors.* Analytical Chemistry, 1999. **71**(21): p. 4837-4843.
88. Park, E.J., et al., *Ratiometric optical PEBBLE nanosensors for real-time magnesium ion concentrations inside viable cells.* Analytical Chemistry, 2003. **75**(15): p. 3784-3791.
89. Xu, H., J.W. Aylott, and R. Kopelman, *Fluorescent nano-PEBBLE sensors designed for intracellular glucose imaging.* Analyst, 2002. **127**(11): p. 1471-1477.
90. Srivastava, A. and G. Krishnamoorthy, *Time-resolved fluorescence microscopy could correct for probe binding while estimating intracellular pH.* Analytical Biochemistry, 1997. **249**(2): p. 140-146.
91. Sumner, J.P. and R. Kopelman, *Alexa Fluor 488 as an iron sensing molecule and its application in PEBBLE nanosensors.* Analyst, 2005. **130**(4): p. 528-533.
92. Brasuel, M., et al., *Production, characteristics and applications of fluorescent PEBBLE nanosensors: Potassium, oxygen, calcium and pH imaging inside live cells.* Sensors and Materials, 2002. **14**(6): p. 309-338.
93. Buck, S.M., et al., *Optochemical nanosensor PEBBLEs: photonic explorers for bioanalysis with biologically localized embedding.* Current Opinion in Chemical Biology, 2004. **8**(5): p. 540-546.
94. Kopelman, R., *Fluorescent pebble nano-sensors for real-time intracellular chemical analysis.* Abstracts of Papers of the American Chemical Society, 2004. **227**: p. U111-U111.
95. Webster, A., S.J. Compton, and J.W. Aylott, *Optical calcium sensors: development of a generic method for their introduction to the cell using conjugated cell penetrating peptides.* Analyst, 2005. **130**(2): p. 163-170.
96. Koo, Y.E.L., et al., *Photonic explorers based on multifunctional nanoplatforms for biosensing and photodynamic therapy.* Applied Optics, 2007. **46**(10): p. 1924-1930.
97. Kopelman, R., *Award Address: From nano-domain spectroscopy to single cell spectrochemical imaging.* Abstracts of Papers of the American Chemical Society, 2005. **230**: p. U196-U196.
98. Kopelman, R., et al., *The world's smallest sensors: Intracellular opto-chemical probes.* Abstracts Of Papers Of The American Chemical Society, 1998. **216**: p. 093-IEC.
99. Peterson, J.I., et al., *Fiber Optic Ph Probe for Physiological Use.* Analytical Chemistry, 1980. **52**(6): p. 864-869.
100. Webster, A., et al., *The delivery of PEBBLE nanosensors to measure the intracellular environment.* Biochemical Society Transactions, 2007. **035**(3): p. 538-543.
101. Arriagada, F.J. and K. Osseo-Asare, *Synthesis of nanosize silica in a nonionic water-in-oil microemulsion: Effects of the water/surfactant molar ratio and ammonia concentration.* Journal Of Colloid And Interface Science, 1999. **211**(2): p. 210-220.
102. Poulsen, A.K., et al., *Unusually large acrylamide induced effect on the droplet size in AOT/Brij30 water-in-oil microemulsions.* Journal of Colloid and Interface Science, 2007. **306**(1): p. 143-153.
103. Hunkeler, D., *Mechanism and Kinetics of the Persulfate-Initiated Polymerization of Acrylamide.* Macromolecules, 1991. **24**(9): p. 2160-2171.
104. Orakdogen, N. and O. Okay, *Influence of the initiator system on the spatial inhomogeneity in acrylamide-based hydrogels.* Journal of Applied Polymer Science, 2007. **103**(5): p. 3228-3237.
105. Brookhaven, *http://www.brookhaven.co.uk/zeta-potential.html.* 2007.
106. Colloids, S., *http://www.silver-colloids.com/Tutorials/Intro/pcs18.html.* 2005.
107. Malvern, *http://www.malvern.co.uk/LabEng/technology/zeta_potential/zeta_potential_LDE.htm.* 2000.
108. Sigma-Aldrich, *DEXTRAN Product Number D9260, D4626, D4133, D1662, D4751, D3759, D1390, D1537, D4876, D5251, D1037, D5376, and D5501.* Product Information, 2007 (3/21/01).
109. Sigma-Aldrich, *FLUORESCEIN ISOTHIOCYANATE-DEXTRAN Sigma Stock Nos. FD-4, FD-10S, FD-20S, FD-20, FD-40S, FD-40, FD-70S, FD-70, FD-150S, FD-150, FD-250S, FD-500S, and FD-2000S.* Product Information, 2007(01/01/97).

110. Anderson, S., et al., *Preparation and Characterization of 2,2'-Bipyridine-4,4'-Disulphonic and Bipyridine-5-Sulfonic Acids and Their Ruthenium(Ii) Complexes - Excited-State Properties and Excited-State Electron-Transfer Reactions of Ruthenium(Ii) Complexes Containing 2,2'-Bipyridine-4,4'-Disulphonic Acid or 2,2'-Bipyridine-4,4'-Dicarboxylic Acidp.* Journal of the Chemical Society-Dalton Transactions, 1985(11): p. 2247-2261.
111. Castellano, F.N. and J.R. Lakowicz, *A water-soluble luminescence oxygen sensor.* Photochemistry and Photobiology, 1998. **67**(2): p. 179-183.
112. Whitaker, J.E., R.P. Haugland, and F.G. Prendergast, *Spectral and Photophysical Studies of Benzo[C]Xanthene Dyes - Dual Emission Ph Sensors.* Analytical Biochemistry, 1991. **194**(2): p. 330-344.
113. Sun, H., et al., *Synthesis and characterization of ratiometric, pH sensing nanoparticles with covalently attached fluorescent dyes.* Chemistry of Materials, 2006. **18**(15): p. 3381-3384.
114. Loewenstein, W.R., *The Touchstone of Life, Molecular Information, Cell Communication, and the FoundTations of Flife.* 2000: Oxford University Press. 384.
115. Chakravarthy, B, and J.F. Whitfield., *Calcium The Grand-Master Cell Signalar*, ed. P.B. Cavers. 2001, Ottawa, Ontario, Canada: NRC Research Press. 247.
116. Takahashi, A., Camacho, Patricia., Lechleiter, James., Herman, Brian., *Measurement of intracellular Calcium* Physiological Reviews, 1999. **79**(4): p. 1089 - 1125.
117. Campbell, A.K., *Intracellular Calcium Its Role as Regulator.* Monographs in Molecular Biophysics and Biochemistry, ed. H. Gutfreund. 1983, Chichester, UK: John Wiley and Sons Ltd. 556.
118. Cobbold, P.H.and J.G.McCormack., *Cellular Calcium.* A Practical Approach, ed. D.R.a.B.D. Hames. 1991, Oxford, UK: Oxford University Press. 418.
119. Silver, R.B., *Imaging structured space-time patterns of Ca2+ signals: essential information for decisions in cell division.* Faseb Journal, 1999. **13**: p. S209-S215.
120. Tuffet-Anghileri, A.M. and L.J.Anghileri., *The Role of Calcium in Biological Systems Volume I.* 1982, Boca Raton, Florida, USA: CRC Press. 276.
121. Tuffet-Anghileri, A.M. and L.J.Anghileri., *The Role of Calcium in Biological Systems Volume II.* 1982, Boca Raton, Florida, USA. 229.
122. Whelan, J. and D. Evered., *Calcium and the Cell*, ed. C. Foundation. 1986, Chichester, UK: John Wiley and Sons Ltd. 300.
123. Herbst, C., *The divergence of crenation and tissue cells in a lime-free medium.* Archiv Fur Entwicklungsmechanik Der Organismen, 1900. **9**(3): p. 424-463.
124. Shooter, R.A. and H.V. Wyatt, *Mineral Requirements for Growth of Staphylococcus-Pyogenes - Effect of Magnesium and Calcium Ions.* British Journal of Experimental Pathology, 1955. **36**(4): p. 341-350.
125. Kornberg, A., et al., *Origin of Proteins in Sporulation.* Annual Review of Biochemistry, 1968. **37**: p. 51-&.
126. Manery, J.F., *Connective Tissue Electrolytes.* Federation Proceedings, 1966. **25**(6P1): p. 1799.
127. Manery, J.F., *Effects of Ca Ions on Membranes.* Federation Proceedings, 1966. **25**(6P1): p. 1804.
128. Brink, F., *The Role of Calcium Ions in Neural Processes.* Pharmacological Reviews, 1954. **6**(3): p. 243-298.
129. Reuter, H., Blaustei.Mp, and G. Haeusler, *Na-Ca Exchange and Tension Development in Arterial Smooth-Muscle.* Philosophical Transactions of the Royal Society of London Series B-Biological Sciences, 1973. **265**(867): p. 87-94.
130. Fearon, D.T. and K.F. Austen., *The human complement system: biochemistry, biology, and pathobiology.* Essays Med. Biochem., 1976. **2**: p. 1 - 35.
131. Hallet, M.B., Hodges, R., Cadman, M., Blanchfield, H., Dewitt, S., Pettit, E.J., Laffafian, I., Davies, E.V., *Techniques for measuring and manipulating free Ca2+ in the cytosol and organelles of neutrophils.* Journal of Immunological Methods, 1999. **232**(1-2): p. 77-88.
132. Peterson, O.H., Burdakova, N., *Fluorescent probes used for measuring intracelluar calcium.* Encyclopedia of life sciences. 2003, Chichester: Jon Wiley & Sons Ltd.
133. Oconnor, S.E., *Recent Developments in the Classification and Functional-Significance of Receptors for Atp and Utp, Evidence for Nucleotide Receptors.* Life Sciences, 1992. **50**(22): p. 1657-1664.
134. Iredale, P.A. and S.J. Hill, *Increases in Intracellular Calcium Via Activation of an Endogenous P(2)-Purinoceptor in Cultured Cho-K1 Cells.* British Journal of Pharmacology, 1993. **110**(4): p. 1305-1310.

135. Iredale, P.A., et al., *Inositol 1,4,5-Trisphosphate Generation and Calcium Mobilization Via Activation of an Atypical P-2 Receptor in the Neuronal Cell-Line, N1e-115.* British Journal of Pharmacology, 1992. **107**(4): p. 1083-1087.
136. Probes, M., *Fluo Calcium Indicators.* Invitrogen Product Information, 2005(MP 01240): p. 1 - 5.
137. McGuigan, J.A.S., D. Luthi, and A. Buri, *Calcium Buffer Solutions And How To Make Them - A Do It Yourself Guide.* Canadian Journal Of Physiology And Pharmacology, 1991. **69**(11): p. 1733-1749.
138. Biotek, *http://www.biotek.com/products/tech_res_detail.php?id=131.* 2006.
139. Kao, J.P.Y., *Practical Aspects of Measuring [Ca^{2+}] with Fluorescent Indicators.* Methods in Cell Biology. Vol. 40. 1994. 155 - 181.
140. Probes, M., *19.1 Technical Focus: Loading and Calibration of Intracellular Ion Indicators,* in *The Handbook — A Guide to Fluorescent Probes and Labeling Technologies* Invitrogen, Editor. 2007.
141. Barsoum, J., et al., *Tat-Mediated Delivery of Heterologous Macromolecules into Living Cells.* Restorative Neurology and Neuroscience, 1995. **8**(1-2): p. 11-12.
142. Fawell, S., et al., *Tat-Mediated Delivery of Heterologous Proteins into Cells.* Proceedings of the National Academy of Sciences of the United States of America, 1994. **91**(2): p. 664-668.
143. Futaki, S., *Arginine-rich peptides. An abundant source of membrane-permeable peptides having potential as carriers for intracellular protein delivery.* Journal Of Biological Chemistry, 2001. **276**(8): p. 5836-5840.
144. Gariepy, J. and K. Kawamura, *Vectorial delivery of macromolecules into cells using peptide-based vehicles.* Trends in Biotechnology, 2001. **19**(1): p. 21-28.
145. Lundberg, P. and U. Langel, *A brief introduction to cell-penetrating peptides.* Journal Of Molecular Recognition, 2003. **16**(5): p. 227-233.
146. Snyder, E.L. and S.F. Dowdy, *Cell penetrating peptides in drug delivery.* Pharmaceutical Research, 2004. **21**(3): p. 389-393.
147. Green, M. and P.M. Loewenstein, *Autonomous Functional Domains of Chemically Synthesized Human Immunodeficiency Virus Tat Trans-Activator Protein.* Cell, 1988. **55**(6): p. 1179-1188.
148. Elliott, G. and P. Ohare, *Intercellular trafficking and protein delivery by a herpesvirus structural protein.* Cell, 1997. **88**(2): p. 223-233.
149. Derossi, D., G. Chassaing, and A. Prochiantz, *Trojan peptides: the penetratin system for intracellular delivery.* Trends in Cell Biology, 1998. **8**(2): p. 84-87.
150. Richard, J.P., et al., *Cell-penetrating peptides - A reevaluation of the mechanism of cellular uptake.* Journal Of Biological Chemistry, 2003. **278**(1): p. 585-590.
151. Tung, C.H. and R. Weissleder, *Arginine containing peptides as delivery vectors.* Advanced Drug Delivery Reviews, 2003. **55**(2): p. 281-294.
152. Derossi, D., et al., *The 3rd Helix of the Antennapedia Homeodomain Translocates through Biological-Membranes.* Journal of Biological Chemistry, 1994. **269**(14): p. 10444-10450.
153. Derossi, D., et al., *Cell internalization of the third helix of the antennapedia homeodomain is receptor-independent.* Journal of Biological Chemistry, 1996. **271**(30): p. 18188-18193.
154. Langel, U., *Cell-penetrating Peptides, Processes and Applications.* 2002.
155. Green, M., *Autonomous functional domains of chemically synthesized human immunodeficiency virus Tat trans-activator protein.* Cell, 1988. **55**(6): p. 1179 - 1188.
156. Silhol, M., et al., *Different mechanisms for cellular internalization of the HIV-1 Tat-derived cell penetrating peptide and recombinant proteins fused to Tat.* European Journal Of Biochemistry, 2002. **269**(2): p. 494-501.
157. Vives, E., *Cellular uptake of the Tat peptide: an endocytosis mechanism following ionic interactions.* Journal Of Molecular Recognition, 2003. **16**(5): p. 265-271.
158. Futaki, S., S. Goto, and Y. Sugiura, *Membrane permeability commonly shared among arginine-rich peptides.* Journal Of Molecular Recognition, 2003. **16**(5): p. 260-264.
159. Kabouridis, P.S., *Biological applications of protein transduction technology.* Trends In Biotechnology, 2003. **21**(11): p. 498-503.
160. Wender, P.A., et al., *The design, synthesis, and evaluation of molecules that enable or enhance cellular uptake: Peptoid molecular transporters.* Proceedings of the National Academy of Sciences of the United States of America, 2000. **97**(24): p. 13003-13008.
161. Caron, N.J., et al., *Intracellular delivery of a Tat-eGFP fusion protein into muscle cells.* Molecular Therapy, 2001. **3**(3): p. 310-318.
162. Lewin, M., et al., *Tat peptide-derivatized magnetic nanoparticles allow in vivo tracking and recovery of progenitor cells.* Nature Biotechnology, 2000. **18**(4): p. 410-414.

163. Zhao, M., et al., *Differential conjugation of Tat peptide to superparamagnetic nanoparticles and its effect on cellular uptake.* Bioconjugate Chemistry, 2002. **13**(4): p. 840-844.
164. Josephson, L., et al., *High-efficiency intracellular magnetic labeling with novel superparamagnetic-Tat peptide conjugates.* Bioconjugate Chemistry, 1999. **10**(2): p. 186-191.
165. Frankel, A.D. and C.O. Pabo, *Cellular Uptake of the Tat Protein from Human Immunodeficiency Virus.* Cell, 1988. **55**(6): p. 1189-1193.
166. National Institute of Allergy and Infectious Diseases., *How HIV Causes AIDS.* http://www.niaid.nih.gov/factsheets/howhiv.htm, 2006.
167. Gilbert, W., *Why Genes in Pieces.* Nature, 1978. **271**(5645): p. 501-501.
168. Chen, L.L., et al., *Increased Cellular Uptake of the Human Immunodeficiency Virus-1 Tat Protein after Modification with Biotin.* Analytical Biochemistry, 1995. **227**(1): p. 168-175.
169. Loret, E.P., et al., *Activating Region of Hiv-1 Tat Protein - Vacuum Uv Circular-Dichroism and Energy Minimization.* Biochemistry, 1991. **30**(24): p. 6013-6023.
170. Efthymiadis, A., L.J. Briggs, and D.A. Jans, *The HIV-1 Tat nuclear localization sequence confers novel nuclear import properties.* Journal of Biological Chemistry, 1998. **273**(3): p. 1623-1628.
171. Truant, R. and B.R. Cullen, *The arginine-rich domains present in human immunodeficiency virus type 1 Tat and Rev function as direct importin beta-dependent nuclear localization signals.* Molecular and Cellular Biology, 1999. **19**(2): p. 1210-1217.
172. Ensoli, B., et al., *Release, Uptake, and Effects of Extracellular Human-Immunodeficiency-Virus Type-1 Tat Protein on Cell-Growth and Viral Transactivation.* Journal of Virology, 1993. **67**(1): p. 277-287.
173. Schwartz, J.J. and S.G. Zhang, *Peptide-mediated cellular delivery.* Current Opinion in Molecular Therapeutics, 2000. **2**(2): p. 162-167.
174. Thoren, P.E.G., et al., *Membrane binding and translocation of cell-penetrating peptides.* Biochemistry, 2004. **43**(12): p. 3471-3489.
175. Vives, E., *Present and future of cell-penetrating peptide mediated delivery systems: "Is the Trojan horse too wild to go only to Troy?"* Journal of Controlled Release, 2005. **109**(1-3): p. 77-85.
176. Vives, E., et al., *TAT peptide internalization: Seeking the mechanism of entry.* Current Protein & Peptide Science, 2003. **4**(2): p. 125-132.
177. Chan, W.C. and P.D. White, *Fmoc Solid Phase Peptide Synthesis: A Practical Approach.* Practical Approach Series, ed. B.D. Hames. Vol. 222. 2000, Oxford: Oxford Universoty Press.
178. Shriver-Lake, L.C., et al., *Covalent binding of genetically engineered microorganisms to porous glass beads.* Analytica Chimica Acta, 2002. **470**(1): p. 71-78.
179. Briddon, S.J., *Hanks Buffered Saline Solution with 1.3 mM calcium chloride for increased chance of successful intracellular calcium flux*, P. Coupland, Editor. 2006, Nottingham University: Nottingham.
180. Christie, R.J. and D.W. Grainger, *Design strategies to improve soluble macromolecular delivery constructs.* Advanced Drug Delivery Reviews, 2003. **55**(3): p. 421-437.
181. Chu, G.L., et al., *The Role of Intracellular Ph and Its Variance in Low Ph Sensitization of Killing by Hyperthermia.* Radiation Research, 1990. **122**(3): p. 288-293.
182. Kneen, M., et al., *Green fluorescent protein as a noninvasive intracellular pH indicator.* Biophysical Journal, 1998. **74**(3): p. 1591-1599.
183. Chaloin, L., et al., *Design of carrier peptide-oligonucleotide conjugates with rapid membrane translocation and nuclear localization properties.* Biochemical and Biophysical Research Communications, 1998. **243**(2): p. 601-608.
184. Hoekstra, D., et al., *Gene delivery by cationic lipids: in and out of an endosome.* Biochemical Society Transactions, 2007. **35**: p. 68-71.
185. Watt, F.M. and B.L.M. Hogan, *Out of Eden: Stem cells and their niches.* Science, 2000. **287**(5457): p. 1427-1430.
186. Friedens.Aj, Chailakh.Rk, and K.S. Lalykina, *Development of Fibroblast Colonies in Monolayer Cultures of Guinea-Pig Bone Marrow and Spleen Cells.* Cell and Tissue Kinetics, 1970. **3**(4): p. 393-&.
187. Pittenger, M.F., et al., *Multilineage potential of adult human mesenchymal stem cells.* Science, 1999. **284**(5411): p. 143-147.
188. Kopen, G.C., D.J. Prockop, and D.G. Phinney, *Marrow stromal cells migrate throughout forebrain and cerebellum, and they differentiate into astrocytes after injection into neonatal*

mouse brains. Proceedings of the National Academy of Sciences of the United States of America, 1999. **96**(19): p. 10711-10716.
189. Sato, Y., et al., *Human mesenchymal stem cells xenografted directly to rat liver are differentiated into human hepatocytes without fusion.* Blood, 2005. **106**(2): p. 756-763.
190. Lange, C., et al., *Hepatocytic gene expression in cultured rat mesenchymal stem cells.* Transplantation Proceedings, 2005. **37**(1): p. 276-279.
191. Choi, K.S., et al., *In vitro trans-differentiation of rat mesenchymal cells into insulin-producing cells by rat pancreatic extract.* Biochemical and Biophysical Research Communications, 2005. **330**(4): p. 1299-1305.
192. Houghton, J., et al., *Gastric cancer originating from bone marrow-derived cells.* Science, 2004. **306**(5701): p. 1568-1571.
193. Baksh, D., L. Song, and R.S. Tuan, *Adult mesenchymal stem cells: characterization, differentiation, and application in cell and gene therapy.* Journal of Cellular and Molecular Medicine, 2004. **8**(3): p. 301-316.
194. Meirelles, L.D.S., P.C. Chagastelles, and N.B. Nardi, *Mesenchymal stem cells reside in virtually all post-natal organs and tissues.* Journal of Cell Science, 2006. **119**(11): p. 2204-2213.
195. Tuan, R.S., G. Boland, and R. Tuli, *Adult mesenchymal stem cells and cell-based tissue engineering.* Arthritis Research & Therapy, 2003. **5**(1): p. 32-45.
196. Musina, R.A., E.S. Bekchanova, and G.T. Sukhikh, *Comparison of mesenchymal stem cells obtained from different human tissues.* Bulletin of Experimental Biology and Medicine, 2005. **139**(4): p. 504-509.
197. Jiang, Y.H., et al., *Pluripotency of mesenchymal stem cells derived from adult marrow.* Nature, 2002. **418**(6893): p. 41-49.
198. Kolf, C.M., E. Cho, and R.S. Tuan, *Mesenchymal stromal cells - Biology of adult mesenchymal stem cells: regulation of niche, self-renewal and differentiation.* Arthritis Research & Therapy, 2007. **9**(1).
199. Abdel-Latif, A., et al., *Adult bone marrow-derived cells for cardiac repair - A systematic review and meta-analysis.* Archives of Internal Medicine, 2007. **167**(10): p. 989-997.
200. Bunnell, B.A., et al., *Potential application for mesenchymal stem cells in the treatment of cardiovascular diseases.* Canadian Journal of Physiology and Pharmacology, 2005. **83**(7): p. 529-539.
201. Pittenger, M.F. and B.J. Martin, *Mesenchymal stem cells and their potential as cardiac therapeutics.* Circulation Research, 2004. **95**(1): p. 9-20.
202. Chen, X., M.A. Armstrong, and G. Li, *Mesenchymal stem cells in immunoregulation.* Immunology and Cell Biology, 2006. **84**(5): p. 413-421.
203. Trzaska, K.A. and P. Rameshwar, *Current advances in the treatment of Parkinson's disease with stem cells.* Current Neurovascular Research, 2007. **4**(2): p. 99-109.
204. Wang, G.S., et al., *Adult stem cells from bone marrow stroma differentiate into airway epithelial cells: Potential therapy for cystic fibrosis.* Proceedings of the National Academy of Sciences of the United States of America, 2005. **102**(1): p. 186-191.
205. Altman, G.H., et al., *Cell differentiation by mechanical stress.* Faseb Journal, 2001. **15**(14): p. 270.
206. Jones, R., *Surface markers of undifferentiated mesenchymal stem cells*, P. Coupland, Editor. 2007, University of Nottingham: Nottingham.
207. Zola, H., Swart, B., Nicholson, I., Aasted, B., Bensussan, A., Boumsell, L., Buckley, C., Clark, G. et al., *CD molecules 2005: human cell differentiation molecules.* Blood, 2005. **106**(9): p. 3123 - 3126.
208. Smith, A.G., *Embryo-derived stem cells: Of mice and men.* Annual Review of Cell and Developmental Biology, 2001. **17**: p. 435-462.
209. Xu, C.H., et al., *Immortalized fibroblast-like cells derived from human embryonic stem cells support undifferentiated cell growth.* Stem Cells, 2004. **22**(6): p. 972-980.
210. Xu, C.H., et al., *Feeder-free growth of undifferentiated human embryonic stem cells.* Nature Biotechnology, 2001. **19**(10): p. 971-974.
211. Promega, *Sequencing Grade Modified Trypsin*, in *Promega product literature* 2007, Promega Corporation: Madison, USA. p. 1 - 2.